

3462

JNCASR
Acc No. 3462
LIBRARY

JNCASR
548.8 P



**INVESTIGATIONS OF MOLECULAR CRYSTALS
USING EXPERIMENTAL CHARGE DENSITY**

A Thesis
Submitted for the Degree of
Doctor of Philosophy

By
R. SRINIVASA GOPALAN



TO
MANIPAL ACADEMY OF HIGHER EDUCATION
THROUGH
JAWAHARLAL NEHRU CENTRE FOR ADVANCED SCIENTIFIC
RESEARCH, BANGALORE 560 064, INDIA
AUGUST 2000

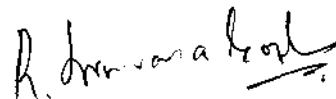
548.8
P

In the loving memory of my mother

DECLARATION

I hereby declare that the matter embodied in this thesis entitled **“Investigations of molecular crystals using experimental charge density”** is the result of investigations carried out by me in the Chemistry and Physics of Materials unit, Jawaharlal Nehru Centre for Advanced Scientific Research, Jakkur, Bangalore, India, under the supervision of Dr. G. U. Kulkarni and Professor C.N.R. Rao.

In keeping with the general practice of reporting scientific observations, due acknowledgement has been made whenever the work described has been based on the findings of the other investigators. Any omission which might have been occurred by oversight or error of misjudgement is regretted.



R. SRINIVASA GOPALAN



Chemistry & Physics of Materials unit
JAWAHARLAL NEHRU CENTRE FOR ADVANCED SCIENTIFIC RESEARCH
Jakkur P.O., Bangalore 560 064, INDIA

28, August, 2000

CERTIFICATE

Certified that the work described in the thesis entitled "**INVESTIGATIONS OF MOLECULAR CRYSTALS USING EXPERIMENTAL CHARGE DENSITY**" is the result of investigations carried out by Mr. R. Srinivasa Gopalan in the Chemistry and Physics of Materials Unit, Jawaharlal Nehru Centre for Advanced Scientific Research, Jakkur, Bangalore 560 064 under our supervision and the results presented in the thesis have not previously formed the basis for the award of any other diploma, degree or fellowship.

Dr. G. U. Kulkarni

Prof. C. N. R. Rao

ACKNOWLEDGEMENTS

I am grateful to my research supervisors Dr. G. U. Kulkarni and Prof. C.N.R.Rao for suggesting problems and for taking keen interest in me. From them, I have learnt to tackle various scientific problems and face them with confidence. I have gained immense knowledge from them in form of very productive discussions. It has been a wonderful experience doing research in a centre with highly advanced facilities.

I thank Dr. P. Kumaradhas for his initial help in data collection and multipole refinement. I would like to acknowledge the sincere efforts by the technical staff, Srinivas and Srinath, who have been extremely helpful in maintaining the single crystal diffractometer in excellent condition. I thank Dr. G. Acharya for the ethylenedicarbonitrile derivatives and Dr. T. P. Radhakrishnan for the DMPDQ crystals.

I am thankful to all the faculty members of both JNCASR and Chemistry division, IISc who have offered courses and have been extremely generous. In particular, I would like to thank Profs. S. Chandrasekharan, S. Ramasesha, J. Chandrasekhar, T.N. Guru Row and Dr. P. K. Das. I would also like to thank Dr. Balasubramanian for maintaining excellent computing facilities. I am thankful Dr. V. R. Pedireddi and Dr. S. Natarajan for their help in various crystallographic programs.

I have had an extremely helpful atmosphere in the Crystallography lab thanks to Anupama, Neeraj, Vaidhya, Amitava, Ayi, Shivshankar and Jayaram. I am especially thankful to Anupama, John and Shivshankar for helping me in the thesis work.

I thank Profs. Phillip Coppens (SUNY, Buffalo), Paul Mallinson (University of Glasgow, Scotland), Richard. F. W. Bader (McMaster University, Canada), George Sheldrick (University of Gottingen, Germany), Drs. Krystof Wozniak (University of Warsaw, Poland) and Sian Howard (University of Wales, Cardiff) for patiently answering many of my questions. I thank Prof. Mark Spackman (University of New England, Australia) for sending the reprints of his papers.

I would like to acknowledge the help of Drs. Ayyappan and Mahesh during the initial stages of my Int. Ph. D. I am thankful to my classmates Kalai, Bala, Yamuna and Saifi for all their help during course work. I would like to thank all the students especially Gargi, John, Vinod, Vaidhya, Sudhee, Sarathy, Jaya, Sujay, Praveen and Sachin who have been helpful at various times during the course of my research work.

I would like to acknowledge the help from Mr. Jarali (SSCU) for DSC measurements and Vasu for IR measurements. Vinayak and Rajesh have been

extremely good maintaining the computers failing which many things would have come to a stand still.

I thank the office staff of JNCASR and CSIR-COE. They have made my stay in the centre convenient and saved my time from usual official chores. I am obliged to Jawaharlal Nehru Centre for giving me a scholarship.

I am glad to have got a lot of friends here as well as in IISc who have made my stay pleasant. Those who have really made a mark in my life include Neeraj, Anupama, Swarna, Anoop, Joy, Prashanth, Praveen, Shobha and Akash.

I thank my school chemistry teacher, Mrs. Sujata, who inspired me to take up chemistry for my further studies. I thank my college chemistry teachers, Mr. Vannamuthu, Ms. Nirmala Devi and Prof. R. S. Raghavan for taking keen interest in me.

I thank my family members for all their love and affection. Finally, I would like to thank my parents for allowing me to do what I wanted rather than imposing their views on me. They have been a constant source of encouragement and inspiration to me. My mother especially had been a great source of ideas and encouragement to me. This thesis is dedicated in the memory of my mother.

CONTENTS

DECLARATION	i
CERTIFICATE	ii
ACKNOWLEDGEMENTS	iii
PREFACE	viii

INVESTIGATIONS OF MOLECULAR CRYSTALS USING EXPERIMENTAL CHARGE DENSITY

SUMMARY	1
1. INTRODUCTION	
1.1 Background	6
1.2 Description of charge density.....	8
1.3 Critical points	9
1.4 Charge density from X-ray diffraction.	17
1.5 Data refinement and Computer codes.....	20
1.6 Dipole moments from experimental charge density.....	22
2. SCOPE OF THE THESIS	
2.1 A study of N-methyl-N-(2-nitrophenyl)cinnamanilide.....	24
2.2 Photodimerization <i>o</i> -ethoxy cinnamic acid.....	24
2.3 Photoreaction of <i>p</i> -nitrophenol.....	26
2.4 Properties of aliphatic dicarboxylic acids.....	26
2.5 Structural Phase Transition in Adipic Acid.....	30
2.6 Non-linear Optical Molecular crystals.....	30
3. EXPERIMENTAL AND RELATED ASPECTS	
3.1 Crystals.....	34
3.2 Diffractometer.....	36

3.3	Structure and multipole refinement.....	41
4.	RESULTS AND DISCUSSION	
4.1	Hydrogen bonds in N-methyl-N-(2-nitrophenyl)cinnamanilide	45
	Charge density distribution	45
	Molecule in the crystal versus a free molecule.....	55
	Conclusions.....	59
4.2	Photodimerization of <i>o</i>-ethoxy cinnamic acid and its dependence on the polymorphic form.....	60
	Molecular packing of α and γ forms.....	60
	Charge density in the α and the γ forms.....	70
	The photodimer.....	76
	Conclusions.....	79
4.3	Photocoloration of <i>p</i>-nitrophenol.....	81
	Molecular packing.....	81
	Charge density analysis.....	84
	Conclusions.....	89
4.4	Properties of a series of aliphatic dicarboxylic acids.....	93
	Structural aspects.....	93
	Charge density analysis.....	98
	Conclusions.....	103
4.5	Effects of the non-centric crystal field on the molecular properties of organic NLO materials.....	105
4.5.1	5-nitrouracil.....	105
4.5.2	1,1-ethylenedicarbonitriles.....	115
	Conclusions.....	125
4.6	The molecular dipole moment of 7,7-di(S(+)-2-(methoxymethyl)pyrro- lidino) -8,8-dicyanoquinodimethane, a NLO material.. ..	126
	Molecular structure.....	126
	Charge density analysis.....	126
4.7	Structural Phase Transition in Adipic Acid.....	135

Structural aspects.....	135
Electrostatic potential analysis.....	144
5. REFERENCES.....	148
6. OTHER WORK DONE BY THE AUTHOR.....	154

SUPPLEMENTARY INFORMATION

PREFACE

The thesis deals with the analysis of charge density distribution in molecular systems in terms of topological properties. Several organic molecular crystals have been investigated with definitive objectives in mind. Some of the important aspects studied are: the effect of intermolecular hydrogen bonding, polymorph-specific photoreactivity and non-linear optical (NLO) properties.

The effect of intermolecular hydrogen bonding on the molecular geometry has been investigated in the case of N-methyl-N-(2-nitrophenyl)cinnamanilide. The geometry obtained from semi-empirical AM1 calculations on the free molecule provides the reference state. Molecular cohesion in a series of alkane dicarboxylic acids has been studied with specific interest in the alternation of physical properties with the chain length. In this context, the single crystal-single crystal phase transition in adipic acid has also been investigated using the electrostatic potential approach.

The polymorph-specific photochemical behavior of *o*-ethoxy cinnamic acid has been examined by carrying out a detailed investigation of the structure and charge density of the light-sensitive polymorph in comparison with the corresponding light-stable forms. The photochemical reactivity of one of the polymorphs of *p*-nitrophenol has also been studied.

A few organic NLO materials have been investigated using the experimental charge density method to understand how a non-centric crystal field influences molecular properties, such as the dipole moment. The systems studied are: non-centric and centric polymorphs of 5-nitouracil and differently substituted 1,1-ethylenedicarbonitriles. For the purpose of comparison, semi-empirical calculations have been carried out on the frozen as well as optimized geometries of the molecules. An important finding from the study is that there is an enhancement in the molecular dipole moment in NLO crystals due to the non-centric field. Such an effect was also observed in 7,7-di(S(+)-2-(methoxymethyl)pyrrolidino)-8,8-dicyanoquinodimethane, where the donors and acceptors are well separated by an intermediate π -system.

INVESTIGATIONS OF MOLECULAR CRYSTALS USING EXPERIMENTAL CHARGE DENSITY*

SUMMARY

The thesis deals with investigations on the charge density distribution in molecular solids using high-resolution X-ray diffraction. Although the possibility of extracting molecular properties from charge density was known since the early days of X-ray diffraction, it is only in the last decade due to technical and computational developments that the charge density method has gained enough confidence for accurate applications. The experimentation used by the candidate involves a sophisticated diffractometer attached with a CCD area detector and a low temperature set-up. The data refinement is done using the program package, XD, based on multipole formalism. It allows one to refine multipole populations around each atom in addition to atomic and thermal parameters. From the topography of the charge distribution, one can uniquely define various chemical entities such as atom-cores, bonding regions, lone-pairs, rings and cages. Moreover, a detailed analysis can provide information on electrophilic and nucleophilic sites in a molecule, strengths of attractive and repulsive interactions and many other bond properties. The experimental charge density method is unique in that the in-crystal molecular dipole moment can be estimated. This value is often compared with the dipole moment of the molecule in the free state obtained computationally. The candidate undertook to study various aspects of molecular crystals such as hydrogen bonding, reactivity and non-linear optical property. The molecular systems were chosen carefully to bring focus on the individual aspects. The systems studied include N-methyl-N-(2-nitrophenyl)cinnamamide, polymorphs of *o*-ethoxy cinnamic acid, *p*-nitrophenol, a homologous series of aliphatic dicarboxylic acids, polymorphs of 5-nitouracil, derivatives of 1,1-ethylenedicarbonitrile and 7,7-di(S(+)-2-(methoxymethyl)pyrrolidino)-8,8-dicyanoquinodimethane.

In N-methyl-N-(2-nitrophenyl)cinnamamide, the molecules are held only by C—H...O contacts, the prominent being a pair of centrosymmetrically related bifurcated hydrogen contacts from the amidic oxygen. The oxygens of the nitro group form C—H...O contacts at much higher distances. The cinnamide part of the molecule is nearly planar while it is twisted at the nitrobenzene link by 63.3°. In contrast, a semi-empirical energy optimisation of the free molecule showed that the two phenyl rings lie in a plane while the intervening bonds are buckled, as though the molecule in the crystal was held twisted to favour hydrogen bonding from the amidic oxygen. The question posed for the charge density investigation pertains to the relative strength of the hydrogen bonds from the amidic oxygen in comparison to those from the nitro oxygens. The critical point analysis has revealed that the hydrogen bonds from the amidic oxygen carry higher densities and Laplacians, characteristic of strong interactions.

The photoinduced (2+2) cycloaddition reaction in the α -form of o-ethoxy cinnamic acid has been investigated in terms of structure and charge density in comparison with the light stable γ -form. The reactive double bonds in the reactive α -form (4.514 Å) are closer as compared to those in the γ -form (5.253 Å). The molecule is planar in the α -form and forms dimeric hydrogen bonds involving the carboxylic groups. In the photostable γ -form however, the molecule is non-planar and exhibits near-symmetric hydrogen bonds. Solid state IR spectroscopy on the two forms lends further evidence on the nature of the hydrogen bonds. Charge density analysis shows that the near-symmetric hydrogen bond in the γ -form is ionic and appears to restrict conjugation by way of distorting the molecule. This unusual feature in the γ -form keeps the cinnamoyl double bonds away from each other, rendering it photochemically unreactive. In the α -form, however, there is some charge redistribution in the ethoxy and the cinnamoyl regions. The cyclobutyl ring of the photodimer, 2,2'-diethoxy α -truxillic acid, consists of weak and strained single bonds.

Aliphatic dicarboxylic acids show an alternation in their physical properties with the number of methylene units in the chain, a property common to alkyl chains. We have studied the first few members of the homologous series of aliphatic dicarboxylic acid namely, malonic, succinic, glutaric, adipic and pimelic acids using structure and charge density. The study shows interesting systematics along the series. The C—C bond connecting to the carboxylic group is shorter by $\sim 0.03 \text{ \AA}$ compared to the inner C—C bonds, the latter attaining the ideal value of 1.54 \AA only in higher members. The density in the C—C, C—O and the O—H bonds is maximum in glutaric acid and decreases on either side of the series. The C=O and the C—H bonds exhibit the opposite trend. The molecules are held by acid dimeric hydrogen bonds and side-chain interactions, the latter being present only in the solid state. The densities associated with the side-chain interactions have been calculated as fraction of the total densities involved in intermolecular interactions. This is taken to indicate the cohesion of the molecules in the lattice. Interestingly, an undulatory behavior is observed along the series in compliance with that observed for melting point.

The single-crystal to single-crystal phase transition in adipic acid at $\sim 136 \text{ K}$ has been investigated in detail using structure and electrostatic potential. On lowering the temperature, the a parameter of the room temperature monoclinic cell decreases by $\sim 0.25 \text{ \AA}$. Accompanying the transition, the b parameter nearly triples while a reverts back to the room temperature value. Two-thirds of the molecules in the structure lose centre of symmetry. Packing diagrams of the high- and the low-temperature phases on superposition reveal that there exist alternating domains perpendicular to the b direction which contain molecules with and without symmetry. The deviation of the inner and the outer torsion angles from 180° , if taken to represent the strain in the molecule shows that upon phase transition, the evenly distributed strain in the high-temperature phase segregate into two domains comprising unstrained molecules in one domain (HM) and highly strained molecules without inversion symmetry in the other

(FM). The electrostatic potential maps of the molecules in the low- and the high-temperature phases show that the FM fragment exhibits a relatively larger spread in the potential due to inter-chain interactions compared to the high-temperature and the HM fragment. This is the first charge density study on a single-crystal to single-crystal phase transition.

In our pursuit of extracting physical properties of molecular materials, we have carried out thorough investigations on non-linear optical materials. In order to understand the manner in which the non-centric nature of the crystal-field affects the molecular dipole moment and other properties in the solid, two systems have been examined- one where the center of symmetry is destroyed by crystallizing the molecule in a related polymorphic structure and the other where the non-centric nature is introduced by changing the pattern of substitution. For the former case we have studied centric and non-centric polymorphs of 5-nitrouracil and for the latter case we have studied differently substituted 1,1-ethylenedicarbonitriles. We find that in the non-centric polymorph of 5-nitrouracil, the charge separation is more and hence the dipole moment obtained from experimental charge density is higher than in the centric polymorph. Semi-empirical calculations show the frozen molecular geometries of both the forms have similar dipole moments close to that in the centric polymorph. Among the 1,1-ethylenedicarbonitriles, there is an increased charge separation in the non-centric thioamino derivative leading to an enhanced dipole moment of 15D compared to the centric diamino (5 D) and dithio (6 D) derivatives. The effect of the crystal field is also borne out by semiempirical AM1 calculations on the two systems. Dipole moments calculated for the molecules in the frozen geometries match closely with those obtained for centric crystals from the experimental charge densities. The calculated values of the dipole moment in the frozen or optimized geometries in the non-centric structures are, however, considerably lower than the observed value. Furthermore, the conformation of the S—CH₃ group in the non-centric crystal is anti with respect to the central C=C bond while the syn conformation is predicted for the free molecule in the optimized

geometry. We have also carried out a structural and charge density study on 7,7-di(S(+)-2-(methoxymethyl)pyrro-lidino)-8,8-dicyanoquinodimethane where the donor and the acceptor groups are separated by a long π -system ($\sim 6\text{\AA}$). We find that the donor and the acceptor groups carry large positive and negative charges respectively while the π -system carries no net charge and the dipole moment obtained from the charge density is very high ($\sim 44\text{ D}$). Frozen and optimised geometries of this molecule carries smaller but similar charges and the calculated dipole moments from these geometries are quite small ($\sim 20\text{ D}$). These observations clearly ascertain that an asymmetric crystal field of a non-centric structure can significantly enhance the dipole moment of a molecule. The effect is well pronounced in this case due to a larger separation between the donor and the acceptor.

* Papers based on the above studies have appeared in J. Mol. Struct (Theochem) (2000), J. Mol. Struct (2000), J. Mol. Struct. (2000), Proc. Ind. Acad. Sci (1999), J. Solid State Chem. (1999), ChemPhysChem (2000)

1. INTRODUCTION

1.1 Background

The description of charge distribution in crystalline lattices has come a long way since the first quantum model of the atom. It was known from early days that a quantitative account of the chemical bonds in molecules and crystals would require the calculation of the probability density of the electron cloud between atoms. The possibility of probing the electronic structure was recognized almost immediately after the discovery of X-ray diffraction by von Laue in 1912, as is evident from Debye's statement [1] in 1915.

"It seems to me that experimental study of scattered radiation, in particular from light atoms, should get more attention, since along this way it should be possible to determine the arrangement of electrons in the atoms".

Convinced that X-rays were scattered by electrons, Debye joined by Scherrer, turned his attention to chemical bonding and thereby initiated the field of X-ray charge density studies. Debye and Scherrer wondered how the valency dashes, used by the chemists to describe the bond between atoms, could be replaced by an electron model that was consistent with their results with the newly discovered powder diffraction method and with Bragg's ionization counter measurements.

The first problem addressed was the covalent bond in diamond [2]. They first assumed the electrons occupy the space between the neighboring atoms as in the Lewis dot model, which had become widely used. But this model was not in agreement with the diffraction results of Bragg, since it would yield a strong 222 reflection, which is not observed in the diffraction pattern. They concluded that electron clouds in the bonding regions could not be detected in diamond or other comparable solids.

A second model consisted of a spherical carbon atom with electrons moving rapidly so as to give a constant average distribution within a spherical volume centered at the nucleus. This model provided a quantitative account of the observed decrease of the atomic scattering factor at higher diffraction angles. The dimension of the atom-sphere derived from this model was consistent with the interatomic distances, and was of the same order of magnitude as calculated by Bohr on the basis of his quantum theory.

The measurement techniques were too crude to show any deviations from spherical atomic distributions. Most of the efforts were on simple ionic compounds such as NaCl and MgO, for which the deviations from spherical symmetry were very small. Thus, the measurement of charge densities in the bonding regions remained a distant goal for decades, even though attempts were not lacking.

Technical developments that occurred in the 1960s and 1970s provided much needed impetus to the X-ray diffraction field. High-precision diffractometers, low-temperature set-up, automation in data collection and advances in computing power and the software have become regular feature of modern experimentation. Neutron diffraction provided an independent source of positional and thermal parameters, unbiased by the isolated-atom assumptions. The past three decades have seen increased activity in this area of research with significant contributions from several workers worldwide, F.L.Hirshfeld, P.Coppens, B.Craven, R.F.Stewart and N.K.Hansen to name a few. The program package, XD, has been developed since 1995 from a European commission on charge density. The contributions of Lecomte, Blessing, Pinkerton, Baert and Fiel are indispensable especially in the charge density of non-centrosymmetric systems. There have been notable progress in the theoretical approach as well. Pople's Gaussian program [3] and Schmidt's Gamess package [4] are being used extensively for *ab initio* charge density on isolated molecules. Saunders, Roetti and Dovesi have extended the Hartree-Fock analysis to crystals in their CRYSTAL program [5]. Kohn-Sham's Density Functional approach has also been used for crystals. R.F.W.Bader has made significant contributions in the last four decades to the understanding of

the topology of charge density distribution in molecular crystals. In his "Quantum theory of Atoms in Molecules" [6] he has defined bond properties in terms of various topological entities. The transferability of charge distribution between molecules carrying identical functional groups is one of the important contributions by him. He has also defined the reactivity and stability of bonds in terms of the charge distribution. The above mentioned developments in the charge density method have laid the foundation for its wider applications in diverse fields. In the recent years, the charge density method has been applied extensively on various types of organic and biological molecules, inorganic complexes, organometallic compounds, transition metal clusters and non-linear optic materials [7-12].

1.2 Description of Charge density

Charge density in a N-electron system is the probability density of finding any of the electrons in the phase space $d\tau$.

$$\rho(r) = N \int \psi^* \psi d\tau \quad \dots(1)$$

where ψ is the stationary state function; τ denotes the spin coordinates of all the electrons and the cartesian coordinates of all electrons but one. It is expressed in $e\text{\AA}^{-3}$ or a.u (1 a.u = $6.7483 e\text{\AA}^{-3}$). The description of electronic structure of a molecule in real space therefore relates to the charge density distribution around the constituent atoms. The density in a molecule can be conveniently modelled by partitioning into core, spherical valence and deformation valence around each atom (the deformation being caused by the interatomic bonding) [13],

$$\rho_{atom}(r) = \rho_{core}(r) + \rho_{valence}(r) + \rho_{deformation}(r, \theta, \phi) \quad \dots(2)$$

and thus one may look at the total electron density, core, valence or deformation density. Topological properties are dealt with using the total electron density or using its derivatives, while the bonding features can be visualised using the deformation density.

Charge density distribution in a molecule or a crystal may be obtained by *ab initio* Hartree-Fock calculations [14]. In this method, the electrons are assumed to move in a symmetric field generated by the nuclei and the other electrons. Since, the wavefunction and the potential are correlated, one obtains the wave function using an iterative procedure till such a time when a change in potential does not produce a significant change in the wave function. Once the wave function is obtained, the electron density distribution could be readily determined. Commercial programs such as Gaussian [3] and Gamess [4] are used regularly for this purpose. Calculations for crystals can be performed using the periodic Hartree-Fock method or using the Density functional theory. Both of these options have been incorporated in the CRYSTAL program of Dovesi and co-workers [5]. Within the density functional formalism, calculations can be done either at Local density approximation (LDA) or using Generalised Gradient Approximation (GGA). Either of the methods are known to yield good results.

1.3 Critical points

The topology of a charge distribution has many rich features- maxima, minima, saddles and nodes which help characterise intuitional elements like atom cores, bonds, lone-pair electrons etc. These are analysed in terms of critical points, the points where the electron density exhibits an extremum. As an example, the charge density distribution in water molecule [6] is depicted in Fig.1 in the form of contour as well as relief maps. The density is maximum at the oxygen core position and decreases steeply towards the mid-region between oxygen and hydrogen reaching the minimum value at the 'critical point' ($\nabla\rho = 0$). This point carries maximum densities from the other two perpendicular directions. A quantitative description of charge density thus boils down to examining the number and the nature of such critical points in and around a molecule. A critical point (CP) is characterised not only by its density and location but also by the curvatures and the associated signs.

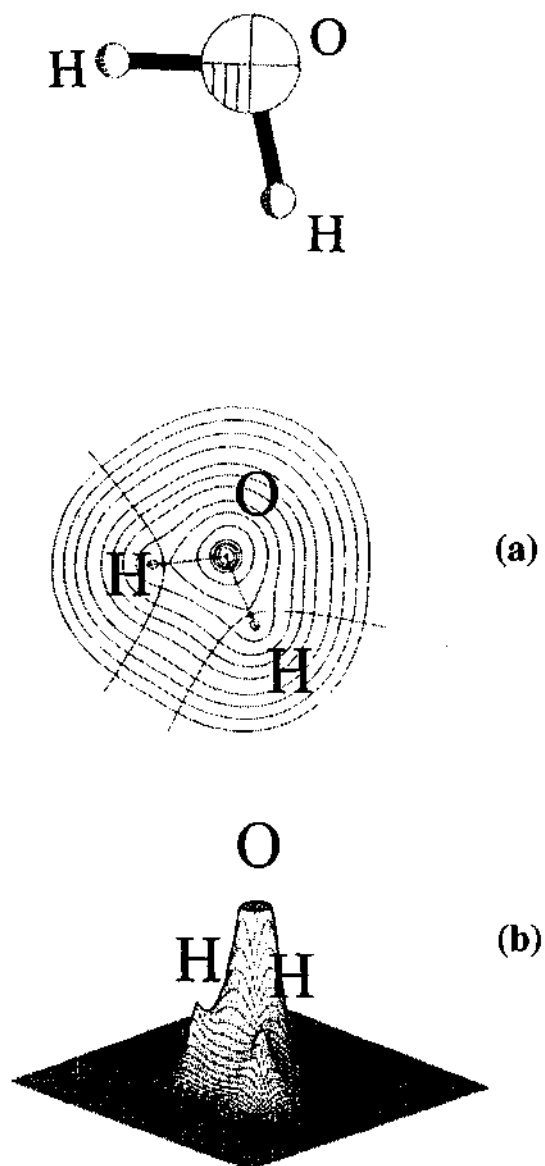


Fig.1. Water: Charge density in the molecular plane, a) the contour map. The outermost contour has the value $0.0067 \text{ e}\text{\AA}^{-3}$. The density increases almost exponentially for inner contours. The bond paths, the interatomic surfaces and the bond critical points are also indicated. b) The relief map where the atom-cores are seen as peaks (from ref. 6).

Table 1

Critical point	Meaning
(3,-3)	All curvatures are negative and the property is a local maximum at r_c
(3,-1)	Two curvatures are negative and property is a maximum at r_c in the plane defined by their corresponding axes. The property is a minimum at r_c along the third axis which is perpendicular to this plane
(3,+1)	Two curvatures are positive and the property is a minimum at r_c in the plane defined by their corresponding axes, property is a maximum at r_c along the third axis which is perpendicular to this plane
(3,+3)	All curvatures are positive and property is a local minimum at r_c

Table 2

Chemical entity defined in terms of critical points

Chemical entity	Property	Critical point
Atom cores	ρ	3, -3
Bonds	ρ , esp	3, -1
Rings	ρ , esp	3, +1
Cages	ρ	3, +3
Lone-pair	$\nabla^2\rho$	3, +3

For an arbitrary choice of coordinate axes, one encounters nine second derivatives of the form, $\partial^2\rho/\partial x\partial y$ in the determination of the curvatures of ρ at a point in space. Their ordered 3 x 3 array is called as the Hessian matrix of the charge density. Thus,

$$\text{Hessian, H} = \begin{pmatrix} \partial^2\rho/\partial x^2 & \partial^2\rho/\partial x\partial y & \partial^2\rho/\partial x\partial z \\ \partial^2\rho/\partial y\partial x & \partial^2\rho/\partial y^2 & \partial^2\rho/\partial y\partial z \\ \partial^2\rho/\partial z\partial x & \partial^2\rho/\partial z\partial y & \partial^2\rho/\partial z^2 \end{pmatrix}$$

is a real, symmetric matrix and can be diagonalized. The new axes about which the Hessian is a diagonalized is called as the principal axes of curvature, so called because the magnitude of the three second derivatives of ρ calculated with respect to these axes are extremized.

$$\begin{pmatrix} \partial^2\rho/\partial x^2 & \partial^2\rho/\partial x\partial y & \partial^2\rho/\partial x\partial z \\ \partial^2\rho/\partial y\partial x & \partial^2\rho/\partial y^2 & \partial^2\rho/\partial y\partial z \\ \partial^2\rho/\partial z\partial x & \partial^2\rho/\partial z\partial y & \partial^2\rho/\partial z^2 \end{pmatrix} \xrightarrow{\text{Diagonalize}} \begin{pmatrix} \lambda_1 & 0 & 0 \\ 0 & \lambda_2 & 0 \\ 0 & 0 & \lambda_3 \end{pmatrix}$$

The trace of the Hessian matrix, i.e the sum of the diagonal elements, is invariant to the rotation of the coordinate system. Thus, the curvature of charge density $\nabla^2\rho$, called as the Laplacian, obtained as the sum of eigen values- $\lambda_1, \lambda_2, \lambda_3$ of the Hessian matrix is invariant to the choice of the rotational axis.

$$\text{Trace} = \lambda_1 + \lambda_2 + \lambda_3 \equiv \text{Laplacian} \quad \dots(3)$$

The nature of the critical points is uniquely defined by the set (rank, signature). The rank of the critical point refers to the number of non-zero eigen values of the Hessian matrix, while the signature refers to the sum of their signs. In addition, to the charge density maps, sometimes it is necessary to draw Laplacian maps to unravel the nature of interaction in the interatomic regions as well as the shape of the lone-pairs. Figure 2 shows a Laplacian map of 3,3,6,6-tetramethyl-S-tetrathiane [15], an example from the literature, in the plane formed by C(1), S(1) and S(1a) atoms. The lone pairs on the sulphur

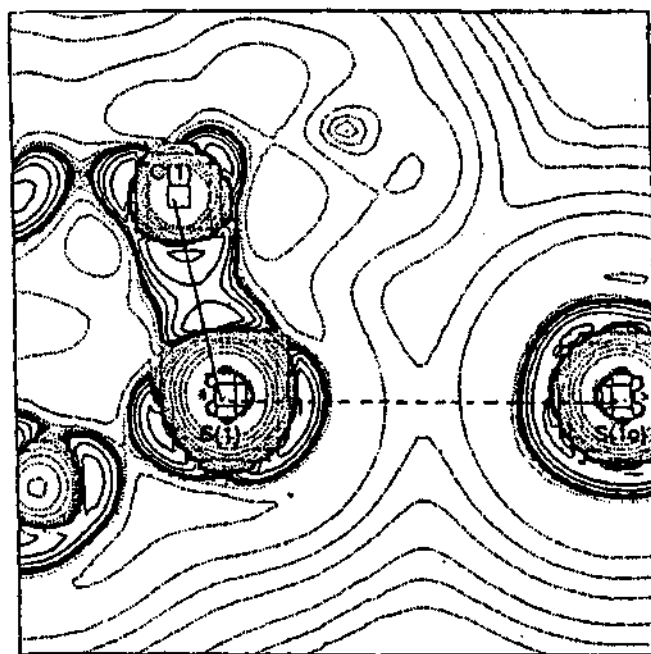
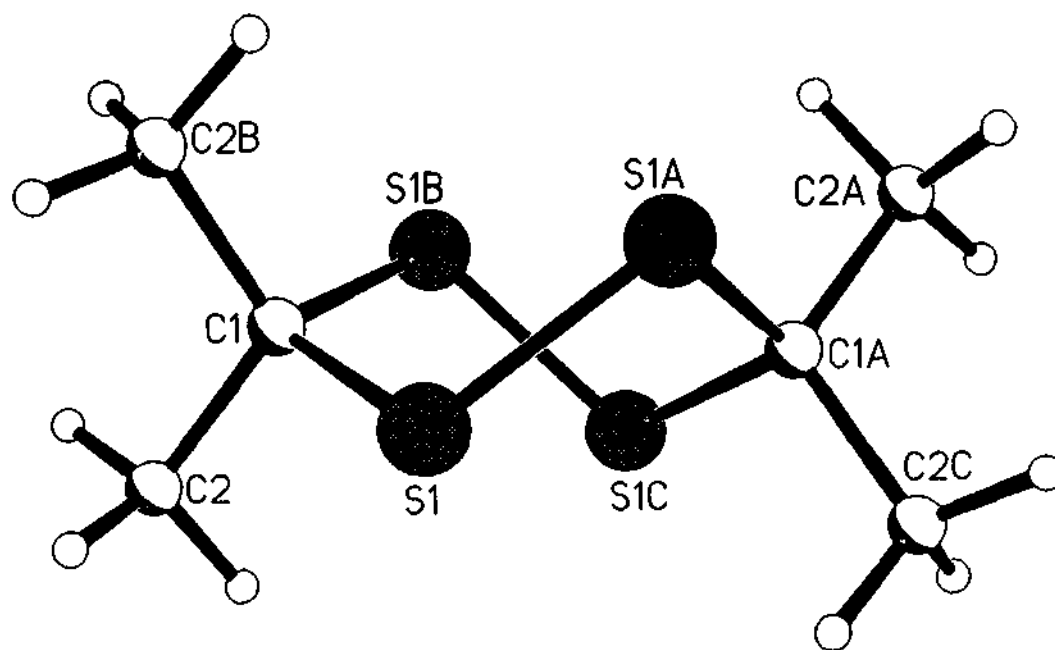


Fig.2. 3,3,6,6-tetramethyl-S-tetrathiane: Laplacian distribution in C(1), S(1), S(1A) plane. Molecular diagram is shown at the top (from ref. 15).

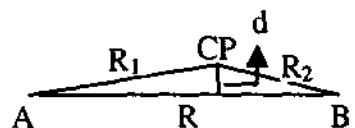
are seen as lobes. We observe that there exists shared (covalent) interaction between the carbon and sulphur while there is a closed (ionic) interaction between the two sulphur atoms.

The relative magnitudes of the curvatures perpendicular to the bond direction (λ_3) determine the ellipticity [16] associated with a bond.

$$\varepsilon = (\lambda_1/\lambda_2) - 1 \quad \dots(4)$$

Theoretically, cylindrically symmetric bonds (single and triple bonds) have ellipticity zero while double bonds have a value of 0.74.

An estimate of bond polarization [16] can be obtained from the location of the bond CP with respect to the internuclear vector,



$$\Delta_B \% = 100 \times (R_m - R_1) / R_m \quad \dots(5)$$

where $R_m = (R_1 + R_2) / 2$. The Δ value is used to describe relative electronegativities of atoms involved. The strain involved in a bond can be estimated [16] in terms of the vertical displacement, d of the bond path from the internuclear vector

$$d = 2 \times \sqrt{s \times (s - R_1) \times (s - R_2) \times (s - R)} / R \quad \dots(6)$$

where $s = (R_1 + R_2 + R) / 2$

Covalent bonds are usually associated with high charge densities ($1.5 - 3 \text{ e}\text{\AA}^{-3}$) and negative Laplacians, while ionic bonds are characterised by small densities and positive Laplacians. Thus, a typical C—C bond carries a density of $\sim 1.7 \text{ e}\text{\AA}^{-3}$ and a Laplacian of $\sim -16.0 \text{ e}\text{\AA}^{-5}$ at the CP while a KF bond carries a density of $0.37 \text{ e}\text{\AA}^{-3}$ and a Laplacian of $7.47 \text{ e}\text{\AA}^{-5}$. Hydrogen bonds are associated with even smaller densities and Laplacians. The hydrogen bond in water carries a density of $0.133 \text{ e}\text{\AA}^{-3}$ and a Laplacian of $1.50 \text{ e}\text{\AA}^{-3}$. Following Cramer and Kraka [16], the charge density at critical point, ρ_{CP} , is a measure of the bond strength in covalent bonds, the value at the critical

point depending upon the atoms involved and the bond order. Accordingly, a C=C bond exhibits a density of $\sim 2.5 \text{ e}\text{\AA}^{-3}$. And a C \equiv C bond is associated with a higher value of $\sim 2.8 \text{ e}\text{\AA}^{-3}$. The ellipticity of a bond, ε , is a measure of its extent of double bond character. For cylindrically symmetric bonds, the ellipticity is therefore zero while in the case of ideal carbon double bonds, the theoretical estimate gives $\varepsilon \sim 0.74$. These quantities in combination with bond polarity (Δ), pseudoatomic charges and the bent bond character (d) describe a bond quantitatively.

The electrostatic potential (esp) generated by a molecule containing nuclear charges, z_i , placed at R_i , with a charge distribution $\rho(r)$, is given by [17,18]

$$V(r) = \sum_i \frac{z_i}{|r - R_i|} - \int \frac{\rho(r')}{|r' - r|} d^3 r' \quad \dots(7)$$

As the electrostatic forces are relatively long range forces, they determine the path along which an approaching reactant will travel towards a molecule. A nucleophilic reagent will be first attracted to the regions where the potential is positive while an electrophile will approach the negative regions of the molecule. Thus, it is useful in describing attractive and repulsive interactions and also in determining the electrophilic and nucleophilic sites in molecules. Figure 3 shows the electrostatic potential map of imidazole [19]. We see an extension of the electrostatic potential near the N—H and a minimum near the opposite nitrogen atom. This represents the hydrogen bonding interactions between this hydrogen and the nitrogen. They act as donor and acceptor sites respectively in the N—H \cdots N hydrogen bonding interactions in the interatomic regions.

The other quantity of interest is the kinetic energy density at the critical point, G_{CP} [20] which is obtained by

$$G_{CP} = \frac{3}{10} (3\pi)^{2/3} \rho_{CP}^{5/3} + \frac{\nabla^2 \rho_{CP}}{6} \quad \dots(8)$$

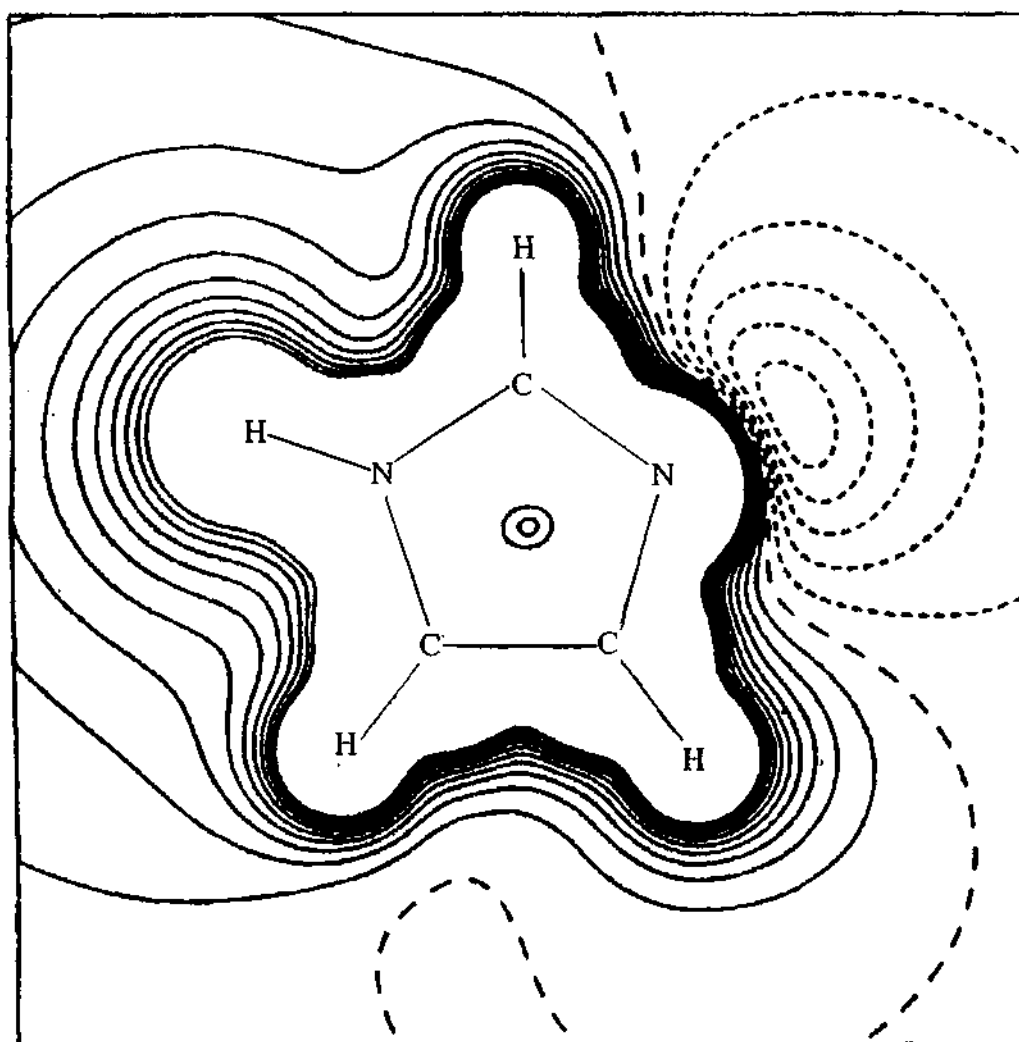


Fig.3. The electrostatic potential for imidazole in the least square plane of all atoms. Contours at $0.05 \text{ e}\text{\AA}^{-1}$ (from ref.19).

It has been used in some cases for the calculation of hydrogen bond energies [21] and their classification [22].

1.4 Charge density from X-ray diffraction

Experimental determination of charge density mostly relies on X-ray diffraction although other techniques have been applied in some instances. X-ray diffraction arises from scattering by electrons and therefore carries information on the distribution of electronic charge in real space [7]. The intensity of a Bragg reflection, $I(\mathbf{h})$, at a given temperature, is proportional to the square of its structure factor,

$$I(\mathbf{h}) \propto |F(\mathbf{h})|^2$$

$$\propto \left| \sum_i f_i(\mathbf{h}) e^{2\pi i \mathbf{h} \cdot \mathbf{r}_i} \right|^2 \quad \dots(9)$$

where $f_i(\mathbf{h})$ is the scattering factor of the i th atom in the unit cell of volume, V . The charge density is obtained by the Fourier summation of the experimentally measured reflections.

$$\rho(\mathbf{r}) = \frac{1}{V} \sum_{\mathbf{h}} F(\mathbf{h}) e^{-2\pi i \mathbf{h} \cdot \mathbf{r}} \quad \dots(10)$$

In conventional structure determination, $f_i(\mathbf{h})$ is approximated to the scattering factor from spherical electronic density, while for a complete description of bonding, accurate modeling of $f_i(\mathbf{h})$ becomes necessary. In parallel to $\rho(\mathbf{r})$ (see equation 2),

$$f(\mathbf{h}) = f_{core}(\mathbf{h}) + f_{valence}(\mathbf{h}) + f_{deformation}(\mathbf{h}) \quad \dots(11)$$

Such a partitioning of $f(\mathbf{h})$ is justifiable in X-ray diffraction since one can select regions of reciprocal space where core scattering is predominant. In Fig.4, we show variation of $f(\mathbf{h})$ with scattering angle, θ for various elements.

Each curve is composed of two regions. At low angles or Bragg vector ($\mathbf{h} = 2\sin\theta/\lambda$), $f(\mathbf{h})$ decreases steeply and above $\sim 0.5 \text{ \AA}^{-1}$, the fall is gradual. The first part has contributions from both the atom-core and the valence

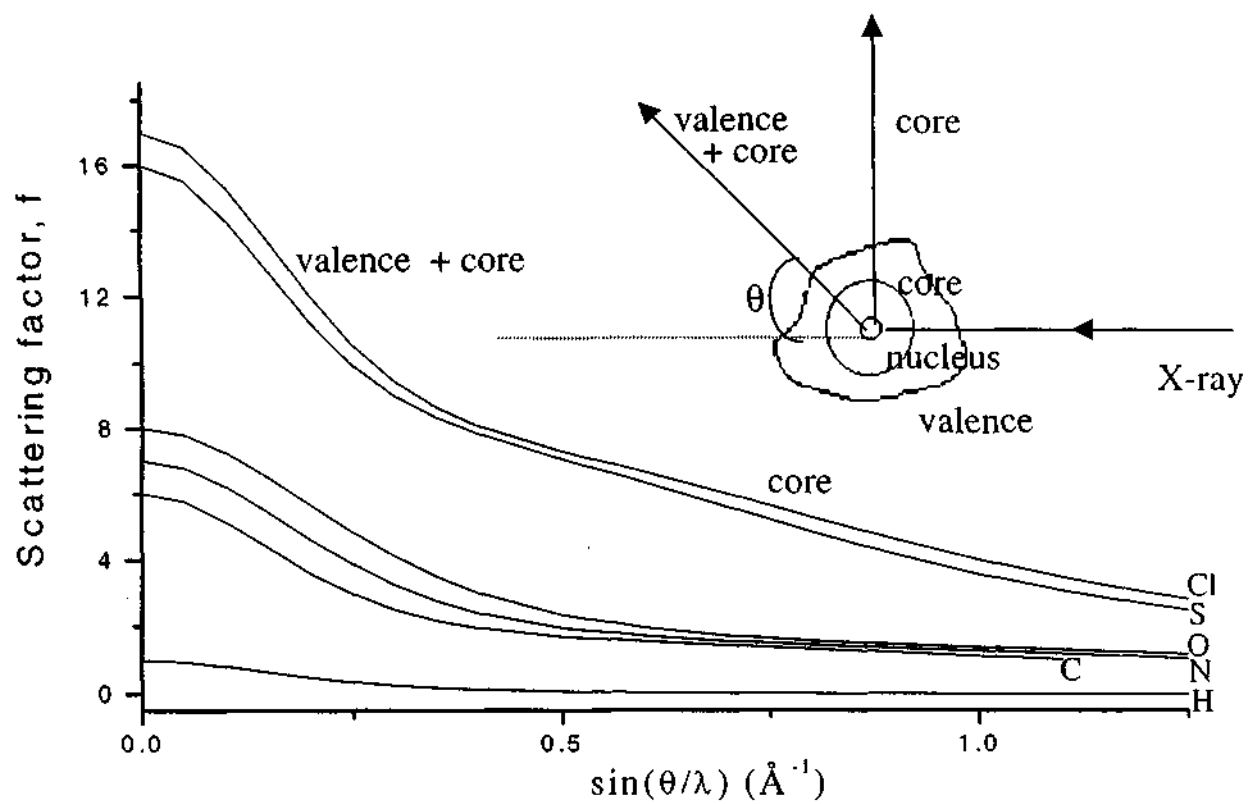


Fig.4. Variations of the scattering factor with $\sin\theta/\lambda$ for different atoms. Above 0.5 \AA^{-1} , the scattering due to valence electrons decreases gradually and the atom core becomes visible. This is shown schematically in the inset. The scattering factors were obtained from the International Tables for Crystallography, Vol. IV, page 71 (1974).

density while the second arises mainly due to the core. Thus, X-ray diffraction facilitates extraction of the bonding or the deformation density,

$$\rho_{\text{deformation}} = \rho_{\text{total}} - \rho_{\text{promolecule}} \quad \dots(12)$$

where promolecule is obtained by the superposition of atoms without any interaction between them. This is called the (X-X) method. In the (X-N) method, the core positions along with the thermal parameters are obtained from a neutron diffraction experiment. The latter is particularly useful while dealing with hydrogen atom positions though it requires two data sets, which can be expensive besides having to grow bigger crystals. In the recent years, the (X-X) method has become more popular. In this thesis work, only (X-X) method has been used.

Equation (8) above necessitates data collection covering a wide range of the reciprocal space. For small unit cells with dimensions $\sim 30 \text{ \AA}$, data collection up to moderately high resolution (1.25 \AA^{-1}) can be achieved using short wavelength radiations such as MoK α (0.71 \AA). Moreover, data collection strategy critically depends on the type of the diffractometer. In the past, point detectors mounted on a four circle diffractometers were used for charge density measurements with the data collection extending in some cases to a period of few weeks. Of late, area detectors or image plates are preferred over the conventional ones, as the experiments can be carried out faster with greater redundancy [23]. Area detectors in combination with synchrotron radiation is becoming increasingly popular [24, 25]. Koritsanszky *et al.* [25] demonstrated that the charge density data can be collected within a day.

Thermal smearing of charge density caused by atomic vibrations can hamper extraction of subtle features of bonding as described by,

$$f(T)_{(h,k,l)} = f(0) \exp\left(-\left(b_{11}h^2 + b_{12}hk + b_{13}hl + b_{22}k^2 + b_{23}kl + b_{33}l^2\right)\right) \quad \dots(13)$$

where

$$\begin{aligned} 2\pi^2 a^2 U_{11} &= b_{11} \\ 2 \times 2\pi^2 a^* b^* U_{12} &= b_{12} \quad \text{etc.,} \end{aligned}$$

where U_{ij} 's are the anisotropic displacements parameters. Low temperature experiments at ~ 100 K, are carried out allowing a stream of liquid nitrogen to fall on the crystal. In some cases however, much lower temperature (~ 20 K) have been achieved using one or two stage He-closed-cycle cryostats [26]. It is also necessary to choose a good quality, least mosaic crystal for charge density work.

1.5 Data refinement and Computer codes

A preliminary knowledge of the crystal structure is important prior to a detailed charge density analysis. Direct methods are commonly used to solve structures in the spherical atom approximation. The most popular code is SHELX from Sheldrick [27] which provides excellent graphical tools for visualization. The refinement of the atom positional parameters and anisotropic temperature factors are carried out by applying the full-matrix least-squares method on a data corrected if found necessary, for absorption and diffuse scattering. Hydrogen atoms are either fixed at idealized positions or located using the difference Fourier technique. SHELX-93 program was used for all structure refinements reported in this thesis.

In the absence of inputs from neutron diffraction, a higher order refinement of X-ray data ($> 0.6 \text{ \AA}^{-1}$) becomes essential to obtain accurate core positions and the associated thermal parameters (the X-X method). In this case, the hydrogen atom positions are often adjusted to the average neutron diffraction values [28] and are held there during the refinement. Often, the rigid bond test [29] is carried out and the parameters are corrected for translation-libration motions of the molecule [30]. In the usual structural analysis, one makes use of an Independent Atom Model (IAM), where the atoms are considered to be non-interacting spheres. However, in order to study the effect of bonding in molecules and materials, it is necessary to work beyond the IAM. One of the most successful approaches to charge density involves the multipolar method. In this method, the electron density in the molecule is segregated in to the electron density of the constituent atoms, which themselves are expressed in terms of multipoles, the dipole and higher

poles reflecting the asphericity of the electron distribution. The expansion or contraction of the electron shell due to the electron transfer between the atoms during bonding is expressed in terms of kappa parameters. Thus, the electron density is obtained in a local coordination system using the Hansen-Coppens formalism [13] as

$$\rho(\mathbf{r}) = \rho_c(r) + P_v \rho_v(\kappa r) + \sum_l R_l(\kappa' r) \sum_{m=-l}^l P_{lm} y_{lm}\left(\frac{\mathbf{r}}{r}\right) \quad \dots(14)$$

Here, ρ_c and ρ_v are the spherically averaged Hartree-Fock core and valence densities with ρ_v normalized to one electron. The Slater type radial functions $R_l = N_l r^n \exp(-\kappa' \xi r)$, modulated by the multipolar spherical harmonic angular functions y_{lm} define the deformation density. The population parameters, P_v and P_{lm} , are floated along with κ and κ' during the refinement. The multipoles on the first row atoms are generally refined up to octapole moments, while for the heavier ones, moments up to hexadecapole are used. Hydrogen atoms are restricted to dipole, although occasionally quadrupole moments are included in the refinement. Kappa values greater than unity indicate contraction while lesser than unity indicate expansion. As the core is not affected by bonding there is no kappa on core, while on the valence shell various types of kappa's namely, spherical, deformation, monopole, dipole, quadrupole, octupole and hexadecapoles are applied. Generally the deformation kappa and the kappa's on higher poles take the same values, though in some rare instances, separate kappa's have been used. As hydrogen has only one electron, the kappa value for hydrogen is quite high (close to being 1.2) compared to other atoms (which are close to 1). The above formalism is well adopted in the recently developed user-friendly program package- XD [31]. Older codes such as MOLLY [13], VALRAY [32], LSEXP [33], POP [34] are also still in use. The quality of a refined model can be monitored based on the residuals and the goodness of fit parameter besides closely inspecting the deformation density maps.

$$R1 = \sum | |F_o| - |F_c| | / \sum |F_o| \quad \dots(15)$$

$$wR2 = [\sum [w(F_o^2 - F_c^2)^2] / \sum [w(F_o^2)^2]^{1/2} \quad \dots(16)$$

$$S = [\Sigma[w(F_o^2 - F_c^2)^2] / (n-p)]^{1/2} \quad \dots(17)$$

where n refers to the number of reflections and p is the total number of parameters refined.

1.6 Dipole moments from experimental charge density

As described in section 1.3, many chemical properties can be obtained from charge density. It is customary to evaluate molecular dipole moments from charge density using the multipole populations or using the direct integration method. In the multipolar method, the population coefficients P^i can be used to estimate the pseudo-atomic charges on the different atoms according to the equation,

$$q_i = n_i - P^i \quad \dots(18)$$

where n_i is the total number of electrons of atom i. The molecular dipole moment is given by,

$$\mathbf{p}_i = \sum_i z_i \mathbf{R}_i + \int_V \mathbf{r} \rho_i(\mathbf{r}_i) d\mathbf{r} \quad \dots(19)$$

where \mathbf{R}_i refers to the nuclear position vector and $\mathbf{r}_i = \mathbf{r} - \mathbf{R}_i$. In the direct integration method, the corresponding equation is,

$$\boldsymbol{\mu} = \int \mathbf{r} \rho(\mathbf{r}) d\mathbf{r} \quad \dots(20)$$

Molecular dipole moment obtained from experimental charge density can be conveniently compared with that obtained using semi-empirical methods like MOPAC [35].

2. SCOPE OF THE THESIS

Cohesion of molecules in crystalline state has been a topic of great interest for both structural and quantum chemists. It is well known that during crystallization, the lattice imposes restrictions on the conformation and symmetry of the molecules and the molecules often distort so as to maximize the intermolecular interactions. It is of considerable importance to understand the symmetries prevailing in a molecular solid in terms of the distortion of the molecules and the nature of intermolecular interactions.

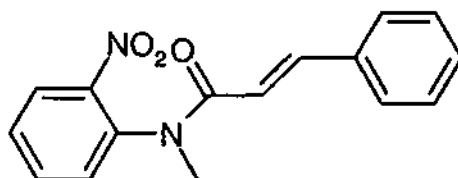
Hydrogen bonding forms an important ingredient for molecular packing in most of the organic crystals. They are of different types - with a wide variety of hydrogen bond donors and acceptors. The N—H...O, N—H...N, N—H...S, O—H...O and C—H...O are some typical examples. These hydrogen bonds in a crystalline lattice form different kinds of repeat units (motifs). Etter [36] has proposed a graph-set notation to denote the various motifs. Each motif could be any of the four types namely C (chain), R (Ring), D (dimer or any other finite set) or S (intramolecular hydrogen bond). The number of donors (d) and the acceptors (a) used in each motif are assigned as subscripts and superscripts respectively, and the size or the degree of the motif (corresponding to the number of atoms in the motif) is indicated in parenthesis.

The hydrogen bond interactions in the intermolecular regions often provide more than one nearly equi-energetic packing possibilities leading to polymorphism in the crystalline state. A slight change in the intermolecular hydrogen bonding can bring about polymorphism in molecular crystals. The difference in free energy between two polymorphs is typically of the order of a few kcal mol⁻¹. The free energies may exhibit different trends with temperature. More importantly, the different polymorphic forms of a molecule may exhibit different reactivities in the solid state. We have carried out structure and charge

density investigations of various molecular crystals to address some of the issues mentioned above, in addition to several other aspects of interest.

2.1 A study of N-methyl-N-(2-nitrophenyl)cinnamanilide

In order to understand how crystal packing induces molecular distortions, we chose to study N-methyl-N-(2-nitrophenyl)cinnamanilide (shown below)



which exhibits a bifurcated hydrogen bonded ring structure in the lattice and is also considerably distorted. In order to examine molecular distortion and bonding in this molecule, we have carried out a high-resolution X-ray diffraction measurement at 130 K and analysed the charge densities in the intramolecular as well intermolecular regions. We have also compared the structure of the molecule in the lattice with that in the free state obtained by geometry optimization.

2.2 Photodimerization of *o*-ethoxy cinnamic acid

The photochemical dimerization in cinnamic acid and its derivatives, first investigated by Cohen *et al.* [37] is a classic in organic solid state chemistry. We chose to study *o*-ethoxy cinnamic acid which exists in three polymorphic forms α , β and γ forms with the α - and the β -forms being photoreactive while the γ -form is photostable. The α -form undergoes photodimerization to give centrosymmetric α -truxilic acid and the β -form gives mirror related β -truxinic acid (Fig.5). We have carried out structure and charge density investigation on the α -form, the γ -form and the photodimer of the α -form. We have analysed the intramolecular bonding regions in terms of the total charge density and the intermolecular hydrogen bond region using the Laplacian description. The molecule is quite planar in the α -form, but in the γ -form, the side groups deviate

Photodimerization in *o*-ethoxy cinnamic acid

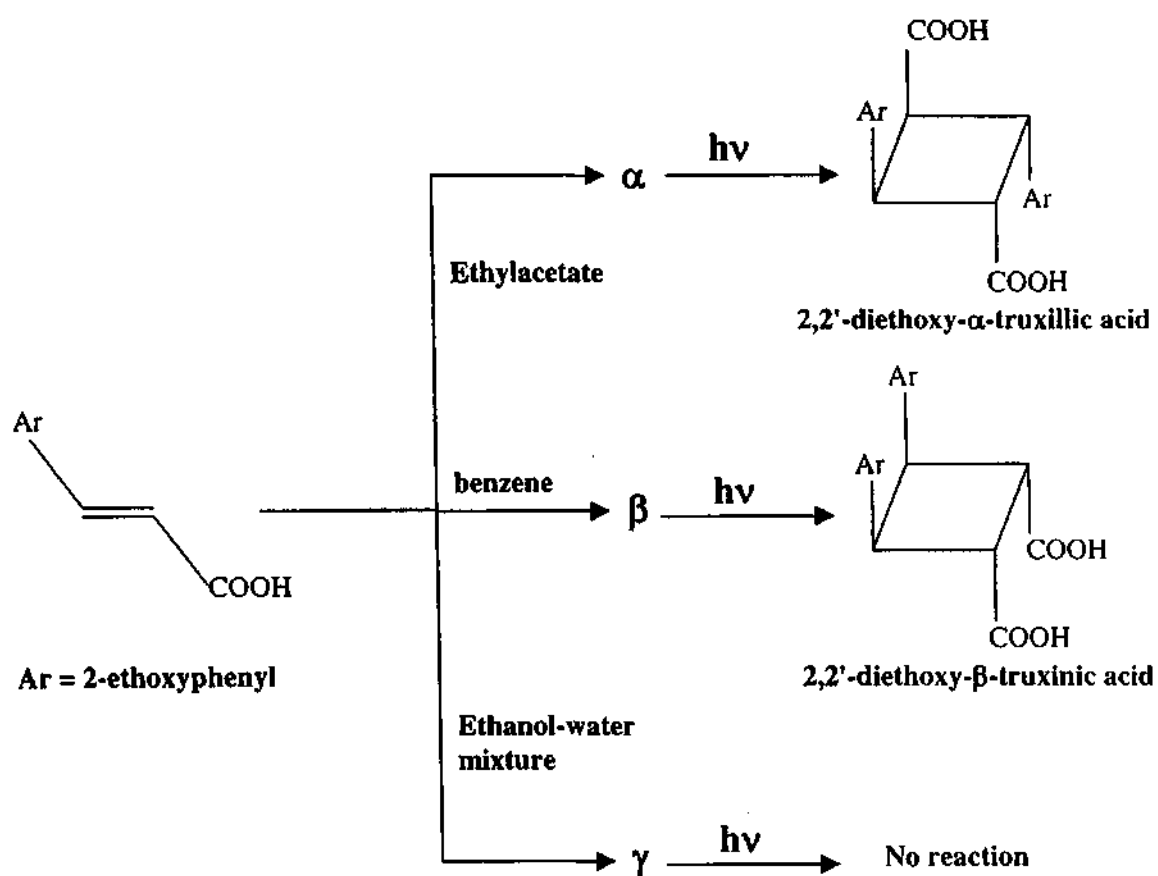


Fig.5. Scheme showing the polymorphism and photoreactivity in *o*-ethoxy cinnamic acid.

significantly from the plane of the benzene ring. The carboxylic groups form normal cyclic hydrogen bonds in the α -form and near-symmetric hydrogen bonds in the γ -form. The nature of the hydrogen bond in the two forms was also confirmed by IR spectroscopy. The charge density analysis has shown that the near-symmetric hydrogen bond in the γ -form is ionic and appears to restrict conjugation by way of distorting the molecule. This unusual feature keeps the cinnamoyl double bonds away from each other, rendering it photochemically unreactive. In the α -form, however, the double bonds have a closer approach. The cyclobutyl ring of the photodimer consists of weak and strained single bonds.

2.3 Photoreaction of *p*-Nitrophenol

p-Nitrophenol is another system whose polymorphic forms exhibit different behavior towards light. The α form undergoes a topochemically controlled photochemical transformation [38], manifesting itself in an irreversible color change of the crystal from yellow to red while the β form is stable towards photoirradiation [Fig.6]. The origin of the color change in the α -form is, however, not clear. We have carried out charge density analysis of the irradiated crystal to examine the effect of photoirradiation on the crystal structure as well as the topography of the charge distribution, using low temperature X-ray diffraction measurements. For the sake of comparison, previous results from this laboratory on the pristine α and the β forms have been used [39]. Our charge density analysis has revealed significant changes in the intra- and intermolecular regions following irradiation, although the crystal and molecular structures showed small variations.

2.4 Properties of aliphatic dicarboxylic acids

Alkanedioic acids are good examples of molecular solids that exhibit polymorphism [40,41]. The first few members of this series except adipic acid

p-nitrophenol

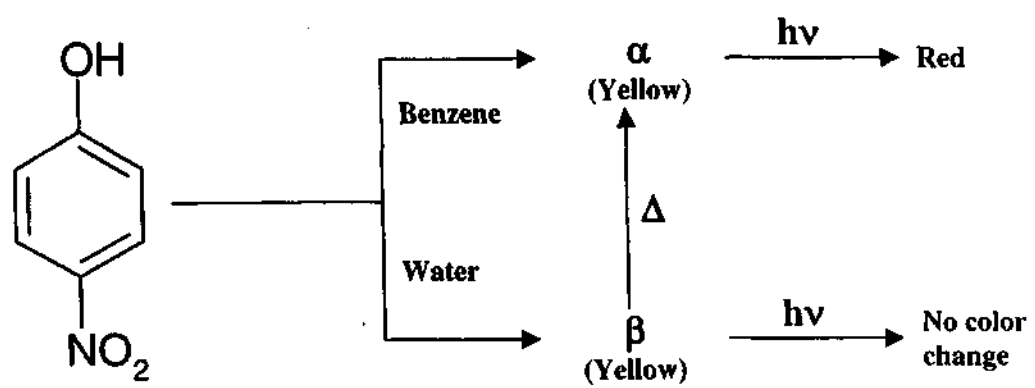
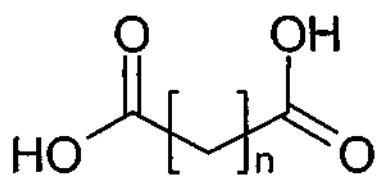


Fig.6. Scheme showing the polymorphism and photoreactivity in *p*-nitrophenol

are known to exist in two forms, α and β , the latter being more stable at room temperature. In the β form other than that of malonic, the molecule possesses an internal symmetry. In the even membered case, there is an inversion centre on the central C—C bond and the molecular backbone is virtually planar. The odd members on the other hand, have a two-fold axis of symmetry through the central carbon atom and the chain is slightly twisted. Malonic acid however, does not possess any element of symmetry and the two carboxylic groups are almost perpendicular to each other. The $\beta \rightarrow \alpha$ transitions for the dicarboxylic acids occur in the temperature range, 340 to 410 K. In the case of odd acids, the two-fold axis of symmetry is lost in the high-temperature phase while the even acids retain their inversion centre. Besides polymorphism, the dicarboxylic acids have been found to exhibit many interesting properties such as alternation in the melting point (Fig.7) with the number of methylene units [42]. As shown in the figure, the even members exhibit higher melting points compared to their odd counterparts. The difference in melting points between the neighbours decreasing as the chain length increases.

The various studies on aliphatic dicarboxylic acids do not reveal discernible structure-property relations in these compounds. Since the properties would be related to subtle variations in cohesion and packing of molecules, we considered that an experimental charge density study would provide useful information on these molecules. For this purpose, we have collected high resolution X-ray diffraction data at low temperature on malonic, succinic, glutaric, adipic and pimelic acids. We have examined the intra- and intermolecular charge distributions in these solids. Such a study was not only expected to throw light on the nature of the dicarboxylic acids but also on the hydrocarbon chain involved in the odd-even effect in such alkane derivatives. The present study has indeed provided some insight into the cohesion of the aliphatic dicarboxylic acids in the solid state and shown certain unusual features of some members of the series.



$n = 1, 2, 3, 4, 5$

Malonic, succinic, glutaric, adipic, pimelic

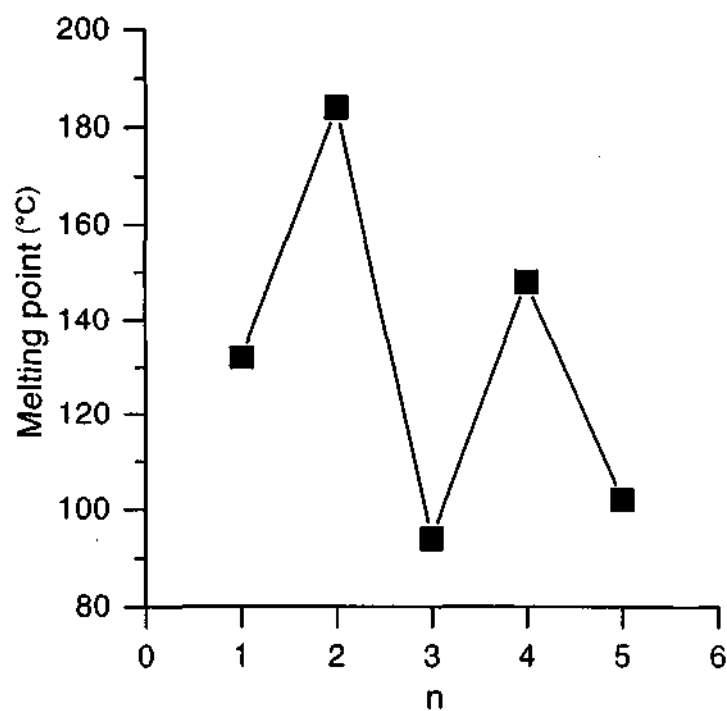
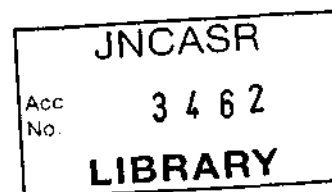


Fig.7. Melting points of the various acids. Here, n denotes the number of methylene groups in the acid. Formula diagram is shown at the top.

548.8
P



2.5 Structural Phase Transition in Adipic acid

While collecting low temperature data on the various dicarboxylic acids, we chanced upon a phase transition in adipic acid at $\sim 136\text{K}$. This transition was previously reported by Ohki *et al.* [43] based on thermal measurements and Raman spectroscopy. The thermal anomaly associated with the transition was found to be small and exhibited a λ -type behavior without hysteresis, indicating the phase transition to be of second or higher order. Raman spectroscopy on powder samples showed the appearance of a weak band below the transition whose intensity increased on further cooling. The authors also reported that single crystal studies were fruitless as the crystals cracked on cooling near the phase transition temperature. We have investigated the structural aspects of the phase transition and have therefore carried out X-ray diffraction measurements on both the high- and the low-temperature phases using the same crystal. Our results have shown that the phase transition is induced due to increased interchain interactions involving carboxylic oxygens and methylene hydrogens. This is one of the very few examples of structural analysis on single crystal-single crystal transformation [44-46] and is indeed the only charge density study of its kind. The results of the study are presented in a separate section (4.5) towards the end of thesis.

2.6 Non-linear Optical Molecular crystals

An excellent example of application of the charge density method in studying molecular properties in the solid state is in the case of organic NLO materials. Nitroaniline and push-pull ethylenes are typical examples of NLO materials involving intramolecular charge transfer. Besides having a polarizable π -cloud with electron-donating and accepting-groups, an essential feature of such compounds is that they crystallize in non-centrosymmetric space groups. A knowledge of intramolecular charge transfer and the associated dipole moments provide definite clues on the polarisation of the molecule, P in an electric field, [47]

$$P = \alpha E + \beta E^2 + \gamma E^3 + \delta E^4 + \dots \quad \dots(21)$$

Charge density studies of 2-methyl-4-nitroaniline [48] and urea [49] show that there is a considerable enhancement of the molecular dipole moment in the solid state. Espinosa *et al.* [50] have reported a charge density study of L-arginine phosphate. Based on a charge density study on N-(4-Nitrophenyl)-L-prolinol, Fkyerat *et al.* [51,52] extracted hyperpolarizability from the octapole moments. While there is some speculation as to whether charge densities can provide hyperpolarizability [53], it is generally accepted that reliable molecular dipole moments can be extracted from charge densities [7]. Thus, Hamazaoui *et al.* [54] have obtained the dipole moment of 3-methyl-4-nitropyridine-N-oxide from charge density which agrees well with that from semi-empirical calculations. Recently, Madsen *et al.* [55] have evaluated the dipole moment of phosphangulene from the charge density to be 42% higher than that measured in a chloroform solution. They also obtained the pyroelectric coefficient by combining the derived dipole moment with temperature-dependent measurements of the unit cell volume.

We have carried out an experimental charge density investigation of organic NLO systems in order to understand the manner in which the non-centric nature of the crystal-field affects the molecular dipole moment and other properties in the solid. For this purpose, we have examined three systems - one where the center of symmetry is destroyed by crystallizing the molecule in a related polymorphic structure and the other where the non-centric nature is introduced by changing the pattern of substitution (Fig.8). The third system provides an example of a molecule where the donor and the acceptor are separated by a large π -system. For the first system, we have chosen the two polymorphic forms of 5-nitrouracil, I, which crystallizes in orthorhombic P2(1)2(1)2(1) and Pbc_a space groups, the former being non-centrosymmetric. The NLO activity of the non-centric form at 1.06 μ m is ~ 160 times that of KDP [56]. In order to explore the effect of substitution, we have studied 1,1-ethylene-

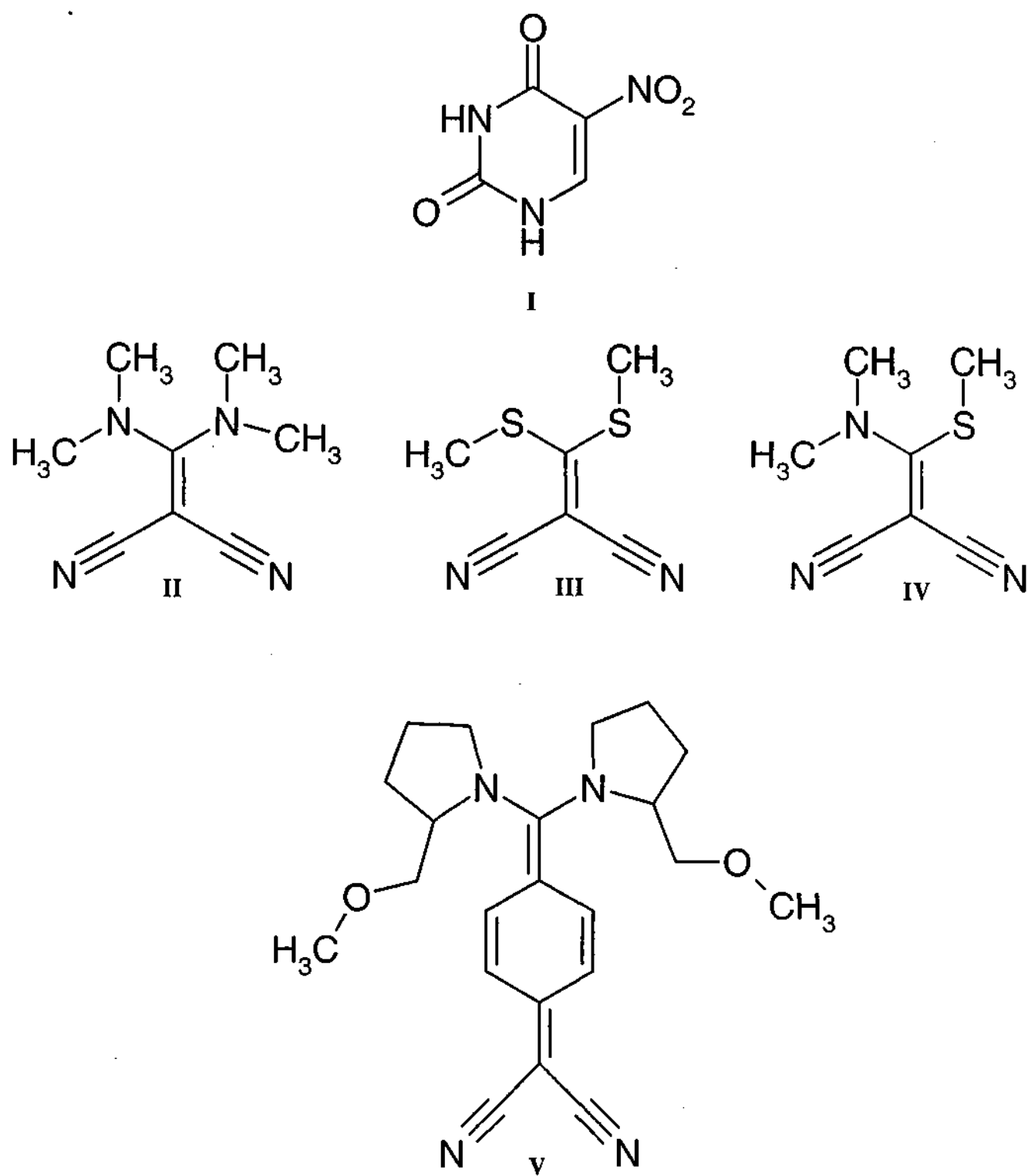


Fig.8. Formula diagrams of 5-nitouracil (I), diamino (II), dithio (III) and the thioamino (IV) derivatives of 1,1-ethylenedicarbonitriles and DMPDQ (V)

dicarbonitriles (abbreviated EDCN) in which the positions of the dimethylamino and methylthio substituents, have been varied to give the symmetric and unsymmetric molecules, bis(N,N-dimethylamino)-EDCN (II); 2,2-bis(methylthio)-EDCN (III) and 2-(N,N-dimethylamino)-2-methylthio-EDCN (IV). The diamino and the dithio derivatives, II and III, crystallize in centric structures while the thioamino, IV, occurs in a non-centrosymmetric structure exhibiting NLO properties.

The molecule, 7,7-di(S(+)-2-(methoxymethyl)pyrrolidino)-8,8-dicyanoquinodimethane (DMPDQ) forms the third system. It crystallises in a non-centric, polar space group, P2(1) with an NLO activity of 55 times that of urea [57]. In all the three systems, we have examined the intramolecular bonding using the Laplacian of the total electron density. Where necessary, we have analyzed the intermolecular interactions in terms of the electrostatic potential. We have computed the dipole moments from the experimental charge densities and compared the results with those from semi-empirical AM1 calculations. Our results show that the experimental dipole moments of the centric structures are generally close to those predicted from the semi-empirical calculations on the frozen or the optimized molecular geometries, but the experimental dipole moments in the non-centric structures are considerably larger.

The results obtained from the investigations of the various materials are presented in section 4, providing adequate information on the structures and charge densities. Details related to the analysis have been given at the end of the thesis as Supplementary information, for the sake of clarity and elegance. Crystallographic information files (CIF) have been deposited in the Cambridge Crystallographic Data Centre.

3. EXPERIMENTAL AND RELATED ASPECTS

3.1 Crystals

The crystals were grown either by the slow evaporation of the solvent as in most cases or by slow cooling from an elevated temperature. Typical growth periods were about one week.

N-methyl-N-(2-nitrophenyl)cinnamanilide: The compound was synthesized dissolving pyridine and *o*-nitroaniline in dichloromethane and adding cinnamoyl chloride in drops to the reaction mixture. Once the reaction was complete, dichloromethane was distilled off and the reaction mixture poured into water. The product was purified by repeated crystallization from a mixture of hexane and dichloromethane [58].

o-Ethoxy cinnamic acid: It was prepared by the Knoevenagel reaction of *o*-ethoxy benzaldehyde and malonic acid in pyridine containing traces of bipyridine [59]. The α -form was obtained by the slow evaporation of a concentrated solution in ethyl acetate while slow cooling of a solution in ethanol-water mixture gave the γ -form. The process of cooling from 75° C to room temperature was carried out over a period of three days. In order to obtain the photodimer, 2,2'-diethoxy α -truxillic acid (trans-2,4-bis(2-ethoxyphenyl) trans-1,3-cyclobutane dicarboxylic acid), crystals of the α -form were irradiated at room temperature using a mercury vapor lamp. After about an hour, the compound was cleaned with copious amounts of ether, when the unreacted parent material went into the solution while the product remained insoluble. This process was carried out a few times in order to remove traces of the parent compound. The photodimer was dissolved in hot glacial acetic acid and filtered before crystallizing it under slow evaporation.

p-nitrophenol: Pale yellow crystals of the α form were grown from the benzene solution and were exposed to indirect sunlight for two weeks when

the color of the crystals changed to deep red. The beta form was obtained by the evaporation of a solution in water.

Aliphatic dicarboxylic acids: All the dicarboxylic acids were obtained commercially (Merck, Germany). Crystals of malonic, succinic, adipic and pimelic acids were grown by the slow evaporation of ethyl acetate solutions, while crystals of glutaric acid were grown from water.

5-Nitrouracil: The compound was obtained commercially (FLUKA). On cooling an aqueous solution of 5-nitrouracil, I (see Fig.8), from 70°C crystals of the centrosymmetric polymorph were obtained. The non-centric crystals were obtained from acetonitrile solution at room temperature.

1,1-Ethylenedicarbonitriles: Reaction between stoichiometric amounts of $\text{Na}_2(\text{S}_2\text{C}_4\text{N}_2) \cdot 3\text{H}_2\text{O}$ and methyl iodide in methanol yielded 2,2-Bis(methylthio)-1,1-ethylenedicarbonitrile (III) [60]. Treating monosodium salt of dicyanomethane with N,N-dimethyl-C-p-chlorophenylsulfonlthio formamide in benzene / dimethylformamide at room temperature gives 2-(N,N-dimethylamino)-2-methylthio-1,1-ethylenedicarbonitrile (IV) [61]. On heating 2,2-Bis(methylthio)-1,1-ethylenedicarbonitrile (III) mildly with dimethylamine in benzene gave 2,2-Bis(N,N-dimethylamino)-1,1-ethylene dicarbonitrile (II) [62]. The crystals of the three compounds (II, III and IV) were grown from toluene, ethyl acetate and benzene solutions respectively.

7,7-di(S(+)-2-(methoxymethyl)pyrrolidino)-8,8-dicyanoquinodimethane:

Tetracyanoquinodimethane (TCNQ, 0.1g, 0.49 mmol) was dissolved in 20 ml of tetrahydrofuran (reshly distilled and dried over sodium). To this solution, 0.18 ml (1.46 mmol) of S(+)-2-(methoxymethyl)-pyrrolidine was added. The solution turned dark green immediately and changed to greenish yellow on heating at 50 °C and stirring for ~2 min. A greenish yellow precipitate appeared slowly. The solution was then cooled to 30 °C and kept for 2h. After further cooling to 5 °C for half an hour, the precipitate was filtered out and washed with cold tetrahydrofuran to give 60% yield of a greenish yellow

compound. Recrystallization from acetonitrile gave pale yellow, transparent, prism-like crystals, melting at 250 °C [57].

A polarizing microscope, LEICA MZ8 was used to examine the crystals. Crystals with dimensions in the range of ~ 0.1 to 0.25 mm were chosen for the investigations. Charge density data was routinely collected at ~ 130K using a low temperature set-up shown in Fig.9. The cold nitrogen gas from the dewar is made to shower on the crystal. The temperature of the stream could be recorded using a Chromel-Alumel (K-type) thermocouple. The temperature of the crystal could be maintained within $\pm 1^\circ$ using the thermocontroller. The temperature (130 K) was chosen such that the consumption of liquid nitrogen was optimal (~ 5 liters/h). In order to circumvent ice formation on the crystal, Cu pips specially designed for the purpose were used. A thin glass fiber at the end of the pip carried the crystal under measurement. With this kind of an arrangement, the data collection could be carried out without any interruption for a period of 2 to 3 days.

3.2 Diffractometer

All data sets have been collected using a SIEMENS 3-circle diffractometer with κ -axis fixed at 54.7° in which the positive and the negative limits for 2θ and $(\omega-2\theta)$ axes are 30 and -85° ; 26 and -208° respectively. The ϕ axis on the other hand could be moved in the whole range of 0 to 360° . A photograph of the diffractometer is shown in Fig.10. The Mo $K\alpha$ radiation generated from a sealed X-ray tube (50 kV, 40 mA) is monochromatised using a graphite monochromator held at 6° . The beam is then passed through a 0.5mm collimator before falling on the crystal. The direct beam from the collimator is stopped using a beam-stop which is placed beyond the crystal. A charge coupled device (CCD) serves as the detector. It has a 1024×1024 pixelated phosphor screen protected by a Be window. At each pixel point on the screen, the X-ray photons are converted to optical photons which are then carried to the CCD chip. The charge built-up is a measure of the diffracted intensity. Before a data collection, dark current

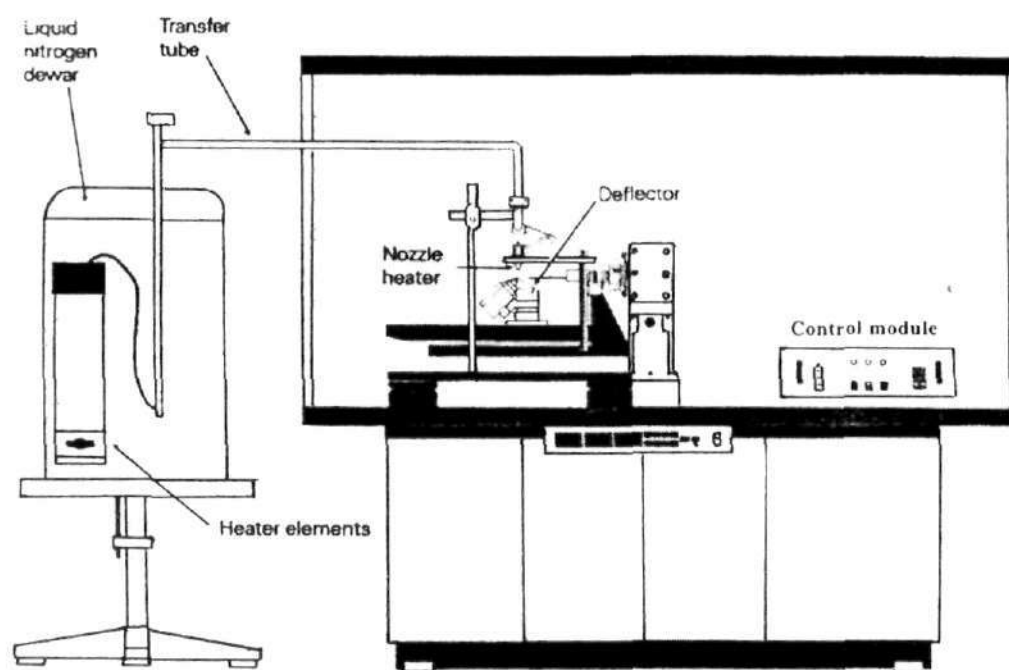


Fig.9. Diagram of the low temperature set-up on the SMART 3-circle goniometer

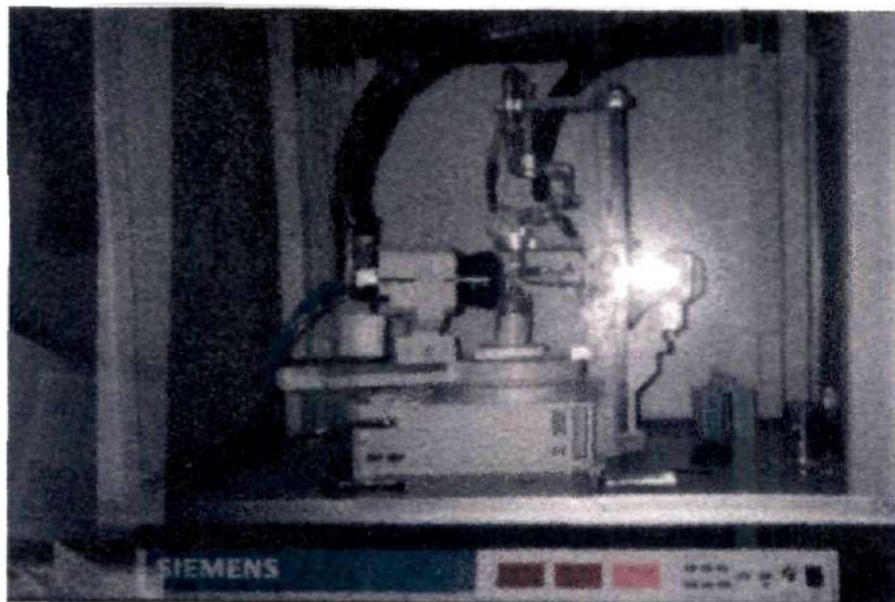


Fig.10. A photograph showing the SMART CCD diffractometer system

measurement is done without opening the shutter in order to estimate background. The dark frames (16 frames) are collected for the same exposure time as the data and are averaged to obtain the background.

The copper pip with a crystal on top, is mounted on the goniometer-head and the sleds on the goniometer head are adjusted to center the crystal with respect to the cross-hairs of the optical microscope attached to the diffractometer. The data collection/reduction is done on a Pentium-DOS machine connected to the diffractometer using the SMART software [63]. Initially, the orientation of crystal with respect to the diffractometer is determined by collecting over a range of $\sim 7^\circ$ in ω in ~ 45 frames, each frame being read for 10 seconds. The width of each frame was 0.3° . By this method, the cell parameters and the orientation of the crystal could be obtained. For extended data, a separate SGI workstation connected to the Pentium PC over the LAN (100 Mbps) is used. In many instances, prior to the data collection, the ASTRO program [63] was involved for the optimal range of θ , ϕ and ω for which the estimated coverage is maximum at a detector distance of 5.0 cm. A room temperature hemisphere data is usually recorded to check the quality of the data at various resolution levels. Depending upon the intensity of diffraction, the data is collected for 20 to 40 seconds per frame. The data reduction is carried out using the SAINT software on the SGI workstation. This computer also houses SHELXTL [64] for structure solution and other programs like PLATON [65]. The structure can be solved with a partial data set when the data collection is still on. This arrangement provided means of monitoring the data during collection the experiment and any problems encountered could be identified and corrected immediately. The crystal is then cooled to 130 K and a hemisphere (for centric crystals) or a full sphere (for non-centric crystals) data were collected both at low and high resolution ($2\theta = 28^\circ, 75^\circ$), the maximum resolution achievable being $\sim 0.45\text{\AA}$. The values of 2θ , ϕ and ω used for the hemisphere and the full sphere data are listed in Table 3 and Table 4 respectively.

Table 3Optimal 2θ , ϕ and ω for hemispherical data at low and high resolutions

Run #	2θ	ω	ϕ	Width	# of frames
0	-28	-26	0	-0.3	606
1	-28	-21	88	-0.3	435
2	-28	-23	180	-0.3	230
3	-75	-73	0	-0.3	606
4	-75	-68	88	-0.3	435
5	-75	-70	180	-0.3	230

Table 4Optimal 2θ , ϕ and ω for full-spherical data at low and high resolutions

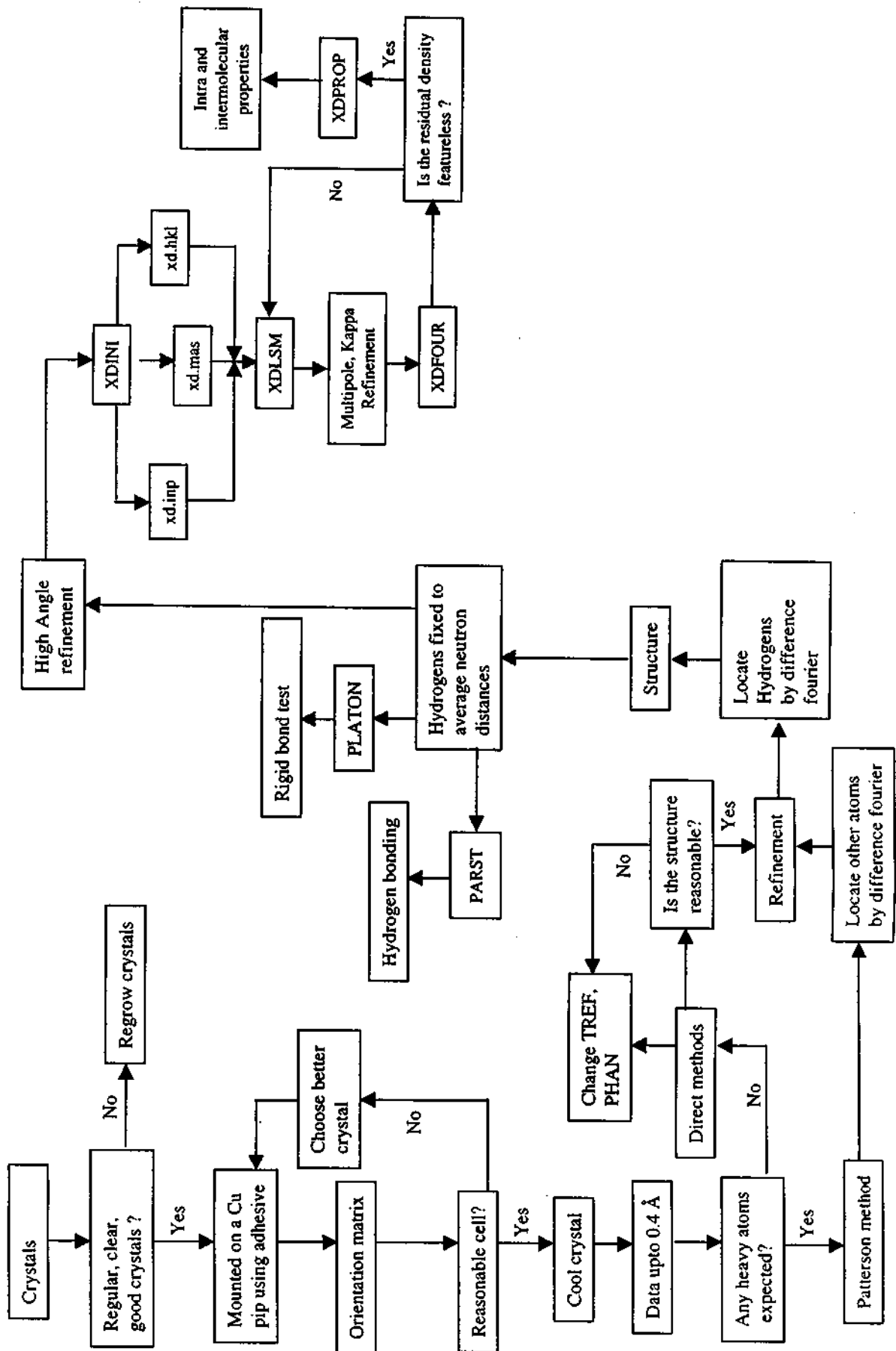
Run #	2θ	ω	ϕ	width	# of frames
0	-28	-26	0	-0.3	636
1	-28	-21	88	-0.3	465
2	-28	-23	180	-0.3	636
3	-28	-26	270	-0.3	465
4	-75	-73	0	-0.3	636
5	-75	-68	88	-0.3	465
6	-75	-70	180	-0.3	636
7	-75	-73	270	-0.3	465

During the data reduction, the original orientation matrix along with the lattice parameters is refined every 40 frames and the orientation matrix and the lattice parameters obtained using the total data is used for structure refinement and charge density.

3.3 Structure and multipole refinement

The total data and the refined matrix is used as input in the program, XPREP. The centric or the non-centric nature of the crystal is determined based on the normalized structure factor, E ; Mean $|E^2 - 1|$ being 0.968 (for centric) and 0.736 for non-centric crystal structures [66]. The exact space group is determined from the systematic absences. The graphic routine XP was used for the visualization purposes. All the structures were solved using direct methods of the XS routine of SHELXTL [64]. The XL routine of SHELXTL [64] was used for the structure refinement over F^2 . In all the cases, the non-hydrogen atoms were first located and refined anisotropically. The hydrogens were located using difference Fourier technique and refined isotropically. In some instances, extinction corrections were needed. In the non-centric cases, the structure determination was additionally guided by the FLACK parameter [67]. The weights, w_1 and w_2 were adjusted in order to obtain the goodness of fit close to unity. A high-order refinement was performed on the structure so obtained, using the high-resolution reflections, $\sin\theta/\lambda > 0.6 \text{ \AA}^{-1}$. During this refinement the hydrogens were moved to average neutron diffraction distances [28] ($C_{sp^2}-H$, 1.075; $C_{Ar}-H$, 1.085; $C_{sp^3}-H$, 1.06; $O-H$, 0.96; $N-H$, 1.01Å). The positional and thermal parameters of hydrogens were kept fixed thereafter. The resultant file of the high-order refinement served as the initial input to the charge density analysis.

The multipolar refinement is done using a full-matrix least squares refinement routine, XDLSM of XD. The flowchart shown below illustrates the various steps involved in the structure and charge density refinements. Additional details of the multipolar refinement are listed below.



1. Coordinates and thermal parameters from high-angle refinement ($\sin\theta/\lambda > 0.6 \text{ \AA}^{-1}$) is taken as the input to charge density analysis.
2. Scaling refinement
3. P_{00} refined.
4. P_{1m} ($l, m > 0$) refined
5. Spherical kappa (κ) refined on all atoms
6. P_{00} refined
7. P_{1m} ($l, m > 0$)
8. Deformation kappa (κ') refined on all non-hydrogen atoms
9. P_{00} refined
10. P_{1m} ($l, m > 0$)
11. Atom positions of non-hydrogen atoms refined
12. P_{00} refined
13. P_{1m} ($l, m > 0$) refined
14. P_{00} and P_{1m} refined

Each step is repeated till the shift/esd values become small. The quality of the refinement is constantly monitored through goodness of fit (S), R1, wR2. For a reliable electron density calculation, caution is exercised to maintain study N_{ref}/N_v greater than 10.

The electronic properties like dipole, electron density, Laplacian etc are calculated using XDPROP [31]. The experimental deformation map is obtained using the calculated multipole phases with the observed structure factors F_o .

$$\delta\rho^{exp}(r) = \frac{1}{V} \sum_h \left[|F_o(h)| e^{i\phi_{mul}} - |F_{sph}(h)| e^{i\phi_{sph}} \right] e^{-2\pi i h \cdot r} \quad \dots(22)$$

$F_{sph}(h)$ is computed with atomic positions and thermal parameters obtained from the multipole refinement. The dynamic model map is obtained from the calculated multipole factors, i.e. the Fourier coefficients are the difference of the two values of F_c

$$\delta\rho^{dyn}(r) = \frac{1}{V} \sum_h \left[|F_{mul}(h)| e^{i\phi_{mul}} - |F_{sph}(h)| e^{i\phi_{sph}} \right] e^{-2\pi i h \cdot r} \quad \dots(23)$$

Since the use of multipole phases makes the maps slightly model dependent; to check that all the significant density features of the experimental data are included in the model, one computes the residual density. This is defined as the difference between the total electron density and that obtained

$$\delta\rho^{res}(r) = \frac{1}{V} \sum_{\mathbf{h}} [|F_0(\mathbf{h})| - |F_{mul}(\mathbf{h})|] e^{i\phi_{mul}} e^{-2\pi\mathbf{h}\cdot\mathbf{r}} \quad \dots(24)$$

by the multipole model and is obtained using the routine XDFOUR and plotted using XDGRAPH [31]. A featureless, flat residual density means a good modeling of the electron density by multipole model. The aspherical atom used in the multipole refinement gives the structure factor phases closer to the true phases in the non-centrosymmetric crystals than does the spherical atom model. Thus it permits mapping of the density by Fourier synthesis in many ways.

4. RESULTS AND DISCUSSION

4.1 Hydrogen bonds in N-methyl-N-(2-nitrophenyl)cinnamanilide

N-methyl-N-(2-nitrophenyl)cinnamanilide exhibits a bifurcated hydrogen bonded ring structure in the lattice and is considerably distorted [58]. The molecule was found to crystallize in a monoclinic cell ($a=10.3397(1)$, $b=10.0008(1)$, $c=13.8310(1)$ Å, $\beta = 107.019(1)^\circ$) with four molecules in the unit cell (Table 5). In Table 6, we list the bond lengths, bond angles and torsion angles. In Fig.11 we show the packing of N-methyl-N-(2-nitrophenyl)cinnamanilide showing the most favorable intermolecular contacts. The most striking feature is that the molecule is twisted at the amide-phenyl (N(11)—C(13)) link with the cinnamide portion being nearly planar (torsion angle C(2)—C(1)—C(7)—C(8), -6.24°). The nitrobenzene ring is highly non-planar, the nitro group being rotated with respect to phenyl ring by 43.5° . The nitrobenzene group as whole is twisted away from the mean cinnamide plane making an angle of 63.3° . From the Fig.11, we see that each molecule forms bifurcated C—H...O hydrogen bonds [68] with the amidic oxygen of the centrosymmetric partner. The contacts from H(6) and H(7) are at 2.369 and 2.440 Å with C—H...O angle of 149.3° and 152.7° respectively (Table 7). The angle of bifurcation is $\sim 60.4^\circ$. These hydrogen bonds are of $R_1^2(6)$ type [36] and the two pairs are related by a center of inversion. As expected of a bifurcated hydrogen bond, the ring hydrogen bonds, the amidic oxygen forms hydrogen contact of D(2) type with phenyl hydrogens, H(16) and H(17). The latter contact appears to be more favourable (2.331 Å, 153.7°). Besides those from the amidic oxygen, there exist C—H...O contacts atoms H(6), H(7), O(10A) and C(9A) are coplanar [69] within 0.0161 Å. In addition to from the nitro-oxygens as well (see Table 7). It may be noted that the intermolecular bonding in this crystal is only through C—H...O contacts.

Charge density distribution

We now discuss the charge density analysis of both the intra- and intermolecular regions. In Fig.12, we show the deformation map of the molecule in

Table 5
Crystal data and experimental details

Crystal	Cinnamanilide
Chemical formula	$C_{16}H_{14}N_2O_3$
Formula weight (g)	282.29
Cell System	Monoclinic
Space group	P2(1)/n
a (Å)	10.3397(1)
b (Å)	10.0008(1)
c (Å)	13.8310(1)
β (°)	107.019(1)
V (Å ³)	1367.6(4)
Z	4
ρ (Mg m ⁻³)	1.371
Radiation type	Mo K α
Wave length (Å)	0.71073
No. of reflections for cell parameters	60
μ (mm ⁻¹)	0.1
Crystal form	Cuboidal
Crystal size (mm)	0.45 x 0.3 x 0.5
Crystal color	Colorless
Data collection temperature	130 K
Diffractometer	Siemens CCD
Crystal-detector distance (cm)	5.0
No. of measured reflections	22993
No. of independent reflections	11258
No. of observed reflections	7936
R_{merge}	0.0369
R_{int}	0.0298
θ_{max} (°)	49.43
Range of h, k, l	
	-19 ≤ h ≤ 21
	-20 ≤ k ≤ 19
	-29 ≤ l ≤ 29
Refinement	
R1	0.0464
wR2	0.0668
S	1.0876
No of variables	393
N_{ref}/N_v	36.1

Table 6
Bond lengths, bond angles and torsion angles involving non-hydrogen atoms from X-ray crystallography and AM1 calculation

Bond Length (Å)	X-ray	AM1
C(1)-C(2)	1.414(2)	1.4029
C(1)-C(6)	1.407(1)	1.4044
C(1)-C(7)	1.482(1)	1.4536
C(2)-C(3)	1.407(1)	1.394
C(3)-C(4)	1.402(2)	1.3945
C(4)-C(5)	1.397(2)	1.3932
C(5)-C(6)	1.412(2)	1.3969
C(7)-C(8)	1.354(1)	1.3413
C(8)-C(9)	1.497(1)	1.4837
C(9)-O(10)	1.241(2)	1.2455
C(9)-N(11)	1.373(1)	1.404
N(11)-C(12)	1.466(2)	1.4398
N(11)-C(13)	1.445(1)	1.4218
C(13)-C(14)	1.406(1)	1.4125
C(13)-C(18)	1.394(1)	1.4182
C(14)-C(15)	1.412(2)	1.3894
C(15)-C(16)	1.390(2)	1.3961
C(16)-C(17)	1.407(2)	1.389
C(17)-C(18)	1.408(2)	1.4069
C(18)-N(19)	1.479(1)	1.4899
N(19)-O(20)	1.243(2)	1.2022
N(19)-O(21)	1.225(2)	1.2012

Bond angle (°)	X-ray	AM1
C(6)-C(1)-C(7)	119.14(9)	118.85
C(2)-C(1)-C(7)	122.79(8)	122.04
C(2)-C(1)-C(6)	118.03(9)	119.1
C(1)-C(2)-C(3)	120.79(9)	120.39
C(2)-C(3)-C(4)	120.5(1)	120.23
C(3)-C(4)-C(5)	119.3(1)	119.82
C(4)-C(5)-C(6)	120.4(1)	120.29
C(1)-C(6)-C(5)	121.0(1)	120.17
C(1)-C(7)-C(8)	125.8(1)	124.83
C(7)-C(8)-C(9)	119.8(1)	120.35
C(8)-C(9)-N(11)	118.8(1)	118.16
C(8)-C(9)-O(10)	121.8(1)	121.99
O(10)-C(9)-N(11)	119.4(1)	119.79
C(9)-N(11)-C(13)	117.7(1)	119.24
C(9)-N(11)-C(12)	127.0(1)	122.44
C(12)-N(11)-C(13)	115.3(1)	115.77
N(11)-C(13)-C(18)	122.5(1)	123.3
N(11)-C(13)-C(14)	120.3(1)	118.94
C(14)-C(13)-C(18)	117.2(1)	117.75
C(13)-C(14)-C(15)	121.7(1)	121.02
C(14)-C(15)-C(16)	120.0(1)	120.48
C(15)-C(16)-C(17)	119.3(1)	120.05

C(16)-C(17)-C(18)	119.7(1)	119.91
C(13)-C(18)-C(17)	122.0(1)	120.77
C(17)-C(18)-N(19)	118.3(1)	117.54
C(13)-C(18)-N(19)	119.7(1)	121.69
C(18)-N(19)-O(21)	117.1(1)	118.41
C(18)-N(19)-O(20)	118.8(1)	119.78
O(20)-N(19)-O(21)	124.1(1)	121.75

Torsion Angle (°)	X-ray	AM1
C(6)-C(1)-C(7)-C(8)	171.9(1)	160.92
C(2)-C(1)-C(7)-C(8)	-6.2(2)	-19.69
C(7)-C(1)-C(6)-C(5)	-176.9(1)	-179.85
C(2)-C(1)-C(6)-C(5)	1.3(2)	0.74
C(6)-C(1)-C(2)-C(3)	-0.2(2)	-0.34
C(7)-C(1)-C(2)-C(3)	177.9(1)	-179.72
C(1)-C(2)-C(3)-C(4)	-0.9(2)	-0.14
C(2)-C(3)-C(4)-C(5)	0.9(2)	0.22
C(3)-C(4)-C(5)-C(6)	0.2(2)	0.19
C(4)-C(5)-C(6)-C(1)	-1.3(2)	-0.67
C(1)-C(7)-C(8)-C(9)	-176.4(1)	178.64
C(7)-C(8)-C(9)-O(10)	2.9(2)	-42.31
C(7)-C(8)-C(9)-N(11)	-177.4(1)	140.58
C(8)-C(9)-N(11)-C(12)	-3.8(2)	-22.39
C(8)-C(9)-N(11)-C(13)	179.2(1)	176.46
O(10)-C(9)-N(11)-C(12)	175.9(1)	160.43
O(10)-C(9)-N(11)-C(13)	-1.0(1)	-0.72
C(9)-N(11)-C(13)-C(14)	-111.2(1)	-111.42
C(9)-N(11)-C(13)-C(18)	68.4(1)	67.74
C(12)-N(11)-C(13)-C(14)	71.5(1)	86.21
C(12)-N(11)-C(13)-C(18)	-109.0(1)	-94.63
N(11)-C(13)-C(18)-N(19)	0.6(1)	2.18
N(11)-C(13)-C(18)-C(17)	-179.5(1)	-177.34
N(11)-C(13)-C(14)-C(15)	-178.1(1)	178.51
C(14)-C(13)-C(18)-N(19)	-179.8(1)	-178.64
C(14)-C(13)-C(18)-C(17)	0.1(2)	1.83
C(18)-C(13)-C(14)-C(15)	2.3(2)	-0.71
C(13)-C(14)-C(15)-C(16)	-2.1(2)	-0.45
C(14)-C(15)-C(16)-C(17)	-0.5(2)	0.51
C(15)-C(16)-C(17)-C(18)	2.8(2)	0.62
C(16)-C(17)-C(18)-C(13)	-2.7(2)	-1.81
C(16)-C(17)-C(18)-N(19)	177.3(1)	178.65
C(17)-C(18)-N(19)-O(20)	-136.5(1)	-145.31
C(13)-C(18)-N(19)-O(20)	43.5(2)	35.15
C(17)-C(18)-N(19)-O(21)	42.2(2)	31.89
C(13)-C(18)-N(19)-O(21)	-137.8(1)	-147.65

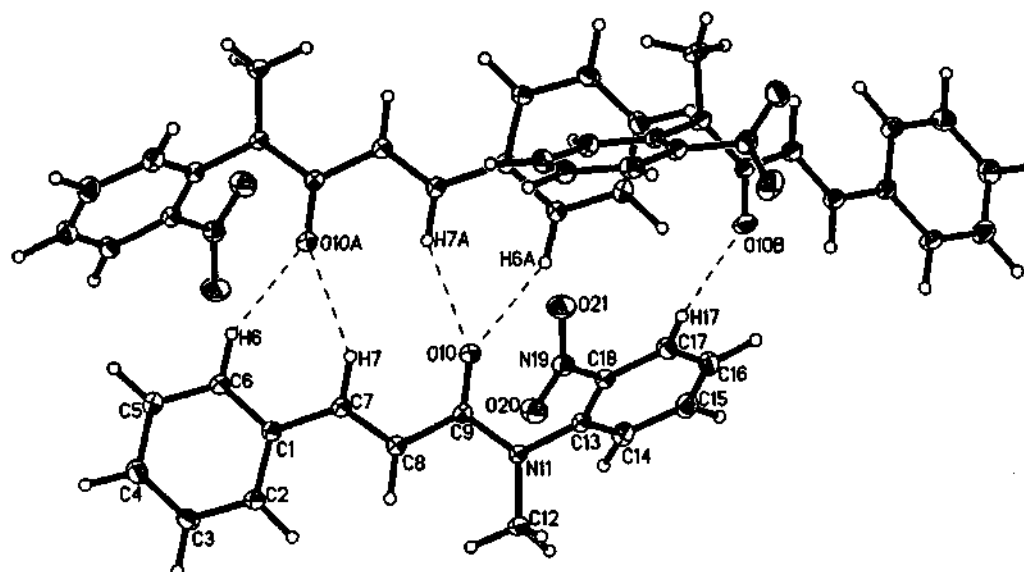
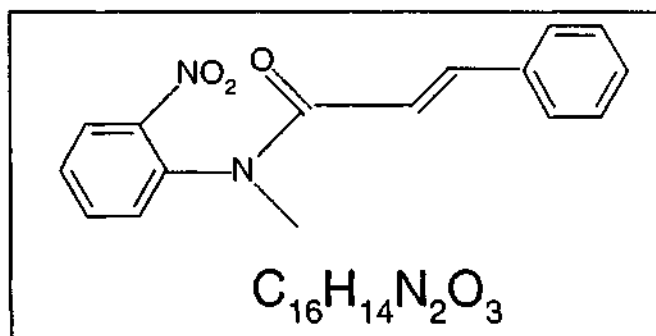


Fig.11. Intermolecular hydrogen bonds in N-methyl-N-(2-nitrophenyl)cinnamanilide. All non-hydrogen atoms are shown at 50% probability ellipsoids. Formula diagram is shown in the inset on the top.

Table 7
Intermolecular Hydrogen Bond contacts

D—H...A	Bond type	H...A (Å)	D...A (Å)	∠D—H...A (°)
C(6)—H(6)...O(10) ^a	R ₁ ² (6)	2.369(1)	3.362(1)	152.7(1)
C(7)—H(7)...O(10) ^a	R ₁ ² (6)	2.440(1)	3.410(1)	149.3(1)
C(17)—H(17)...O(10) ^b	D(2)	2.331(2)	3.330(1)	153.7(1)
C(16)—H(16)...O(10) ^c	D(2)	2.896(1)	3.741(1)	135.5(1)
C(4)—H(4)...O(20) ^d	D(2)	2.695(1)	3.606(1)	142.2(1)
C(2)—H(2)...O(20) ^e	R ₁ ² (7)	2.598(1)	3.622(1)	166.3(1)
C(8)—H(8)...O(20) ^e	R ₁ ² (7)	2.758(1)	3.785(1)	159.4(1)
C(12)—H(12C)...O(20) ^e	R ₁ ² (7)	2.723(1)	3.692(1)	151.9(1)
C(15)—H(15)...O(21) ^e	R ₁ ² (5)	2.802(1)	3.529(1)	124.9(1)
C(16)—H(16)...O(21) ^e	R ₁ ² (5)	2.916(1)	3.579(1)	120.1(1)

Symmetry: a) -x, 1-y, -z; b) 1/2-x, 1/2+y, 1/2-z; c) 1/2+x, 3/2-y, 1/2+z; d) -1-x, 1-y, -z; e) -1/2-x, -1/2+y, 1/2-z;

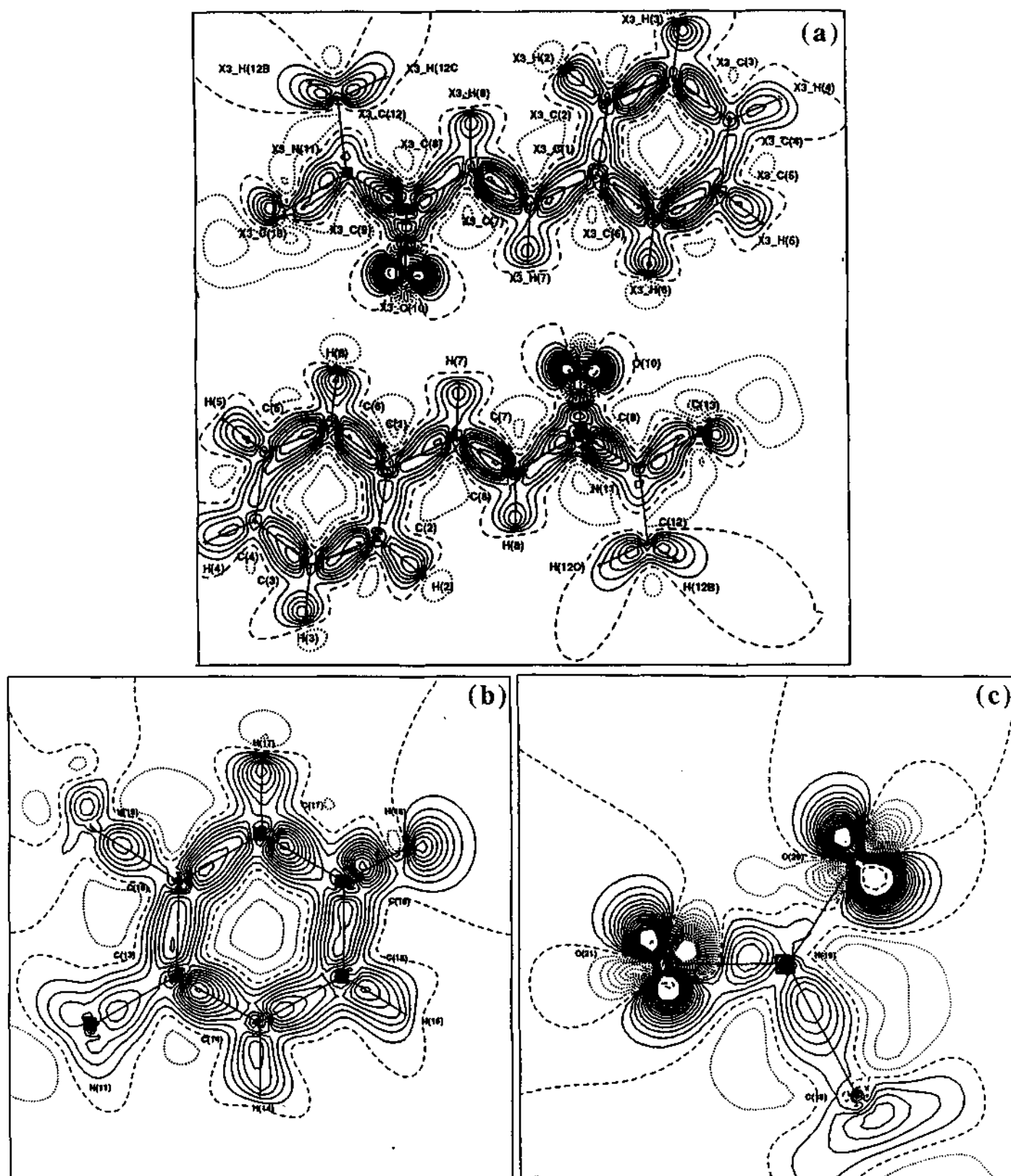


Fig.12. Deformation density map of N-methyl-N-(2-nitrophenyl)cinnamanilide in the mean plane of a) bifurcated hydrogen bond; b) nitrobenzene and c) nitro group. Contour intervals at 0.1 eÅ⁻³.

three parts (a, b and c) since it is highly non-planar. Concentric contours typify the various bonding regions in the molecules between the atom-cores. The charge density distribution is as expected in the various regions of the molecule (Table 8). However, a few points are noteworthy. The topography of the deformation density in the C(7)=C(8) region is distinctly different from those of the neighboring single bonds (Fig.12a). Accordingly, the charge density at the CP is typical of an isolated double bond ($\rho = 2.349 \text{ e}\text{\AA}^{-3}$, $\nabla^2\rho = -21.24 \text{ e}\text{\AA}^{-5}$, $\epsilon=0.23$). The other region of interest is that of the amide group (Fig.12a). The methyl (C(12)—N(11)) and the amidic link (C(9)—N(11)) exhibit widely differing densities (1.49 and $2.45 \text{ e}\text{\AA}^{-3}$ respectively) though both are C—N bonds. Theoretical estimation [16] of bonding density of a C—N bond is $1.86 \text{ e}\text{\AA}^{-3}$. Thus, it appears as though the density has migrated from the methyl link to the amidic region. The density in the C(9)=O(10) bond is also somewhat high, $2.56 \text{ e}\text{\AA}^{-3}$. In Fig.12c, we find that there is very little deformation density in the N—O bonds, which is due to ionic interactions. The topology of the Laplacian field allows one to realize the chemical model of localized bonded and non-bonded pairs (lone-pairs) and to characterize local concentrations ($\nabla^2\rho < 0$) and depletions ($\nabla^2\rho > 0$) in molecular charge distribution [70,71]. Figure 13 shows the contour maps of the Laplacian of the total density in the plane defined by nitro group. The lone pairs on the oxygens (3, +3) critical points. The N-O bonds exhibit as disjoint lobes indicating ionic nature of these bonds, unlike the N-C bonds which shows shared interaction. The large negative charges on the nitro oxygens (O(20), -0.30 e ; O(21), -0.1 e) compared to the amide oxygen (-0.06 e) also reflects the ionic nature of the nitro bonds. The lone-pair electrons around the amidic oxygen, O(10) (Fig.12a) and the nitro-oxygens (Fig.12c) are clearly visible as two sets of concentric contours around each nucleus. In Laplacian, they were found to occur as (3, +3) CPs exhibiting high Laplacians $\sim -220 \text{ e}\text{\AA}^{-5}$. The distance of the CP from the nucleus is ~ 0.31 and 0.38 \AA in the case of O(10) and nitro-oxygens respectively. A contour map of the Laplacian shown in Fig.14a, reveals that the lone-pair density around O(10) is slightly polarized towards H(6) and H(7), of the bifurcated hydrogen bonding region as does the lone pair of the nitro oxygen (Fig.14b). This is also evident from the deformation density map in Fig.12a where the contours of the lone-pair are seen oriented towards the hydrogens. The nature of the intermolecular bonding is best described in terms of the electrostatic potential. In

Table 8
Analysis of the bond critical points

Bond	ρ ($e\text{\AA}^{-3}$)	$\nabla^2\rho$ ($e\text{\AA}^{-5}$)	ϵ
C(1)—C(2)	1.83(2)	-12.40(5)	0.12
C(2)—C(3)	2.08(2)	-15.01(5)	0.28
C(3)—C(4)	2.10(2)	-16.07(6)	0.19
C(4)—C(5)	1.91(3)	-11.64(6)	0.22
C(5)—C(6)	2.15(2)	-18.43(5)	0.11
C(1)—C(6)	2.11(2)	-17.88(5)	0.24
C(2)—H(2)	1.82(5)	-18.0(1)	0.09
C(3)—H(3)	1.59(4)	-10.7(1)	0.07
C(4)—H(4)	1.77(5)	-15.8(2)	0.03
C(5)—H(5)	1.76(6)	-19.6(3)	0.06
C(6)—H(6)	1.74(5)	-16.3(1)	0.09
C(1)—C(7)	1.81(2)	-12.26(4)	0.19
C(7)—C(8)	2.35(2)	-21.24(6)	0.23
C(8)—C(9)	1.72(2)	-9.71(4)	0.3
O(10)—C(9)	2.56(6)	-13.2(1)	0.05
N(11)—C(9)	2.45(2)	-17.42(6)	0.21
N(11)—C(12)	1.49(3)	-2.03(7)	0.17
N(11)—C(13)	1.92(3)	-10.56(7)	0.08
C(7)—H(7)	1.67(4)	-13.1(1)	0.04
C(8)—H(8)	1.61(5)	-11.8(1)	0.02
C(12)—H(12A)	1.71(5)	-11.3(1)	0.31
C(12)—H(12B)	1.69(6)	-12.3(2)	0.19
C(12)—H(12C)	1.61(6)	-13.1(3)	0.14
C(13)—C(14)	2.11(3)	-18.03(8)	0.13
C(14)—C(15)	2.07(3)	-15.82(6)	0.15
C(15)—C(16)	2.21(3)	-17.92(6)	0.12
C(16)—C(17)	2.02(3)	-15.37(9)	0.11
C(17)—C(18)	2.20(2)	-19.82(6)	0.14
C(13)—C(18)	2.17(2)	-19.06(6)	0.15
C(14)—H(14)	1.79(6)	-18.2(2)	0.05
C(15)—H(15)	1.77(6)	-17.1(3)	0.05
C(16)—H(16)	1.31(6)	3.7(3)	0.64
C(17)—H(17)	1.85(5)	-18.8(1)	0.06
N(19)—C(18)	1.71(3)	-10.13(8)	0.17
O(20)—N(19)	2.85(9)	5.2(1)	0.14
O(21)—N(19)	3.3(1)	-6.7(2)	0.2

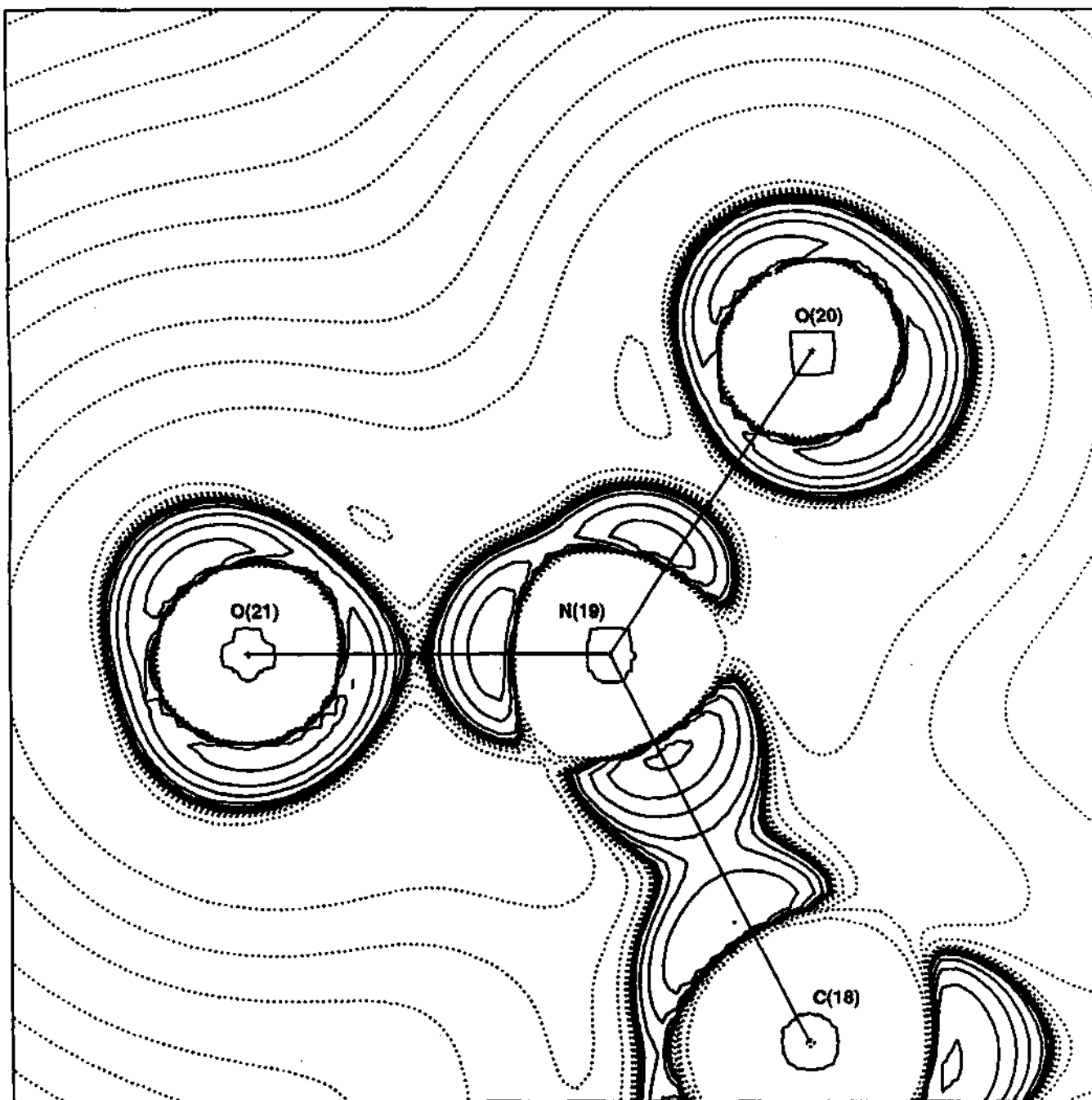


Fig.13. Contour map of Laplacian of the total electron density in the plane of the nitro group.

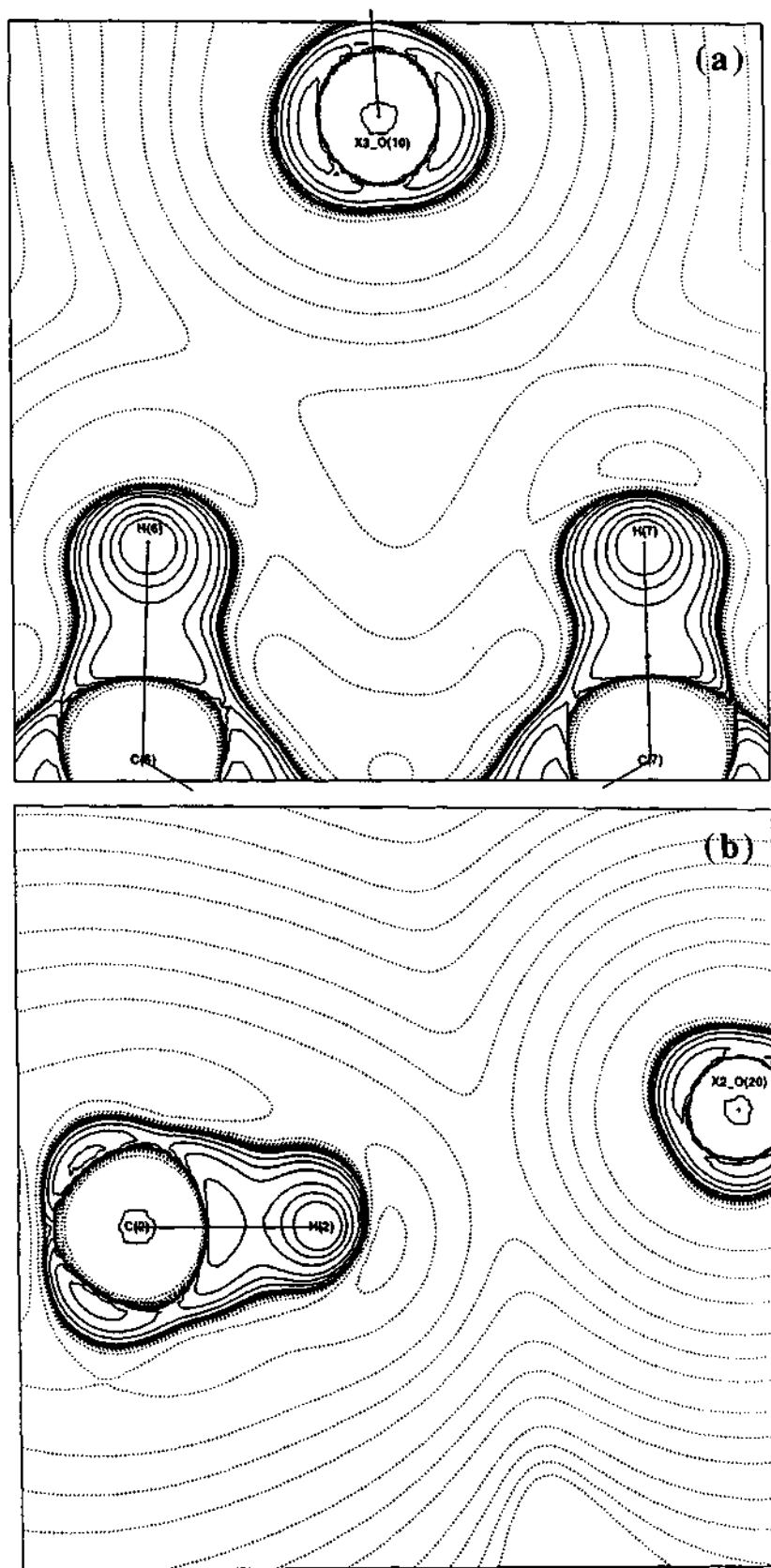


Fig.14. Contour map of Laplacian of the total electron density in the plane formed by a) H(6), H(7) and X3_O(10); b) C(2), H(2) and X2_O(20) atoms.

Fig.15, we show contour maps of the electrostatic potential in the hydrogen bond regions of the amido and the nitro oxygens. As shown in the figures, the contours originating from the C-H region overlap with those from the amido and nitro oxygens. In the former case, the penetration is significant indicating that these are strong contacts [19]. They are associated with (3, -1) critical points in ρ as well as in the electrostatic potential. They carry a small density of $-0.05 \text{ e}\text{\AA}^{-3}$ and small positive Laplacians, $\sim 0.8 \text{ e}\text{\AA}^{-5}$, typical of closed shell interactions [6]. The hydrogen bonding between the phenyl hydrogen H(17) and the amidic oxygen O(10) forms the next strongest hydrogen bond with a density of $0.047 \text{ e}\text{\AA}^{-3}$ and a Laplacian of $0.877 \text{ e}\text{\AA}^{-5}$. The Laplacian at the CPs are small and positive as is generally found in hydrogen bonds [6].

In the latter case of nitro oxygen however, the penetration of the electrostatic potential is relatively small indicating weaker interactions (see Fig.15b). The strength of these interactions are also reflected in their densities and Laplacians. We find ρ_{mean} of $0.034 \text{ e}\text{\AA}^{-3}$ and $\nabla^2\rho$ of $0.526 \text{ e}\text{\AA}^{-5}$. The trends associated with the various hydrogen bonds are better understood by plotting $\nabla^2\rho$ vs. ρ [70] as shown in Fig.16. We could clearly mark two regions of interactions as shown – one region where the hydrogen bonds exhibit low values for both the density and the Laplacian and the other, where both quantities are disproportionately higher. What is interesting is that all the bonds involving the nitro-oxygens belong to the first region and those from the amidic oxygen fill the second region. Clearly, the amidic oxygen forms stronger hydrogen bonds compared to the more ionic nitro-oxygens. This appears to govern the molecular geometry and packing in the solid state.

Molecule in the crystal versus a free molecule

The molecular structure in the lattice as discussed above, was compared with that of a “free” molecule, shown in Fig.17b. The latter was obtained using a semi-empirical calculation (AM1, PRECISE) after optimizing bond lengths, angles and torsion angles using MOPAC [35]. The experimental coordinates served as the initial input. SCF was achieved and the heat of formation and the dipole moment of the molecule so obtained are $49.73 \text{ kcalmol}^{-1}$ and 5.215 D respectively. An important finding from the calculation is that the benzene rings are parallel within 8° while the

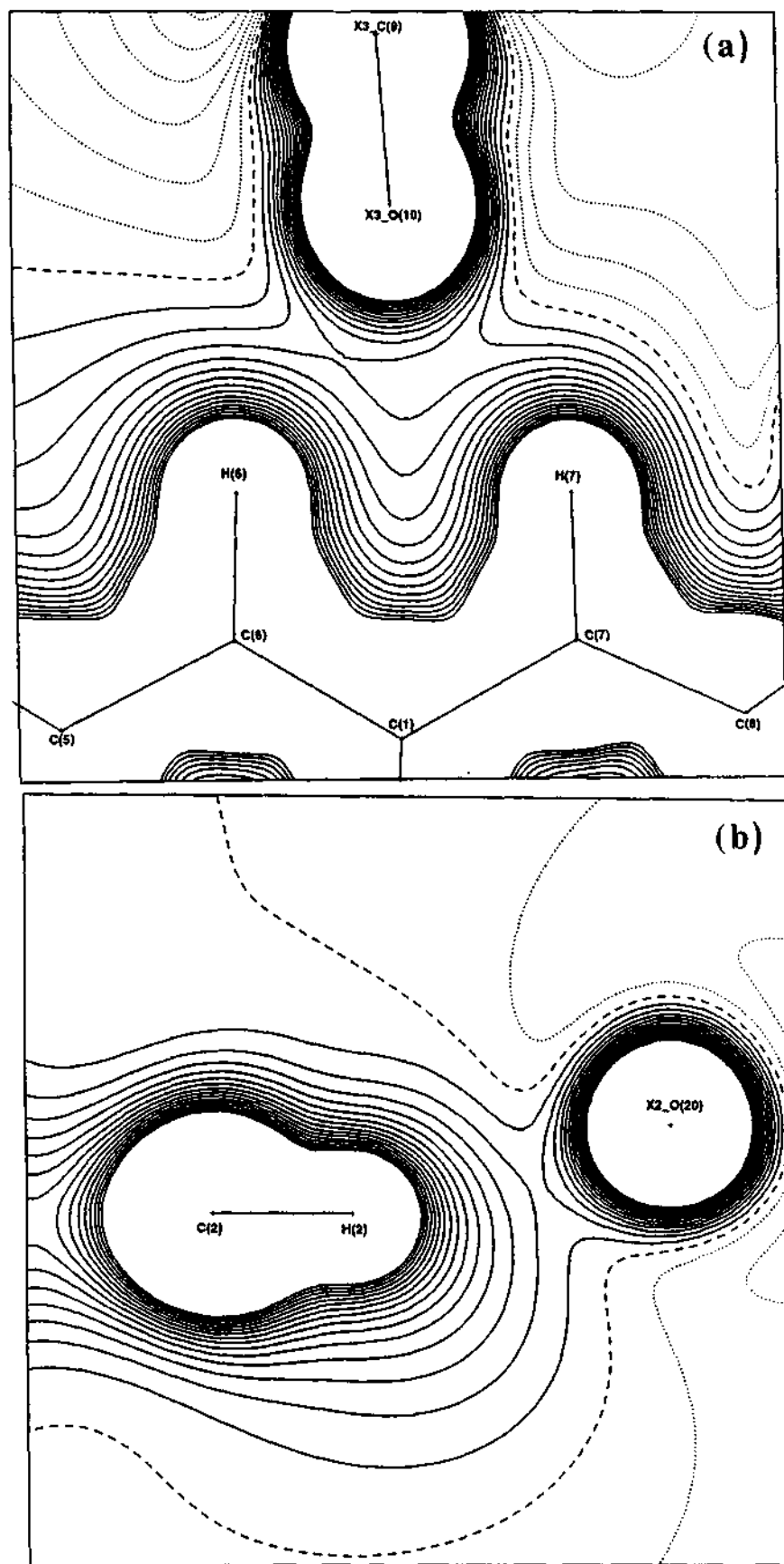


Fig.15. Electrostatic Map in the plane formed by a) H(6), H(7) and X3_O(10); b) C(2), H(2) and X2_O(20) atoms. Contours at $0.05 \text{ e}\text{\AA}^{-1}$.

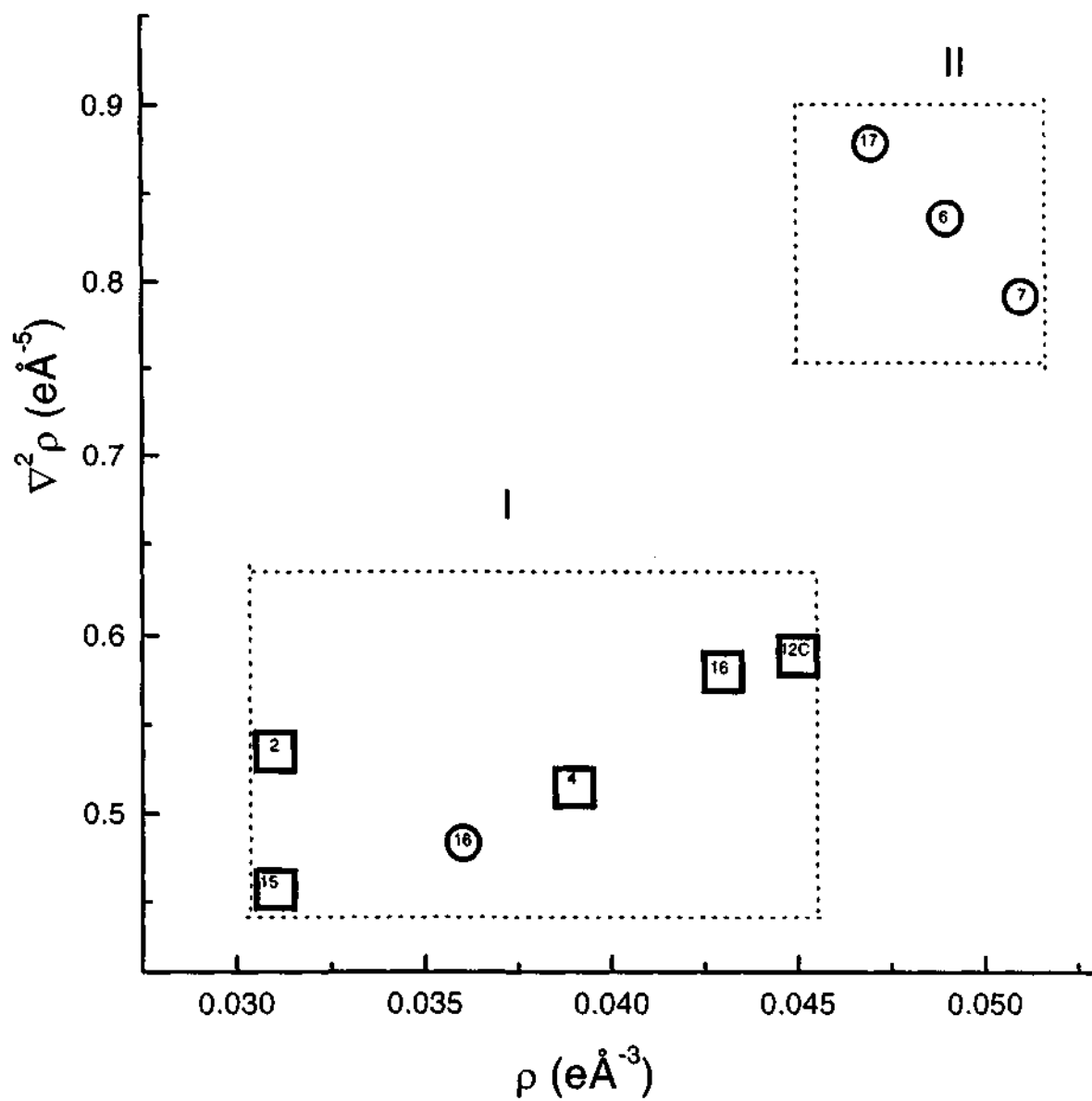


Fig.16. Variation of $\nabla^2\rho_{CP}$ with ρ_{CP} for various hydrogen bonds, $O_{\text{amido}}\cdots H$, circles; $O_{\text{nitro}}\cdots H$, squares. The numbers inside the symbols refer to the hydrogens involved in bonding. Regions I and II emphasise different trends in the plot.

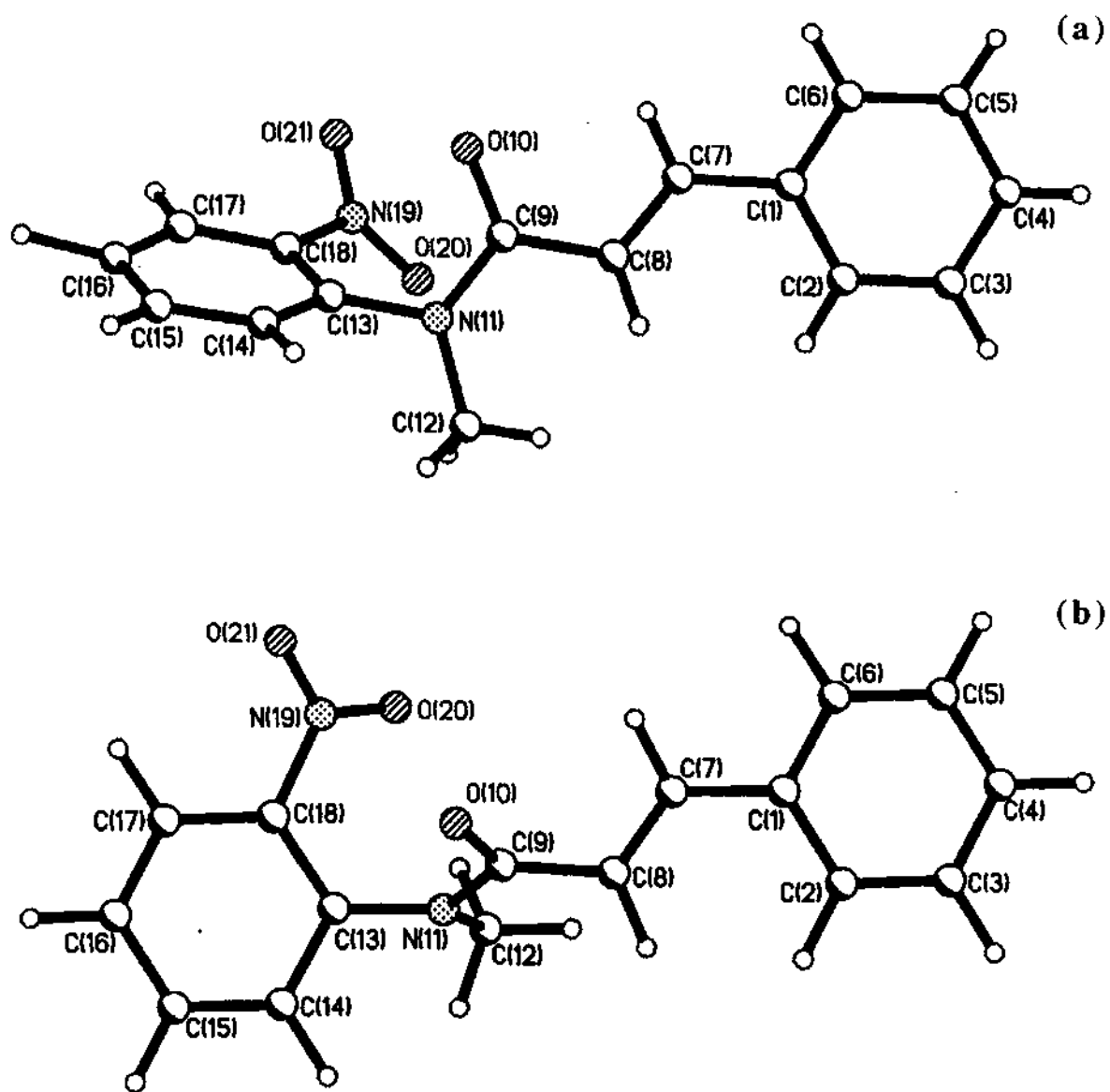


Fig.17. Molecular structure of N-methyl-N-(2-nitrophenyl)cinnamanilide from (a) X-ray crystallography and (b) AM1 calculation.

intervening bonds are buckled with torsion angles from C(2)—C(1)—C(7)—C(8) through C(8)—C(9)—N(11)—C(13) being -19.69° , 178.64° , 140.58° and 176.46° respectively as compared to -6.24° , -176.36° , -177.31° and 179.24° in solid state (Table 6). The O(10)—C(9)—N(11)—C(12) torsion angle is 160.83° as compared to 175.95° found in solid state. However, the bond lengths and angles are quite similar in the two cases (see Table 6). Thus, our calculation provides a reference state of the molecule using which constraints imposed by packing in a lattice could be examined.

Conclusions

We have drawn the following conclusions from the above charge density study.

- 1) N-methyl-N-(2-nitrophenyl)cinnamanilide crystallizes in P2(1)/n and exhibits centrosymmetrically related $R_1^2(6)$ hydrogen bond ring structure in the intermolecular region.
- 2) The amidic oxygen appears to be the active center for hydrogen bonding with both ρ and $\nabla^2\rho$ being higher as compared to those involving nitro-oxygens. Our study has shown that hydrogen bond interactions from the amidic oxygen are stronger compared to those from nitro-oxygens leading to the distortion of the molecule relative to the free state.
- 3) It is as though to favor bifurcated hydrogen bonding from the amidic oxygen, the molecule is highly twisted at the amide-nitrobenzene link. Semi-empirical calculations show that in the "free" molecule, the two phenyl rings are coplanar within 8° while the intervening groups are buckled out of plane.

The above investigation strengthens the general notion that hydrogen bonding involving strong donors and acceptors dictate the molecular structure in a given lattice. The less acidic protons such as those in acetylenes, aldehydes or activated aromatic and aliphatic compounds influence the molecular geometry to a lesser extent and participate in hydrogen bonding if a packing is found favorable.

4.2 Photodimerization of o-ethoxy cinnamic acid and its dependence on the polymorphic form

Molecular packing of α and γ forms

The α -polymorph exists in a centrosymmetric triclinic system ($a=6.69530(10)\text{\AA}$, $b=8.67300(10)\text{\AA}$, $c=9.98270(10)\text{\AA}$, $\alpha=72.0270(10)^\circ$, $\beta=71.1900(10)^\circ$, $\gamma=67.7830(10)^\circ$). The γ -form crystallizes in a monoclinic cell ($C2/c$, $a=16.9695(2)\text{\AA}$, $b=5.46140(10)\text{\AA}$, $c=23.0688(3)\text{\AA}$, $\beta=110.8560(10)^\circ$) (Table 9). In both these polymorphs, the asymmetric unit comprises of a full molecule. We show the molecular packing diagrams of the α - and γ - forms in Fig.18. The structural parameters of the two forms are listed in Table 10 along with those of the photodimer, to highlight the differences. The geometric parameters in both the polymorphs are similar in almost all the regions except for the carboxylic group and in the torsion angles made by the side groups with the phenyl ring. The molecule is non-planar in the γ -form, the groups being twisted by as much as 9° away from the plane of the benzene ring. In the α -form, the heavy atom framework of the molecule is essentially planar, the side groups being out of plane of the benzene ring by -3° .

In Table 11, we list favorable hydrogen contacts in the α - and γ -structures. There are intermolecular O—H \cdots O contacts between the carboxyl groups in both the forms, but the nature of these contacts is entirely different. Thus, the C(9)—O bond lengths in the α -form are 1.240(2) and 1.3161(14) \AA respectively, while these distances are nearly equal (~ 1.275 \AA) in the γ -form. The intermolecular O \cdots O distance in the α -form is slightly longer than in the γ -form (α , 2.633(1); γ , 2.617(2) \AA). The C(8)—C(9)—O(1) and C(8)—C(9)—O(2) bond angles show some differences as well. The angles are $123.5(2)^\circ$ and $113.61(11)^\circ$ respectively in the α -form and are more closer in the γ -form, $120.49(10)^\circ$ and $116.56(10)^\circ$ respectively. These structural features suggest the presence of a near-symmetric hydrogen bond in the carboxylic dimer in the γ -form and normal dimer hydrogen bond in the α -form. The two carboxylic bond angles approaching a common value and the bonds becoming nearly equal is in accordance with the VSEPR model. In order to explore how common such a feature is, a search was carried out using the Cambridge

Table 9
Crystal data and experimental details

Crystal	α	γ	α - dimer
Chemical formula	$C_{11}H_{12}O_3$	$C_{11}H_{12}O_3$	$C_{22}H_{24}O_6$
Formula weight (g)	192.21	192.21	384.41
Cell System	Triclinic	Monoclinic	Monoclinic
Space group	P -1	C 2/c	P 2 ₁ /c
a (Å)	6.69530(10)	16.9695(2)	8.333(4)
b (Å)	8.67300(10)	5.46140(10)	8.444(2)
c (Å)	9.98270(10)	23.0688(3)	13.975(4)
α (°)	72.0270(10)	90	90
β (°)	71.1900(10)	110.8560(10)	106.64(3)
γ (°)	67.7830(10)	90	90
V (Å ³)	496.326(11)	1997.87(5)	942.0(6)
Z	2	8	2
F ₀₀₀	204	816	408
ρ (Mg m ⁻³)	1.286	1.278	1.355
Radiation type	Mo K α		
Wave length (Å)	0.71073		
No. of reflections for cell	60	60	60
μ (mm ⁻¹)	0.093	0.093	0.10
Crystal form	Cuboidal	Needle	Cuboidal
Crystal size (mm)	0.3 x 0.2 x 0.2	0.3 x 0.15 x 0.15	0.15 x 0.1 x 0.1
Crystal color	Colorless	Colorless	Colorless
Data collection temperature	130(2) K	130(2) K	130(2) K
Diffractometer	Siemens CCD		
Crystal-detector distance (cm)	5.0		
No. of measured reflections	7405	14190	9163
No. of independent reflections	6365	8371	4928
No. of observed reflections	4120	5079	3711
R _{int}	0.0205	0.0299	0.0535
θ_{min} (°)	2.21	1.89	2.55
θ_{max} (°)	49.48	49.60	49.49
Range of h, k, l			
	-11 ≤ h ≤ 13	-36 ≤ h ≤ 36	-16 ≤ h ≤ 17
	-18 ≤ k ≤ 18	-10 ≤ k ≤ 10	-17 ≤ k ≤ 18
	-16 ≤ l ≤ 21	-49 ≤ l ≤ 27	-25 ≤ l ≤ 28
After multipole refinement			
Weighting Scheme	0.07160, 0.1721	0.0737, 0.4	0.0731, 2.7123
R1	0.0426	0.0557	0.0417
WR2	0.0467	0.0654	0.0677
S	0.9808	0.9622	0.9388
No of variables	278	278	278
N _{ref} /N _v	14.3	18.3	13.3

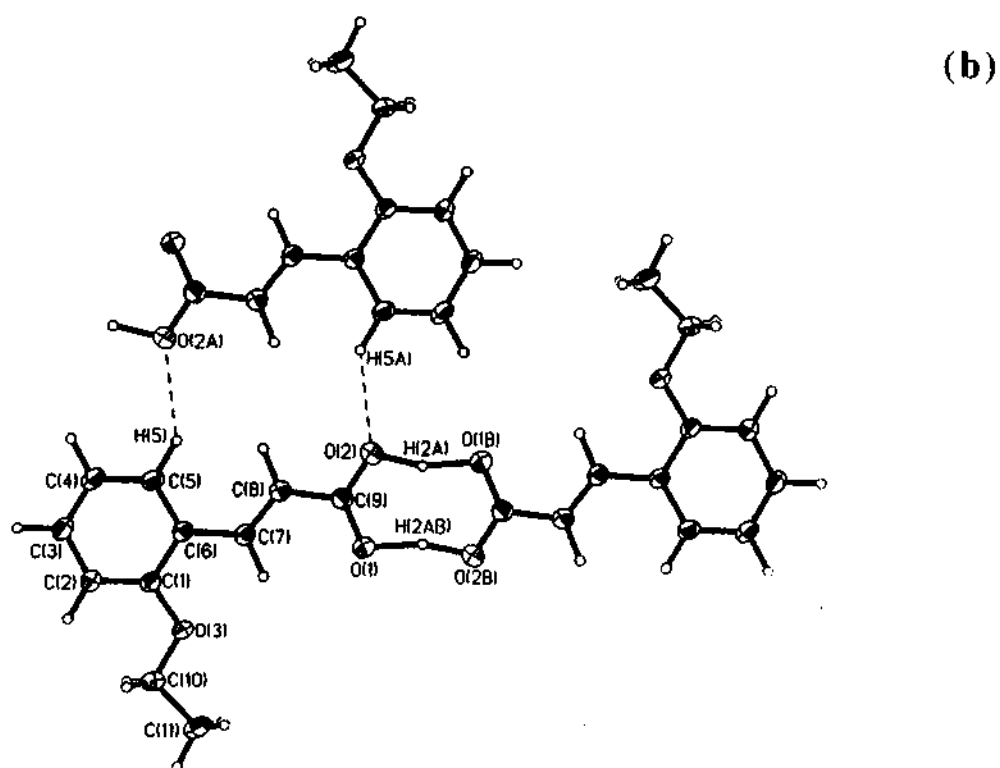
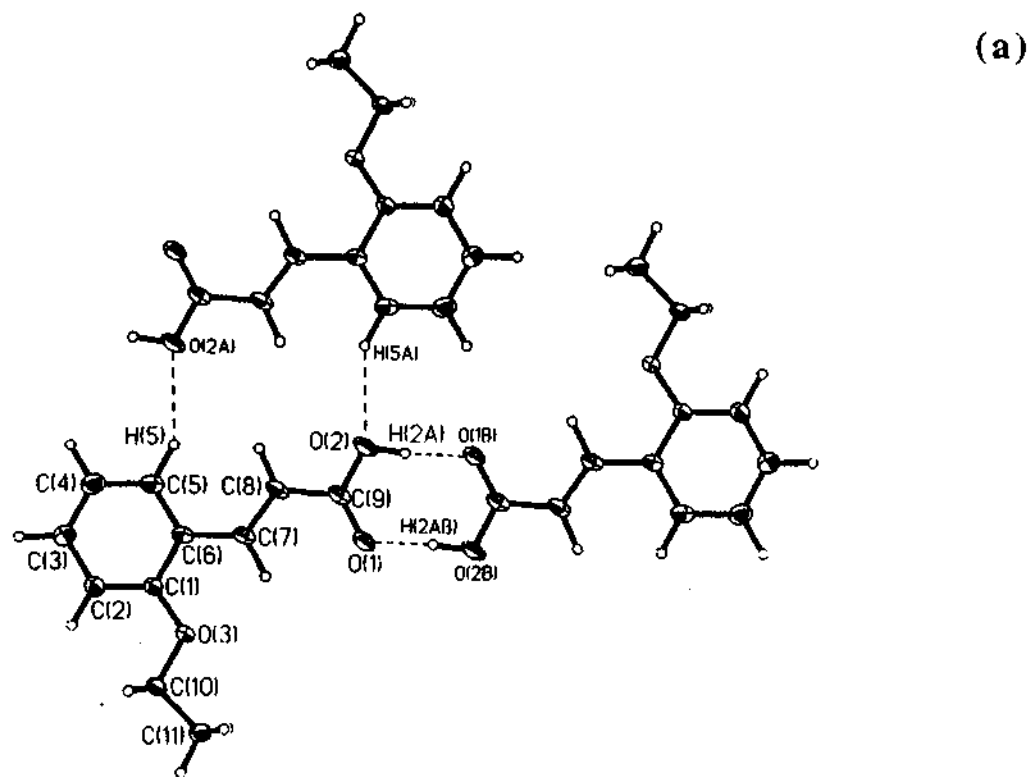


Fig.18. Packing diagrams of *o*-ethoxy cinnamic acid molecules in a) the α - and b) the γ -forms. Intermolecular contacts are also shown. All non-hydrogen atoms are shown at 50% probability ellipsoids.

Table 10

Important differences in the molecular structure in the α - and γ - forms and the α -dimer

	α	γ	α -dimer
a) Bond length (Å)			
C(6)—C(7)	1.461(2)	1.462(2)	1.509(4)
C(7)—C(8)	1.345(2)	1.335(2)	1.549(4)
C(7)—C(8A) ^a			1.580(4)
C(8)—C(9)	1.468(2)	1.468(2)	1.497(4)
O(1)—C(9)	1.240(2)	1.2710(14)	1.239(4)
O(2)—C(9)	1.3161(14)	1.278(2)	1.307(4)
O(2)—H(2A)	0.96	1.25	0.96
C(1)—O(3)	1.3648(14)	1.3675(13)	1.373(4)
O(3)—C(10)	1.4371(13)	1.431(2)	1.436(4)
C(10)—C(11)	1.506(2)	1.514(2)	1.507(6)
b) Bond angle (°)			
C(5)—C(6)—C(7)	122.20(10)	122.74(10)	119.7(2)
C(6)—C(7)—C(8)	125.43(12)	125.78(10)	118.9(2)
C(7)—C(8)—C(9)	121.06(12)	121.87(10)	115.1(2)
C(1)—C(6)—C(7)	119.57(10)	119.18(9)	122.4(2)
O(2)—C(9)—C(8)	113.61(11)	116.56(10)	114.7(2)
O(1)—C(9)—C(8)	123.5(2)	120.49(10)	121.9(3)
O(3)—C(1)—C(6)	116.23(10)	115.88(9)	114.3(3)
C(1)—O(3)—C(10)	117.79(9)	118.03(9)	118.3(2)
O(3)—C(10)—C(11)	107.35(10)	106.97(11)	107.0(3)
c) Torsion angle (°)			
C(5)—C(6)—C(7)—C(8)	1.6(2)	5.05(18)	-125.8(3)
C(2)—C(1)—C(6)—C(7)	-178.68(12)	-179.28(10)	176.5(3)
C(1)—C(6)—C(7)—C(8)	-179.56(12)	-175.68(11)	54.4(4)
C(6)—C(7)—C(8)—C(9)	-178.34(12)	177.94(10)	109.9(3)
C(7)—C(8)—C(9)—O(2)	-177.01(12)	175.33(11)	160.4(2)
C(7)—C(8)—C(9)—O(1)	3.7(2)	-5.60(18)	-22.6(4)
C(1)—O(3)—C(10)—C(11)	-178.87(11)	174.06(11)	-174.7(3)
C(10)—O(3)—C(1)—C(6)	-177.98(11)	-173.18(11)	-179.0(3)
C(10)—O(3)—C(1)—C(2)	1.67(18)	7.07(17)	2.7(5)

a) The distances between the shortest double bond contact in α - and γ -form are 4.514 and 5.253 Å respectively

Table 11
Intra- and intermolecular Hydrogen Bond contacts

Polymorph	D-H...A	Bond type	H...A	D...A	∠D-H...A
α	O(2)—H(2A)...O(1) ^a	Acid dimer	1.68(2)	2.633(1)	172.1(6)
	C(5)—H(5)...O(2) ^b	Intralayer	2.437(1)	3.404(2)	148.9(1)
	C(4)—H(4)...O(1) ^c	Interlayer	2.637(1)	3.634(2)	153.9(1)
	C(10)—H(10A)...O(3) ^d	Interlayer	2.930(2)	3.616(2)	122.9(1)
	C(10)—H(10B)...O(1) ^e	Interlayer	2.600(1)	3.315(1)	124.3(1)
	C(11)—H(11C)...O(2) ^f	Interlayer	2.675(2)	3.648(2)	152.4(1)
γ	O(2)—H(2A)...O(1) ^g	Acid dimer	1.40(1)	2.617(2)	162.4(8)
	C(5)—H(5)...O(2) ^h	Intralayer	2.481(1)	3.386(1)	141.2(1)
	C(4)—H(4)...O(1) ⁱ	Interlayer	2.615(1)	3.641(1)	159.4(1)
	C(10)—H(10B)...O(3) ^j	Interlayer	2.818(1)	3.690(1)	139.6(1)
	C(11)—H(11B)...O(1) ^k	Interlayer	2.939(1)	3.714(1)	130.3(1)
	α- dimer	O(2)—H(2A)...O(1) ^l	Acid dimer	1.67(2)	2.627(3)
C(7)—H(7)...O(3) ^m		Intramolecular	2.42(4)	2.938(4)	108(2)
C(8)—H(8)...O(3) ⁿ		Intramolecular	2.75(4)	3.176(3)	103(2)
C(11)—H(11B)...O(1) ^m		Intramolecular	2.67(5)	3.525(5)	137(4)
C(4)—H(4)...O(2) ^p		Intermolecular	2.60(3)	3.493(4)	140(3)
C(11)—H(11A)...O(1) ^q		Intermolecular	2.55(5)	3.490(4)	148(3)

Symmetry: a) -1-x, 2-y, -z; b) -1-x, 3-y, -z; c) x, 1+y, z; d) -x, 2-y, 1-z; e) 1+x, y, z; f) -x, 2-y, -z; g) 1/2-x, 5/2+y, 1/2-z; h) -1/2-x, -1/2+y, z; i) 1/2-x, -1/2+y, 1/2-y; j) x, y-1, z; k) -1-x, -y, z; l) -x, -y, -z; m) x, y, z; n) x, y, z; p) x, 1/2-y, -1/2+z; q) x, 1/2-y, 1/2-z

Structural Database (version 5.7) for carboxylic acids having the two C—O bonds differing within 0.01 Å. Of the total 3334 acid groups found, only 3% could satisfy this criterion. Among half of these, HFIX had been applied for positioning hydroxyl hydrogen. Where hydrogen has been located, the O—H bond length spans between 1.0 and 1.31 Å. Accordingly, the carboxylic hydrogen, H(2A) in the γ -form was located midway in the intermolecular region with O—H and H...O distances being 1.25 and 1.40 Å respectively. This hydrogen was held at this position in the subsequent refinements. The corresponding distances in the α -form are 0.96 and 1.68 Å respectively (see Table 10 and 11).

As shown in Fig.18, each molecule is held by two C—H...O contacts from an adjacent molecule related by inversion. In the α -form, this contact is at 2.437(1) Å, almost perpendicular to the O—H...O contacts. The contact in the γ -form is longer by ~ 0.05 Å and is slightly tilted following reorientation of the carboxylic group. The molecules pack in layers in both the forms, the spacing between the layers being ~ 3.45 and 3.39 Å respectively in the α - and the γ -forms. The relative positions of the benzene rings in a layer do not differ appreciably in the two polymorphs and the crystal densities are also comparable (see Table 9). The layers are held by C—H...O contacts, four in the α -form and three in γ -form, the distances ranging between 2.60 and 2.94 Å (see Table 11). The adjacent layers are less displaced with respect to each other in the α -form, with more favorable contacts in terms of the distance and the angle. The differences in the structural features of the α - and the γ -forms discussed hitherto play an important role in determining the photoreactivity. We shall discuss this aspect along with the charge density, later in this section.

We felt that the difference between the α - and the γ -forms with respect to the nature of hydrogen bonding in the carboxylic acid dimer needs further proof by an independent method. Since infrared (IR) spectroscopy is ideally suited to distinguish symmetric and asymmetric hydrogen bonds [72,73], we carried out a comparative study of the IR spectra of the α - and the γ - forms in the 4000-400 cm^{-1} region. The spectra were recorded in the form of KBr pellets as well as nujol mulls. The nujol mull spectra were considered essential in order to avoid spurious bands due to any moisture in KBr. In Fig.19, we show the IR spectra of the two forms in the 3300-

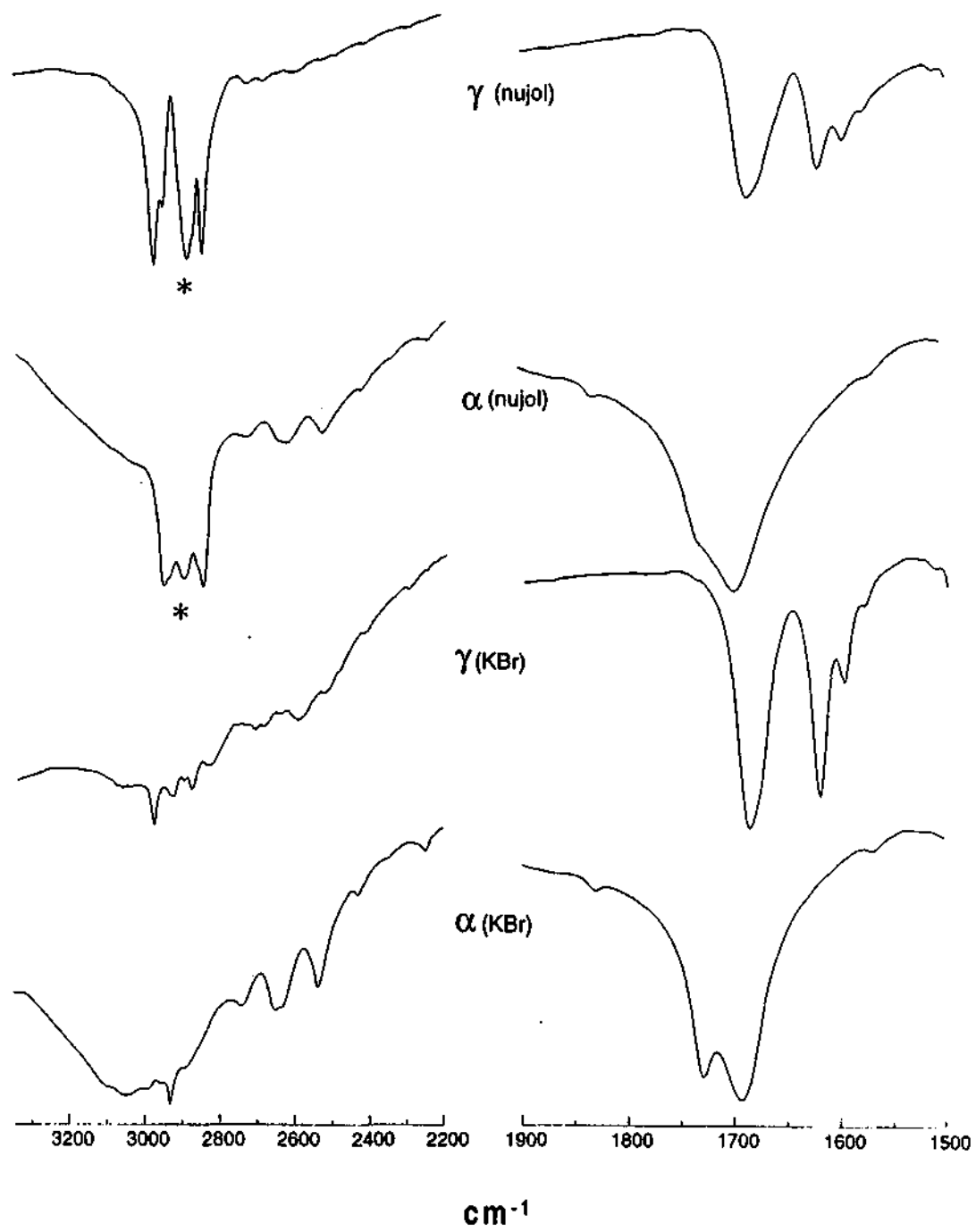


Fig.19. Infrared spectra of the α - and the γ -forms of *o*-ethoxy cinnamic acid in KBr pellet and nujol mull. Asterisks denote nujol bands.

2200 and 1900-1500 cm^{-1} regions. While the spectrum of the γ -form shows a larger number of features due to the lower symmetry as expected, the most prominent difference in the spectra of the two forms is seen in the 3300-2200 cm^{-1} region. The α -form shows a broad intense band centered around 3000 cm^{-1} , in addition to weak features between 2800 and 2500 cm^{-1} . Such features are characteristic of carboxylic acid dimers [72,74]. The intense band centered around 3000 cm^{-1} is completely absent in the spectrum of the γ -form. One of the characteristic features of symmetric hydrogen bonds is the absence of 3000 cm^{-1} band in the hydrogen bond region [73,75]. The α -form shows bands at ~ 1730 and 1694 cm^{-1} due to the OH bending and the C=O stretching modes respectively. We observe the C=O stretching mode at $\sim 1688 \text{ cm}^{-1}$ in the spectrum of the γ form, the lower C=O frequency being consistent with the stronger hydrogen bonds present in the dimer. The absence of the OH bending frequency suggests that the hydrogen bond in the γ -form is different from that in the ordinary cyclic dimers. A symmetric H-bond does not exhibit such a bending vibration frequency. Furthermore, the appearance of additional bands at 1622 and 1598 cm^{-1} in the spectrum of the γ -form also supports this observation [73,75]. The IR spectrum of maleate ion shows the O-H stretching band below 1650 cm^{-1} . Based on the IR studies, we can safely conclude that the γ -form has symmetric hydrogen bonds while the α -form possesses the usual carboxylic acid dimers.

In Fig.20 we show two centrosymmetric molecules in the α -form undergoing photodimerization. The molecules belong to the adjacent layers and are related by $(-x, 2-y, -z)$. The double bonds ($1.345(2) \text{ \AA}$) between the C(7) and C(8) atoms of the cinnamoyl groups may be viewed as the opposite sides of an imaginary rectangle distorted to the extent of $\sim 3.1^\circ$. Although the distance between the double bonds (4.514 \AA) is somewhat larger than required by the Schmidt criterion [37], the bonds are potentially reactive. In the photostable γ -form, however, the C(7)=C(8) bond sticks out of the molecular plane (C(1)—C(6)—C(7)—C(8), $-175.68(11)^\circ$, C(5)—C(6)—C(7)—C(8), $5.05(18)^\circ$ as compared to $-179.56(12)^\circ$ and $1.6(2)^\circ$ in the α -form) and as a result its reactive partner ($1/2-x, 3/2-y, -z$) is placed farther apart ($\sim 5.251 \text{ \AA}$) in an oblique parallelogram (see Fig.21), the acute angle being 80.7° . The cyclobutane ring formed by the dimerization of the α -form is not an exact

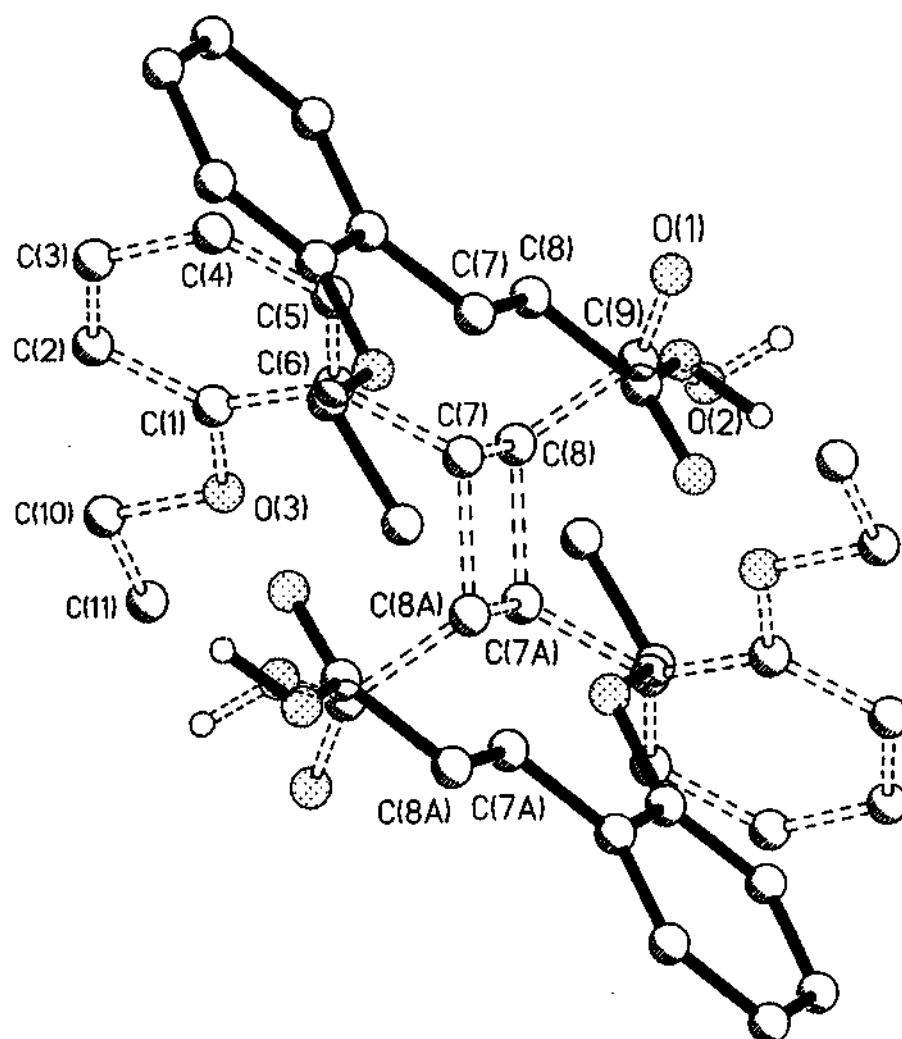


Fig.20. Photodimerization in *o*-ethoxy cinnamic acid. Two centrosymmetric molecules of the α -form before (full lines) and after (dashed lines) the reaction. Hydrogen atoms other than the hydroxylic are omitted from the figure for the sake of clarity.

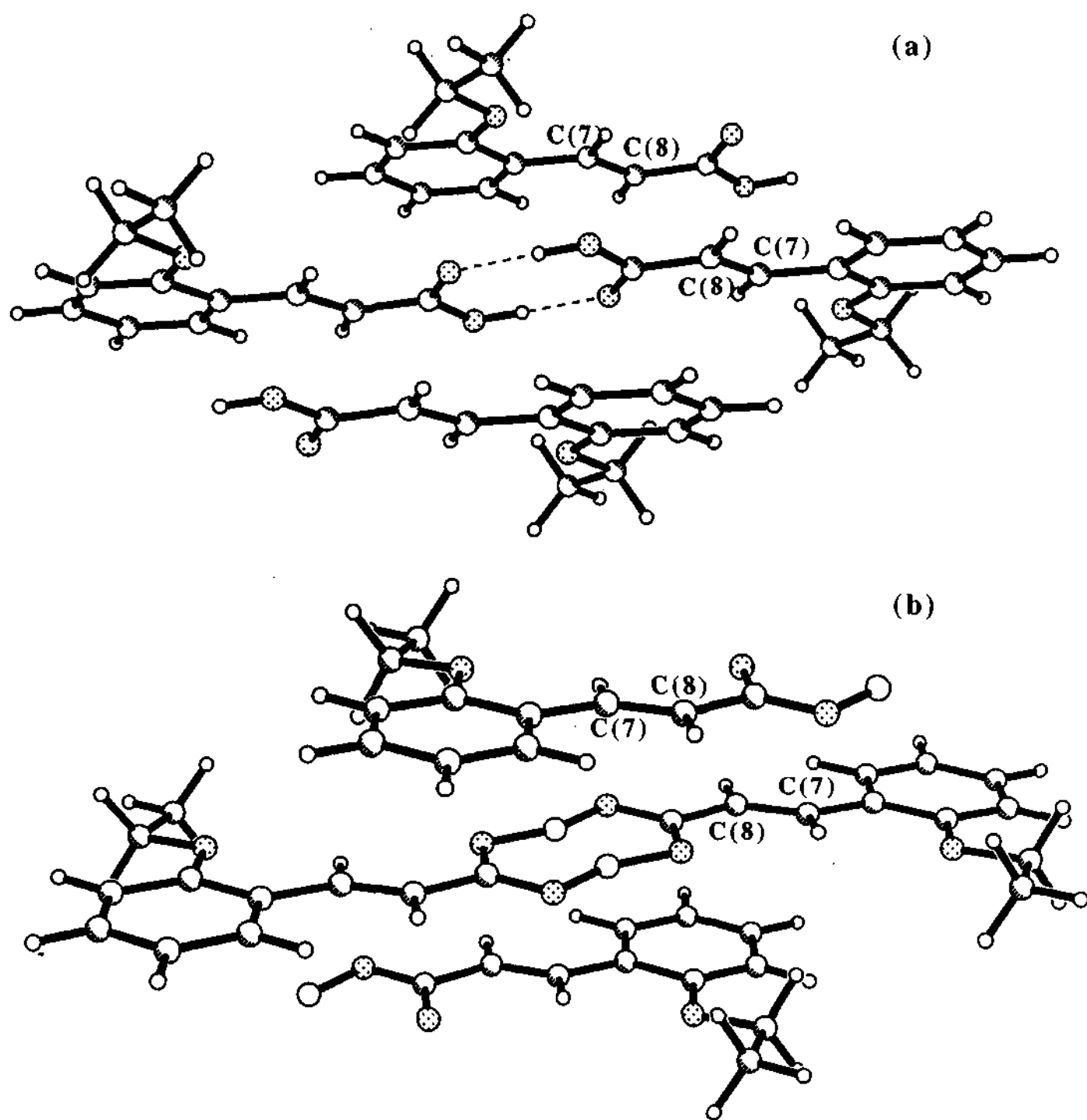


Fig.21. Packing diagram showing dimeric hydrogen bonding and reactive double bonds in a) α and b) γ forms of o-ethoxy cinnamic acid

square (1.549 Å x 1.580 Å), the new C(7)—C(8A) and C(8)—C(7A) bonds are slightly longer than the C(7)—C(8) bonds and the angular distortion is 1.8°. The two halves of the dimer are related by inversion as expected from the topochemistry of the dimerization.

Charge density in the α and the γ forms

We now turn to the charge density analysis of the cinnamic acid monomers in the α - and the γ -forms and of the photodimer. In Fig.22, we show the deformation density in a plane containing C(4), C(9) and C(11) atoms of the α - and γ -polymorphs. Concentric contours typify the various bonding regions in the molecules between the atom-cores. The lone-pair electrons on the ethoxy and carboxylic oxygens are clearly seen as pairs of lobes. The total electron densities and the Laplacians at the critical points are listed for the various bonds in Table 12 along with the polarization and ellipticity parameters. The average ρ_{CP} of the phenyl ring is 2.11 eÅ⁻³ in the α -form as compared to 2.19 eÅ⁻³ in the γ -form. Similarly, the C(6)—C(7) and C(8)—C(9) single bond regions in the α -form have densities of 1.78(4) and 1.82(5) eÅ⁻³ respectively while those in the γ -form exhibit somewhat higher values, 1.96(4) and 1.95(5) eÅ⁻³ respectively. In the γ -form, the topography of the deformation density in the C(7)=C(8) region is as expected of a carbon-carbon double bond [76]. In the α -form, on the other hand, the contours are less dense (see Fig.22a). This is reflected in the properties of the bond CPs. In the γ -form, the density between C(7) and C(8) is 2.55(5) eÅ⁻³, typical of an isolated double bond [16] while in the α -form, it is considerably lower (2.27(5) eÅ⁻³) though the corresponding bond lengths hardly differ (Table 10). The bond in the α -form is associated with slightly higher ellipticity. The ethoxy groups in the α - and γ -forms also show differences in bond densities. The C(1)—O(3) bond in the α -form has much higher density (2.21(5) eÅ⁻³) than the O(3)—C(10) bond (1.80(5) eÅ⁻³), indicating that the density has migrated from one bond to the other. The difference is much smaller in the γ -form (~ 0.2 eÅ⁻³). Considering that the molecule is quite planar in the α -form we would expect such differences due to conjugation [42].

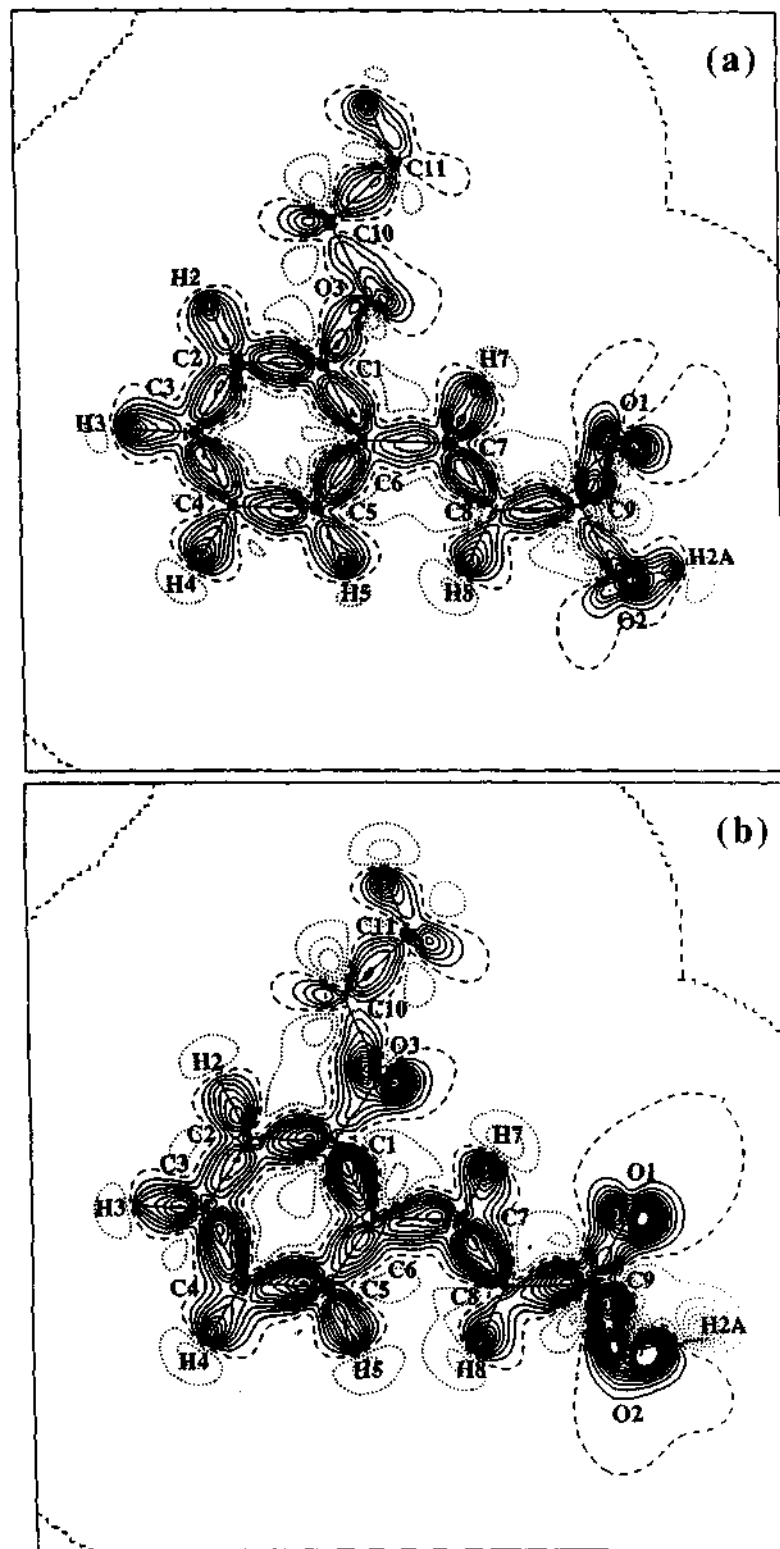


Fig.22. Deformation density maps in the mean plane of the molecule in a) the α - and b) the γ -forms. Deformation density was obtained as the difference between the total density and the spherical density without thermal smearing. Contour interval at $0.1 \text{ e}\text{\AA}^{-3}$.

Table 12
Analysis of bond critical points

Bond	α				γ				α -dimer			
	P	$\nabla^2\rho$	ϵ	$\Delta(\%)$	P	$\nabla^2\rho$	ϵ	$\Delta(\%)$	P	$\nabla^2\rho$	ϵ	$\Delta(\%)$
O(1)-C(9)	2.90(7)	-38.9(4)	0.38	22	2.71(7)	-38.1(4)	0.21	25	3.55(9)	-66.4(5)	0.24	23
O(2)-C(9)	2.22(7)	-26.0(3)	0.41	25	3.21(6)	-41.3(3)	0.27	15	2.83(9)	-34.4(6)	0.11	36
O(2)-H(2A)	2.3(1)	-23.8(8)	0.01	54	0.9(1)	-2.8(5)	0.1	53	2.6(2)	-39(1)	0.06	51
C(1)-C(2)	2.12(5)	-18.9(1)	0.25	2	2.22(5)	-20.9(1)	0.31	3	2.56(6)	-28.6(2)	0.32	1
C(1)-C(6)	2.02(5)	-15.9(1)	0.36	1	2.28(5)	-22.9(1)	0.35	12	2.51(7)	-31.5(3)	0.24	16
C(2)-C(3)	2.09(5)	-17.6(1)	0.26	1	2.05(5)	-15.6(1)	0.34	3	2.33(7)	-22.7(3)	0.12	13
C(3)-C(4)	2.11(5)	-17.1(2)	0.3	4	2.30(5)	-19.6(2)	0.3	5	2.29(7)	-26.3(2)	0.3	10
C(4)-C(5)	2.04(5)	-16.9(2)	0.29	5	2.27(5)	-17.9(1)	0.3	8	2.27(6)	-22.9(2)	0.1	13
C(5)-C(6)	2.14(5)	-19.9(1)	0.3	3	2.00(5)	-16.5(1)	0.28	7	2.21(9)	-22.0(5)	0.87	34
C(2)-H(2)	1.7(1)	-12.9(3)	0.15	34	1.9(1)	-20.1(4)	0.08	39	1.9(1)	-19.9(5)	0.1	38
C(3)-H(3)	1.8(1)	-15.5(2)	0.06	29	1.8(1)	-18.9(4)	0.07	42	1.9(1)	-17.1(3)	0.06	28
C(4)-H(4)	1.8(1)	-16.9(3)	0.07	28	1.9(1)	-16.9(3)	0.03	27	2.1(1)	-32.2(6)	0.09	47
C(5)-H(5)	1.8(1)	-15.6(3)	0.15	32	2.0(1)	-21.7(4)	0.1	35	1.9(1)	-19.4(3)	0.07	24
C(6)-C(7)	1.78(4)	-12.3(1)	0.23	3	1.96(4)	-14.2(1)	0.21	3	1.82(5)	-17.8(1)	0.11	1
C(7)-C(8)	2.27(5)	-21.9(2)	0.42	3	2.55(5)	-24.3(2)	0.25	5	1.63(5)	-11.7(1)	0.13	8
C(7)-C(8A)	1.9(1)	-19.1(3)	0.09	37	1.84(8)	-16.3(2)	0.09	20	1.54(8)	-10.6(2)	0.19	1
C(7)-H(7)	1.82(5)	-14.0(1)	0.3	1	1.95(5)	-17.8(2)	0.26	14	1.8(1)	-19.4(4)	0.07	38
C(8)-H(8)	1.8(1)	-17.4(3)	0.11	27	1.74(8)	-14.1(2)	0.14	22	2.10(6)	-25.8(2)	0.22	18
O(3)-C(1)	2.21(5)	-16.0(2)	0.11	14	2.12(5)	-15.1(2)	0.15	17	1.8(1)	-17.6(3)	0.03	34
O(3)-C(10)	1.80(5)	-6.9(2)	0.06	13	1.91(6)	-11.6(2)	0.04	17	2.28(8)	-30.9(4)	0.09	26
C(10)-C(11)	1.71(4)	-11.1(1)	0.14	2	1.73(5)	-12.6(1)	0.17	3	2.32(6)	-14.9(2)	0.08	6
C(10)-H(10A)	1.74(7)	-11.8(2)	0.06	32	1.9(1)	-19.0(4)	0.09	36	1.70(7)	-12.3(2)	0.26	17
C(10)-H(10B)	1.82(8)	-15.0(3)	0.07	38	1.8(1)	-16.2(3)	0.11	29	1.8(1)	-11.1(3)	0.41	27
C(11)-H(11A)	1.82(8)	-12.8(3)	0.1	29	1.8(1)	-14.1(5)	0.1	40	1.8(1)	-13.2(4)	0.12	33
C(11)-H(11B)	1.6(1)	-11.1(3)	0.16	32	1.8(1)	-13.0(4)	0.13	32	2.1(1)	-24.4(4)	0.11	31
C(11)-H(11C)	1.70(8)	-10.6(2)	0.06	21	1.7(1)	-13.9(3)	0.19	25	1.7(1)	-11.8(5)	0.13	34
					1.7(1)	-13.9(3)	0.19	25	1.8(1)	-15.2(3)	0.13	11

ρ in eA^{-3} ; $\nabla^2\rho$ in eA^{-5}

As regards the C—H...O hydrogen contacts, all except C(10)—H(10B)...O(1) are associated with small densities and Laplacians in both the polymorphs. The C(10)—H(10B)...O(1) contact exists only in the α -form and carries a density of 0.052(7) $e\text{\AA}^{-3}$ and a positive Laplacian (0.759(4) $e\text{\AA}^{-5}$) as expected. Following Mallinson *et al.* [70], it can be considered as a moderately strong C—H...O interaction. However, the intermolecular O—H...O contacts in the two forms exhibit major differences in charge density in parallel to the structural differences discussed earlier. In this context, the deformation density maps in the carboxylic dimer region are revealing. We see from Fig.22 that there are considerable differences in the charge density in this region (see Tables 12 and 13). Thus, the C(9)=O(1), C(9)—O(2) and the O(2)—H(2A) regions in the α -form have ρ_{CP} values of 2.90(7), 2.22(7) and 2.3(1) $e\text{\AA}^{-3}$ respectively. The O(2)—H(2A)...O(1A) bond carries a small density of 0.28(7) $e\text{\AA}^{-3}$ and a positive Laplacian of 5.13(8) $e\text{\AA}^{-5}$, characteristic of closed-shell interaction in the intermolecular region. The near absence of distinction between the two C—O bond lengths of the carboxyl group in the γ -form is reflected in the charge distribution. The densities associated with C(9)=O(1) and C(9)—O(2) bonds are unusually high, 2.71(7) and 3.21(6) $e\text{\AA}^{-3}$ respectively. Moreover, we find comparable densities in the O—H and the H...O bonds (0.9(1) and 0.6(1) $e\text{\AA}^{-3}$ respectively), the associated Laplacians being -2.8(5) and 1.9(2) $e\text{\AA}^{-5}$ respectively. Contour maps of the Laplacian shown in Fig.23 illustrate the ionic nature of the O—H bond in the γ -form as compared to a shared interaction in the α -form. This is one of the few instances where the charge density distribution of a near-symmetric intermolecular hydrogen bond has been studied. In maleates containing intramolecular symmetric hydrogen bonds (O...H \sim 1.21 \AA) the values of ρ_{CP} and Laplacian are \sim 1.1 $e\text{\AA}^{-3}$ and $-6 e\text{\AA}^{-5}$ respectively [77].

An inspection of the pseudo-atomic charges reveal that there is an interplay between the resonance and the inductive effects in the molecule. The charge on O(1), O(2) and H(2A) in the γ -form was found to be higher (-0.47, -0.48 and 0.63 e) than those in the α -form (-0.27, -0.28 and 0.19 e). The ethoxy oxygen, O(3) exhibited charges of -0.39 and -0.16 in the γ - and α -forms respectively. The molecular geometry in the two forms can be rationalized based on the above discussion. If the molecule in the γ form were planar, the ethoxy group at the ortho

Table 13
Hydrogen bond critical points

Polymorph	D-H...A	Bond type	$\rho(\text{e}\text{\AA}^{-3})$	$\nabla^2\rho(\text{e}\text{\AA}^{-5})$
α	O(2)—H(2A)...O(1) ^a	acid dimer	0.28(7)	5.13(8)
	C(5)—H(5)...O(2) ^b	intralayer	0.04(2)	0.811(4)
	C(4)—H(4)...O(1) ^c	interlayer	0.02(1)	0.438(5)
	C(10)—H(10A)...O(3) ^d	interlayer	0.023(3)	0.355(2)
	C(10)—H(10B)...O(1) ^e	interlayer	0.052(7)	0.759(4)
γ	O(2)—H(2A)...O(1) ^b	acid dimer	0.6(1)	1.9(2)
	C(5)—H(5)...O(2) ^f	intralayer	0.03(1)	0.648(5)
	C(4)—H(4)...O(1) ⁱ	interlayer	0.011(8)	0.300(4)
	C(10)—H(10B)...O(3) ^j	interlayer	0.016(7)	0.319(4)
	C(11)—H(11B)...O(1) ^k	interlayer	0.017(6)	0.277(4)
α - dimer	O(2)—H(2A)...O(1) ^l	acid dimer	0.18(8)	5.31(8)
	C(7)—H(7)...O(3) ^m	intramolecular	0.034(6)	0.576(4)
	C(8)—H(8)...O(3) ⁿ	intramolecular	0.07(1)	1.146(5)
	C(11)—H(11B)...O(1) ^m	intramolecular	0.05(1)	0.683(7)
	C(4)—H(4)...O(2) ^p	intermolecular	0.02(1)	0.427(5)
	C(11)—H(11A)...O(1) ^q	intermolecular	0.03(2)	0.622(7)

Symmetry: a) $-1-x, 2-y, -z$; b) $-1-x, 3-y, -z$; c) $x, 1+y, z$; d) $-x, 2-y, 1-z$; e) $1+x, y, z$;
f) $-x, 2-y, -z$; g) $1/2-x, 5/2+y, 1/2-z$; i) $-1/2-x, -1/2+y, z$; j) $1/2-x, -1/2+y, 1/2-y$;
k) $x, y-1, z$; l) $-1-x, -y, z$; m) $-x, -y, -z$; n) x, y, z ; p) $x, 1/2-y, -1/2+z$; q) $x, 1/2-y, 1/2-z$

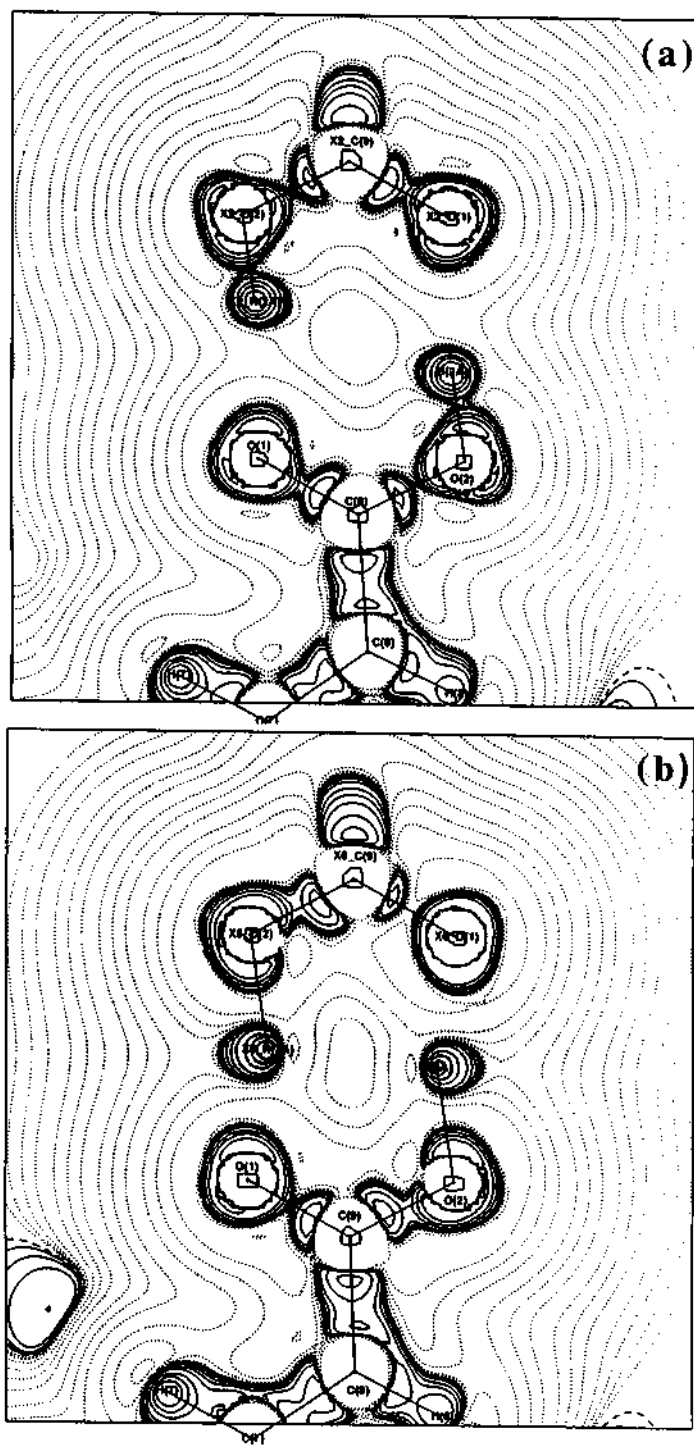


Fig.23. Contour maps of the Laplacian of the total density in the O(1), O(2) and C(9) plane for a) α and b) γ -forms.

position would pump in more charge through resonance which should simply destabilize the charge separation in the molecule. Thus, it is clear that the ionic nature of the near symmetric hydrogen bond in the γ -form goes hand in hand with the localization of charge density in the respective bond regions and the non-planarity of the molecule.

The photodimer

The photodimer of the α -polymorph, 2,2'-diethoxy α -truxillic acid, crystallizes in a centrosymmetric space group, $P2_1/c$ ($a=8.333(4)$ Å, $b=8.444(2)$ Å, $c=13.975(4)$ Å, $\beta = 106.64(3)^\circ$) with two molecules per unit cell, the asymmetric unit being half the molecule. The C(7)—C(8) distance in the cyclobutyl ring is 1.549(4) Å, about 0.2 Å longer compared to the pristine α -form. The internal geometry of this ring is quite comparable to that found in α -truxillic acid [78]. The bond angles change dramatically, the angles around C(7) and C(8) become nearly tetrahedral on dimerization (see Table 10). The C(6)—C(7) and C(8)—C(9) distances increase by ~ 0.04 Å and 0.03 Å respectively. The bond distances increase by ~ 0.01 Å in the ethoxy groups. The regions of the benzene ring exhibit minor changes on dimerization, but the angular relations with the side groups undergo major changes. Thus, the cyclobutyl ring and the acid groups subtend angles of $\sim 89.4^\circ$ and 46.3° respectively with the phenyl ring while the ethoxy group makes an angle of 5.4° with the phenyl ring (compared to 2.6° in the α -form). In Fig.24, we show the packing diagram of the photodimer viewed along the b -axis. The O—H \cdots O contacts of the acid dimeric units run parallel to the a -axis, providing enough scope for several C—H \cdots O side interactions (Table 11). The methyl hydrogen, H(11A) establishes an intermolecular contact with a carbonyl oxygen and H(11B) forms an intramolecular contact with it. The phenyl hydrogen, H(4) enters into intermolecular contact with a neighboring hydroxyl oxygen, O(2). Unlike the monomers, H(5) in the dimer is no longer in a position to form a C—H \cdots O contact. The intermolecular contacts help stack the molecules in the ac -plane (Fig.24).

We now turn to the nature of charge distribution in the photodimer in comparison with the monomers in the two polymorphs (Fig.25). The geometry and

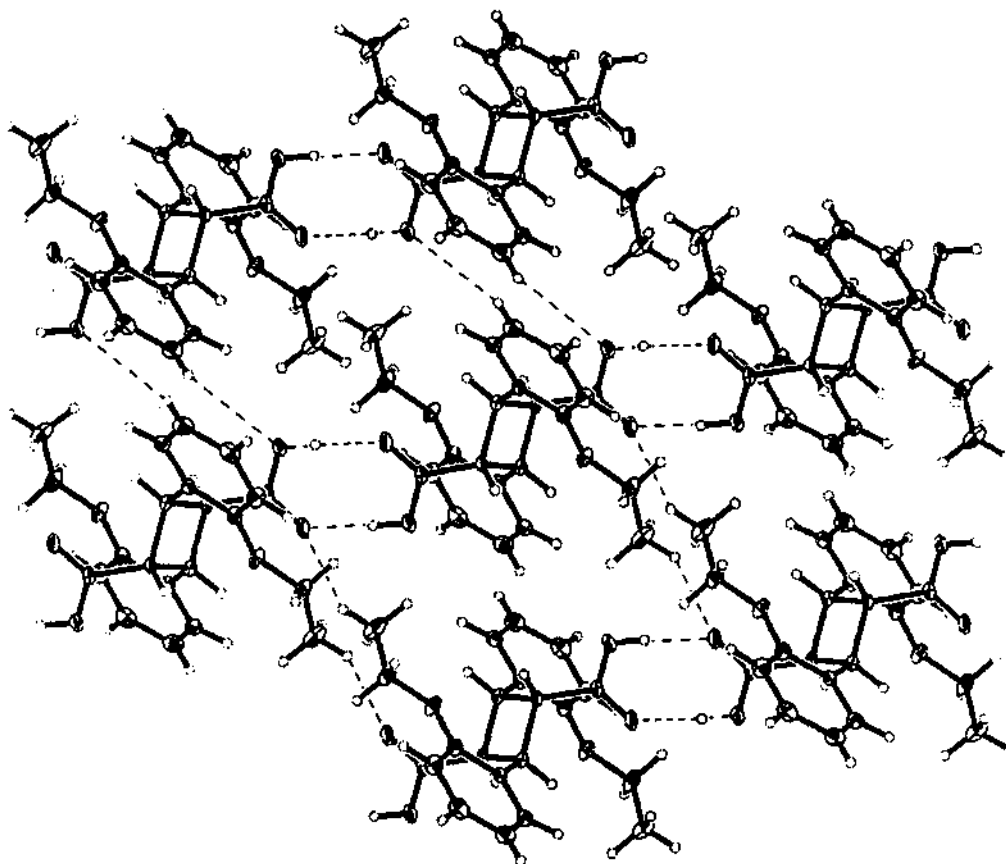


Fig.24. Packing diagram of the photodimer, 2,2'-diethoxy α -truxillic acid. Intra- and intermolecular contacts are also shown. All non-hydrogen atoms are shown at 50% probability ellipsoids.

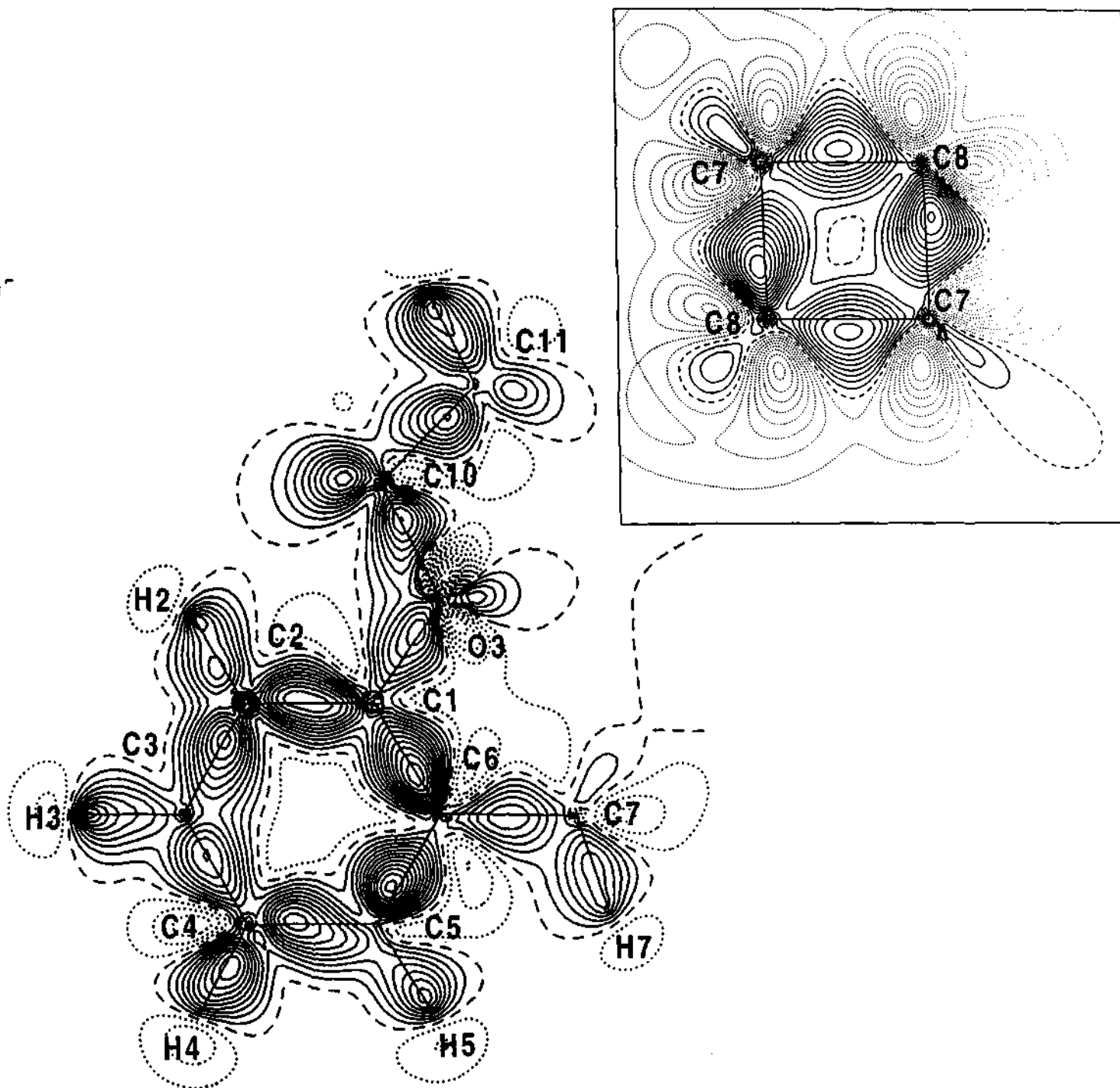


Fig.25. Deformation density map of the photodimer, 2,2'-diethoxy α -truxillic acid in the plane of the phenyl ring. The inset shows the deformation density in the plane of the cyclobutane ring. Contour interval at 0.075 eÅ⁻³.

the bond properties of the dimer differ significantly not only in the reaction region but also in the other parts of the molecule. The benzene ring, however, remains essentially unaffected upon dimerization. The mean ρ_{CP} of the benzene ring is $2.36 \text{ e}\text{\AA}^{-3}$ is slightly larger than that found in the α - and the γ -polymorphs. Considering that dimerization results in a non-planar structure (Fig.24), the ρ_{CP} of the C(1)—O(3) and O(3)—C(10) bonds are $2.28(8)$ and $2.32(6) \text{ e}\text{\AA}^{-3}$. The ρ_{CP} of C(6)—C(7) and C(8)—C(9) are typical of single bonds. The bonding within the carboxylic group resembles that in the α -form with ρ_{CP} values of $3.55(9)$, $2.83(9)$ and $2.6(2) \text{ e}\text{\AA}^{-3}$ for C(9)=O(1), C(9)—O(2) and O(2)—H(2A) respectively. The intermolecular O(2)—H(2A)···O(1) bond carries a small density of $\sim 0.18(8) \text{ e}\text{\AA}^{-3}$ with a Laplacian of $\sim 5.31(8) \text{ e}\text{\AA}^{-5}$ as in the α -form. The C—H···O contacts exhibit low densities (mean value $0.04 \text{ e}\text{\AA}^{-3}$) and small Laplacians as listed in Table 13. The cyclobutane ring resulting from the photodimerization of the α -form is shown in the inset of Fig.25. The ring exhibits a (3, +1) CP [5] at the inversion center with a density of $\sim 0.62 \text{ e}\text{\AA}^{-3}$ and a Laplacian of $\sim 5.8 \text{ e}\text{\AA}^{-5}$. The C—C bonds of the cyclobutane ring exhibit low values of ρ_{CP} and the Laplacians ($\sim 1.58 \text{ e}\text{\AA}^{-3}$ and $\sim -11.2 \text{ e}\text{\AA}^{-5}$ respectively), implying that the bonds are weak. The contours of the C(7)—C(8) and C(7A)—C(8A) bonds lie outside the interatomic vector. This indicates that the bonds are considerably bent [16] which is characteristic of strained rings [79,80]. The ellipticity values of the C(7)-C(8) and C(7)-C(8A) bonds are high (0.13 and 0.19 respectively) compared to an ideal single bond for which ellipticity is zero. The polarization associated with C(7)—C(8) bond is noticeably higher (8%) compared to C(7)—C(8A) which exhibits values characteristic of a single bond (1%). Probably, the eclipsing interactions between C(6) of the phenyl ring and C(9A) of the carboxylic group bring about subtle differences in bond lengths and polarization between the two pairs of bonds in the cyclobutyl ring.

Conclusions

The present study of the reactivity of *o*-ethoxy cinnamic acid has provided some fine details related to the solid state photoreactivity of this compound, involving (2+2) cycloaddition. The molecule in the reactive α -form is essentially planar, but in the γ -form, the side groups are out of the plane of the benzene ring.

The adjacent cinnamoyl double bonds in the α -form face each other at a favorable distance ($\sim 4.514 \text{ \AA}$) while in the γ -form, the double bonds are not only placed at a larger distance ($\sim 5.251 \text{ \AA}$) but are also not properly oriented with respect to each other. This is due to the significant differences between the structures in the two forms, the most noteworthy one being the presence of near-symmetric O—H \cdots O hydrogen bonds in the γ -form compared to the ordinary carboxylic dimer contacts in the α -form. The nature of the hydrogen bonds is confirmed by IR spectroscopy measurements. The O-H stretching frequency at $\sim 3000 \text{ cm}^{-1}$, common to carboxylic acid dimers, is not observed in the spectrum of the γ -form. Instead, two additional bands appear around 1600 cm^{-1} due to the symmetric hydrogen bond. The intermolecular C—H \cdots O contacts in the γ -form are considerably weakened due to the presence of the near-symmetric hydrogen bonded dimer.

There are also important differences in the charge density distribution between two forms. The molecule being planar in the α -form, effects due to conjugation are clearly seen in the charge density. The ρ_{CP} of the double bond is considerably smaller (2.27 e\AA^{-3}) compared to that in the γ -form (2.55 e\AA^{-3}). The ethoxy link to the phenyl ring carries some extra density due to charge migration from the ethoxy bond. Such effects are not observed in the case of the γ -form. The symmetric hydrogen bond of the latter being ionic, the molecule prefers a non-planar geometry. The cyclobutane ring formed by the dimerization is not exactly a square, the angular distortion being 1.8° . New C—C bonds are slightly longer compared to the other pair. The ring is strained, all the bonds being associated with small densities and Laplacians.

4.3 Photocoloration of p-nitrophenol

Molecular packing

The crystal packing in the β and α modifications is noticeably different. The β form crystallizes in the $P2_1/n$ space group, with the cell dimensions of $a=3.6812(3)$, $b=11.152(9)$, $c=14.6449(12)$ Å and $\beta = 92.804(2)^\circ$. We find no orientational relation of this cell with that of the α form [81], which occurs in the $P2_1/c$ space group with $a=6.1664(1)$, $b=8.8366(3)$, $c=11.5435(4)$ Å and $\beta = 103.390(1)^\circ$. Upon irradiation, the cell parameters are $a=6.1414(1)$, $b=8.8032(2)$, $c=11.5013(2)$ Å and $\beta = 103.338(1)$ (Table 14). The densities are comparable to those obtained by Coppens and Schmidt [82,83]. We find that the bond lengths and the angles are similar in both the alpha forms before and after the irradiation, though there are some small differences in their torsion angles involving the nitro groups. There exist small differences in the bond angles between the alpha and the beta forms in the nitro group region. The important structural differences between the irradiated α , pristine α and β forms are listed in the Table 14.

In Fig.26 we show the molecular packing diagrams of the p-nitrophenol in the after irradiation and have compared with those in the pristine α and β -forms. The adjacent nonparallel molecules subtend an angle of 74.58° compared to 74.73° in the pristine α form. The value of this angle in the β form is 29.26° [82,83]. The intermolecular hydrogen contacts also appear unaffected following irradiation. There are nine contacts as in the pristine α form (see Fig.26) with the $O(3)\cdots H(1)$ contact at ~ 1.88 Å being the shortest ($\angle O(3)\cdots H(1)-O(1) \sim 167^\circ$). It is interesting that the N and O(2) atoms of the same nitro group make weak contacts with H(1) at ~ 2.47 Å. As though to favor such an interaction, the H(1) atom is displaced from the phenyl plane by 0.29 Å. This value is 0.03 Å less than that found before irradiation. Other atoms N, O(2), O(3) and O(1) exhibit small displacements of 0.05, 0.05, 0.09 and 0.03 Å respectively, regardless of irradiation. In the β form however, the H(1) atom remains in the plane of the phenyl ring and it is the O(2) atom which shows the maximum displacement (0.22 Å). We find six hydrogen contacts in this structure with $O(3)\cdots H(1)$ as the main contact similar to that in the α structure except that the

Table 14
Important structural differences between the different forms of p-Nitrophenol

	Irradiated α	Pristine α	β
Unit cell parameters			
a (Å)	6.1414(1)	6.1664(1)	3.6812(3)
b (Å)	8.8032(2)	8.8366(2)	11.1152(9)
c (Å)	11.5013(2)	11.5435(2)	14.6449(12)
β (°)	103.338(1)	103.390(1)	92.802(2)
Space group	P2 ₁ /c	P2 ₁ /c	P2 ₁ /n
ρ (Mg m ⁻³)	1.527	1.510	1.544
Bond lengths (Å)			
N—O(2)	1.229(2)	1.237(1)	1.235(1)
N—O(3)	1.247(2)	1.251(1)	1.238(1)
\angle C—C—O inequality (°)	5.57	5.48	6.24
\angle C—C—N inequality (°)	0.96	1.2	0.31
Deviation from the plane of benzene ring (Å)			
O(1)	0.0296	0.03	0.046
H(1)	0.293	0.319	0.030
N	0.049	0.045	0.001
O(2)	0.044	0.043	0.221
O(3)	0.087	0.088	0.079
Shortest intermolecular hydrogen contact O(1) —H(1)···O(3)			
O(1)···O(3)	2.825(1)	2.832(1)	2.832(1)
H(1)···O(3)	1.881(1)	1.890(1)	1.909(1)
\angle O—H···O	167.1(1)	166.39(5)	160.55(6)

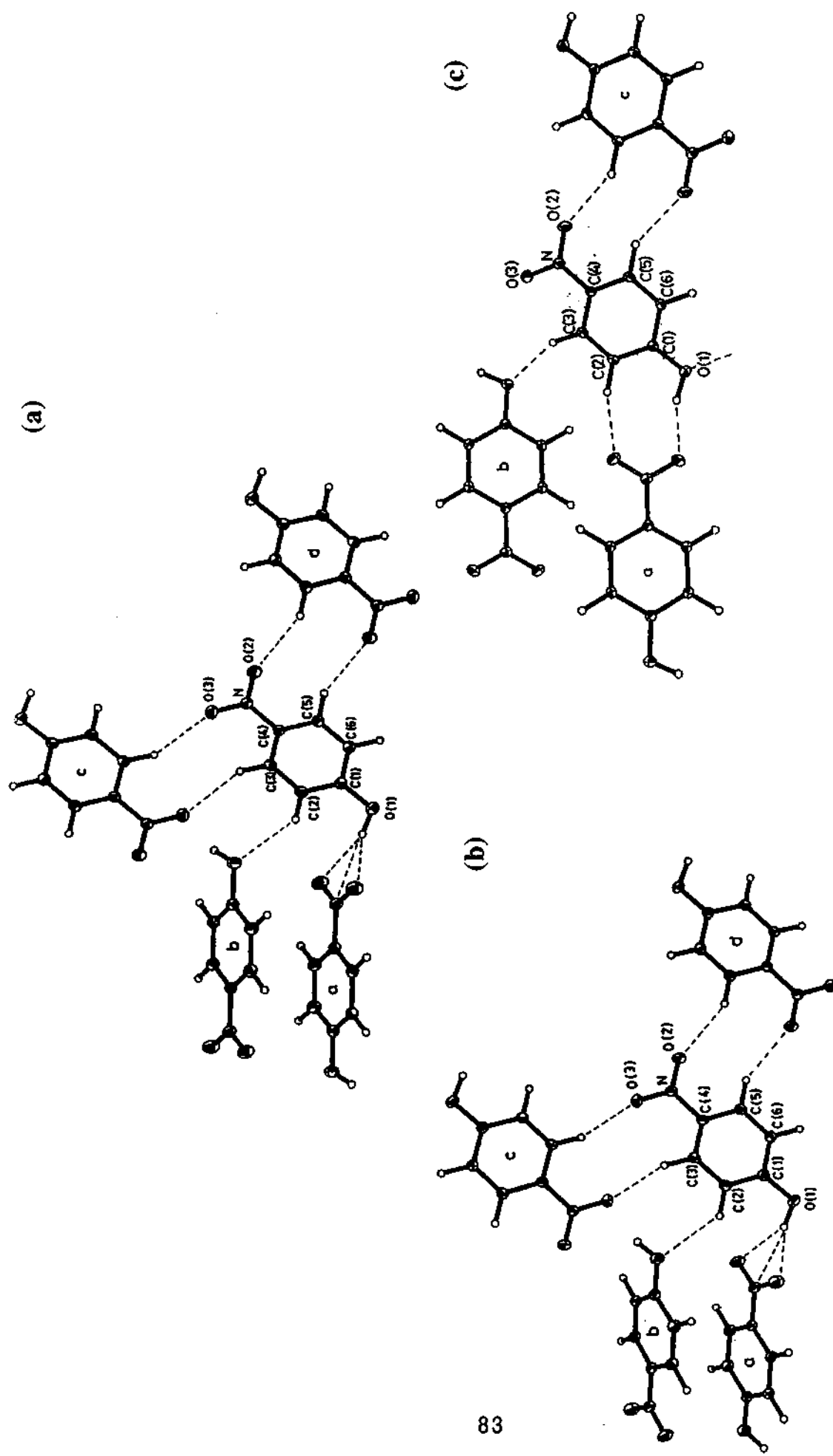


Fig.26. Molecular packing diagram in the plane of the phenyl ring in a) irradiated α , b) pristine α and c) β forms of *p*-nitrophenol. All non-hydrogen atoms are shown at 50% probability ellipsoids.

bond angle in this case is $\sim 160^\circ$ (see Fig. 26).

Charge density analysis

We shall first compare the intramolecular bonding in the irradiated and pristine α and the β -forms. The static deformation density, $\Delta\rho$, is shown in Fig.27 in the plane of the benzene ring. The deformation density due to bonding builds up as concentric contours in the regions of the C—C bonds of the benzene ring, the C—N bond, the N—O bonds of the nitro group as well as in the C—O and the O—H bonds of the hydroxyl group. The lone-pair of the oxygen atoms are also clearly seen in Fig.27. The residual density map was featureless, the magnitude of the random peaks being less than $0.12 \text{ e}\text{\AA}^{-3}$. The intramolecular CPs are found to be (3,-1) type, characteristic of a covalently bonded molecular system [6]. The ρ_{CP} of the six C-C bonds in the benzene ring vary in a rather narrow range, $2.05 - 2.19 \text{ e}\text{\AA}^{-3}$ (see Table 15) the mean value being $2.13 \text{ e}\text{\AA}^{-3}$. Following Cremer and Kraka [16], this corresponds to a mean bond order of 1.77, akin to those in aromatic rings. This value may be compared with that obtained before irradiation (1.70) and also that of the β form (2.02) [39]. The ellipticity ϵ , is slightly higher in the irradiated crystal (0.24) as compared to the pristine α polymorph (~ 0.21), but much lower than the theoretical value of 0.33. The homonuclear bonds are little polarized, some up to 12% due to perturbation caused by the two functional groups. The mean density in the C—H bond regions of the benzene ring is very similar to those obtained with the two polymorphs ($\sim 1.9 \text{ e}\text{\AA}^{-3}$) and is close to the theoretical density of $1.85 \text{ e}\text{\AA}^{-3}$. The polarity of the C—H bonds, Δ , is expected to be 26.6% towards hydrogen and we obtained a mean Δ value of 23.9%. A value of $\sim 21\%$ had been obtained for the pristine α and the β forms.

The C(1)—O(1) bond connecting the hydroxyl group to the benzene ring is associated with ρ_{CP} values of $2.12 \text{ e}\text{\AA}^{-3}$ corresponding to a bond order of 1.25. The pristine α and the β forms exhibit C-O bond orders of 1.23 and 1.43 respectively. The bond is polarized towards C(1) with $\Delta = 17.4\%$ in the irradiated crystal while the polarization is much higher in both the pristine α (22.9%) and the β forms (35.4%). The O(1)—H(1) bond region also exhibits noticeable differences (Table

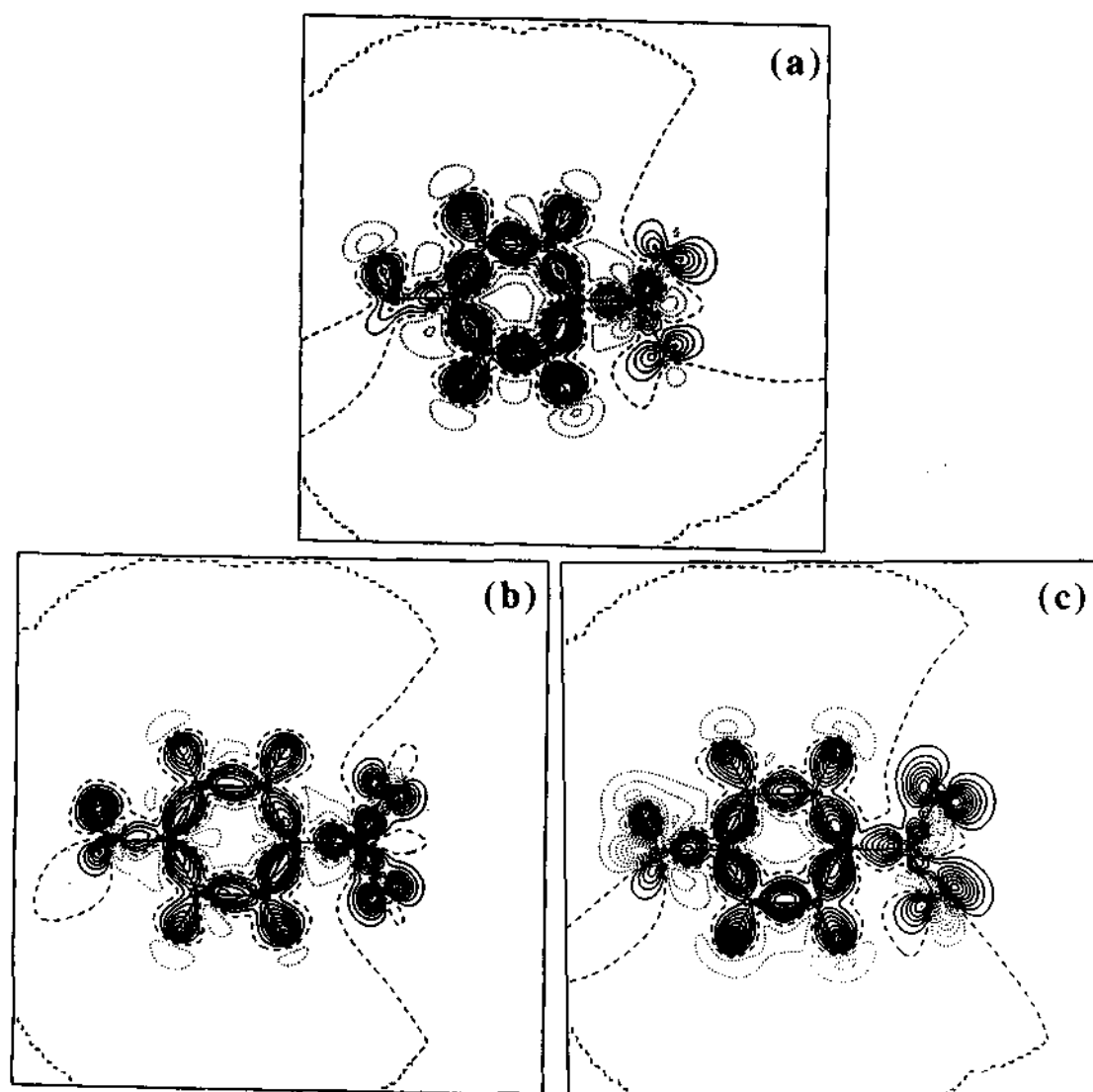


Fig.27. Static deformation density in the plane of the phenyl ring in a) irradiated α , b) pristine α and c) β forms of *p*-nitrophenol. Contours at $0.1 \text{ e}\text{\AA}^{-3}$

Table 15

Analysis of the bond critical points for the irradiated α (top row),
pristine α (middle row) and β (bottom row) forms

Bond	ρ	$\nabla^2\rho$	ϵ	$\Delta\%$	d
C(1)—C(2)	2.11(3)	-18.1(1)	0.28	8.8C(2)	0.021
	2.08(5)	-18.1(1)	0.27	1.5 C(2)	0.011
	2.21(5)	-22.4(2)	0.26	5.6 C(2)	0.014
C(2)—C(3)	2.19(3)	-19.8(1)	0.21	2.1C(3)	0.015
	2.09(5)	-18.0(1)	0.22	1.3 C(3)	0.005
	2.20(5)	-21.7(1)	0.24	4.0 C(2)	0.009
C(3)—C(4)	2.05(3)	-17.5(1)	0.22	2.5C(4)	0.013
	2.01(5)	-17.8(1)	0.21	5.3 C(3)	0.012
	2.24(5)	-23.0(2)	0.18	12.7 C(3)	0.016
C(4)—C(5)	2.14(3)	-18.9(1)	0.26	2.1C(4)	0.018
	2.20(5)	-19.4(1)	0.22	1.1 C(5)	0.014
	2.34(6)	-23.4(2)	0.19	5.1 C(5)	0.019
C(5)—C(6)	2.10(3)	-20.8(1)	0.22	12.8C(6)	0.018
	2.10(5)	-18.0(1)	0.18	3.9 C(5)	0.007
	2.35(6)	-24.2(2)	0.17	0.3 C(6)	0.018
C(6)—C(1)	2.17(3)	-21.6(1)	0.27	4.1C(1)	0.009
	2.04(5)	-18.4(1)	0.24	6.4 C(6)	0.008
	2.27(6)	-22.3(2)	0.22	6.4 C(6)	0.013
C(2)—H(2)	1.87(5)	-17.1(1)	0.04	23.1H(2)	0.021
	1.89(4)	-21.0(1)	0.07	20.0 H(2)	0.017
	1.89(5)	-16.6(2)	0.04	23.9 H(2)	0.015
C(3)—H(3)	1.88(6)	-18.5(2)	0.09	30.3H(3)	0.006
	1.97(4)	-20.2(1)	0.10	24.6 H(3)	0.007
	2.01(4)	-19.0(2)	0.12	20.9 H(3)	0.015
C(5)—H(5)	1.93(5)	-20.1(1)	0.09	18.1H(5)	0.002
	1.97(4)	-20.3(1)	0.06	18.5 H(5)	0.007
	1.96(4)	-19.9(2)	0.09	18.5 H(5)	0.014
C(6)—H(6)	1.85(5)	-17.1(1)	0.09	24.0H(6)	0.007
	1.82(3)	-17.7(1)	0.13	20.0 H(6)	0.017
	1.96(4)	-19.6(2)	0.14	19.3 H(6)	0.015
O(1)—C(1)	2.12(5)	-17.5(2)	0.13	17.4C(1)	0.027
	2.09(6)	-21.1(3)	0.05	22.9 C(1)	0.027
	2.32(6)	-20.0(3)	0.04	35.4 C(1)	0.022
O(1)—H(1)	2.40(10)	-42.4(7)	0.04	55.9H(1)	0.020
	2.91(6)	-45.2(6)	0.09	46.5 H(1)	0.041
	2.68(11)	-36.4(4)	0.14	47.7 H(1)	0.026
N—C(4)	1.80(3)	-12.3(1)	0.22	19.1C(4)	0.006
	1.78(5)	-14.0(2)	0.29	25.5 C(4)	0.016
	1.91(5)	-12.5(2)	0.20	17.2 C(4)	0.018
O(2)—N	3.15(6)	-2.3(2)	0.16	4.5N	0.004
	3.49(8)	-8.7(3)	0.14	2.1 N	0.009
	3.14(14)	2.5(4)	0.08	1.8 N	0.025
O(3)—N	3.18(6)	3.3(2)	0.12	1.2O(3)	0.006
	3.39(8)	5.0(3)	0.20	0.6 O(3)	0.006
	3.03(2)	10.6(5)	0.25	0.6 N	0.031

ρ ($e\text{\AA}^{-3}$) is the electron density, $\nabla^2\rho$ ($e\text{\AA}^{-5}$) is the Laplacian, ϵ is the ellipticity, Δ is the bond polarity in %, d (\AA) is the perpendicular distance between the critical point and the internuclear vector

15). The ρ_{CP} value in the α form decreases remarkably upon irradiation from 2.91 to 2.40 $\text{e}\text{\AA}^{-3}$. The β form exhibits a moderate density of 2.68 $\text{e}\text{\AA}^{-3}$. We notice that in all the cases, the CPs in the C(1)—O(1)—H(1) region deviate significantly ($d \sim 0.03 \text{ \AA}$) from the intermolecular vectors due to the bending of the orbitals, which is also reflected in the inequality of the C—C—O bond angles, a feature common to many other phenolic compounds [84].

The C(4)—N bond linking the nitro group to the benzene ring in the α form remains essentially unchanged on irradiation (bond order ~ 0.94) though bonding within the nitro group varies significantly. The irradiated crystal exhibits moderate densities of 3.15 and 3.18 $\text{e}\text{\AA}^{-3}$ in the N—O(2) and N—O(3) bond regions respectively as compared to the pristine α form (3.49 and 3.39 $\text{e}\text{\AA}^{-3}$ respectively) and the β form (3.14 and 3.03 $\text{e}\text{\AA}^{-3}$ respectively). We notice from Table 15 that some of the Laplacians in the nitro group are small positive numbers in contrast to the negative values observed in general for covalently bonded systems. This may be due to the higher ionicity of the nitro bonds.

In Table 16 we list the pseudoatom charges in the different forms. The group charges of NO_2 and OH of the irradiated crystal are -0.39 and 0.25 respectively. These values are quite different from those found before irradiation (-1.26 and -0.26 respectively) as well as from those of the β form [39] (-0.83 and 0.37 respectively). The charge distribution appears to be less polarized after irradiation.

The lone-pair electrons on the oxygen atoms of the nitro group occur as (3,-3) critical points in the deformation density [85] and show significant differences between the three cases. The mean total density at lone pair-CPs is $\sim 6.97 \text{ e}\text{\AA}^{-3}$ in the irradiated crystal compared to $\sim 7.6 \text{ e}\text{\AA}^{-3}$ and $\sim 5.5 \text{ e}\text{\AA}^{-3}$ in the pristine α and β forms respectively. We also find that the lone-pair lobes move slightly closer to the nucleus after irradiation by $\sim 0.02 \text{ \AA}$.

We have carried out critical point analysis along the hydrogen contacts and found the presence of small densities associated with small, positive Laplacians. These observations imply a closed shell interaction typical of intermolecular

Table 16
Pseudoatomic charges

ATOM	Irradiated α	Pristine α	β
O(1)	-0.08(7)	-0.29(10)	-0.09(9)
O(2)	-0.10(8)	-0.36(10)	-0.14(9)
O(3)	-0.04(9)	-0.30(10)	-0.22(9)
N	-0.25(20)	-0.60(22)	-0.47(21)
C(1)	-0.06(8)	0.29(13)	0.00(13)
C(2)	-0.08(7)	0.32(12)	-0.01(12)
C(3)	-0.15(7)	0.30(13)	-0.08(13)
C(4)	0.00(7)	0.21(11)	-0.49(13)
C(5)	-0.13(7)	0.20(13)	-0.06(12)
C(6)	0.04(7)	0.30(12)	-0.10(12)
H(1)	0.33(6)	0.03(11)	0.46(6)
H(2)	0.11(5)	0.03(11)	0.32(7)
H(3)	0.20(5)	-0.02(11)	0.30(7)
H(5)	0.11(5)	-0.06(11)	0.30(7)
H(6)	0.12(5)	0.02(10)	0.27(8)

hydrogen bonding [6]. The structural features of the intermolecular hydrogen bonding remained similar before and after irradiation. The α form exhibits a density of $0.19 \text{ e}\text{\AA}^{-3}$ with the shortest contact (O(3)···H(1)). Following irradiation, the density decreases to $0.11 \text{ e}\text{\AA}^{-3}$ much like that obtained for the same contact in the β form. There are some differences in weaker contacts as well (see Table 17). An interesting feature in the α structure is that a common critical point is present with a density of $\sim 0.016 \text{ e}\text{\AA}^{-3}$ for the N···H(1) and O(2)···H(1) contacts, providing evidence for the participation of the entire nitro group in hydrogen bonding with H(1). The density at the common critical point increases marginally after irradiation. These intermolecular hydrogen bond interactions are represented using relief maps of the negative Laplacian. We show such maps in Fig.28, for the α form before and after irradiation, in the plane of the oxygen atoms of the nitro and the hydroxyl groups involved in the intermolecular bonding. We see from the figure that the oxygen lone-pair lobes are polarized in the direction of the hydrogen atom. We find that the relief map resembles that of the pristine α form in that the hydroxyl group appears to have rotated and moved closer to the nitro group compared to the situation in the β form [39]. However, the lone-pair polarization as well as the magnitude of the hydrogen peak is much less, similar to the β form.

Conclusions

The structure of the parent α form of p-nitrophenol shows only marginal changes on turning red. Small differences are observed in the intermolecular hydrogen contacts. On the contrary, the deformation density map of the irradiated crystal modification of the α form resembles more closely that of the β form than that of the pristine α form. The densities at the bond CPs in the nitro group region are much like the values obtained with the β form. The density on the hydroxyl bond is far less than that observed before irradiation. The density at the oxygen lone-pairs decreases following irradiation and the contours resemble more like those in the β form. The charge appears to migrate outwardly from the benzene ring to the nitro and the hydroxyl groups when the crystal structure changes from β to α . On irradiation, the charge migrates inwardly and the distribution becomes more even across the whole molecule.

Table 17
Intermolecular Hydrogen bond critical points

Bond	Bond length	\angle donor-H...acceptor	ρ	$\nabla^2\rho$
Irradiated α				
O(2)···H(1 ^a)	2.466(2)	131.75(1)	0.03(1)	0.946(1)
O(3)···H(1 ^a)	1.881(1)	167.10(1)	0.11(4)	3.07(3)
N···H(1 ^a)	2.466(1)	157.48(9)	0.03(1)	0.948(1)
O(1)···H(2 ^b)	2.498(1)	132.2(1)	0.039(9)	0.804(2)
O(3)···H(3 ^c)	2.603(1)	130.60(8)	0.030(4)	0.499(2)
O(2)···H(5 ^d)	2.392(1)	145.96(8)	0.018(7)	0.600(3)
Pristine α				
O(2)···H(1 ^a)	2.461(1)	133.24(5)	0.016(13)	0.897(8)
O(3)···H(1 ^a)	1.890(1)	166.39(5)	0.19(3)	2.43(4)
N···H(1 ^a)	2.467(1)	159.46(5)	0.016(13)	0.897(8)
O(1)···H(2 ^b)	2.509(1)	132.14(4)	0.029(9)	0.814(6)
O(3)···H(3 ^c)	2.617(1)	130.74(4)	0.035(5)	0.562(2)
O(2)···H(5 ^d)	2.406(1)	145.71(4)	0.040(10)	0.890(9)
Symmetry codes: a) $x+1, -y+1/2, z+1/2$; b) $-x, y-1/2, -z-1/2$; c) $-x+1, -y+1, -z$; d) $-x+2, -y, -z$				
β				
O(2)···H(2 ^a)	2.382(1)	143.34(6)	0.076(14)	1.147(10)
O(3)··· H(1 ^a)	1.909(1)	160.55(6)	0.11(3)	4.66(5)
O(1)···H(3 ^b)	2.345(1)	157.26(6)	0.039(13)	0.66(1)
O(2)···H(5 ^c)	2.400(1)	139.89(5)	0.007(8)	0.257(4)
Symmetry codes: a) $x-1/2, -y+1/2+1, Z+1/2$; b) $-x+1/2, y-1/2, -x+1/2+1$; c) $-x-1, -y+1, -z+2$				

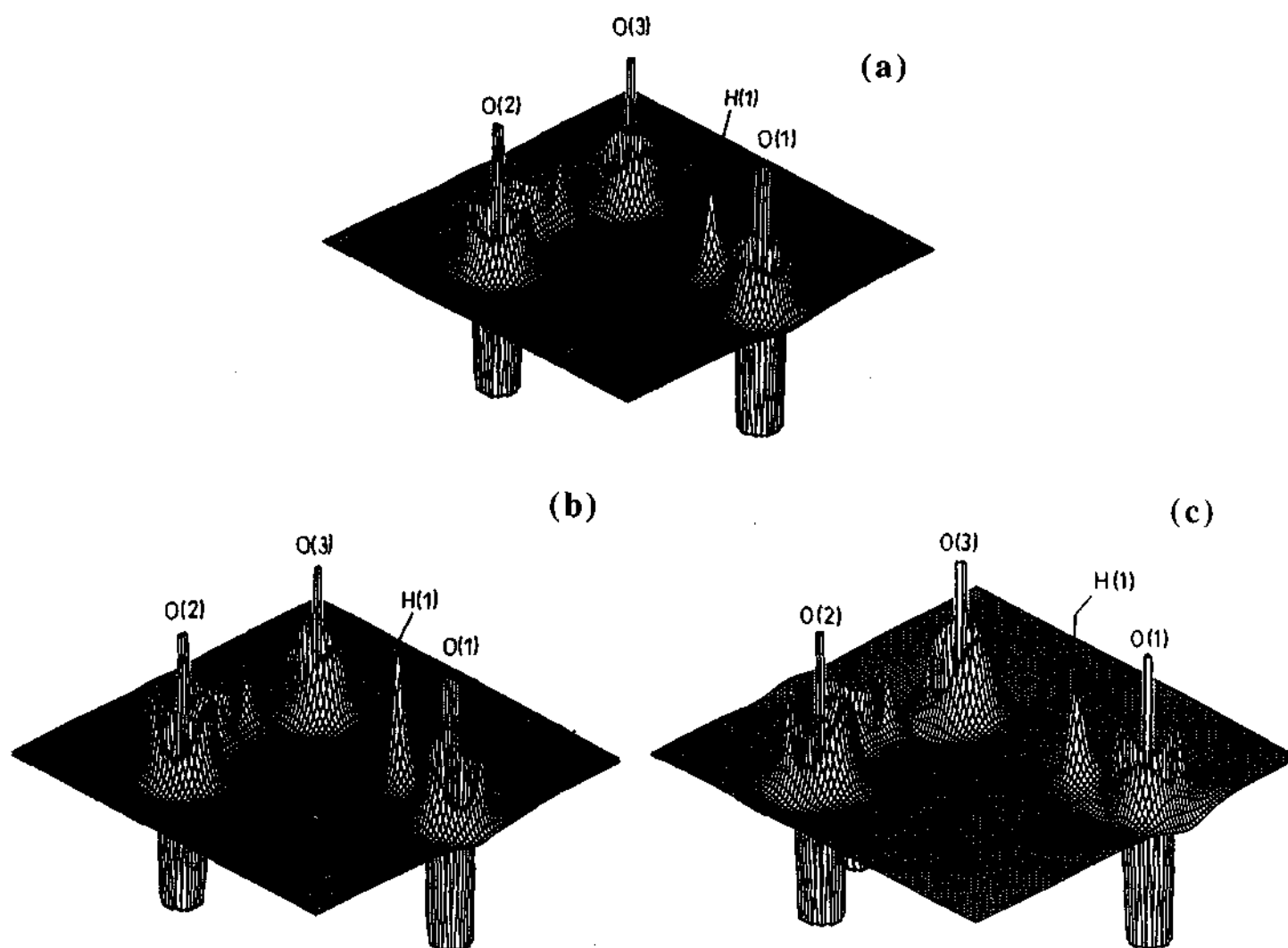


Fig.28. Relief maps of the negative Laplacian in the plane of the hydrogen bond (range -250 to $250 \text{ e}\text{\AA}^{-5}$) in a) irradiated α , b) pristine α and c) β forms of *p*-nitrophenol.

Photoreactivity of a molecule in a given structure depends on the local bonding and approach of the neighboring molecules. As shown in section 4.2, a (2+2) addition involves a vivid change of structure both molecular and of the lattice. On the other hand, the photochemical activity in *p*-nitrophenol is gentle in that the structural changes are hardly visible. However, the electron density distribution changes noticeably. Thus, structure in combination with charge density analysis provides a powerful tool to investigate such systems. The above studies have also shed light on the nature of bonding and molecular geometry in light-stable polymorphs.

4.4 Properties of a series of aliphatic dicarboxylic acids

Structural aspects

While malonic acid crystallizes in a triclinic cell, the higher members occurⁿ in the monoclinic system (Table 18). The crystal density decreases gradually along the series from 1.66 g/cm⁻³ in malonic to 1.37 g/cm⁻³ in pimelic acid. In general, there is good agreement between the structures obtained by us and those reported earlier in the literature [86-92], except that we do not observe any alternation in the bond lengths of the even members. We shall briefly summarize the important results from the structural study. In Fig.29, we show the molecular diagrams of the acids along with the bond distances derived from our study. At room temperature, the even members possess a center of inversion in the central C—C bond while the odd members other than malonic exhibit a two-fold rotational symmetry about the central carbon atom. The molecular symmetry is a direct consequence of the all-trans arrangement of the carbon backbone. Accordingly, succinic and adipic acids adopt the P2(1)/c space group while glutaric and pimelic acids crystallize in the C2/c space group. The backbone is generally non-planar, except in the case of succinic acid. Malonic acid is the most asymmetric of the acids studied here, with the two carboxylic groups making an angle of ~85° to avoid the close approach of the oxygens. The value of this angle in glutaric and pimelic acids is ~62°. By virtue of the symmetry, the carboxylic groups are parallel in the even acids. The bond between the carboxylic carbon and the backbone is ~1.51 Å in malonic acid and decreases only by a small value (0.01 Å) along the series. The C—C bond connecting to the carboxylic group is shorter by ~0.03 Å compared to the inner C—C bonds, the latter attaining the ideal value of 1.54 Å only in higher members. The C—C—C bond angles of the backbone deviate by as much as 5° from the ideal tetrahedral value except in the case of the glutaric acid.

The O—H...O hydrogen bonds between carboxylic groups are the strongest intermolecular bonds in all the acids with bond lengths around 1.7 Å and the O—H...O angles ~ 170° (Table 19). Each dicarboxylic acid molecule is linked by two dimeric units in the lattice. Some examples are shown in Fig.30. Besides the O—H...O bonds, we find several C—H...O contacts with the most favorable ones at

Table 18
Crystal structure data of aliphatic dicarboxylic acids

Compound	Malonic	Succinic	Glutaric	Adipic	Pimelic
Chemical Formula	C ₃ H ₄ O ₄	C ₄ H ₆ O ₄	C ₅ H ₈ O ₄	C ₆ H ₁₀ O ₄	C ₇ H ₁₂ O ₄
Formula weight	104.06	118.09	132.12	146.15	160.18
Cell setting	Triclinic	Monoclinic	Monoclinic	Monoclinic	Monoclinic
Space group	P -1	P 2(1)/c	C 2/c	P 2(1)/c	C 2/c
a (Å)	5.1618(1)	5.4773(1)	12.9802(2)	7.184(1)	17.7190(2)
b (Å)	5.3321(1)	8.7897(1)	4.7555(1)	5.1575(7)	4.7303(1)
c (Å)	8.1947(2)	5.0269(1)	9.7045(2)	9.995(1)	9.6703(1)
α (°)	108.113(1)	90.000	90.000	90.000	90.000
β (°)	101.285(1)	92.905(1)	98.286(1)	110.875(3)	106.643(1)
γ (°)	95.257(1)	90.000	90.000	90.000	90.000
ρ (Mg m ⁻³)	1.660	1.623	1.480	1.403	1.370
μ (mm ⁻¹)	0.16	0.15	0.13	0.12	0.11
Crystal size (mm)	0.5 x 0.3 x 0.5	0.6 x 0.5 x 0.4	0.4 x 0.5 x 0.3	0.4 x 0.5 x 0.4	0.5 x 0.4 x 0.3
Crystal color	Colorless	Colorless	Colorless	Colorless	Colorless
Data collection					
Diffractometer	Siemens CCD				
Radiation type	Mo Kα				
Wavelength (Å)	0.71073				
Crystal-detector distance (cm)	5.0				
Temperature (K)	130	130	130	145	130
No. of measured reflections	4368	4445	5145	5069	5194
No. of independent reflections	3883	2122	2446	2735	3387
No. of observed reflections	2098	1940	1929	1785	2655
R _{merge}	0.0334	0.0203	0.0307	0.0311	0.0470
R _{int}	0.0301	0.0171	0.0329	0.0631	0.0416
θ _{max} (°)	49.32	50.12	49.58	49.51	49.41
Range of h, k, l	-10 ≤ h ≤ 10	-9 ≤ h ≤ 10	-27 ≤ h ≤ 27	-12 ≤ h ≤ 15	-34 ≤ h ≤ 37
	-10 ≤ k ≤ 11	-18 ≤ k ≤ 12	-9 ≤ k ≤ 9	-10 ≤ k ≤ 7	-6 ≤ k ≤ 9
	-12 ≤ l ≤ 17	-11 ≤ l ≤ 10	-13 ≤ l ≤ 20	-18 ≤ l ≤ 12	-20 ≤ l ≤ 8
Refinement					
Refinement on F ²					
R(F)	0.0419	0.0283	0.0293	0.0311	0.0433
wR(F ²)	0.1258	0.0457	0.0505	0.0631	0.0797
S	1.6	1.7	0.8	0.9	0.8
No. of reflections used in the refinement	1899	3202	2482	1541	2390
No. of parameters refined	196	123	161	161	205

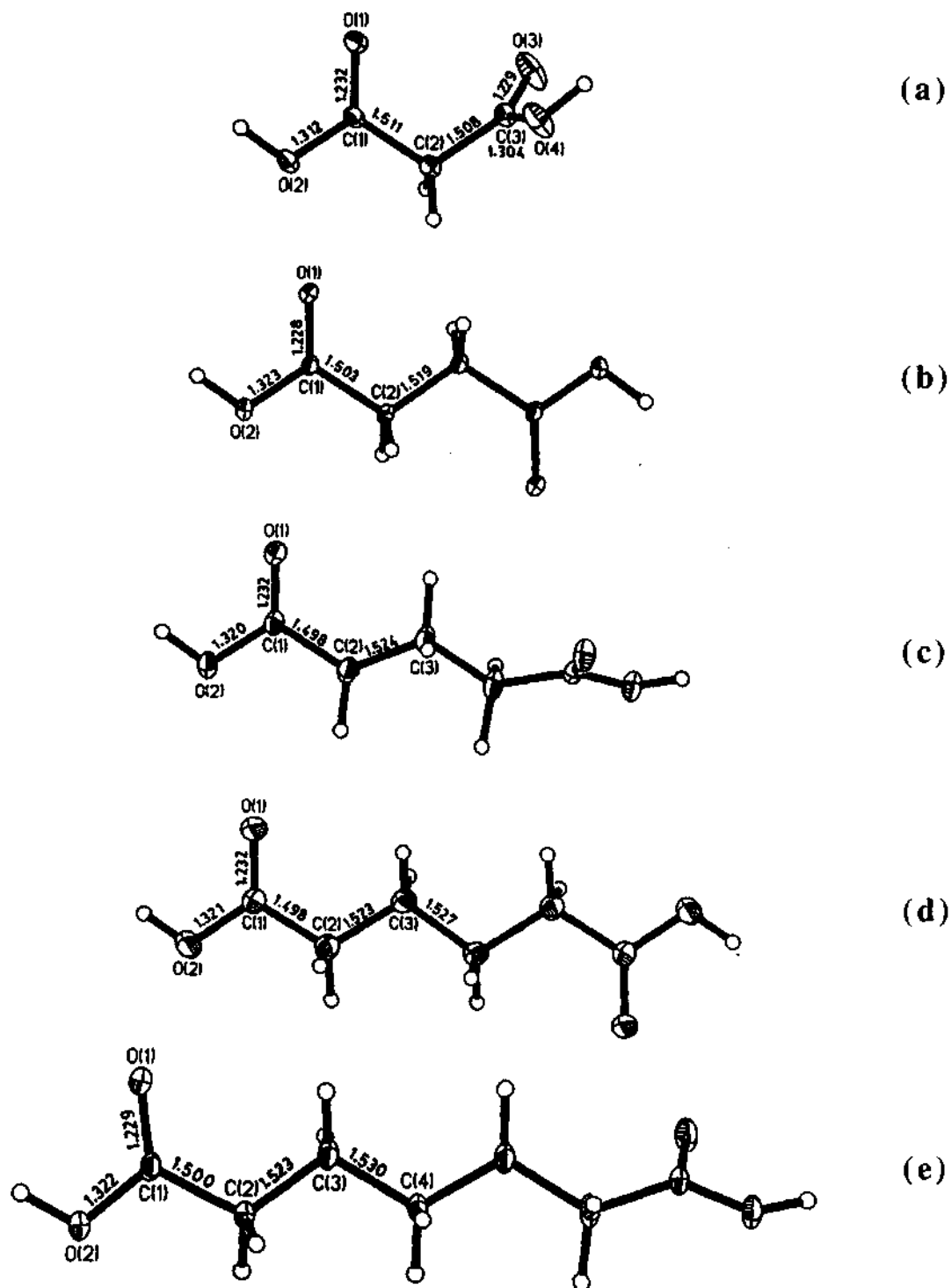


Fig.29. Molecular diagrams showing thermal ellipsoids and interatomic bond lengths for a) malonic, b) succinic, c) glutaric, d) adipic and e) pimelic acids.

Table 19
Structural parameters and charge densities of the hydrogen bonds in dicarboxylic acids

Acids	Bond	Distance (Å)	Angle (°)	ρ (eÅ ⁻³)	$\nabla^2\rho$ (eÅ ⁻⁵)
Malonic	O(2)—H(2)⋯O(1) ^a	1.722(1)	168.7(1)	0.19(5)	4.58(5)
	O(4)—H(4)⋯O(3) ^b	1.717(2)	178.0(1)	0.32(5)	4.58(4)
	O(2)—H(2)⋯O(3) ^c	2.694(1)	111.4(1)	0.025(4)	0.477(3)
	O(4)—H(4)⋯O(1) ^d	2.919(1)	108.6(1)	0.013(4)	0.298(3)
	C(2)—H(2B)⋯O(1) ^e	2.855(1)	112.6(1)	0.030(4)	0.467(3)
	C(2)—H(2B)⋯O(2) ^e	2.545(1)	163.8(1)	0.041(9)	0.737(5)
Succinic	O(2)—H(2)⋯O(1) ^f	1.715(1)	175.9(1)	0.12(6)	5.90(7)
	C(2)—H(2A)⋯O(1) ^g	2.813(1)	127.9(1)	0.020(4)	0.337(3)
	C(2)—H(2A)⋯O(2) ^h	2.710(1)	126.5(1)	0.024(5)	0.426(3)
	C(2)—H(2B)⋯O(1) ⁱ	2.595(1)	165.0(1)	0.021(9)	0.49(4)
Glutaric	O(2)—H(2)⋯O(1) ^j	1.708(1)	171.5(1)	0.13(6)	4.90(5)
	C(2)—H(2A)⋯O(1) ^k	2.733(1)	123.6(1)	0.018(2)	0.260(2)
	C(2)—H(2A)⋯O(1) ^l	2.693(1)	142.7(1)	0.014(3)	0.230(2)
	C(2)—H(2B)⋯O(2) ^m	2.633(1)	151.8(1)	0.010(1)	0.164(1)
	C(3)—H(3A)⋯O(2) ⁿ	2.978(1)	129.4(1)	0.010(1)	0.142(1)
Adipic	O(2)—H(2)⋯O(1) ^o	1.685(2)	174.1(1)	0.11(7)	10.90(9)
	C(2)—H(2A)⋯O(2) ^p	2.709(1)	107.0(1)	0.020(7)	0.504(5)
	C(3)—H(3A)⋯O(2) ^p	2.783(1)	118.9(1)	0.039(9)	0.552(7)
	C(3)—H(3B)⋯O(1) ^r	2.863(1)	119.6(1)	0.017(9)	0.269(6)
Pimelic	O(2)—H(2A)⋯O(1) ^s	1.710(1)	169.4(1)	0.26(6)	4.19(6)
	C(2)—H(2A)⋯O(1) ^t	2.662(1)	149.1(1)	0.032(9)	0.522(7)
	C(2)—H(2A)⋯O(2) ^u	2.724(1)	142.1(1)	0.030(9)	0.485(7)
	C(2)—H(2B)⋯O(1) ^v	2.754(1)	127.1(1)	0.034(9)	0.514(5)
	C(3)—H(3B)⋯O(1) ^w	2.946(1)	174.4(1)	0.015(7)	0.250(5)
	C(4)—H(4B)⋯O(1) ^x	2.713(1)	151.4(1)	0.011(9)	0.406(4)

Symmetry: a) 1-x,1-y,-z; b) 1-x,3-y,1-z; c) 1-x,2-y,-z; d) 1-x,2-y,1-z; e) 2-x,2-y,-z; f) -x,1-y,2-z; g) 1+x,y,z; h) 1/2+x,3/2-y,z; i) 1/2-x, 1/2+y, 1-z; j) 1/2-x,-1/2-y,1-z; k) x,1+y,z; l) -x,-y,1-z; m) 1/2-x,1/2+y,3/2-z; n) -1/2+x,-1/2+y,z; o) -x,1-y,2-z; p) 3/2-x, -1/2+y,-z; r) 5/2-x,1/2+y,-z; s) 1/2-x,3/2-y,-z; t) x,1-y,1/2+z; u) 1/2-x,1/2+y,1/2-z; v) x,y- 1,z; w) x,2-y,1/2+z

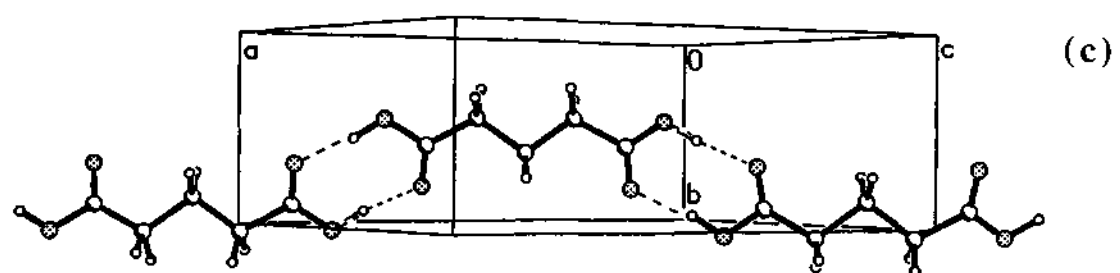
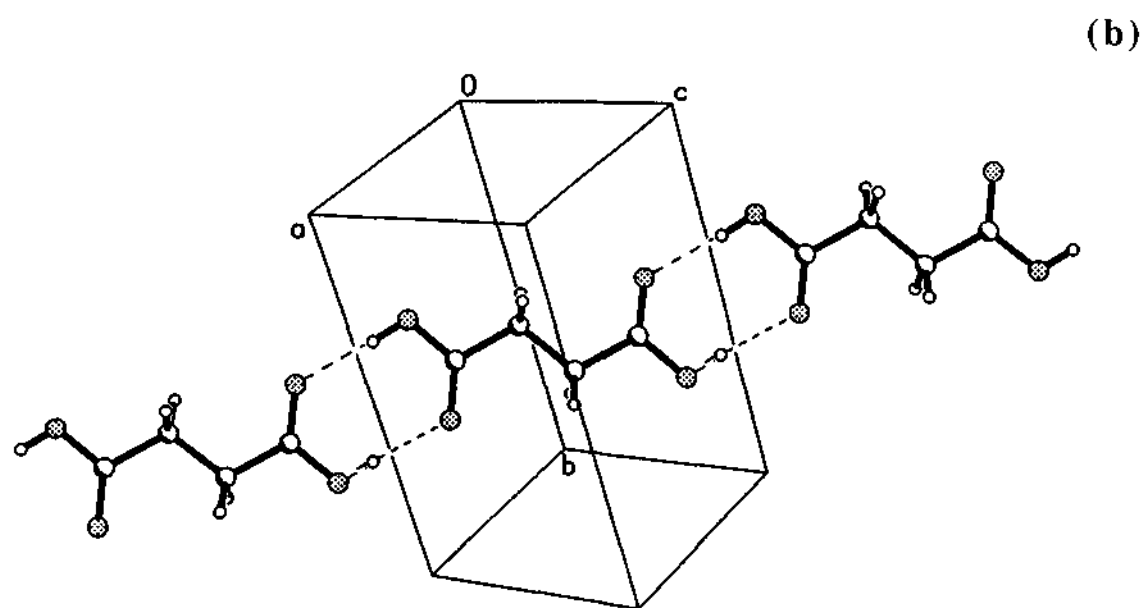
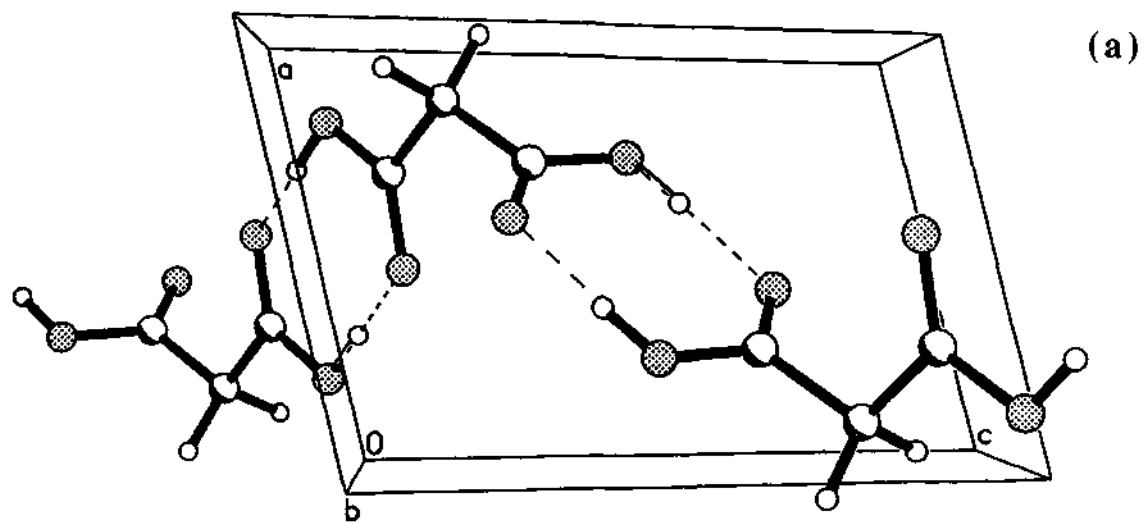


Fig.30. Dimeric hydrogen bonding in a) malonic b) succinic and c) glutaric acids.

$\sim 2.6 \text{ \AA}$ with an angle $\sim 165^\circ$ (see Table 19). In Malonic acid, in addition to the acid dimeric contacts, there are two more $\text{O—H}\cdots\text{O}$ bonds with the neighboring molecules.

Charge density analysis

In Fig.31, we show the static deformation density maps of the dicarboxylic acids close to the mean plane of the molecules. The static deformation density was obtained as the difference between the total density and the spherical density without thermal smearing. In these maps, we observe the bonding electron density as concentric contours along each bond [93,7], though the shape varies considerably along the series. The oxygen lone-pair lobes are also distinctly visible in the maps. As malonic acid is highly asymmetric, the deformation density of the molecule is shown in two parts (Fig.31a and 31b). The succinic molecule being planar exhibits symmetric contours in the map (Fig.31c) along the different bonds. The contours are somewhat denser in glutaric and adipic acids (Fig.31d and 31e). The deformation density of the pimelic acid is shown in Fig.31f. The contours around the central carbon atom are typical of a tetrahedral carbon [94].

We have examined bonding in the dimeric hydrogen bond regions using relief maps of the negative Laplacians. We show the relief maps from the different dicarboxylic acids in Fig.32. Here, the atom positions are marked by the sharp peaks in the plane of hydrogen bonding since they occur as (3,-3) critical points in ρ [6]. The hydrogens involved in hydrogen bonding are well in the dimeric plane except in the case of malonic and pimelic acids (see Fig.32a and f respectively). The oxygen lone-pairs are seen as lobes at a distance of $\sim 0.25 \text{ \AA}$ surrounding the core. The lone pairs are generally polarized in the direction of the hydrogen bond, particularly in the case of even acids (Fig.32c and d). In pimelic acid (Fig.32f), the lobes are somewhat diffuse. The small curved surface between the carbonyl oxygen of one molecule to the hydroxylic hydrogen of another molecule signifies intermolecular hydrogen bonding in the dimeric unit. Accordingly, we observe small electron densities as well as positive Laplacians at the critical points as shown in Table 19 [7]. The end members, malonic and pimelic acids, exhibit slightly higher values of ρ_{CP} ($\sim 0.3 \text{ e\AA}^{-3}$) compared to the other members of the series. Malonic acid shows

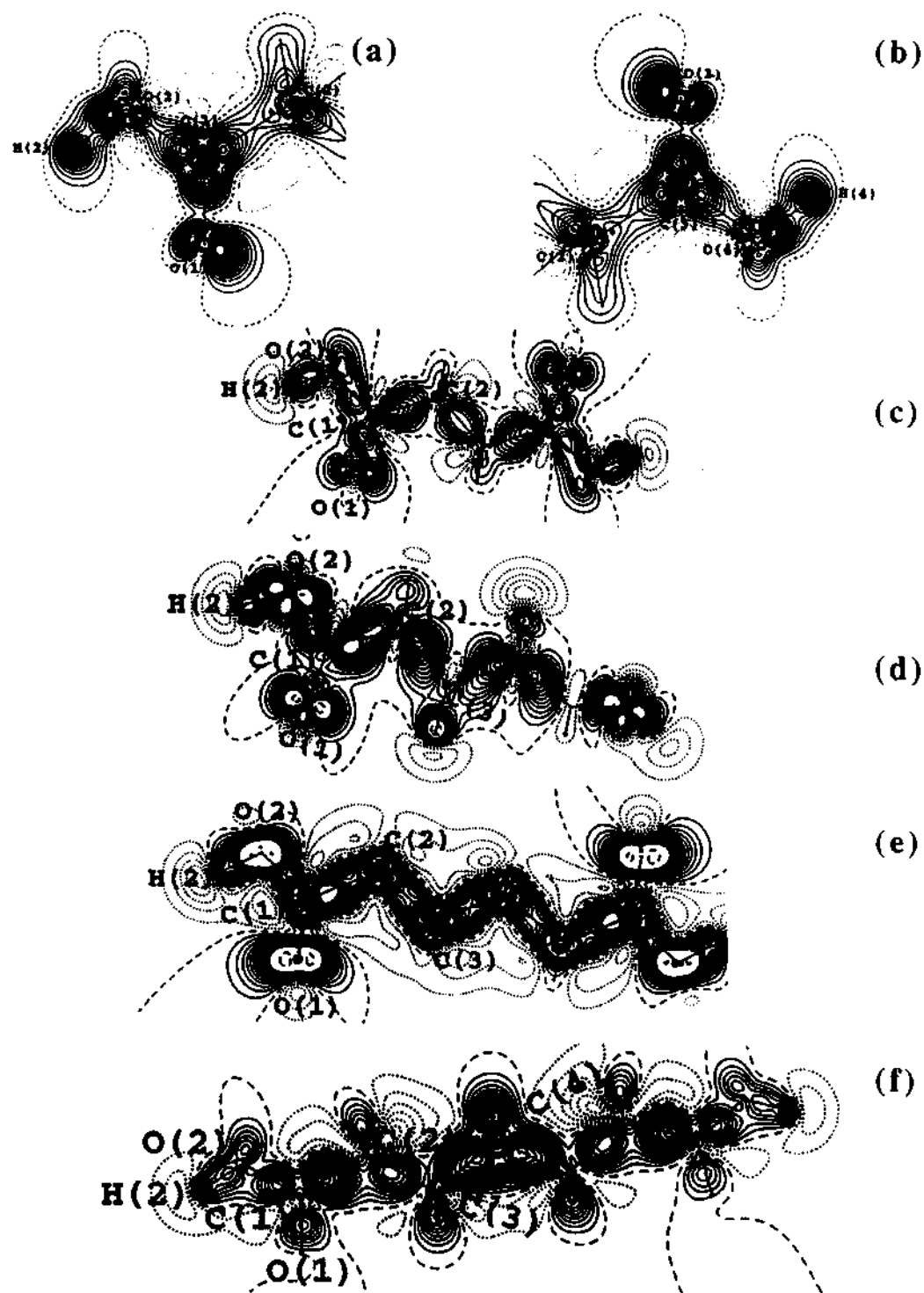


Fig.31. Static deformation density in the mean molecular plane for a) and b) malonic, c) succinic, d) glutaric, e) adipic and f) pimelic acids. Contour intervals at $0.075 \text{ e}\text{\AA}^{-3}$.

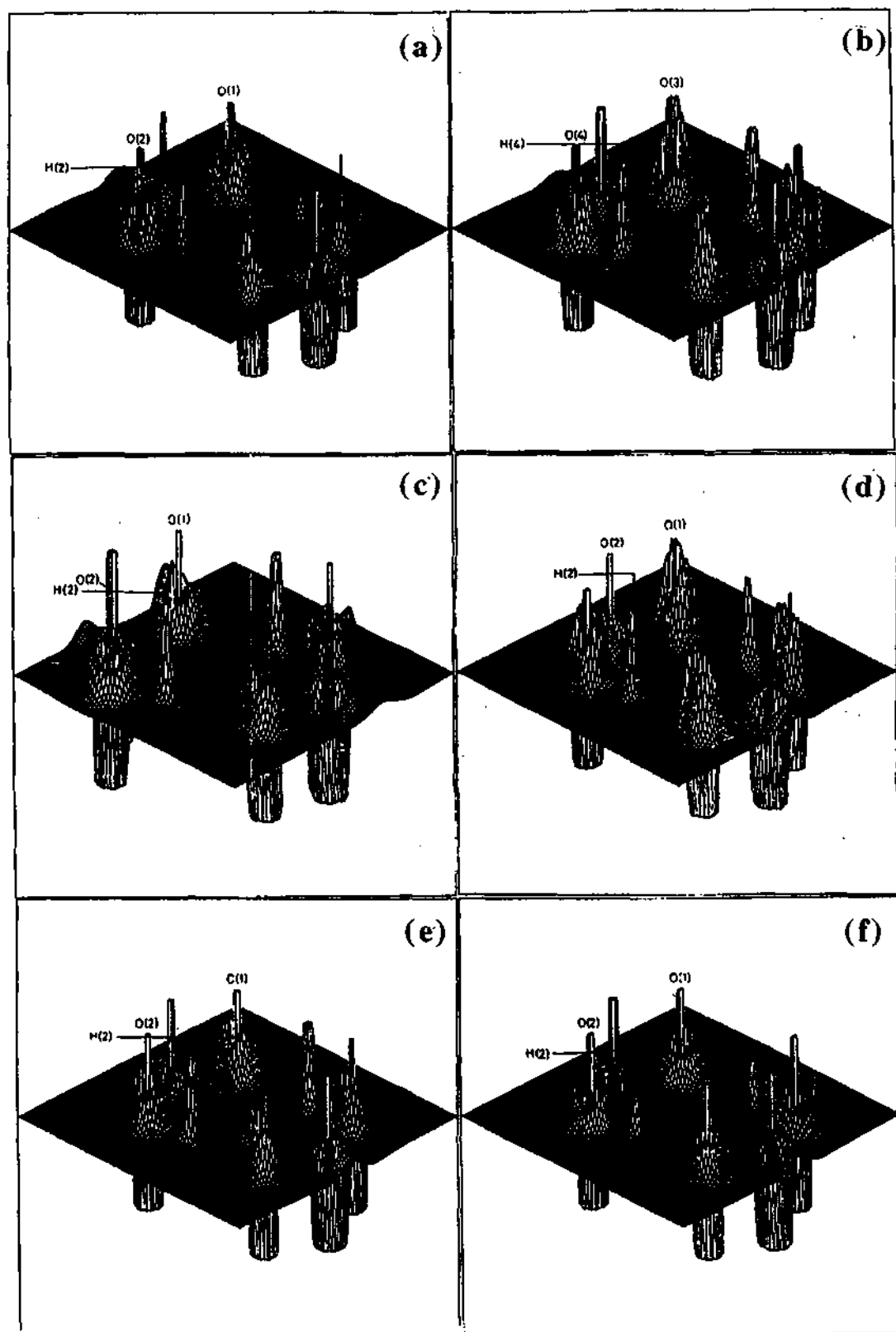


Fig.32. Relief map of the negative Laplacian in the plane of the acid dimeric unit for a) and b) malonic, c) succinic, d) glutaric, e) adipic and f) pimelic acids. Range, -250 to $250 \text{ e}\text{\AA}^{-5}$.

two distinctly different values of ρ_{CP} corresponding to the different dimeric hydrogen bonds present [95], the value being rather large for one of the dimers.

In order to make a systematic study of this homologous series of acids, we have compared the bond lengths and the charge densities of various intramolecular bonds in Table 20. We observe some systematics in the charge densities along the series although the changes in the bond lengths are minimal. The average value of ρ_{CP} for the C—C bonds increases from $1.61 \text{ e}\text{\AA}^{-3}$ in malonic acid to $2.09 \text{ e}\text{\AA}^{-3}$ in glutaric acid, and decreases thereafter. A similar trend is seen in the ρ_{CP} of the C—O and O—H bonds. Interestingly in the case of the C=O and the C—H bonds, an opposite trend is observed. The ρ_{CP} of the C=O bond shows a minimum value of $2.33 \text{ e}\text{\AA}^{-3}$ for glutaric acid, the values on either side of the series being close to $3 \text{ e}\text{\AA}^{-3}$. Moreover in glutaric acid, this value is less than that obtained for the C—O bond ($2.72 \text{ e}\text{\AA}^{-3}$). Clearly, there is an extensive redistribution of charge density among the various bonds, while the interatomic distances seemingly remain rigid.

An overall assessment of the charge distribution among the various bonds can be made by plotting the Laplacian against the density [70] as is shown in Fig.33. We see from this figure that most of the bonds lie in a region where the Laplacian is roughly proportional to the bond density, as one would normally expect. We also observe that like-bonds lie together along a linear region. In Fig.33, the different regions corresponding to C—C, C—H, C—O, O—H and C=O bonds have been delineated. The $\nabla^2\rho - \rho$ plot provides an indication of the bond order and the relative electronegativities of the bonded atoms. Thus, the C—C and the C—H bonds fall in the first region of the plot while the C—O and the O—H bonds group in the second region. The C=O bonds are found in the third region. The C—O and the C=O bonds of the malonic and the glutaric acids are somewhat abnormal. In the case of the malonic acid, the Laplacians of the two bonds are noticeably lower. In glutaric acid on the other hand, the Laplacian of the C=O bond is lower than that of the C—O bond, a trend which is reflected in their charge densities as well (see Table 20).

Inter-chain interactions seem to play an important role in determining the properties of the dicarboxylic acids. We have carried out a careful CP search

Table 20

Interatomic distances, r (Å), and intramolecular bond charge densities, ρ_{cp} ($e\text{Å}^{-3}$) in dicarboxylic acids^(a)

Acids	$(C-C)_{av}$		C_b-C_c		$C_c=O_k$		C_c-O_h		$(C-H)_{av}$		O_h-H_h	
	R	ρ	r	ρ	r	ρ	R	ρ	r	ρ	r	ρ
Malonic	1.509	1.61	1.509(1)	1.64(6)	1.228(1)	3.0(1)	1.306(1)	2.25(10)	1.06	1.90	0.96	2.4(1)
			1.507(2)	1.58(7)	1.226(2)	2.9(1)					1.311(2)	2.5(1)
Succinic	1.503	1.88	1.503(1)	1.88(4)	1.228(1)	2.75(5)	1.323(1)	2.36(5)	1.06	1.77	0.96	2.4(1)
Glutaric	1.511	2.09	1.498(1)	2.24(3)	1.232(1)	2.33(6)	1.320(1)	2.72(4)	1.06	1.66	0.96	2.7(1)
Adipic	1.510	1.93	1.498(3)	2.12(5)	1.232(3)	2.6(1)	1.321(2)	2.36(8)	1.06	1.90	0.96	2.4(1)
Pimelic	1.518	1.74	1.500(1)	1.87(5)	1.229(1)	3.1(1)	1.322(1)	2.29(6)	1.06	1.8	0.96	2.1(1)

^(a) $(C-C)_{av}$, average C—C in the backbone;
 C_b , the backbone carbon;
 C_c , carboxyl carbon;
 O_k , ketonic carbon;
 O_h , hydroxyl hydrogen;
 C_b , backbone linkage

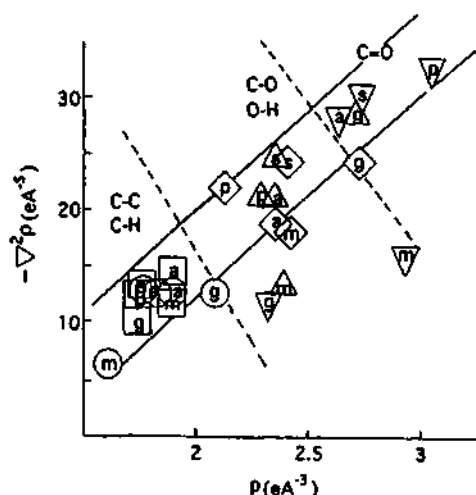


Fig.33. Variation of $\nabla^2\rho_{cp}$ with ρ_{cp} for various bonds, C-C, circle; C-H, square; C-O, uptriangle, C=O, down triangle and O-H, rhombus. The letters m, s, g, a and p marked inside the data symbols represent bonds belonging to malonic, succinic, glutaric, adipic and pimelic acids, respectively. The different bond regions are delineated lines.

analysis on a number of interchain C—H...O contacts and the results are tabulated in Table 19 along with the O—H...O contacts. The C—H...O contacts ($\rho_{cp} \sim 0.04 \text{ e}\text{\AA}^{-3}$) are considerably weaker as compared to the acid dimeric contacts. Malonic acid exhibits only two C—H...O contacts, while succinic and adipic acids make six such contacts. The number of C—H...O contacts in glutaric and pimelic acids is eight and ten respectively. In order to compare the various acids, we have calculated the total density associated with the side-chain interactions as a fraction of the total intermolecular density and the values are plotted against the number of methylene groups in Fig.34. Interestingly, we observe an alternation in this value along the series with the even acids exhibiting higher values compared to their odd neighbors. Thus, it appears that increased side-chain interactions in the even acids lead to relatively higher melting points in the even acids (Fig.7), since side-chain interactions as compared to the dimeric bonds play a decisive role in cohesion of acid molecules in the solid state.

Conclusions

We have arrived at the following conclusions from our combined structural and charge density study.

- a) The even members have a centre of inversion about the central C—C bond while the odd members other than malonic have a two-fold axis about the middle carbon atom. Malonic acid however does not possess any molecular symmetry.
- b) The bond lengths show a trend with the end C—C bonds being shorter and reaching the ideal tetrahedral value as we move in to the molecule.
- c) Fraction of the charge density involved in side chain interactions to the total charge density for all the intermolecular interactions show an alternating behavior with the even members showing a higher fraction compared to the odd ones.
- d) Strong side chain interactions increase the cohesion between the molecules in the even acids and hence the melting point.

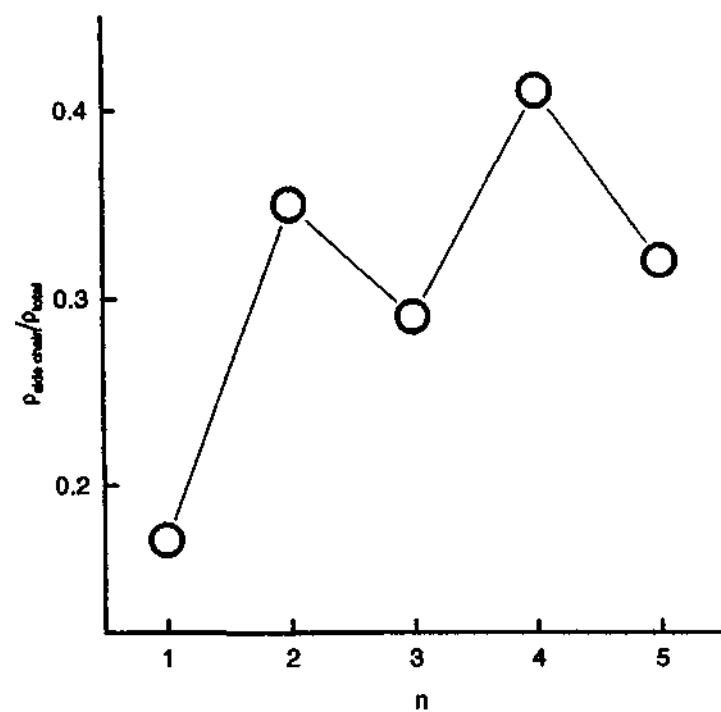


Fig.34. A plot of the sum of ρ_{CP} obtained for the side chain interactions normalised with the total ρ_{CP} due to intermolecular interactions, against the number of methylene groups, n in the acid.

4.5 Effects of the non-centric crystal field on the molecular properties of organic NLO crystals

4.5.1 5-Nitrouracil

Molecular packing

The centric polymorph of 5-nitrouracil crystallizes with eight molecules per unit cell (Pbca; $a = 8.308(3)$, $b = 10.426(3)$, $c = 13.363(4)$ Å) while the non-centric form contains four molecules in the unit cell (P2(1)2(1)2(1); $a = 5.4342(1)$, $b = 9.8406(1)$, $c = 10.3659(1)$ Å). The densities of both the forms are similar (Table 21). The space groups Pbca and P2(1)2(1)2(1) contain the same set of symmetry elements but for the inversion center which makes the problem interesting. In both the polymorphs, the asymmetric unit comprises a whole molecule. The intramolecular geometry is essentially the same in both the cases and the molecule is nearly planar (see Table 22 for bond lengths and angles). The nitro group makes an angle of 1.5° with the plane of the uracil ring in the centric form and this angle is 2.0° in the non-centric polymorph.

In the Fig.35, we show the packing diagram along with the atom labels. In the centric form, the molecule is held by the dimeric N—H...O contacts of $R_2^2(8)$ type [36] with the two neighboring molecules which are coplanar (Fig.35a). The N—H...O contacts in the non-centric form are of D(2) type arising from four different molecules (Fig.35b). In both the cases, the N—H...O bonds are ~ 1.8 Å long, with the \angle N—H...O angles ranging between 155 to 174° . The centric polymorph, in addition, exhibits an intermolecular C—H...O interaction with the nitro group at a relatively short distance of 2.15 Å. The nitro group of the non-centric polymorph is in an unfavorable geometry to establish such a contact (Fig. 35b).

Charge density analysis

The results of the multipolar refinement are described using the Laplacian of the total charge density. The topology of the Laplacian field allows one to obtain a

Table 21
5-nitrouracil: Crystal data and experimental details

Crystal	centric	non-centric
Chemical formula	C ₄ H ₃ N ₃ O ₄	
Formula weight (g)	157.09	
Cell System	Orthorhombic	Orthorhombic
Space group	Pbca	P2(1)2(1)2(1)
a (Å)	8.308(3)	5.4342(1)
b (Å)	10.426(3)	9.8406(1)
c (Å)	13.363(4)	10.3659(1)
V (Å ³)	1157.5(6)	554.32(1)
Z	8	4
F ₀₀₀	640	320
ρ (Mg m ⁻³)	1.803	1.882
Radiation type	Mo Kα	
Wave length (Å)	0.71073	
No. of reflections for cell parameters	45	37
μ (mm ⁻¹)	0.16	0.17
Crystal form	Cuboidal	hexagonal
Crystal size (mm)	0.3 x 0.2 x 0.2	0.15 x 0.15 x 0.1
Crystal color	Colorless	Colorless
Data collection temperature	130 K	130 K
Diffractometer	Siemens CCD	
Crystal-detector distance (cm)	5.0	
No. of measured reflections	16262	16515
No. of independent reflections	5026	8371
No. of observed reflections	3879	3239
R _{merge}	0.0644	0.0434
R _{int}	0.0763	0.0454
θ _{min} (°)	3.0	2.8
θ _{max} (°)	49.4	49.4
Range of h, k, l		
	-12 ≤ h ≤ 16	-10 ≤ h ≤ 11
	-22 ≤ k ≤ 11	-19 ≤ k ≤ 20
	-28 ≤ l ≤ 27	-21 ≤ l ≤ 21
After multipole refinement		
Weighting Scheme	0.02, 0.3	0.02, 0.1
R1	0.0345	0.0391
wR2	0.0416	0.0454
S	1.05	1.00
No of variables	399	404
N _{ref} /N _v	20.5	17.2

Table 22**5-nitrouracil: Bond lengths and bond angles**

Bond length (Å)	centric	non-centric
O(1)—C(1)	1.2284(13)	1.2310(13)
O(2)—C(2)	1.2252(13)	1.2290(12)
O(4)—N(3)	1.2364(12)	1.235(2)
O(3)—N(3)	1.2294(12)	1.2306(14)
N(2)—C(1)	1.3667(13)	1.3663(12)
N(2)—C(2)	1.3945(13)	1.3900(14)
N(2)—H(2)	1.01	1.01
N(1)—C(4)	1.3427(14)	1.341(2)
N(1)—C(1)	1.3807(13)	1.3786(14)
N(1)—H(1)	1.01	1.01
N(3)—C(3)	1.4432(13)	1.4412(14)
C(2)—C(3)	1.4568(14)	1.454(2)
C(3)—C(4)	1.3575(14)	1.3621(14)
C(4)—H(4)	1.08	1.08

Bond angle (°)	centric	non-centric
C(1)-N(2)-C(2)	127.18(9)	127.47(9)
C(1)-N(2)-H(2)	116.41(6)	116.27(6)
C(2)-N(2)-H(2)	116.41(6)	116.27(6)
C(4)-N(1)-C(1)	122.51(9)	122.90(8)
C(4)-N(1)-H(1)	118.74(6)	118.55(6)
C(1)-N(1)-H(1)	118.74(6)	118.55(5)
O(3)-N(3)-O(4)	123.09(9)	123.46(11)
O(3)-N(3)-C(3)	119.36(9)	119.20(11)
O(4)-N(3)-C(3)	117.56(9)	117.33(10)
O(1)-C(1)-N(2)	123.08(9)	122.60(10)
O(1)-C(1)-N(1)	121.61(9)	122.54(9)
N(2)-C(1)-N(1)	115.31(9)	114.85(9)
O(2)-C(2)-N(2)	119.86(9)	118.82(10)
O(2)-C(2)-C(3)	127.55(10)	128.32(10)
N(2)-C(2)-C(3)	112.59(8)	112.85(8)
C(4)-C(3)-N(3)	116.49(9)	116.94(10)
C(4)-C(3)-C(2)	120.79(9)	120.32(10)
N(3)-C(3)-C(2)	122.62(8)	122.73(9)
N(1)-C(4)-C(3)	121.39(9)	121.40(10)
N(1)-C(4)-H(4)	119.30(6)	119.30(6)
C(3)-C(4)-H(4)	119.30(6)	119.30(7)

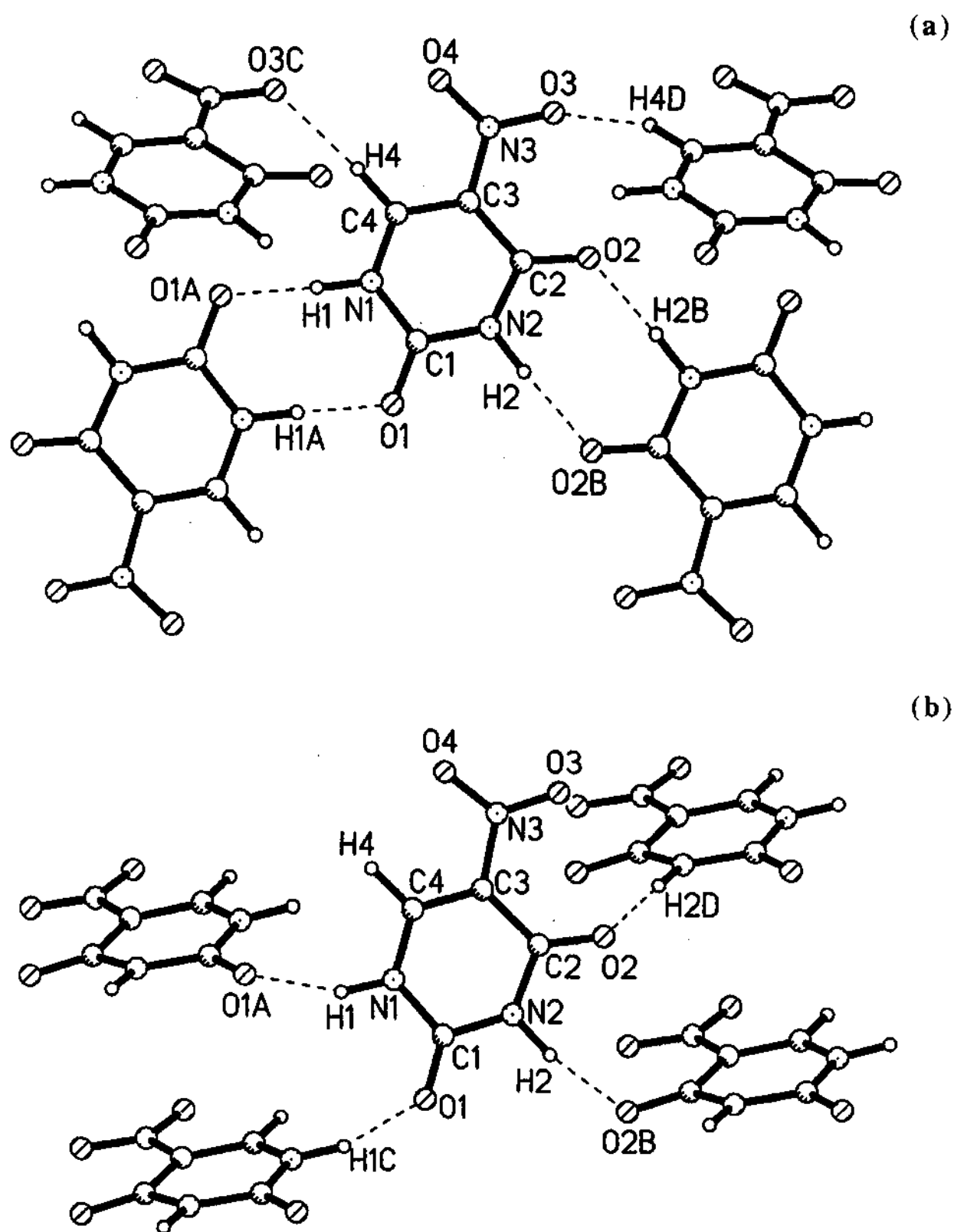


Fig.35. Molecular packing in a) centric and b) non-centric structures showing the intermolecular hydrogen bonds. Atom labels are also shown.

chemical model of the bonded and non-bonded pairs and to characterize the local concentration ($\nabla^2\rho < 0$) and depletion ($\nabla^2\rho > 0$) in the molecular charge distribution [70,71]. Figure 36 shows the contour maps of the Laplacian obtained for the two polymorphs. The lone pairs on the oxygens occur as (3, +3) critical points. There are some differences in the Laplacian maps of the two polymorphs. The atomic basins are generally linked in the centrosymmetric form but they appear to be disjoint in the non-centric case. The N(3)—O(3) bond region in the centrosymmetric form contains non-overlapping atomic lobes indicating a closed shell interaction. This is reflected in the properties of the bond critical points as listed in Table 23. This bond carries a much smaller Laplacian ($-3.0 \text{ e}\text{\AA}^{-5}$) compared to the other N—O bond of the molecule as well as the N—O bonds of the non-centric form, though the electron density itself is quite comparable. We also notice from Table 23 that the densities and the associated Laplacians of the non-hydrogen bonds are somewhat higher in the non-centric form while those of the N—H bonds are higher in the centric form. Moreover, the pseudo atomic charges are generally higher in the non-centric polymorph. This implies that there is an increased charge separation in the non-centric case. For example, the nitro group charge is -0.19 and -0.38 e respectively in the centric and the non-centric forms.

The nature of the intermolecular bonding is described in terms of the electrostatic potential. In Fig.37, we show contour maps of the electrostatic potential maps in the N—H...O and the C—H...O bond regions. The contours originating from the N—H region overlap with those from the oxygen as can be seen from Figs.37a and b. The penetration is significant indicating that these are strong contacts [19]. They are associated with (3, -1) critical points in ρ as well as in electrostatic potential. The Laplacian at the CPs are small and positive (Table 24) as generally found in hydrogen bonds [6]. The C—H...O contact of the centric form also exhibits noticeable overlap of the potentials ($\rho = 0.08(2) \text{ e}\text{\AA}^{-3}$; $V = 0.28(1) \text{ e}\text{\AA}^{-1}$) while in the non-centric form, a zero potential surface passes between the proton and the oxygen indicating no interaction between them (Fig.37c). This is understandable since in the presence of a carbonyl group, a nitro group acts as a secondary hydrogen bond acceptor. The C—H...O contact of the centric form is special in that the oxygen O(3), which participates in intermolecular bonding tends to have nearly ionic

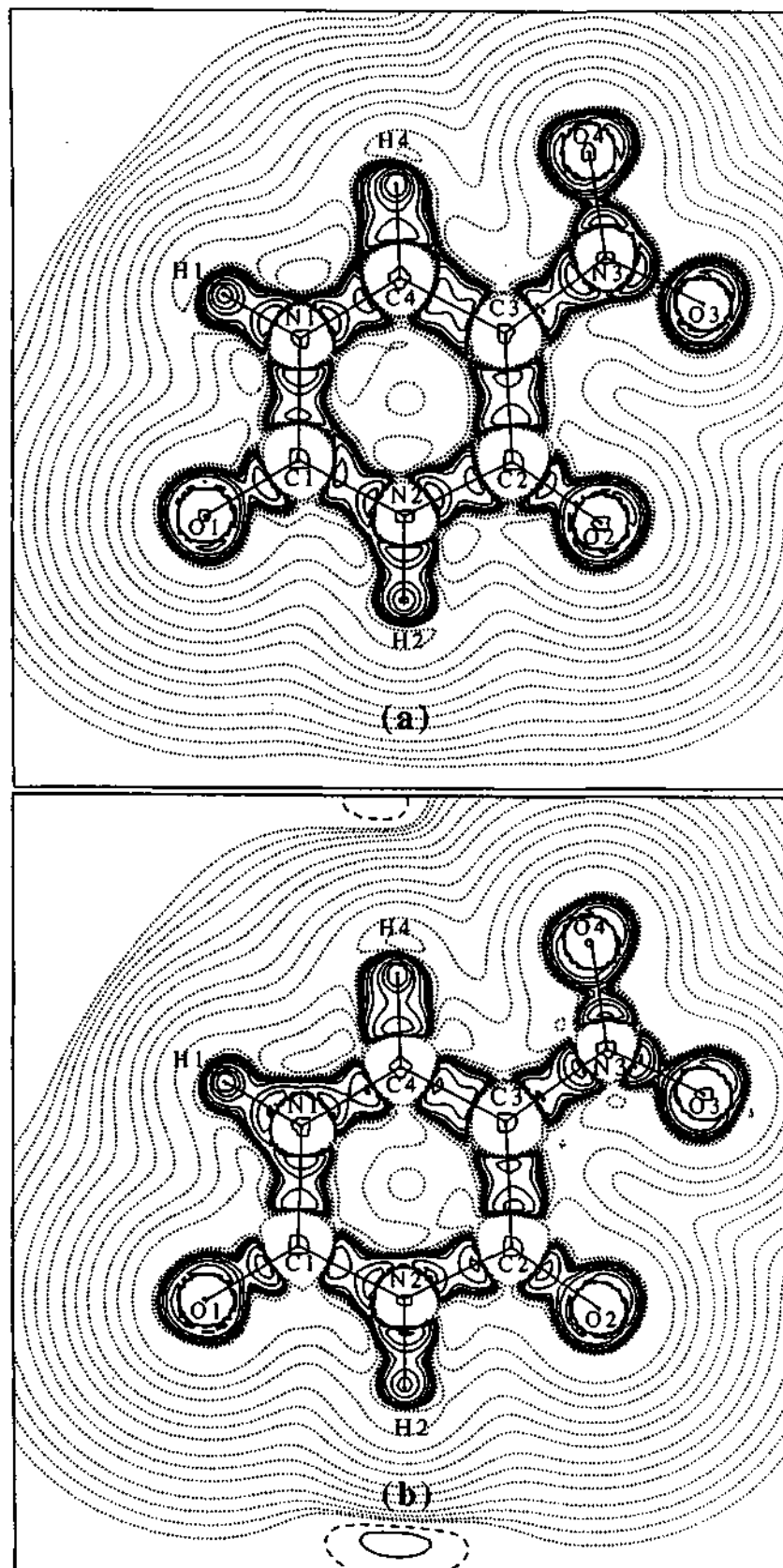


Fig.36. Contour maps of Laplacian of total density in the C(1), C(2) and C(4) plane: a) centric b) non-centric

Table 23
Analysis of the bond critical points in 5-nitrouracil

Bond	centric			non-centric		
	ρ	$\nabla^2\rho$	ϵ	ρ	$\nabla^2\rho$	ϵ
O(1)—C(1)	2.91(5)	-38.2(3)	0.21	3.31(9)	-51.9(5)	0.27
O(2)—C(2)	2.77(6)	-26.8(4)	0.18	3.21(97)	-51.3(4)	0.17
N(1)—C(1)	2.16(5)	-26.8(2)	0.06	2.36(8)	-27.9(3)	0.29
N(1)—C(4)	2.29(5)	-27.3(2)	0.25	2.50(9)	-31.5(4)	0.28
N(1)—H(1)	1.98(6)	-28.8(4)	0.06	1.9(1)	-30.1(8)	0.00
N(2)—C(1)	2.12(4)	-23.9(2)	0.21	2.34(8)	-30.1(3)	0.38
N(2)—C(2)	2.09(4)	-23.5(2)	0.12	2.22(7)	-23.7(3)	0.24
N(2)—H(2)	1.92(6)	-29.8(4)	0.04	1.8(1)	-36(1)	0.04
N(3)—C(3)	1.87(4)	-15.4(2)	0.37	1.96(8)	-17.1(4)	0.39
C(2)—C(3)	1.93(3)	-16.0(1)	0.27	1.98(7)	-7.0(2)	0.46
C(3)—C(4)	2.21(3)	-22.1(1)	0.34	2.31(7)	-24.7(2)	0.43
C(4)—H(4)	1.79(5)	-20.1(2)	0.05	1.9(1)	-29.5(7)	0.07
O(3)—N(3)	3.19(5)	-3.0(2)	0.09	3.48(9)	-14.5(3)	0.05
O(4)—N(3)	3.28(5)	-11.9(2)	0.08	3.61(9)	-18.6(4)	0.08

ρ in $e\text{\AA}^{-3}$; $\nabla^2\rho$ in $e\text{\AA}^{-5}$

Table 24
Hydrogen bond critical points in 5-nitrouracil

Polymorph	D—H...A	ρ ($e\text{\AA}^{-3}$)	$\nabla^2\rho$ ($e\text{\AA}^{-5}$)	V ($e\text{\AA}^{-1}$)
centric	N(1)—H(1)...O(1) ^a	0.18(3)	3.32(2)	0.55(2)
	N(2)—H(2)...O(2) ^a	0.17(3)	2.88(2)	0.47(2)
	C(4)—H(4)...O(3) ^b	0.08(2)	1.39(1)	0.28(1)
non-centric	N(1)—H(1)...O(1) ^c	0.16(5)	2.99(4)	0.52(3)
	N(2)—H(2)...O(2) ^d	0.15(6)	3.05(5)	0.61(4)
	O(1)...H(1)—N(1) ^e	0.14(5)	2.64(5)	0.53(3)
	O(2)...H(2)—N(2) ^f	0.13(5)	2.69(5)	0.60(3)

Symmetry: a) -x, -y, 1-z; b) 1/2-x, 1/2+y, z; c) 1/2+x, 1/2-y, 1-z;
d) -1/2+x, 1/2-y, -z; e) -1/2+x, 1/2-y, 1-z; f) 1/2+x, 1/2-y, -z

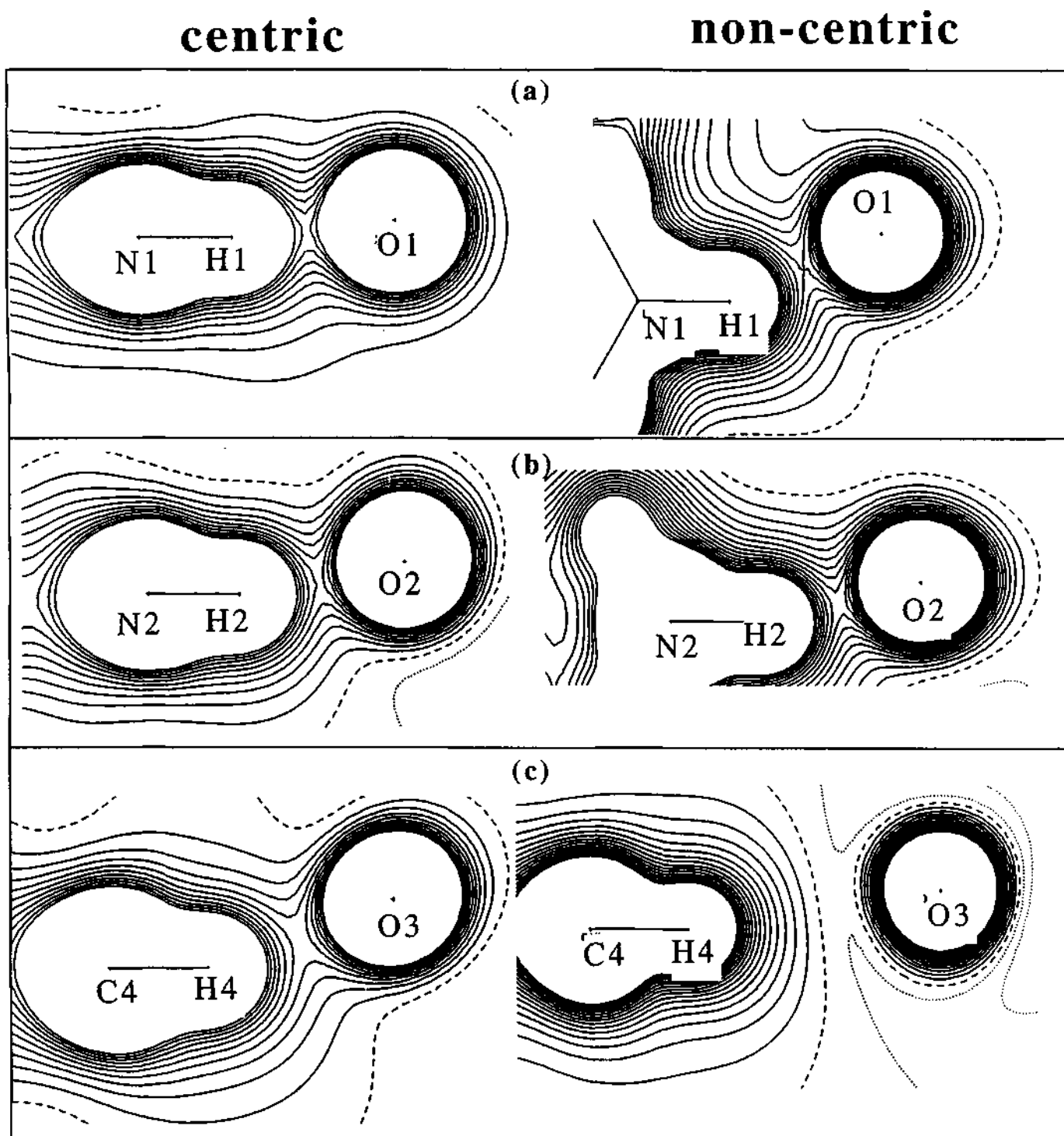


Fig.37. Contour maps of the electrostatic potential in the intermolecular regions (contour level at $0.05e\text{\AA}^{-1}$): a) N(1)—H(1)···O(1), b) N(2)—H(2)···O(2), c) C(4)—H(4)···O(3)

interaction with the nitro group (Fig.36). Such bonding would be favored by the centrosymmetric packing of the molecules. For the same reason, this contact is absent in the non-centric form.

In-situ dipole moments of molecules in crystals can be obtained from charge densities, by using the equation 19,

$$p_i = \sum_j z_j R_j + \int r \rho_i(r_i) dr$$

XDPROP routine of the XD program was used for the calculation of dipole moments and the dipole moment vectors are shown in Fig.38. The vectors lie close to the N(1)—H(1) bond direction in the plane of the molecule. The magnitude of the dipole moments in the centric and the non-centric polymorphs are 5.5(6) and 9(1) D respectively. As the intramolecular geometry remains the same in the two cases (Table 22), the enhancement of the dipole moment in the non-centric structure is likely to arise mainly due to packing. The effect of crystal packing can be understood by calculating the dipole moment of the molecule *ex-situ* in the frozen geometry. For this purpose, we carried out AM1, PRECISE calculations [35] by freezing the molecular geometries obtained from X-ray diffraction. The calculated dipole moments are very similar in the two polymorphs (5.5 and 5.6 D for centric and non-centric cases respectively) and point in the same direction (Fig.38). Interestingly, the vectors obtained from the calculation lie close (in magnitude as well as in direction) to that from experiment for the centric polymorph. This seems to suggest that the packing in the centric form of 5-nitrouracil has minimal effect on the intramolecular charge distribution. This observation also demonstrates that an asymmetric crystal field in a non-centric structure can significantly enhance the dipole moment of a molecule. To our knowledge, this is the first instance of charge density study of a compound crystallizing in closely related space groups exhibiting differing molecular properties.

Conclusions

The present charge density study on the centric and non-centric molecular systems has provided valuable insight into the effect of the crystal field on molecular properties. In the case of 5-nitrouracil, the dipole moment of the molecule

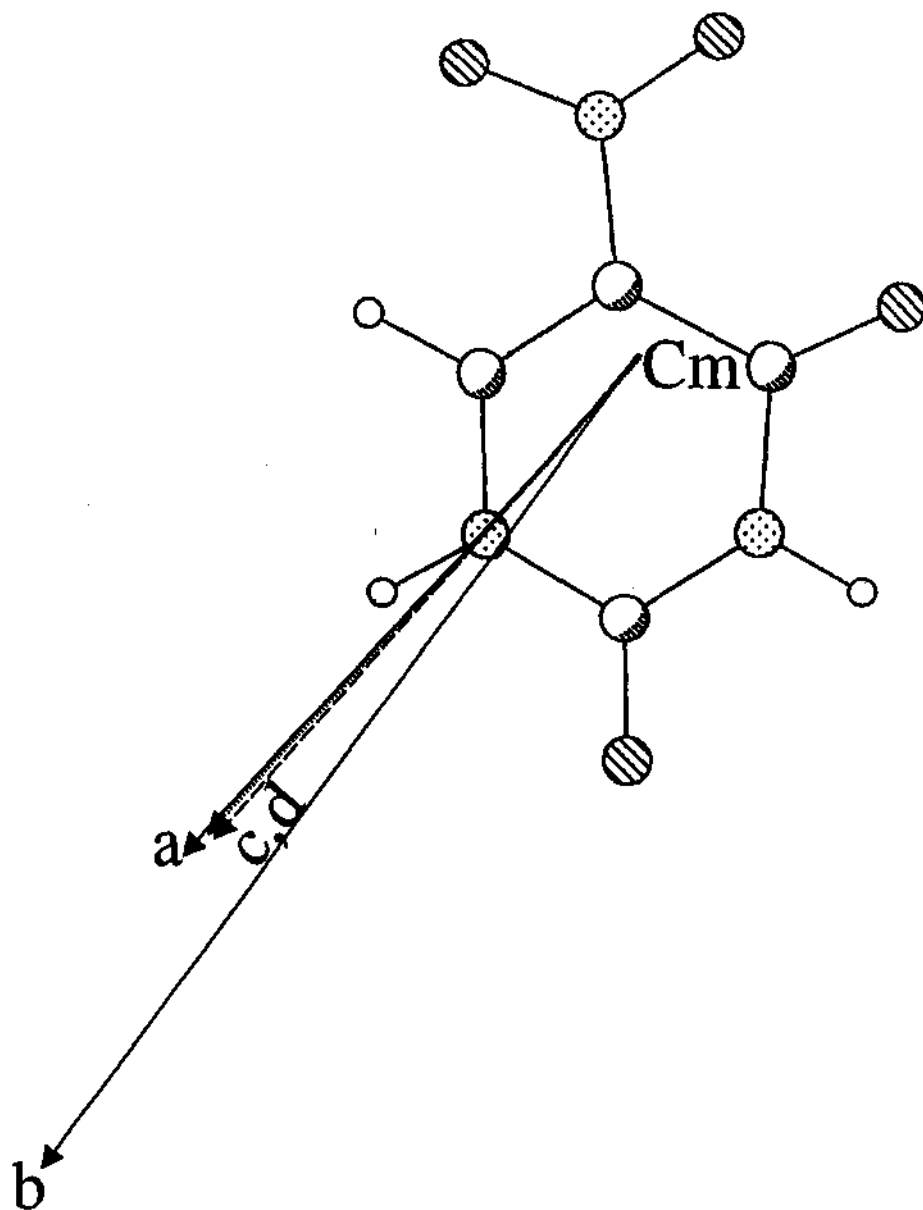


Fig.38. Orientation of the molecular dipole moment of 5-nitrouracil: a) centric, multipole b) non-centric, multipole c) centric, AM1 d) non-centric, AM1. Cm refers to the center of mass of the molecule

in the centric structure (Pbca) is 5.5(6) D and increases to 9(1) D in the noncentric lattice (P2(1)2(1)2(1)), the molecular geometry essentially remaining the same. The difference in the dipole moments clearly arises from the crystal packing. In the centric structure, there are N—H...O hydrogen bonded dimers while in the noncentric, the molecules form N—H...O linear chains. The centric crystal exhibits an additional contact, C—H...O_{nitro} absent in the non-centric structure. The molecular dipole moment in the non-centric crystal is considerably greater than the value calculated for a free molecule at frozen geometry. In centric polymorph, the dipole moment is close to that obtained from the free molecule.

4.5.2 1,1-ethylenedicarbonitriles

Structural aspects

The two nitriles, II and III, crystallize in the centrosymmetric Pcab and P2(1)/n space groups respectively while IV crystallizes in the non-centric Pna2(1) space group (Table 25). We show the molecular diagrams along with the thermal ellipsoids in Fig.39, where the bond lengths and angles associated with the non-hydrogen atoms are also indicated. The diamine, II, possesses a pseudo two-fold symmetry along C(3)—C(4) while the dithio derivative, III, exhibits a syn-anti methylthio conformation. The thioamine, IV, has methylthio group in the anti conformation. The 1,1-ethylenedicarbonitrile moiety, containing a formal C=C bond (C3—C4) and two single bonds (C1—C3 and C2—C3) along with the cyano group, is essentially planar in all the three molecules. The C≡N bond lengths are also similar (1.14(3) Å), being close to those reported in the literature for the nitrile group. There are however, some differences between the formal C—C single and double bonds. In II, the single and the double bonds are of equal length (~1.416 Å), while they are different in III (1.432(2) and 1.427(2) Å as against 1.382(2)). In the thioamine, IV, the differences are moderate (see Fig.39). A survey of formally uncharged molecules containing the ethylenedicarbonitrile moiety (466 hits with r <10%) listed in the Cambridge Crystallographic Database (version 5.7) have the mean C—C and C=C bond lengths of 1.43(2) and 1.37(3) Å respectively. The shortening of the C—C single bonds in this moiety is noteworthy. The C_{sp2}—N (or C_{sp2}—S) bonds are shorter than C_{sp3}—N (or C_{sp3}—S). In the dithio molecule (III),

Table 25

1,1-ethylenedicarbonitriles: Crystal data and experimental details

Crystal	II	III	IV
Chemical formula	$C_8H_{12}N_4$	$C_6H_6N_2S_2$	$C_7H_9N_3S$
Formula weight (g)	164.22	170.25	167.23
Crystal System	Orthorhombic	Monoclinic	Orthorhombic
Space group	Pcab	P2(1)/n	Pna2(1)
a (Å)	7.6280(1)	4.0261(1)	7.904(2)
b (Å)	14.455	13.227	8.630(2)
c (Å)	16.3489(2)	14.3906(1)	12.856(3)
β (°)	90	95.445(1)	90
V (Å ³)	1802.70(3)	762.89(2)	876.9(3)
Z	8	4	4
F ₀₀₀	704	352	352
ρ (Mg m ⁻³)	1.210	1.482	1.267
Radiation type	Mo K α		
Wave length (Å)	0.71073		
No. of reflections for cell parameters	60	60	60
μ (mm ⁻¹)	0.079	0.617	0.309
Crystal form	Cuboidal	Cuboidal	Cuboidal
Crystal size (mm)	0.2 x 0.1 x 0.1	0.2 x 0.15 x 0.1	0.2 x 0.1 x 0.1
Crystal color	colorless	yellow	colorless
Data collection temperature	130 K	130 K	130 K
Diffractometer	Siemens CCD		
Crystal-detector distance (cm)	5.0		
No. of measured reflections	29153	12914	24387
No. of independent reflections	8589	6451	8576
R _{int}	0.0361	0.0301	0.0692
θ_{min} (°)	2.49	2.10	2.84
θ_{max} (°)	49.48	49.47	49.89
Range of h, k, l			
	-15 ≤ h ≤ 15	-8 ≤ h ≤ 7	-16 ≤ h ≤ 15
	-15 ≤ k ≤ 30	-21 ≤ k ≤ 27	-18 ≤ k ≤ 18
	-34 ≤ l ≤ 34	-29 ≤ l ≤ 28	-27 ≤ l ≤ 27
After multipole refinement			
Weighting Scheme			
Shift/esd (max, min)			
R1	0.0501	0.0397	0.0332
wR2	0.0775	0.0475	0.0513
S	0.94	1.06	1.27
No of variables	161	178	197
N _{ref} /N _v	50	50.5	48.9

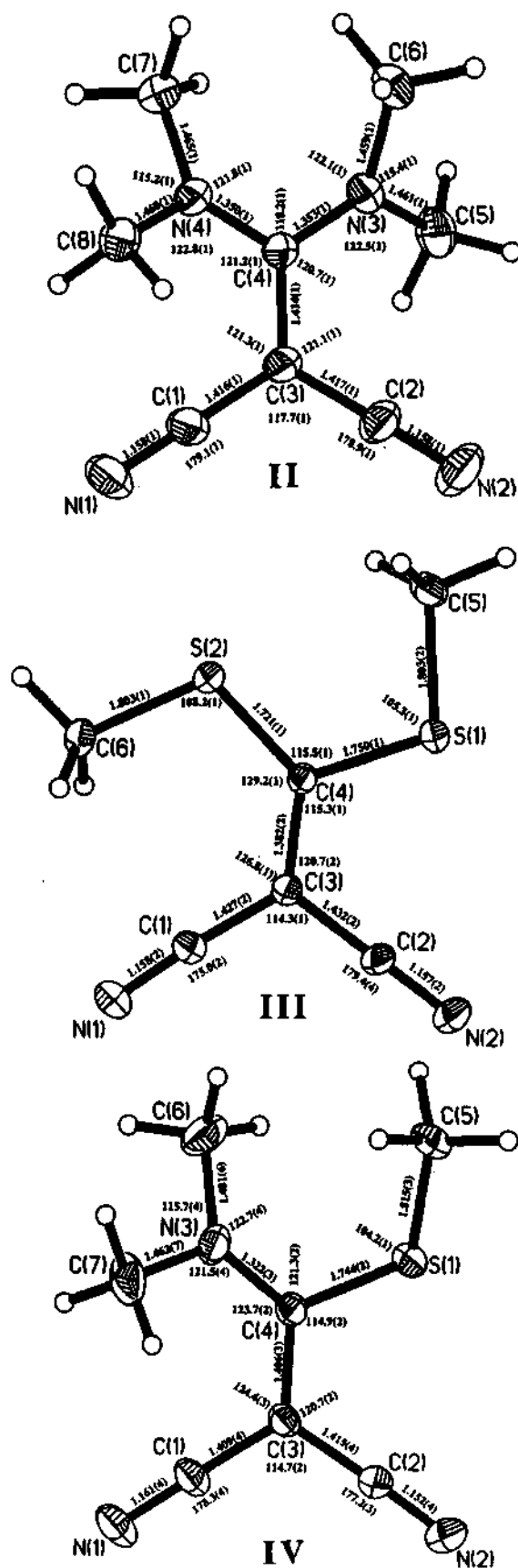


Fig.39. Molecular diagrams showing thermal ellipsoids of 1,1-ethylenedicarbonitriles: diamino (I), dithio (III) and thioamino (IV) derivatives. The figure also shows the bond lengths and angles for all the non-hydrogen bonds.

there exist considerable differences between the bond lengths and the angles associated with the syn and anti conformations of the methylthio groups. The C—C≡N bond angle associated with the syn-methylthio group is 175° instead of ~180°. An earlier structural report on this molecule suggested steric interaction to be responsible for the discrepancy [60]. However, 3,3-bis(methylthio)-2-nitro-2-propene-1-nitrile does not show significant differences in the bond lengths and angles between the syn- and the anti-configurations of the methylthio groups [96].

Charge density analysis

Figure 40 shows the contour maps of the Laplacian of the total density in the plane defined by N(1), N(2) and C(3) atoms. The lone pairs on the nitrogen and sulfur exhibit as (3, +3) critical points. The lobes near sulfur are similar to those shown in Fig.2 in the case of 3,3,6,6-tetramethyl-S-tetrathiane [15]. In the diamine, II, the contours associated with the amino groups are small since this group is out of plane with the rest of the molecule. The C—S bonds of both the dithio (III) and thioamino (IV) derivatives exhibit disjoint lobes.

Figure 41 depicts the critical points in the total density for the various bonds in the molecules. The values of total electron density, the Laplacian and the ellipticity at the critical points are also shown. The C≡N group exhibits similar densities ($\sim 3.2 \text{ e}\text{\AA}^{-3}$) in the three molecules although the Laplacian values are somewhat different, -36, -20 and -16 $\text{e}\text{\AA}^{-5}$ respectively in diamino, dithio and thioamino derivatives. Interestingly, the densities of the C—C single and double bonds are not significantly different in the three compounds (see Fig.41). The Laplacian values are also similar, the differences being less than $\sim 5 \text{ e}\text{\AA}^{-5}$. This result is in contrast with what is expected of normal single and double bonds. The densities associated with the isolated single and double bonds are generally 1.71 and 2.5 $\text{e}\text{\AA}^{-3}$ respectively [16]. In the present case, there is probably some delocalization of electrons in the bonding region. A similar observation was made earlier by Espinosa *et al.* [97] in the case of the BTDMTTF-TCNQ complex. The low values of the densities and the Laplacians in the C—S bonds are characteristic of hypervalent species [15]. A recent study on tetrasulfurtetranitride [98] has reported low values of

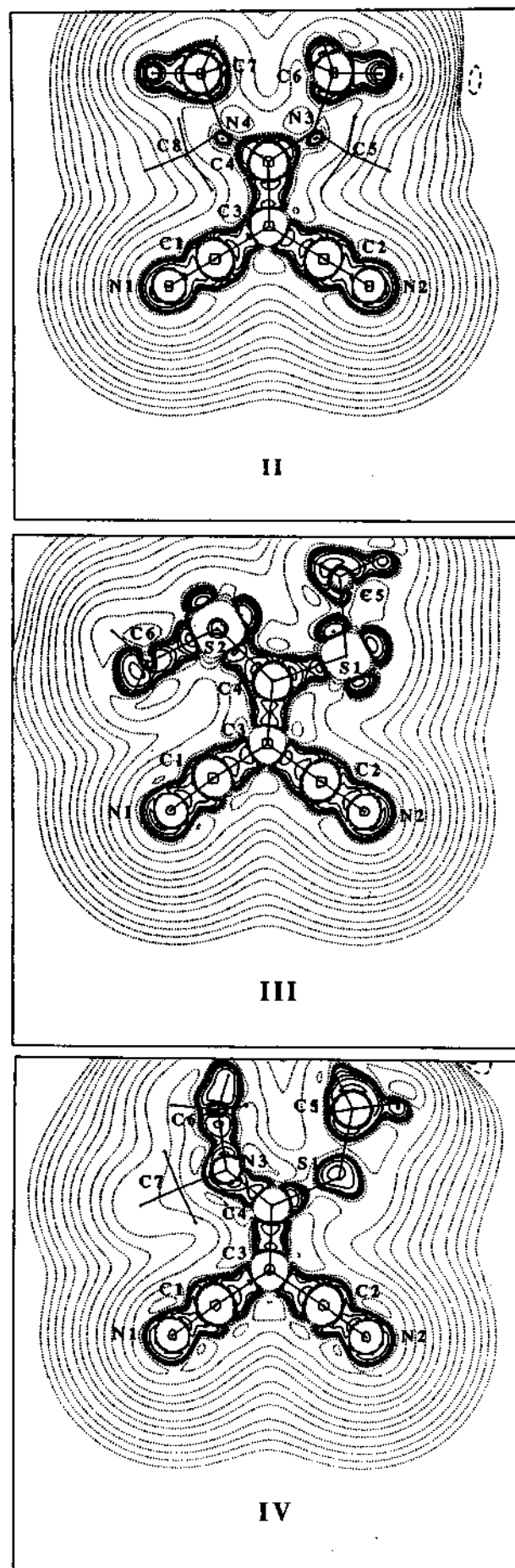


Fig.40. Contour maps of the Laplacian of the total electron density of the diamino, II, dithio, III and thioamino, IV derivatives in the N(1), C(3) and C(4) plane.

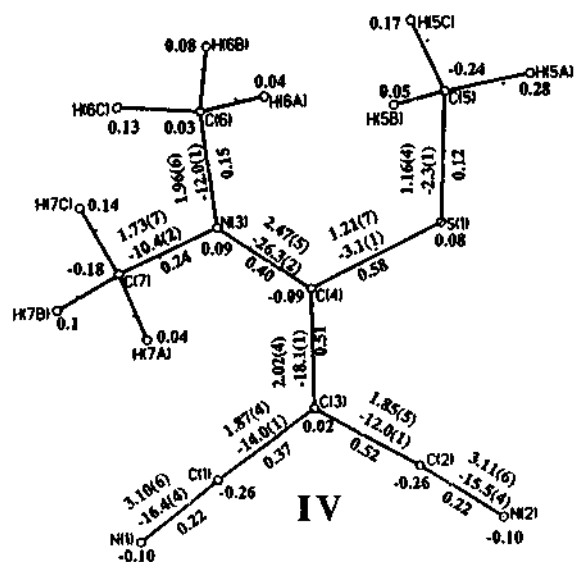
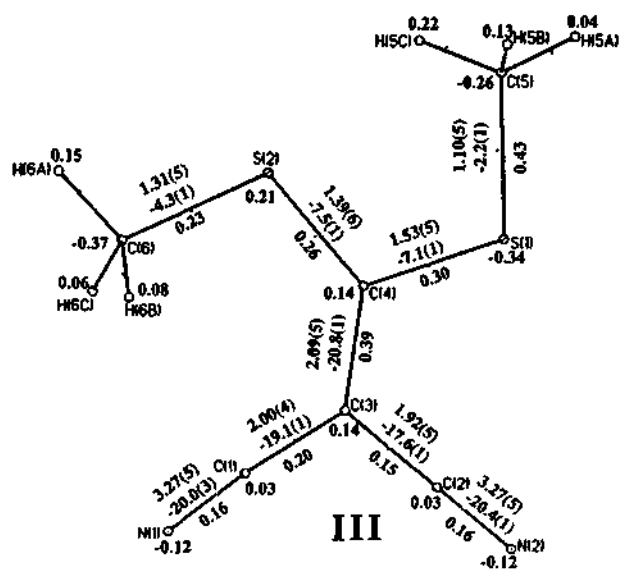
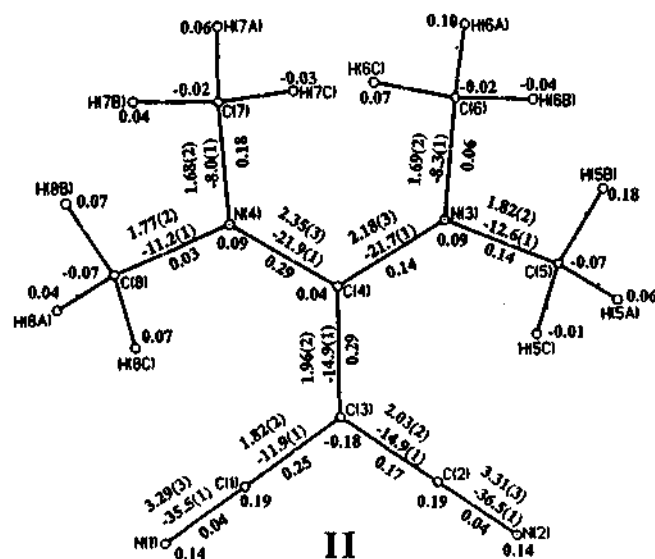


Fig.41. Stick diagrams showing the critical points for the various bonds of the diamino (II), dithio (III) and thioamino (IV) derivatives. The electron density, the Laplacians and the ellipticity associated with each bond are shown by side. The pseudo-atomic charges are also indicated.

densities and Laplacians in the N—S bonds. The charge density analysis reflects the differences between the C_{sp^2} and C_{sp^3} bonding regions as expected to the structural features discussed above. Accordingly, the C_{sp^2} bonding regions carry higher densities and Laplacians (see Fig.41). Based on the pseudoatomic charges shown in Fig.41, there appears to be an increased charge separation in the non-centric thioamine, IV.

The intermolecular contacts of the three structures, II-IV, are listed in Table 26. Both II and (III) exhibit five C—H...N contacts while the thioamine (IV) makes only three such contacts. These are typical C—H...N contacts in terms of both the geometry and the charge density. In addition, there are intermolecular S...S and S...N contacts in the dithio compound and S...N contacts in the thioamine (Table 26). The distances as well as the charge densities associated with these contacts are similar to the contacts found in other molecules [15, 98].

The *in-situ* dipole moments of the molecules in the three crystals are projected in Fig.42. The dipole moment vectors lie close to the mean planes of the molecules. An important observation from Fig.42 is that the dipole moment of the thioamine, IV, in the non-centric structure, is much higher (15(2) D) than the values of the diamino (II) and the dithio (III) derivatives in the centric structures (5(2) D and 6(2) D respectively). The enhancement of the dipole moment in the thioamine could arise from the asymmetric substitution of the electron donating groups or due to the non-centric crystal field. In order to shed more light, we have computed dipole moments of the three molecules in the free state in both the frozen and the optimized (AM1, PRECISE) geometries using MOPAC [35]. In Fig.43, we depict the frozen and the optimized dipole moments projected along with the molecule. The calculated dipole moment remains essentially unchanged between the frozen and the optimized geometries in the case of the diamino and dithio compounds. Compared to the in-crystal dipole moment, these values are slightly higher in the diamino and are comparable in the case of the dithio compound (see Figs.42 and 43). The non-centric thioamine, on the other hand, exhibits much smaller dipole moments outside the lattice, the values in the optimized and frozen geometries being 5.9 and 8.1 D respectively. Both these values are considerably lower than the in-crystal dipole

Table 26
Intermolecular contacts in 1,1-ethylenedicarbonitriles

Hydrogen contacts

D—H...A	H...A (Å)	D...A (Å)	∠D—H...A(°)	ρ (eÅ ⁻³)	∇ ² ρ (eÅ ⁻⁵)
II					
C(5)—H(5A)...N(1) ^a	2.745	3.531	130.9	0.061(3)	0.601(2)
C(7)—H(7A)...N(1) ^b	2.510	3.467	149.6	0.103(5)	0.967(2)
C(8)—H(8C)...N(1) ^c	2.872	3.649	130.4	0.041(2)	0.41(1)
C(8)—H(8B)...N(2) ^d	2.720	3.353	137.2	0.059(3)	0.616(1)
C(7)—H(7B)...N(2) ^e	2.493	3.504	136.8	0.103(5)	0.951(2)
III					
C(6)—H(6C)...N(1) ^f	2.564	3.541	152.8	0.035(6)	0.653(5)
C(6)—H(6A)...N(1) ^g	2.840	3.500	120.6	0.042(5)	0.523(3)
C(5)—H(5B)...N(1) ^h	2.586	3.631	168.6	0.04(2)	0.619(5)
C(5)—H(5A)...N(2) ⁱ	2.560	3.603	167.8	0.040(2)	0.522(2)
C(6)—H(6A)...N(2) ^j	2.886	3.554	121.3	0.048(4)	0.566(3)
IV					
C(5)—H(5B)...N(1) ^k	2.594	3.617	162.0	0.032(8)	0.572(9)
C(6)—H(6B)...N(1) ^k	2.780	3.633	137.5	0.025(8)	0.420(4)
C(5)—H(5A)...N(2) ^l	2.443	3.463	161.2	0.05(1)	0.691(4)

Symmetry: a) x, -1/2+y, 1/2+z; b) 3/2-x, -1/2+y, -z; c) 1/2+x, 3/2-y, z; d) 2-x, 3/2-y, -1/2+z; e) 3/2-x, y, -1/2+z; f) 1+x, y, z; g) -x, 1-y, -z; h) -1/2-x, 1/2+y, 1/2-z; i) 1-x, 1-y, 1-z; j) 1/2-x, 1/2+y, 1/2-z; k) 2-x, -y, 1/2+z; l) 2-x, 1-y, 1/2+z.

Sulfur contacts

Intermolecular contact	Distance (Å)	ρ (eÅ ⁻³)	∇ ² ρ (eÅ ⁻⁵)
III			
S(1)...S(1) ^a	3.515	0.067(1)	0.654(2)
S(1)...S(1) ^b	3.952	0.030(1)	0.305(1)
N(2)...S(2) ^c	3.307	0.055(1)	0.603(1)
N(2)...S(2) ^d	3.549	0.055(1)	0.603(1)
IV			
N(1)...S(1) ^e	3.194	0.055(2)	0.586(3)

Symmetry: a) 1-x, 1-y, 1-z; b) -x, 1-y, 1-z; c) 1/2-x, -1/2+y, 1/2-z; d) -1/2-x, -1/2+y, 1/2-z; e) 3/2-x, -1/2+y, -1/2+z

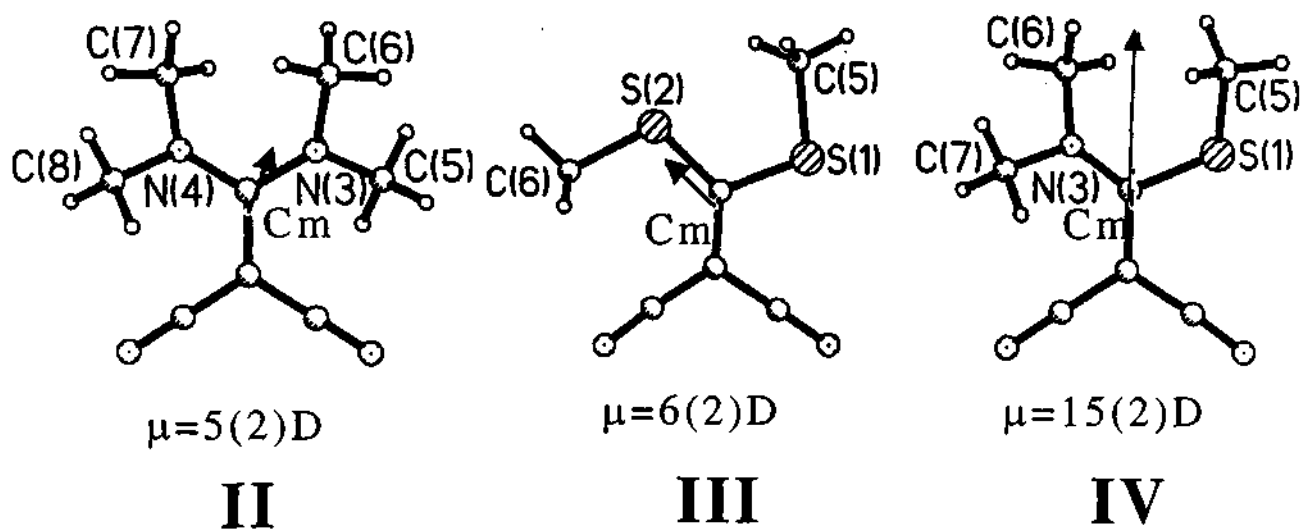


Fig.42. Molecular diagrams showing the dipole moment vectors computed from charge density in II, III and IV. Cm refers to the center of mass of the molecule.

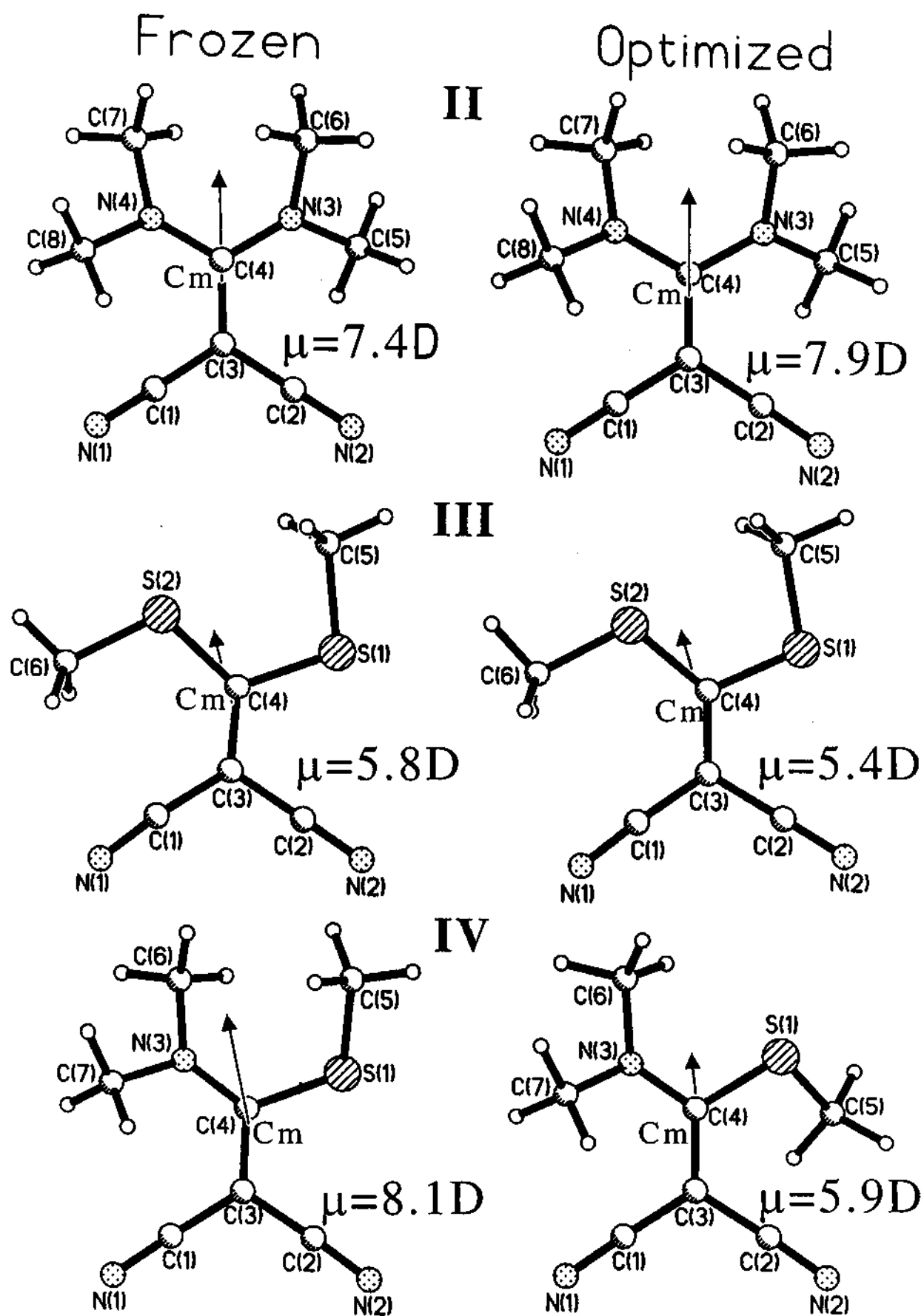


Fig.43. Molecular dipole moments calculated using AM1, MOPAC in the frozen and the optimized geometries of 1,1-ethylenedicarbonitriles: diamino (II), dithio (III) and thioamino (IV) derivatives. Cm refers to the center of mass of the molecule.

moment of 15 D. It is interesting that in the optimized geometry, the thioamine exhibits a syn-methylthio conformation with a smaller dipole moment, ~ 5.9 D (Fig. 43b) compared to the anti-methylthio conformation found in the frozen geometry of the crystal. It appears that the non-centric structure induces significant distortions in the molecule and enhances the dipole moment.

Conclusions

The crystal is centrosymmetric when the two substituents of the ethylenedicarbonitriles are the same as in the diamino (II) and dithio (III) derivatives and they have low dipole moments (~6D). The dipole moment values are close to those obtained by AM1 calculations on the frozen molecular geometries. On the contrary, the thioamine (IV), with the anti-methylthio conformation of the S—CH₃ group, occurs in a non-centric structure where there is an increased charge separation within the molecule and hence a considerably higher dipole moment (15(2)D) than that calculated for the molecule outside the crystal (in the frozen geometry). When the molecule is subjected to optimization (AM1, PRECISE), it adopts a syn-methylthio conformation and the dipole moment falls below to 5.9D. The enhancement of the dipole moment in the thioamino system is partly due to the anti-conformation forced on the molecule by the non-centric crystal field and partly due to the field itself.

4.6 The molecular dipole moment of 7,7-di(S(+)-2-(methoxymethyl)pyrrolidino)-8,8-dicyanoquinodimethane (DMPDQ), a NLO material

Molecular structure

The molecule consists of two methoxymethyl pyrrolidone rings and two cyano groups separated by a quinodimethane ring. The molecule crystallizes in a chiral space group, $P2_1$ ($a = 9.2675(3)$ Å, $b = 8.1573(3)$ Å, $c = 13.8649(5)$ Å, $\beta = 102.9680(10)^\circ$) with two molecules per unit cell, the asymmetric unit being whole molecule (Table 27). We show the molecular diagram in Fig.44 and the bond lengths, angles and torsion angles are listed in Table 28. We find that the molecules in the lattice are held by three intramolecular and three intermolecular hydrogen contacts at distances of ~ 2.5 Å and an angle of $\sim 120^\circ$.

Charge density analysis

The static deformation density in the plane of the phenyl ring as well as in the pyrrolidone ring are shown in Fig.45a and b respectively. The bonds appear as concentric contours while the lone-pairs on the cyano nitrogens appear as lobes. In Table 29, the charge densities as well as the Laplacians at the bond critical points are listed. All the bonds exhibit large densities and high negative Laplacians, characteristic of shared interactions. As was observed in 1,1-ethylenedicarbonitriles, C_{sp^2} -N bonds are stronger than the C_{sp^3} -N bonds. The former are shorter and carry higher densities and Laplacians.

XDPROP routine of the XD program was used for the calculation of dipole moment (Fig.46). The vector lies close to the plane of the phenyl ring nearly bisecting the two pyrrolidone rings. The net charges on the two pyrrolidone rings, the phenyl ring and the two cyano groups are 1.29, 0.02 and -1.31 e respectively. The values clearly indicate the nature of the groups. The pyrrolidone group acts as a donor while the cyano group acts as an acceptor, the conjugated double bonds behaving like a molecular wire connecting the two ends. The magnitude of the dipole moments obtained from the charge density is 44(6) D. A high value of dipole moment is not surprising since the donor and the acceptor are separated by a large distance of ~ 6 Å by the conducting neutral spacer. In order to study the effect of

Table 27

DMPDQ: Crystal data and experimental details

Crystal	DMPDQ
Chemical formula	C ₂₂ H ₂₈ N ₄ O ₂
Formula weight (g)	380.48
Cell System	Monoclinic
Space group	P 2(1)
a (Å)	9.2675(3)
b (Å)	8.1573(3)
c (Å)	13.8649(5)
β (°)	102.9680(10)
V (Å ³)	1021.42(6)
Z	2
F ₀₀₀	408
ρ (Mg m ⁻³)	1.237
Radiation type	Mo K α
Wave length (Å)	0.71073
No. of reflections for cell parameters	45
μ (mm ⁻¹)	0.081
Crystal form	Cuboidal
Crystal size (mm)	0.3 x 0.2 x 0.2
Crystal color	Yellow
Data collection temperature	130 K
Diffractometer	Siemens CCD
Crystal-detector distance (cm)	5.0
No. of measured reflections	21515
No. of independent reflections	16454
No. of observed reflections	16438
R _{int}	0.0462
θ_{\min} (°)	1.51
θ_{\max} (°)	49.30
Range of h, k, l	
	-19 ≤ h ≤ 14
	-16 ≤ k ≤ 17
	-29 ≤ l ≤ 29
After multipole refinement	
Weighting Scheme	
R1	0.0394
wR2	0.0513
S	1.0526
No of Reflections used	7162
No of variables	364
N _{ref} /N _v	19.7

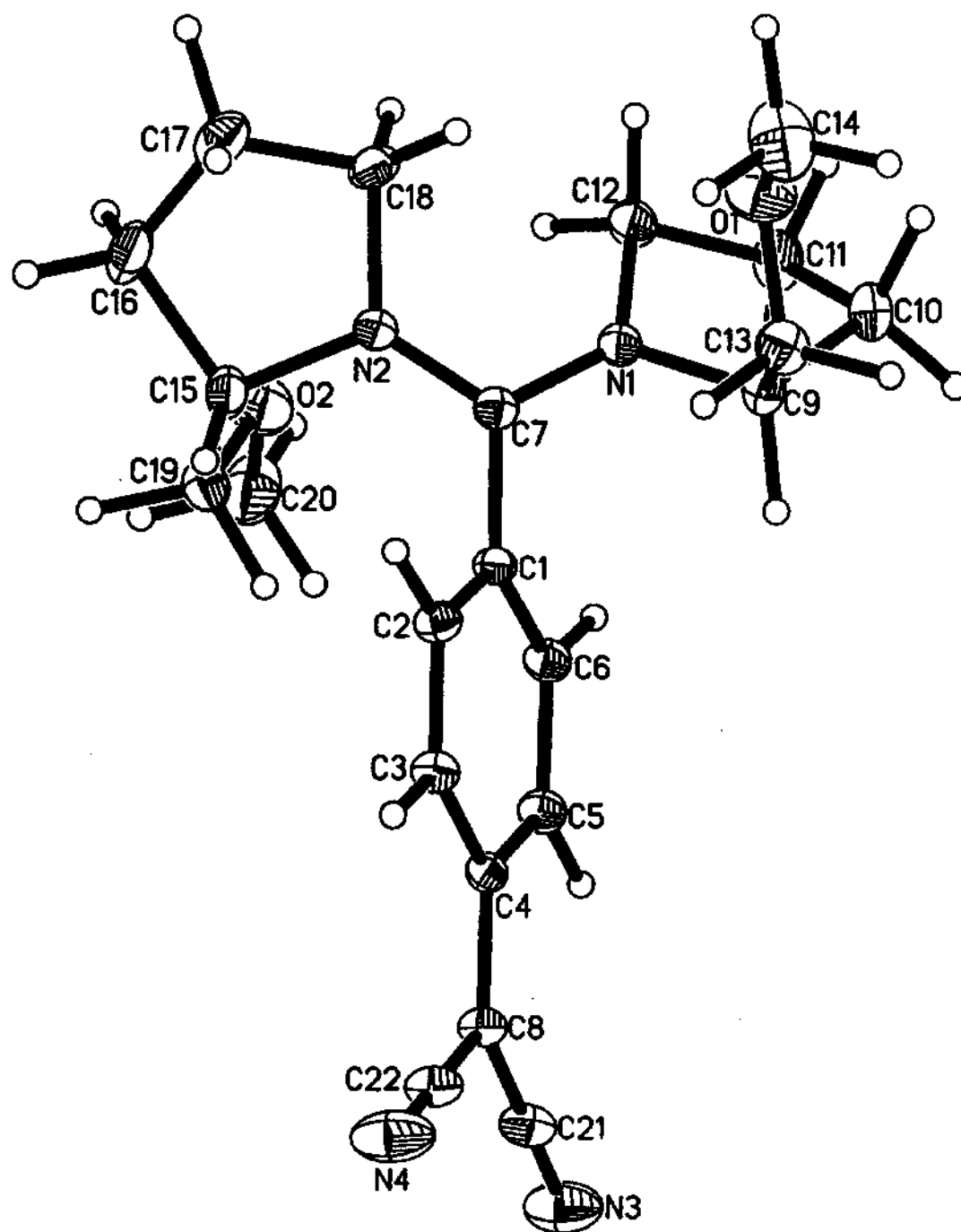


Fig.44. Molecular diagrams showing thermal ellipsoids of DMPDQ. All non-hydrogen atoms are shown at 50 % probability ellipsoids

Table 28
DMPDQ: Bond lengths, bond angles and torsion angles involving non-hydrogen atoms from X-ray crystallography and AM1 calculation

Bond length (Å)	X-ray	AM1
O(1)-C(13)	1.415(3)	1.4261
O(1)-C(14)	1.428(3)	1.4188
O(2)-C(19)	1.421(3)	1.4252
O(2)-C(20)	1.431(3)	1.4192
N(1)-C(7)	1.341(3)	1.3725
N(1)-C(9)	1.487(3)	1.4662
N(1)-C(12)	1.482(3)	1.4541
N(2)-C(7)	1.329(2)	1.3682
N(2)-C(18)	1.482(3)	1.4556
N(2)-C(15)	1.493(3)	1.4688
N(3)-C(21)	1.162(3)	1.1658
N(4)-C(22)	1.160(3)	1.1657
C(1)-C(2)	1.404(3)	1.419
C(1)-C(6)	1.405(3)	1.4211
C(1)-C(7)	1.478(3)	1.4496
C(2)-C(3)	1.389(3)	1.3663
C(3)-C(4)	1.415(3)	1.4366
C(4)-C(5)	1.422(3)	1.4372
C(4)-C(8)	1.442(3)	1.3854
C(5)-C(6)	1.389(3)	1.3656
C(8)-C(21)	1.413(3)	1.4131
C(8)-C(22)	1.408(3)	1.4122
C(9)-C(10)	1.546(3)	1.5457
C(9)-C(13)	1.527(3)	1.5405
C(10)-C(11)	1.535(3)	1.5247
C(11)-C(12)	1.532(3)	1.5385
C(15)-C(16)	1.551(3)	1.545
C(15)-C(19)	1.516(3)	1.538
C(16)-C(17)	1.529(4)	1.5232
C(17)-C(18)	1.528(3)	1.5362

Bond angle (°)	X-ray	AM1
C(13)-O(1)-C(14)	111.9(2)	112.33
C(19)-O(2)-C(20)	111.8(2)	112.29
C(7)-N(1)-C(9)	123.5(2)	122.95
C(7)-N(1)-C(12)	125.5(2)	126.28
C(7)-N(1)-C(9)	111.0(2)	110.76
C(7)-N(2)-C(15)	124.5(2)	123.27
C(7)-N(2)-C(18)	123.5(2)	125.71
C(18)-N(2)-C(15)	112.0(2)	110.96
C(2)-C(1)-C(6)	118.9(2)	118.04
C(2)-C(1)-C(7)	122.6(2)	122.03
C(6)-C(1)-C(7)	118.4(2)	119.93
C(3)-C(2)-C(1)	120.1(2)	121.09
C(2)-C(3)-C(4)	121.9(2)	121.6
C(3)-C(4)-C(5)	117.2(2)	116.48
C(3)-C(4)-C(8)	121.7(2)	121.98
C(5)-C(4)-C(8)	121.1(2)	121.54
C(6)-C(5)-C(4)	120.7(2)	121.49
C(5)-C(6)-C(1)	121.1(2)	121.18
N(2)-C(7)-N(1)	119.7(2)	121.4
N(2)-C(7)-C(1)	121.2(2)	118.87
N(1)-C(7)-C(1)	119.0(2)	119.73
C(22)-C(8)-C(4)	115.9(2)	116.72
C(21)-C(8)-C(4)	122.5(2)	121.5
C(22)-C(8)-C(1)	121.7(2)	121.78
N(1)-C(9)-C(10)	103.8(2)	106.36
N(1)-C(9)-C(13)	109.9(2)	113.34
C(13)-C(9)-C(10)	112.9(2)	111.08
C(11)-C(10)-C(9)	104.9(2)	106.76
C(12)-C(11)-C(10)	103.3(2)	106.06
N(1)-C(12)-C(11)	101.2(2)	106.66
O(1)-C(13)-C(9)	107.4(2)	108.58
N(2)-C(15)-C(16)	102.4(2)	106.54

N(2)-C(15)-C(19)	111.7(2)	114.07
C(19)-C(15)-C(16)	113.9(2)	111.47
C(17)-C(16)-C(15)	104.0(2)	106.9
C(18)-C(17)-C(16)	102.6(2)	106
N(2)-C(18)-C(17)	102.4(2)	107.07
O(2)-C(19)-C(15)	108.6(2)	108.68
N(3)-C(21)-C(8)	179.3(3)	179.71
N(4)-C(22)-C(8)	179.4(2)	179.85

Torsion Angle (°)	X-ray	AM1
C14-O1-C13-C9	-177.8(2)	-177.79
C20-O2-C19-C15	176.9(2)	-179.28
C9-N1-C12-C11	31.2(2)	19.46
C7-N1-C12-C11	-146.8(2)	-161.87
C7-N1-C9-C10	167.9(2)	166.53
C7-N1-C9-C13	-71.1(2)	-71.12
C12-N1-C7-N2	-32.5(3)	-27.57
C9-N1-C7-N2	149.8(2)	150.95
C12-N1-C7-C1	144.3(2)	151.78
C9-N1-C7-C1	-33.5(3)	-29.71
C12-N1-C9-C13	110.9(2)	107.6
C12-N1-C9-C10	-10.2(2)	-14.74
C15-N2-C7-N1	156.7(2)	158.5
C18-N2-C7-N1	-25.0(3)	-18.49
C15-N2-C18-C17	20.8(2)	15.77
C7-N2-C18-C17	-157.7(2)	-166.93
C7-N2-C15-C16	-177.6(2)	173.28
C7-N2-C15-C19	-55.4(3)	-63.3
C18-N2-C7-C1	158.3(2)	162.17
C15-N2-C7-C1	-20.0(3)	-20.84
C18-N2-C15-C19	126.2(2)	114.09
C18-N2-C15-C16	3.9(2)	-9.34
C6-C1-C7-N1	-53.6(3)	-49.66
C2-C1-C7-N1	129.3(2)	130.59
C6-C1-C7-N2	123.2(2)	129.7
C2-C1-C7-N2	-54.0(3)	-50.05
C7-C1-C6-C5	-176.4(2)	-176.76
C2-C1-C6-C5	0.9(3)	3
C6-C1-C2-C3	0.7(3)	-1.64
C7-C1-C2-C3	177.9(2)	178.12
C1-C2-C3-C4	-1.3(3)	-1.56
C2-C3-C4-C5	0.3(4)	3.33
C2-C3-C4-C8	-179.4(2)	-176.03
C3-C4-C8-C21	177.0(2)	179.12
C3-C4-C8-C22	-2.9(3)	-0.44
C3-C4-C5-C6	1.3(3)	-1.97
C5-C4-C8-C21	-2.7(3)	-0.21
C5-C4-C8-C22	177.4(2)	-179.78
C8-C4-C5-C6	-179.0(2)	177.4
C4-C5-C6-C1	-1.9(3)	-1.16
N1-C9-C13-O1	-56.7(2)	-61.47
C10-C9-C13-O1	58.7(2)	58.21
N1-C9-C10-C11	-15.3(2)	3.98
C13-C9-C10-C11	-134.3(2)	-119.77
C9-C10-C11-C12	34.3(2)	7.28
C10-C11-C12-N1	-39.3(2)	-16.09
N2-C15-C19-O2	-47.4(2)	-64.97
C16-C15-C19-O2	68.0(2)	55.75
N2-C15-C16-C17	-27.2(2)	-0.9
C19-C15-C16-C17	-148.0(2)	-125.93
C15-C16-C17-C18	40.4(2)	10
C16-C17-C18-N2	-37.0(2)	-15.65

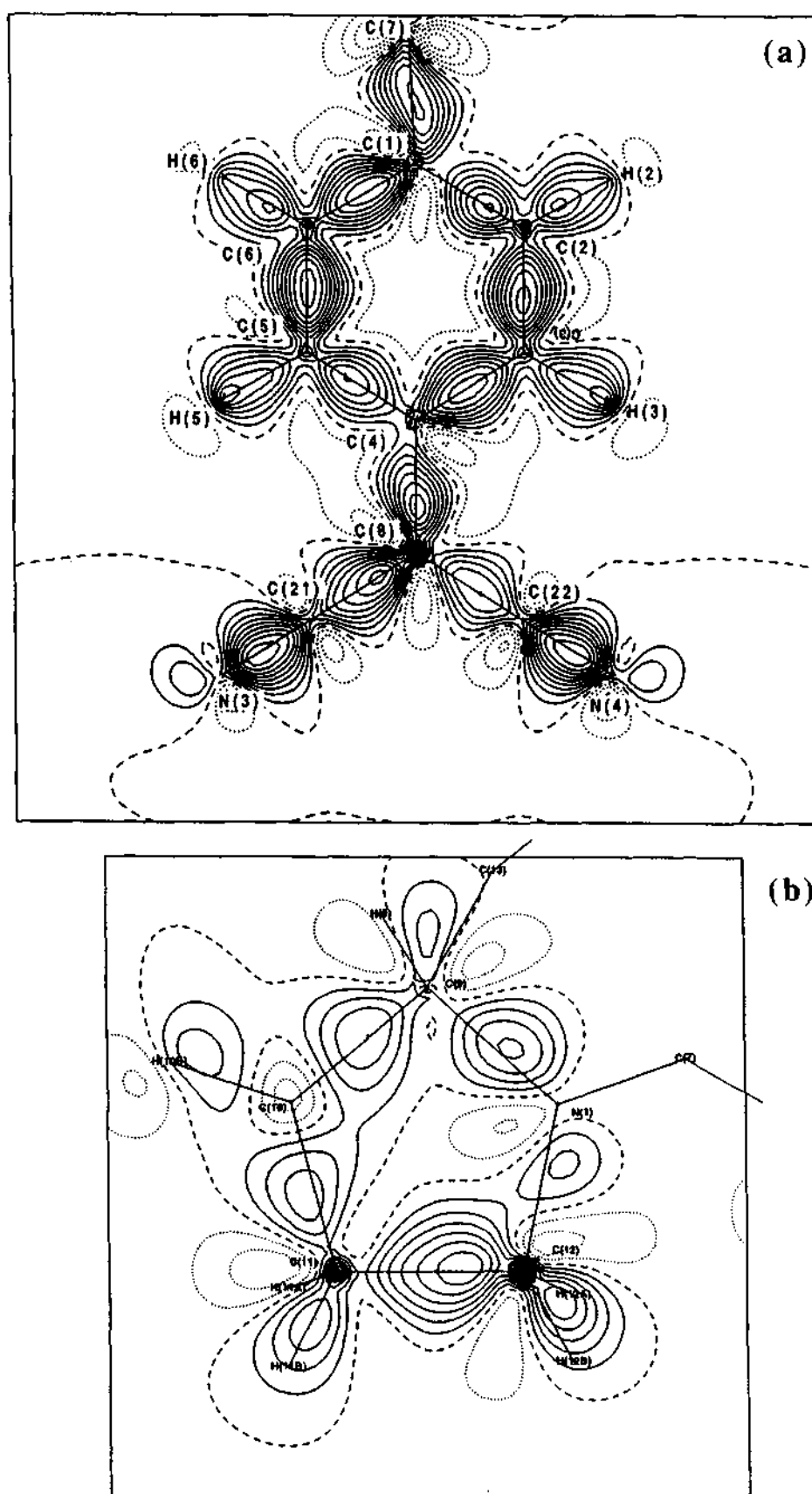


Fig. 45. Static deformation density the plane of a) quinodimethane and b) pyrrolidone rings in DMPDQ. Contour intervals at $0.1 \text{ e}\text{\AA}^{-3}$.

Table 29
Analysis of the bond critical points in DMPDQ

Bond	ρ	$\nabla^2\rho$	ϵ	Δ (%)
O(1)-C(13)	2.11(6)	-25.9(3)	0.33	26.9
O(1)-C(14)	1.98(6)	-17.4(2)	0.05	11.9
O(2)-C(19)	1.79(1)	-12.4(4)	0.1	13.6
O(2)-C(20)	2.21(1)	-33.3(7)	0.07	25.6
N(1)-C(7)	2.42(8)	-37.1(4)	0.12	23.6
N(1)-C(9)	1.85(5)	-15.4(2)	0.17	15.4
N(1)-C(12)	1.67(5)	-10.8(2)	0.11	13.9
N(2)-C(7)	2.88(8)	-32.9(3)	0.28	8.7
N(2)-C(15)	1.84(5)	-15.1(1)	0.18	15.2
N(2)-C(18)	1.68(5)	-11.4(3)	0.12	14.5
N(3)-C(21)	3.20(9)	-15.2(6)	0.16	30.0
N(4)-C(22)	3.20(9)	-15.4(1)	0.16	30.0
C(1)-C(2)	1.91(8)	-19.5(3)	0.39	21.1
C(1)-C(6)	2.25(5)	-22.9(1)	0.35	4.0
C(1)-C(7)	2.01(5)	-18.5(1)	0.28	0.1
C(2)-C(3)	2.33(1)	-25.7(1)	0.26	4.7
C(2)-H(2)	1.72(1)	-16.9(1)	0.08	41.8
C(3)-C(4)	2.19(6)	-21.1(2)	0.29	0.9
C(3)-H(3)	1.81(1)	-18.1(1)	0.15	34.5
C(4)-C(5)	1.97(6)	-17.2(2)	0.38	7.5
C(4)-C(8)	1.97(6)	-18.4(2)	0.47	11.9
C(5)-C(6)	2.44(5)	-26.6(1)	0.2	1.0
C(5)-H(5)	1.78(7)	-17.5(2)	0.15	34.4
C(6)-H(6)	1.73(7)	-17.0(3)	0.08	41.9
C(8)-C(21)	2.18(6)	-18.1(2)	0.2	7.2
C(8)-C(22)	1.97(7)	-16.1(2)	0.35	2.0
C(9)-C(10)	1.74(4)	-12.8(1)	0.04	2.1
C(9)-C(13)	1.77(5)	-15.3(1)	0.06	6.1
C(9)-H(9)	1.72(7)	-17.8(3)	0.05	37.8
C(10)-C(11)	1.71(5)	-13.5(1)	0.16	1.7
C(10)-H(10A)	1.75(9)	-15.9(4)	0.05	44.5
C(10)-H(10B)	1.62(9)	-14.1(3)	0.05	37.3
C(11)-C(12)	1.74(4)	-12.0(1)	0.08	5.5
C(11)-H(11A)	1.80(9)	-15.6(3)	0.03	38.7
C(11)-H(11B)	1.8(1)	-17.7(3)	0.06	36.5
C(12)-H(12A)	1.83(9)	-16.8(3)	0.07	39.3
C(12)-H(12B)	1.7(1)	-16.1(4)	0.04	39.5
C(13)-H(13A)	1.7(1)	-14.2(4)	0.02	45.5
C(13)-H(13B)	1.7(1)	-13.6(4)	0.06	45.4
C(14)-H(14A)	1.7(1)	-18.5(6)	0.19	43.0
C(14)-H(14B)	1.6(1)	-13.9(7)	0.16	50.9
C(14)-H(14C)	1.8(1)	-16.2(3)	0.76	12.0
C(15)-C(16)	1.73(3)	-12.6(3)	0.06	2.2
C(15)-C(19)	1.80(3)	-15.3(3)	0.06	5.0
C(15)-H(15)	1.73(1)	-18.2(1)	0.04	37.8
C(16)-C(17)	1.62(4)	-11.4(3)	0.06	0.8
C(16)-H(16A)	1.8(1)	-14.2(5)	0.05	43.4
C(16)-H(16B)	1.6(1)	-13.1(3)	0.05	35.0
C(17)-C(18)	1.85(4)	-15.2(4)	0.08	3.3
C(17)-H(17A)	1.6(1)	-14.1(4)	0.02	44.0
C(17)-H(17B)	1.6(1)	-13.2(4)	0.04	40.2
C(18)-H(18A)	1.7(1)	-13.8(5)	0.06	43.4
C(18)-H(18B)	1.6(1)	-13.3(4)	0.02	41.5
C(19)-H(19A)	1.6(1)	-15.8(5)	0.06	48.3
C(19)-H(19B)	1.8(1)	-17.3(5)	0.02	44.8
C(20)-H(20A)	1.6(1)	-12.5(2)	0.61	16.5
C(20)-H(20B)	1.9(1)	-20.5(5)	0.18	39.3
C(20)-H(20C)	1.6(2)	-12.4(8)	0.17	51.2

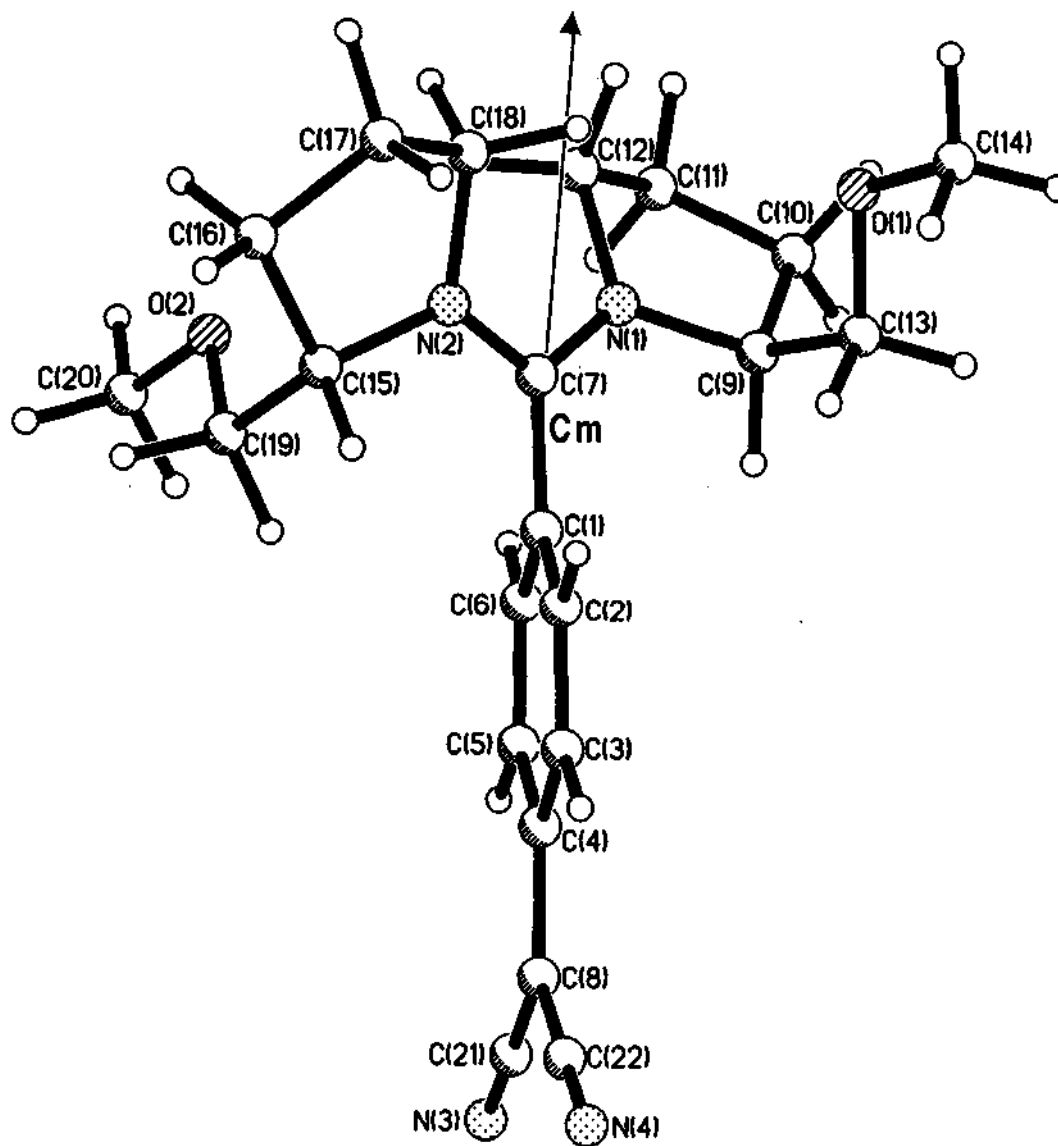


Fig. 46. Molecular diagram showing the dipole moment vector computed from charge density in DMPDQ. Cm refers to the center of mass of the molecule.

crystal field we have carried out AM1, PRECISE calculations [35] at the frozen and optimized molecular geometries (Fig.47). The net charges obtained in the frozen geometry are 0.743, -0.167 and -0.576 for the two pyrrolidone rings, the phenyl ring and the cyano groups respectively. These values are considerably smaller compared to the in-crystal charges but exhibit a similar trend, with the donor group having a positive charge and the acceptor carrying a negative charge. The intervening phenyl ring carries a small negative charge. The bond lengths and the angles in the in-crystal and optimized geometries are quite close while the torsion angles differ quite significantly, especially those involving the ether-side groups (Table 28). The dipole moments computed from the frozen (20 D) and the optimized (17D) geometries are much lower than that obtained in the crystal. The directions of the dipole moments in all the three cases are quite similar. These observations clearly ascertain our previous finding that an asymmetric crystal field of a non-centric structure can significantly enhance the dipole moment of a molecule. The effect is well pronounced in this case due to a larger separation between the donor and the acceptor.

The charge density investigations described in sections 4.5, 4.6 and 4.7 on organic NLO materials have shown that the non-centric field in the crystal can have a significant influence on the molecular conformation, packing and properties. We observe that a relatively higher dipole moment is associated with the molecule in a non-centric structure. The present study which deals with structure and charge density of different families of NLO molecules is one of the very few studies in the literature.

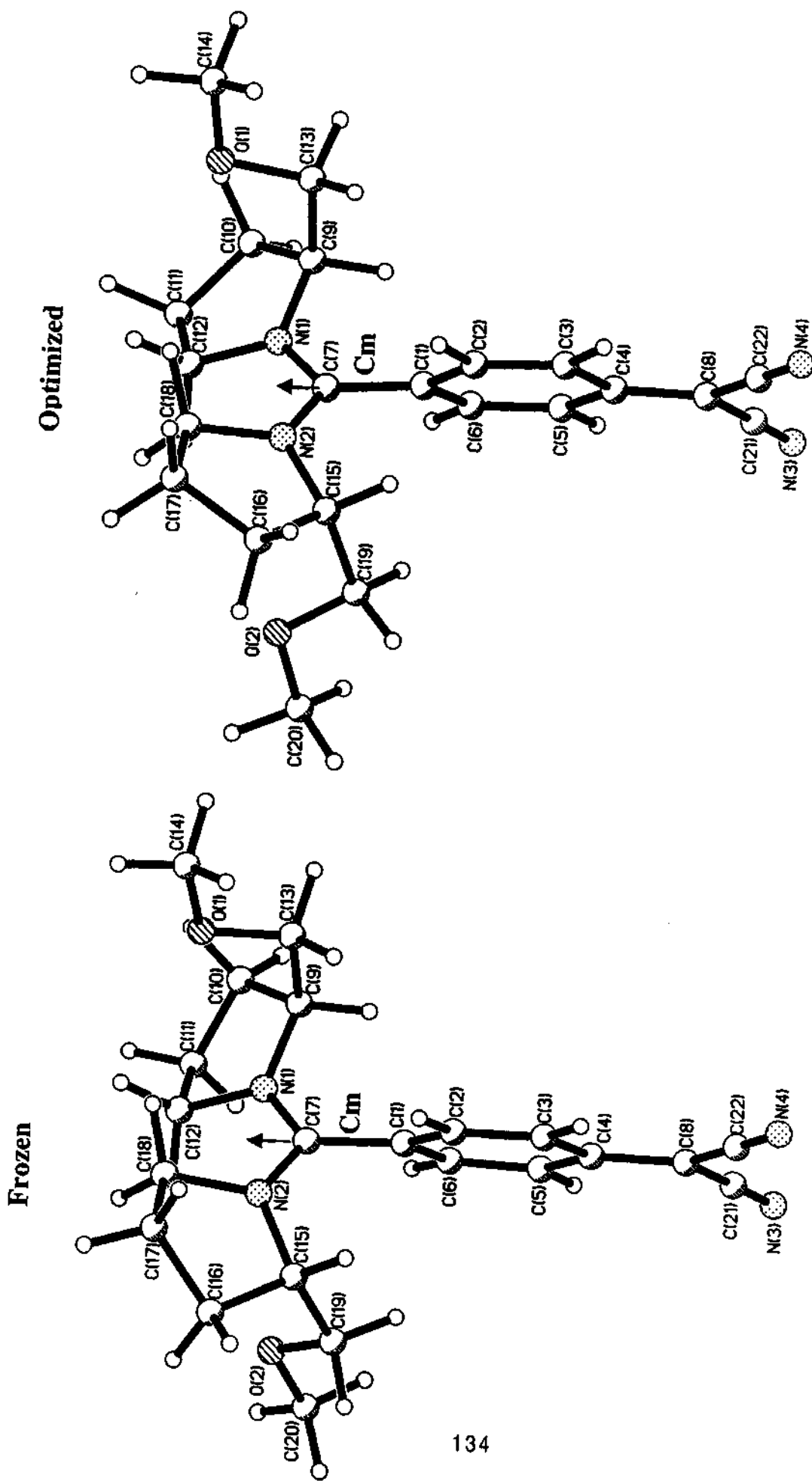


Fig.47. Molecular dipole moments calculated using AM1, MOPAC in the frozen and the optimized geometries of DMPDQ. Cm refers to the center of mass of the molecule.

4.7 Structural Phase Transition in Adipic Acid

Structural aspects

Adipic acid crystallizes in a centrosymmetric monoclinic space group ($P2_1/n$) with two molecules per unit cell ($a=7.3672(3)$, $b=5.1492(2)$, $c=10.0090(2)$ Å and $\beta=110.569(1)^\circ$) (see Table 30). In Fig.48, we show variations in the cell parameters and the crystal density with temperature. As the temperature is decreased from the ambient to close to the transition temperature, the a parameter decreases by ~ 0.25 Å while b and c show only small variations (Fig.48a). Below the transition at 136 K, the cell is still monoclinic with the same space group. As we notice in Table 30, the a parameter reverts back to its room temperature value while the parameter remains essentially unchanged. Interestingly, the b parameter nearly triples to $14.9925(1)$ Å accompanying the transition. It is shorter by ~ 0.5 Å from the ideal tripled value. The angle β shows a gradual increase on cooling and exhibits a cusp near the transition while the density ρ increases steadily (Fig.48b). The phase transition therefore appears to be of second order, which also explains the necessity of slow cooling of the crystal.

In Fig.49, we show the asymmetric units used in structure refinement of the high- and the low-temperature phases. We see from Fig.49 that the asymmetric unit in the high-temperature phase contains only half the adipic molecule [90] and the other half is generated by inversion. We see from Table 31 that the C—C bond length increases gradually from $1.498(2)$ Å for the carboxylic linkage to $1.520(3)$ Å for the central bond. The carbon backbone is non-planar. The torsion angle C(1)—C(2)—C(3)—C(3') is $\sim 173.2(1)^\circ$ while the inner torsion angle C(2)—C(3)—C(3')—C(2') is 180° . The plane containing the carboxylic group makes an angle of $\sim 7^\circ$ with the C(1)—C(2)—C(3) plane. In the low-temperature phase on the other hand, we found that the asymmetric unit comprises of one and a half molecule. The half-molecule fragment resembles the asymmetric unit of the high-temperature phase with the centre of inversion lying on it. It is however, relatively more planar with the torsion angle C(1)—C(2)—C(3)—C(3') being $177.0(1)^\circ$. The angle made by the carboxylic group is also smaller, $\sim 3^\circ$. Obviously, the full-

Table 30
Crystal data and experimental details for Adipic acid

Chemical formula	C ₆ H ₁₀ O ₄	
Formula weight	146.064	
	145 K	116 K
Cell setting	Monoclinic	Monoclinic
Space group	P2 ₁ /n	P2 ₁ /n
a (Å)	7.1761(11)	7.4282(2)
b (Å)	5.1501(8)	14.9925(1)
c (Å)	10.0158(16)	10.1000(3)
β (°)	111.13(2)	111.45(1)
Volume (Å ³)	345.27	1046.90
ρ (Mg m ⁻³)	1.406	1.391
z	4	4
Radiation type	Mo Kα	
Wave length (Å)	0.71073	
μ (mm ⁻¹)	0.12	0.12
Crystal form	Cuboidal	Cuboidal
Crystal size (mm)	0.4x0.3x0.2	0.4x0.3x0.2
Crystal color	Colorless	Colorless
Data collection		
Diffractometer	Siemens CCD	
Data collection	ω scan	
Crystal-detector distance (cm)	5.0	
No. of measured reflections	4329	10144
No. of independent reflections	2735	6928
No. of observed reflections	1787	2057
R _{int}	0.00	0.00
θ _{max} (°)	49.5	49.5
Range of h, k, l	-12→h→15	-8→h→15
	-7→k→10	-24→k→22
	-20→l→15	-20→l→18
Refinement		
Refinement on F ²		
R(F)	0.049	0.056
wR(F ²)	0.087	0.081
S	0.97	0.99
Weights used	0.04, 0.5	0.02, 0.2
No. of reflections used in the refinement	2451	4120
No. of parameters refined	101	271
N _{ref} /N _v	24.5	15.2

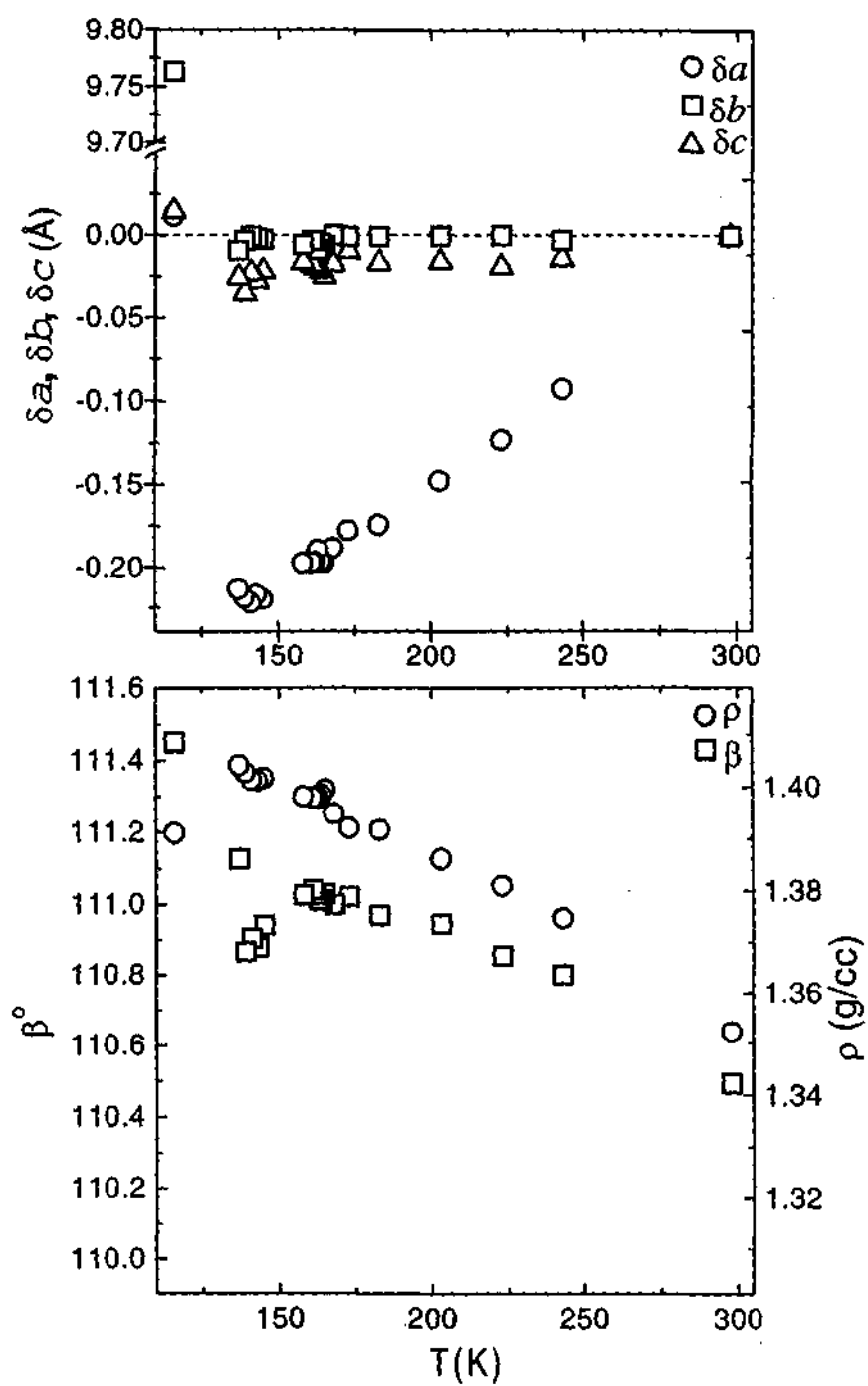


Fig.48. Variations with respect to the room temperature values in (a) a , circles; b , squares; c , triangles and (b) β , squares; ρ , circles with temperature.

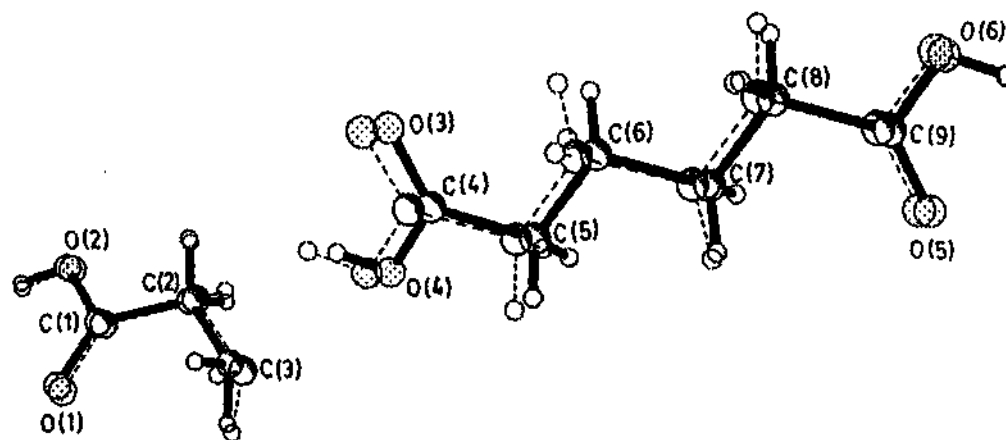


Fig.49. Asymmetric units of adipic acid in the high- (dashed) and the low-temperature (solid line) phases. A 2_1 related full molecule of the high-temperature phase is also shown for comparison.

Table 31

Bond lengths, bond angles and torsion angles of the high- and the low- temperature phases of adipic acid

Bond Lengths (Å)	145 K	116 K
O1—C1	1.224(2)	1.234(3)
O2—C1	1.315(2)	1.324(4)
O2—H2	0.98(3)	0.94(4)
C1—C2	1.498(2)	1.515(4)
C2—C3	1.515(2)	1.524(4)
C2—H2A	0.97(2)	1.00(3)
C2—H2B	0.98(2)	0.99(3)
C3—H3A	0.96(2)	0.99(3)
C3—H3B	1.00(2)	0.98(3)
O3—C4		1.232(3)
O4—C4		1.325(4)
O4—H4		0.94(4)
O5—C9		1.232(3)
O6—C9		1.327(4)
O6—H6		0.93(5)
C4—C5		1.512(4)
C5—C6		1.527(4)
C5—H5A		1.00(3)
C5—H5B		1.02(3)
C6—C7		1.542(4)
C6—H6A		1.02(3)
C6—H6B		0.99(4)
C7—C8		1.527(4)
C7—H7A		0.99(3)
C7—H7B		1.03(3)
C8—C9		1.510(4)
C8—H8A		0.99(3)
C8—H8B		0.96(3)

Bond Angles (°)	145 K	116 K
C1—O2—H2	108(2)	107(2)
O1—C1—O2	123.0(1)	123.2(2)
O2—C1—C2	113.2(1)	113.1(2)
O1—C1—C2	123.8(1)	123.7(3)
C1—C2—H2B	105(1)	107(2)
C1—C2—H2A	107(1)	107(2)
C1—C2—C3	114.1(1)	114.3(2)
H2A—C2—H2B	109(2)	108(2)
C3—C2—H2B	110(1)	111(2)
C3—C2—H2A	112(1)	110(2)
C2—C3—H3B	110(1)	110(2)
C2—C3—H3A	111(1)	110(2)
H3A—C3—H3B	107(1)	107(3)
C4—O4—H4		111(2)
C9—O6—H6		108(3)
O3—C4—O4		123.5(3)
O4—C4—C5		112.8(2)
O3—C4—C5		123.7(3)
C4—C5—H5B		107(2)
C4—C5—H5A		104(2)
C4—C5—C6		114.2(2)
H5A—C5—H5B		105(2)
C6—C5—H5B		111(2)
C6—C5—H5A		115(2)
C5—C6—H6B		110(2)
C5—C6—H6A		109(2)
C5—C6—C7		111.8(2)
H6A—C6—H6B		108(3)
C7—C6—H6B		109(2)
C7—C6—H6A		108(2)
C6—C7—H7B		110(2)
C6—C7—H7A		110(2)
C6—C7—C8		111.0(2)
H7A—C7—H7B		105(2)
C8—C7—H7B		110(2)
C8—C7—H7A		111(2)
C7—C8—H8B		110(2)

C7—C8—H8A	110(2)
C7—C8—C9	114.1(2)
H8A—C8—H8B	110(3)
C9—C8—H8B	106(2)
C9—C8—H8A	108(2)
O6—C9—C8	112.8(2)
O5—C9—C8	124.0(3)
O5—C9—O6	123.2(2)

Torsion angles (°)	145 K	116 K
H2—O2—C1—O1	4(2)	-6(3)
H2—O2—C1—C2	-176(2)	175(3)
O2—C1—C2—C3	173.5(1)	177.1(3)
O1—C1—C2—C3	-6.9(2)	-2.0(4)
O2—C1—C2—H2A	49(1)	-61(2)
O1—C1—C2—H2A	-131(1)	120(2)
O2—C1—C2—H2B	-66(1)	53(2)
O1—C1—C2—H2B	114(1)	-125(2)
C1—C2—C3—H3A	66(1)	-60(2)
C1—C2—C3—H3B	-52(1)	57(2)
H2A—C2—C3—H3B	70(2)	-63(3)
H2A—C2—C3—H3A	-173(2)	179(3)
H2B—C2—C3—H3B	-170(2)	178(3)
H2B—C2—C3—H3A	-52(2)	60(3)
H4—O4—C4—O3		2(3)
H4—O4—C4—C5		-178(3)
H6—O6—C9—O5		-3(3)
H6—O6—C9—C8		178(3)
O4—C4—C5—C6		170.0(2)
O3—C4—C5—C6		-10.2(4)
O4—C4—C5—H5A		43(2)
O3—C4—C5—H5A		-137(2)
O4—C4—C5—H5B		-68(2)
O3—C4—C5—H5B		112(2)
C4—C5—C6—C7		-172.3(2)
C4—C5—C6—H6A		68(2)
C4—C5—C6—H6B		-50(2)
H5A—C5—C6—H6B		70(3)
H5A—C5—C6—H6A		-172(3)
H5A—C5—C6—C7		-52(2)
H5B—C5—C6—H6B		-171(3)
H5B—C5—C6—H6A		-53(3)
H5B—C5—C6—C7		68(2)
C5—C6—C7—C8		-175.7(2)
C5—C6—C7—H7A		61(2)
C5—C6—C7—H7B		-54(2)
H6A—C6—C7—H7B		66(3)
H6A—C6—C7—H7A		-179(3)
H6A—C6—C7—C8		-55(2)
H6B—C6—C7—H7B		-177(3)
H6B—C6—C7—H7A		-62(3)
H6B—C6—C7—C8		62(2)
C6—C7—C8—C9		173.9(2)
C6—C7—C8—H8A		-65(2)
C6—C7—C8—H8B		56(2)
H7A—C7—C8—H8B		178(3)
H7A—C7—C8—H8A		58(3)
H7A—C7—C8—C9		-63(2)
H7B—C7—C8—H8B		-66(3)
H7B—C7—C8—H8A		173(3)
H7B—C7—C8—C9		53(2)
C7—C8—C9—O6		-172.2(2)
C7—C8—C9—O5		8.2(4)
H8A—C8—C9—O6		66(2)
H8A—C8—C9—O5		-114(2)
H8B—C8—C9—O6		-51(2)
H8B—C8—C9—O5		129(2)

molecule fragment of the low-temperature asymmetric unit does not contain a center of inversion. The molecular backbone is buckled, the torsion angles being $172.3(2)^\circ$, $175.7(2)^\circ$ and $173.9(2)^\circ$ along its length. The carboxylic groups also deviate significantly from the mean plane of the hydrocarbon chain ($\sim 10^\circ$). We notice that the central C—C bond of this molecule is close to the ideal tetrahedral value of 1.54 Å (Table 31). The bond angles do not change appreciably following the phase transition.

In Fig.50 we show the packing diagrams in the high- and low-temperature phases. We made use of the simple relationship between the high- and the low-temperature cells and superimposed the crystal structures in order to visualize the deformation of one structure into the other involving translations and rotations of the individual molecules. In Fig.51, we show such a packing diagram along with the unit cells. We observe that in the low-temperature phase, the half-molecule fragment of the asymmetric unit generates molecules which roughly remain in place during phase transition while those generated by the full-molecule fragment show noticeable displacements perpendicular to the screw axis and along the *ac*-diagonal (by ~ 0.8 Å) leading to tripling of the unit cell in the *b* direction. Therefore, the deformation occurs in the alternating domains labelled 'FM' in Fig.51. The HM domains closely resemble the high-temperature structure. The domain interface typifies new interchain interactions resulting from the phase transition. In the regions enclosed by circles in Fig.51 for instance, methylene hydrogens from the FM domain move closer to carboxyl oxygens in the HM domain.

The intermolecular hydrogen contacts of the dimeric units involving the carboxylic groups run perpendicular to the *b* axis and are affected to some extent by the phase transition (see Table 32). In the high temperature phase, the intermolecular H(2)···O(1) distance is 1.72(3) Å with $\angle O(2)—H(2)···O(1)$ of $173(3)^\circ$. Below transition, the carboxylic group in the HM domain exhibits a H···O contact of 1.71 Å with an angle of $168(3)^\circ$ while that in the FM domain has contacts at 1.68(5) and 1.70(4) Å with angles of $170(4)^\circ$ and $176(3)^\circ$ respectively. In addition to the O—H···O contacts, we observe up to six C—H···O contacts per molecule in the range of 2.7 and 2.9 Å in both the high- and the low-temperature phases (Table 32). The

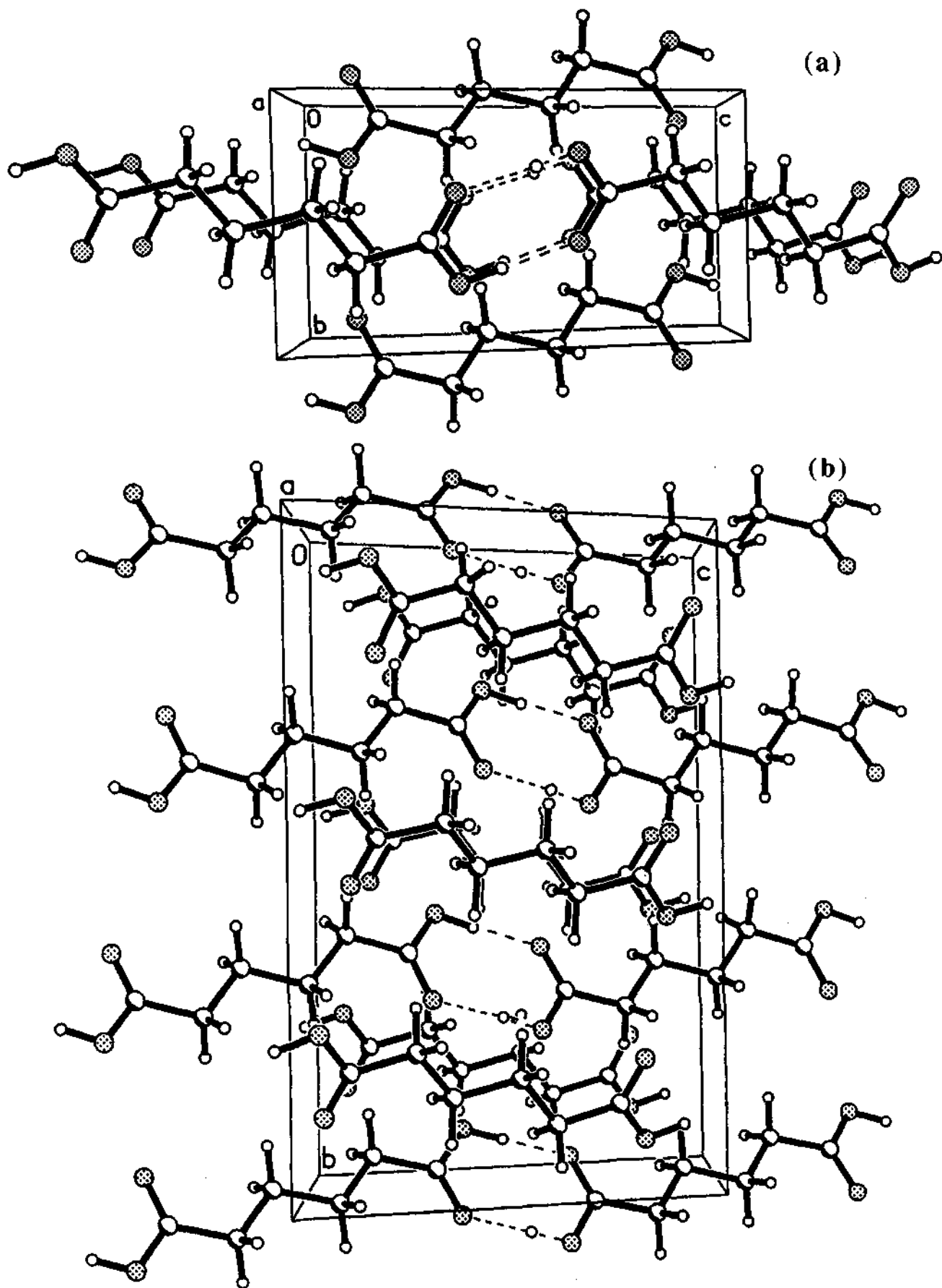


Fig.50. Molecular packing in a) high- and b) low-temperature forms of adipic acids.

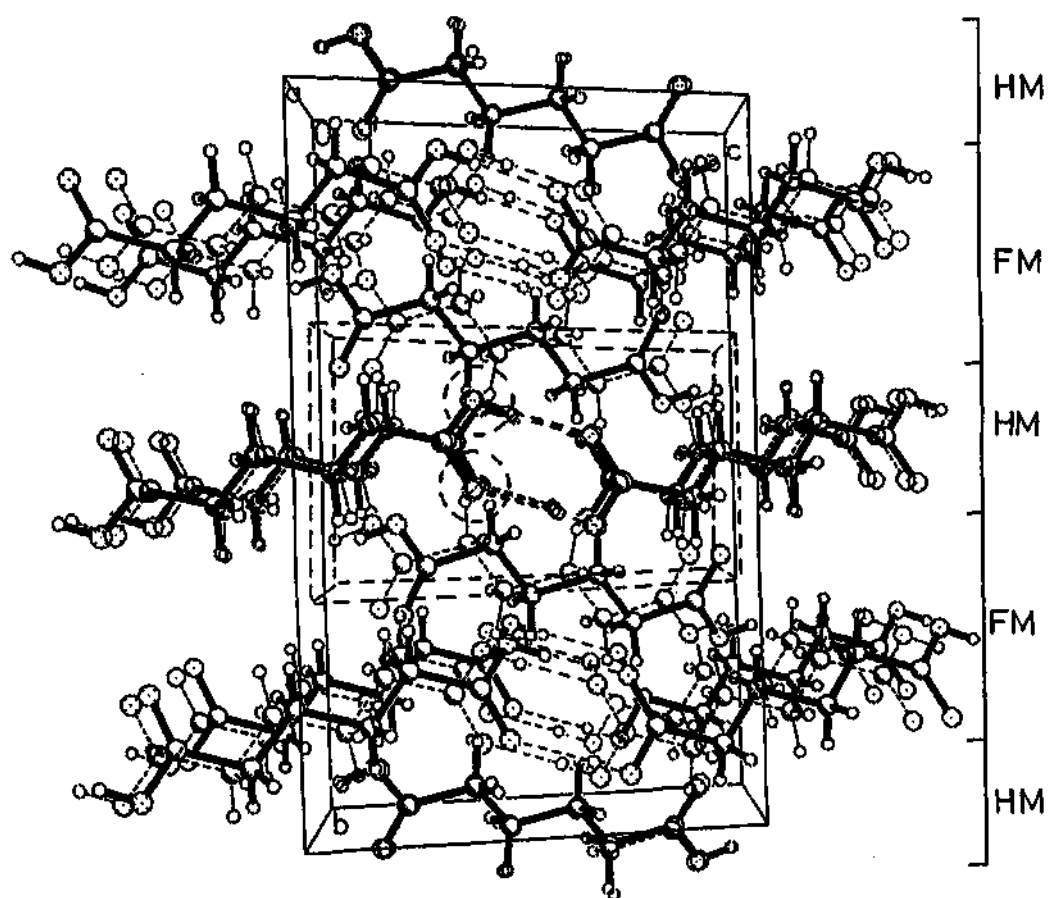


Fig.51. Packing diagrams of the high- and low- temperature phases superimposed to visualise molecular displacements. High temperature, dashed lines; low temperature, solid lines. 'FM' and 'HM' denote domains generated by the full- and the half-molecule fragments of the low temperature asymmetric unit. The unit cells are also shown.

Table 32

Hydrogen bond contacts in the high and low temperature phases

		145 K		116 K	
D—H...A	H...A (Å)	∠D—H...A (°)	D—H...A	H...A (Å)	∠D—H...A (°)
O(2)—H(2)...O(1) ^b	1.72(3)	173(3)	O(2)—H(2)...O(1) ^e	1.71(4)	168(3)
			O(6)—H(6)...O(3) ^b	1.68(5)	170(4)
			O(4)—H(4)...O(5) ^f	1.70(4)	176(3)
C(3)—H(3A)...O(1) ^e	2.92(3)	120(3)	C(5)—H(5A)...O(1) ^g	2.86(3)	147(2)
			C(5)—H(5B)...O(1) ^h	2.85(3)	131(2)
			C(8)—H(8A)...O(1) ⁱ	2.97(3)	141(2)
			C(7)—H(7A)...O(3) ^j	2.87(3)	120(2)
			C(2)—H(2A)...O(5) ^k	2.88(3)	145(2)
C(2)—H(2A)...O(2) ^d	2.73(3)	108(3)	C(8)—H(8B)...O(2) ^g	2.71(3)	115(2)
C(3)—H(3B)...O(2) ^d	2.82(3)	120(3)	C(7)—H(7B)...O(2) ^h	2.65(3)	121(2)
			C(2)—H(2A)...O(4) ^e	2.74(3)	116(2)
			C(5)—H(5A)...O(6) ⁱ	2.81(3)	103(2)
			C(6)—H(6B)...O(6) ^j	2.85(3)	119(2)

Symmetry: a) x, y, z; b) -x, -y, 1-z; c) 1/2-x, -1/2-y, 1/2-z; d) 1/2-x, 1/2-y, 1/2-z; e) 1-x, -y, 1-z; f) 1/2-x, 1/2-y, 3/2-z; g) x-1, y, z; h) x, y, 1+z; i) 1/2-x, 1/2-y, 1/2+z; j) x, y, z-1; k) 1+x, y, z; l) 1/2+x, 1/2-y, -1/2-z.

difference is that in the low-temperature phase, the contact angles are considerably higher making C—H...O interactions more favorable.

From the above discussion, it appears that at room temperature there are only moderate side-chain interactions compromising with the allowable strain in the molecule. On cooling the crystal, the side-chain interactions increase because of closer proximity down to a temperature where the crystal undergoes phase transition giving rise to two types of molecules. It is as though the molecules with evenly distributed strain in the high-temperature phase segregate into two domains comprising *unstrained molecules in one domain (HM) and highly strained molecules without inversion symmetry in the other (FM)*.

This is indeed observed in the molecular geometries. In Fig.52 we show both outer and the inner the torsion angles of the high temperature phase splitting in to two branches each corresponding to HM and FM fragments of the low temperature phase. From the figure, it is clear that the HM fragment is less strained (torsion angles $\sim 180^\circ$) compared to the FM fragment as well as the high temperature fragment. The strain in the FM fragment is even higher than that in the high temperature fragment. Thus the molecular torsion angles can act as 'order parameters' for the phase transition in adipic acid.

Electrostatic potential analysis

We have also examined the electrostatic potential around the molecule in the low- and the high-temperature phases based on XD analysis (Fig.53). We observe positive potential contours engulfing the hydrocarbon chain and the hydroxyl region, the latter being a strong electrophilic site. On the other hand, negative potential contours extend in to intermolecular region from the carbonyl oxygen. We find some major differences between the molecules in the two phases. In the half molecular fragment of the low temperature phase (Fig.53b) the positive contours lie close to the molecular volume especially in the hydrocarbon region and the electrostatic potential distribution is like what one would expect for a less strained molecule. On the contrary, the full molecular fragment of the low-temperature phase (Fig.53c) extends the potential contours well beyond the molecular volume even compared to

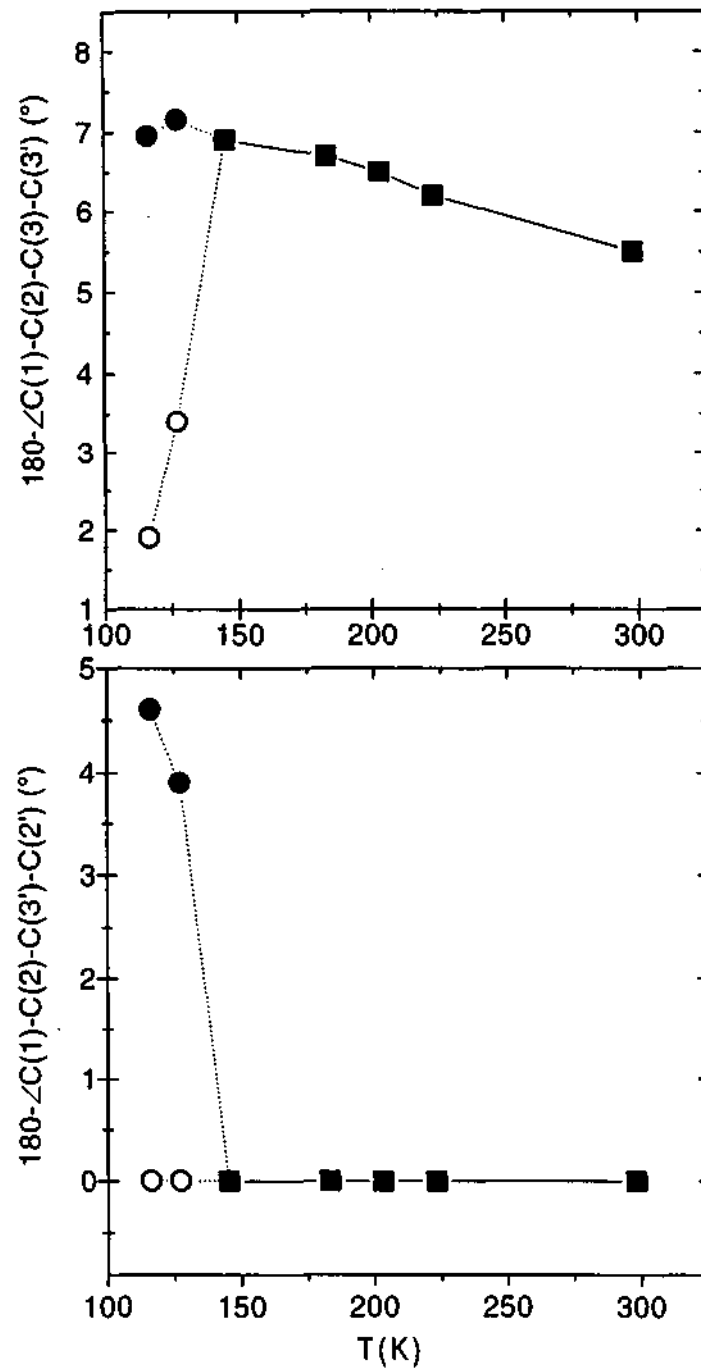


Fig.52. Variation in the torsion angles with temperature in the high- (squares) and low-temperature (circles) phases. Open circles stand for half-molecular fragment and filled circles for full-molecular fragment of the low-temperature phase respectively.

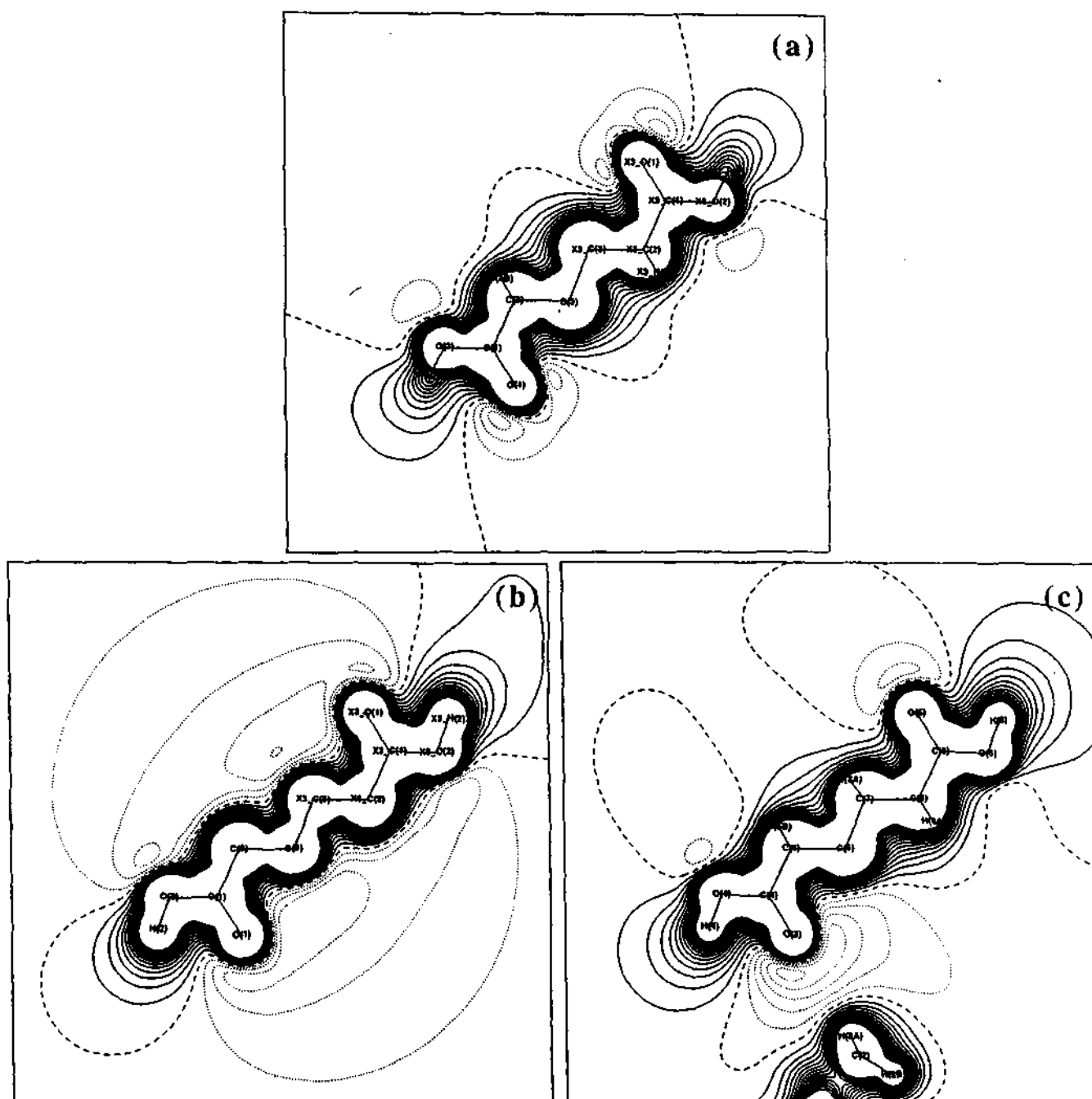


Fig.53. Electrostatic Map in the plane formed by a) C(2), C(3), C(3A) atoms in the high-temperature phase b) C(2), C(3), C(3A) atoms in the half-molecular fragment and c) C(5), C(6), C(7) atoms in the full-molecular fragment in the low-temperature phase. Contours at $0.05 \text{ e}\text{\AA}^{-1}$.

the room-temperature phase (Fig.53a). Thus it is evident that the interchain interactions which drive the phase transition are also responsible for inducing strain in the molecule.

5. REFERENCES

1. P. Debye, Dispersion of Roentgen rays, *Ann. Phys.* **46**, 809 (1915).
2. P. Coppens in *The application of charge density research to Chemistry and Drug Design*; Eds. G. A. Jeffrey, J. F. Piniella, Plenum Press, New York (1991).
3. M. J. Frisch, G. W. Trucks, H. B. Schlegel, P. M. W. Wong, J. B. Foresman, M. A. Robb, M. Head-Gordon, E. S. Replogle, R. Gomperts, J. L. Andres, K. Raghavachari, J. S. Binkley, C. Gonzalez, R. L. Martin, D. J. Fox, D. J. Defrees, J. Baker, J. J. P. Stewart, J. A. Pople, GAUSSIAN 92/DFT, Revision G. 4. Gaussian Inc., Pittsburgh PA, 1993.
4. GAMESS, M. W. Schmidt, K. K. Baldridge, J. A. Boatz, S. T. Elbert, M. S. Gordon, J. H. Jensen, S. Koseki, N. Matsunaga, K. A. Nguyen, S. J. Su, T. L. Windus, M. Dupuis, J. A. Montgomery, *J. Comput. Chem.* **14**, 1347 (1993).
5. R. Dovesi, V. R. Saunders, C. Roetti, M. Causa, N. M. Harrison, R. Orlando, R. Apra *CRYSTAL 95 User's Manual*. University of Torino, Torino, Italy (1996).
6. R.F.W. Bader in *Atoms in Molecules - a Quantum Theory*, Clarendon Press, Oxford, (1990).
7. P. Coppens in *X-ray Charge Densities and Chemical Bonding*, Oxford University Press, 1997.
8. *Studies of Electron Distributions in Molecules and Crystals*, Ed. R. Blessing, Transactions of American Crystallographic Association, Vol. **26** (1990).
9. T. Koritsansky in *Fundamental Principles of Molecular Modelling*, Eds. W. Gans, A. Amann and J. C. A. Boeyens, Plenum, New York, p.143 (1996).
10. M. A. Spackman, A. S. Brown, *Annu. Rep. Prog. Chem., Sect. C, Phys. Chem.* **91**, 175 (1994).
11. M. A. Spackman, *Annu. Rep. Prog. Chem., Sect. C, Phys. Chem.* **94**, 177 (1998).
12. P. Coppens, *Acta. Cryst. A* **54**, 779 (1998).
13. N. K. Hansen, P. Coppens, *Acta. Cryst. A* **34**, 909 (1978).
14. W. J. Hehre, L. Radom, P. v. R. Schleyer, J. A. Pople, *Ab initio Molecular Orbital Theory*, Wiley, New York (1986).

15. K. L. McCormack, P. R. Mallinson, B. C. Webster, D. S. Yufit *J. Chem. Soc., Faraday Trans.*, **92**, 1709 (1996).
16. D. Cremer, E. Kraka, *Croat. Chem. Acta.* **57**, 1259 (1984).
17. *Chemical Applications of Atomic and Molecular Electrostatic Potentials*, Eds. P. Politzer and D. G. Truhlar, Plenum, New York (1981).
18. *Molecular Electrostatic Potentials: Concepts and Applications*, Eds. J. S. Murray and K. D. Sen, Elsevier, Amsterdam (1996).
19. R. F. Stewart in *The application of charge density research to Chemistry and Drug Design*; G. A. Jeffrey, J. F. Piniella, Plenum Press, New York (1991).
20. Y. Abramov, *Acta Cryst. A* **53**, 264 (1997).
21. P. Coppens, Y. Abramov, M. Carducci, B. Korjov, I. Novozhilova, C. Alhambra, M. R. Pressprich, *J. Am. Chem. Soc.* **121**, 2585 (1999).
22. E. Espinosa, E. Mollins, C. Lecomte, *Chem. Phys. Lett.* **285**, 170 (1998).
23. P. Macchi, D. M. Prosperpio, A. Sironi, R. Soave, R. Destro, *J. Appl. Cryst.* **31**, 583 (1998).
24. A. Volkov, G. Wu, P. Coppens, *J. Synchrotron. Rad.* **6**, 1007 (1999).
25. T. Koritsansky, R. Flaig, D. Zobel, H. -G. Crane, W. Morgenroth, P. Luger, *Science* **279**, 356 (1998).
26. *The Application of Charge Density Research to Chemistry and Drug Design*, Eds; G. A. Jeffrey and J. F. Piniella, Plenum Press, New York and London (1991).
27. G. M. Sheldrick, *SHELX-76; Program for crystal structure determination*, University of Göttingen, Germany.
28. F. H. Allen, O. Kennard, D. G. Watson, L. Brammer, A. G. Orpen, R. Taylor, *J. Chem. Soc. Perkin Trans. II.* S1 (1987).
29. F. L. Hirshfeld, *Acta Cryst. A* **32**, 239 (1976).
30. V. Schoemaker, K. N. Trueblood, *Acta Cryst. B* **54**, 507 (1998).
31. T. Koritsansky, S. T. Howard, T. Richter, P. R. Mallinson, Z. Su and N. K. Hansen, *XD, A computer program package for Multipole Refinement and Analysis of charge densities from diffraction data*, Cardiff, Glasgow, Buffalo, Nancy, Berlin (1995).

32. R. F. Stewart and M. A. Spackman, *VALRAY User Manual* (Carnegie Mellon University, Pittsburg, PA)
33. H. L. Hirshfeld, *Acta. Cryst. A* **32**, 239(1976)
34. B. M. Craven, H. P. Weber and X. He, *Tech. Report TR-87-2*, Department of Crystallography, University of Pittsburgh, PA15260 (1987).
35. J. J. P. Stewart, *J. Computer-Aided Molecular Design*, **4**, 1 (1990).
36. M. C. Etter, *Accts. Chem. Res.* **23**, 120 (1990).
37. M. D. Cohen, G. M. J. Schmidt, F. I. Sonntag, *J. Chem. Soc.* 2000 (1964).
38. J. Fritsche, *Liebigs. Ann.* **110**, 157 (1859).
39. G. U. Kulkarni, P. Kumardhas, C. N. R. Rao, *Chem. Mater.* **10**, 3498 (1998).
40. C. N. R. Rao, S. Ganguly, H. R. Swamy, *Croat. Chem. Acta* **55**, 207 (1982).
41. N. R. Jagannathan, C. N. R. Rao, *Chem. Phys. Lett.* **140**, 46 (1987).
42. R. T. Morrison, R. N. Boyd, *Organic Chemistry*, 5th edition, Printice Hall-India Pvt. Ltd (1989).
43. H. Ohki, N. Nakamura, H. Chihara, *J. Phys. Soc. Jpn.* **57**, 382 (1988).
44. P. J. L. Baudour, Y. Delugeard, H. Caileau, *Acta. Cryst. B* **32**, 150 (1976).
45. A. T. H. Lenstra, C. Canalsenoy, K. Verhulst and H. J. Geise, *Acta Cryst. B* **50**, 96 (1994).
46. P. Coppens, T. M. Sabine, *Mol. Cryst. Liquid Cryst.* **3**, 507 (1967).
47. P. N. Prasad, J. D. Williams, *Introduction to Nonlinear Optical Effects in Molecules and Polymers*, John Wiley and sons Inc., New York (1990).
48. S. T. Howard, M. B. Hursthouse, C. W. Lehmann, P. R. Mallinson, C. S. Frampton, *J. Chem. Phys.* **97**, 5616 (1992).
49. C. Gatti, V. R. Saunders, C. Roetti, *J. Chem. Phys.* **101**, 10686 (1994).
50. E. Espinosa, C. Lecomte, E. Molins, S. Veintemillas, A. Cousson, W. Paulus, *Acta. Cryst. B* **52**, 519 (1996).
51. A. Fkyerat, A. Guelzim, F. Baert, W. Paulus, G. Heger, J. Zyss, A. Perigaud, *Acta. Cryst. B* **51**, 197 (1995).
52. A. Fkyerat, A. Guelzim, F. Baert, J. Zyss, A. Perigaud, *Phys. Rev. B* **53**, 16236 (1996).
53. M. A. Spackman, *Annu. Rep. Prog. Chem., Sect. C, Phys. Chem.* **94**, 177 (1998).

54. F. Hamazaoui, F. Baert, J. Zyss, *J. Mater. Chem.* **6**, 1123 (1996).
55. G. K. H. Madsen, F. C. Krebs, B. Lebech, F. K. Larsen, *Chem. Eur. J.* **6**, 1797 (2000).
56. H. Youping, S. Genbo, W. Bochang, J. Rihong, *J. Cryst. Growth.* **119**, 393 (1992).
57. M. Ravi, D. N. Rao, S. Cohen, I. Agranat, T. P. Radhakrishanan, *Chem Mater.* **9**, 830 (1997).
58. E. Subramanian, S. Renganayaki, S. S. S. Raj, H-K. Fun, *Acta Cryst. C* **55**, 764 (1999).
59. B. S. Furniss, A. S. Hannaford, P. W. G. Smith, A. R. Tatchell, Eds., *Vogel's textbook of Practical Organic Chemistry*, Addison Wesley Longman limited, Essex, England (1989).
60. H. U. Hummel, H. Procher *Acta Cryst. C* **42**, 1602 (1986).
61. N. H. Nilsson, J. Sandström, *Synthesis* 433 (1974).
62. E. Ericsson, J. Sandström, I. Wennerbeck, *Acta Chem. Scand.* **24**, 3102 (1970).
63. Siemens Analytical X-ray Instruments Inc., Madison, Wisconsin, USA (1995).
64. SHELXTL (SGI version) Siemens Analytical X-ray Instruments Inc., Madison, Wisconsin, USA (1995).
65. A. L. Spek, *Acta Cryst. A* **46**, C34 (1990).
66. G. H. Stout and L. H. Jensen, *X-ray Structure Determination - A practical guide*, John Wiley & sons, NY, (1989).
67. H. D. Flack, *Acta. Cryst. A* **39**, 876 (1983).
68. I. Rozas, I. Alkorta, J. Elguero, *J. Phys. Chem. A* **102**, 9925 (1998).
69. R. Parthasarathy, *Acta Cryst. B* **25**, 509 (1969).
70. P. R. Mallinson, K. Wozniak, T. Garry, K. L. McCormak, *J. Am. Chem. Soc.* **119**, 11502 (1997).
71. P. R. Mallinson, K. Wozniak, C. C. Wilson, K. L. McCormak, D. M. Yufit, *J. Am. Chem. Soc.* **121**, 4640 (1999).
72. L. J. Bellamy, *The infrared spectra of complex molecules* (3rd Ed.), Chapman and Hall, London (1975).

73. C. N. R. Rao, J. R. Ferraro, *Spectroscopy in inorganic Chemistry*, Vol. 1, Academic Press, New York (1970).
74. J. T. Braunschweig, G. E. Hall, F. G. Mann, N. Sheppard, *J. Chem. Soc.* 868 (1959).
75. R. Blinc, D. Hadzi, *Spectrochem. Acta* **16**, 852 (1960).
76. P. Coppens, *Annu. Rev. Phys. Chem.* **43**, 663 (1994).
77. D. Madsen, C. Flensburg, S. Larsen, *J. Phys. Chem. A* **102**, 2177 (1998)..
78. V. Enkelmann, G. Wegner, K. Novak, K. B. Wagener, *J. Am. Chem. Soc.* **115**, 10390 (1993).
79. K. Angermund, K. H. Claus, R. Goddard, C. Kruger, *Angew. Chem. Intl. Ed. Engl.* **24**, 237 (1985)..
80. H. Irngartinger, S. Strack, *J. Am. Chem. Soc.* **120**, 5818 (1998).
81. M. D. Cohen, P. Coppens, G. M. J. Schmidt, *J. Phys. Chem. Solids* **25**, 258 (1964).
82. P. Coppens, G. M. J. Schmidt, *Acta Cryst.* **18**, 654 (1965).
83. P. Coppens, G. M. J. Schmidt, *Acta Cryst.* **17**, 222 (1964).
84. F. L. Hirshfeld, *Israel J. Chem.* **2**, 87 (1964).
85. S. T. Howard, M. B. Hursthouse, C. W. Lehmann, E. A. Poyner, *Acta Cryst. B* **51**, 328 (1995).
86. J. D. Morrison, J. M. Robertson, *J. Chem. Soc.*, 987 (1949).
87. J. A. Goedkoop, C. H. Macgillavry, *Acta Cryst.* **10**, 125 (1957).
88. J. S. Bradley, D. W. J. Cruickshank, J. D. Morrison, J. M. Robertson and H. M. M. Shearer, *Proc. Roy. Soc. A* **251**, 441 (1959).
89. G. D. Rieck, *Rec. Trav. Chim.*, **63**, 170 (1944).
90. J. D. Morrison, J. M. Robertson, *J. Chem. Soc.*, 1001(1949).
91. P. J. Housty, M. Hospital, *Acta Cryst.*, **18**, 693 (1965).
92. P. J. Housty, M. Hospital, *Acta Cryst.*, **21**, 29 (1966).
93. P. Coppens, *Acta Cryst. A* **54**, 779 (1998).
94. M. A. Spackman, *Acta Cryst. A* **47**, 420 (1991).
95. S. Ganguly, J. R. Fernandes, G. R. Desiraju, C. N. R. Rao, *Chem. Phys. Lett.* **69**, 227 (1980).
96. N. U. Kamath, K. Venkatesan *Acta Cryst. C* **40**, 1211 (1984).

97. E. Espinosa, E. Molins, C. Lecomte, *Phys.Rev. B* **57**, 1820 (1997).
98. W. Scherer, M. Spiegler, B. Pedersen, M. Tafipolsky, W. Hieringer, B. Reinhard, A. J. Downs, G. S. McGrady, *Chem. Commun.* 635 (2000).

6. OTHER WORK DONE BY THE AUTHOR

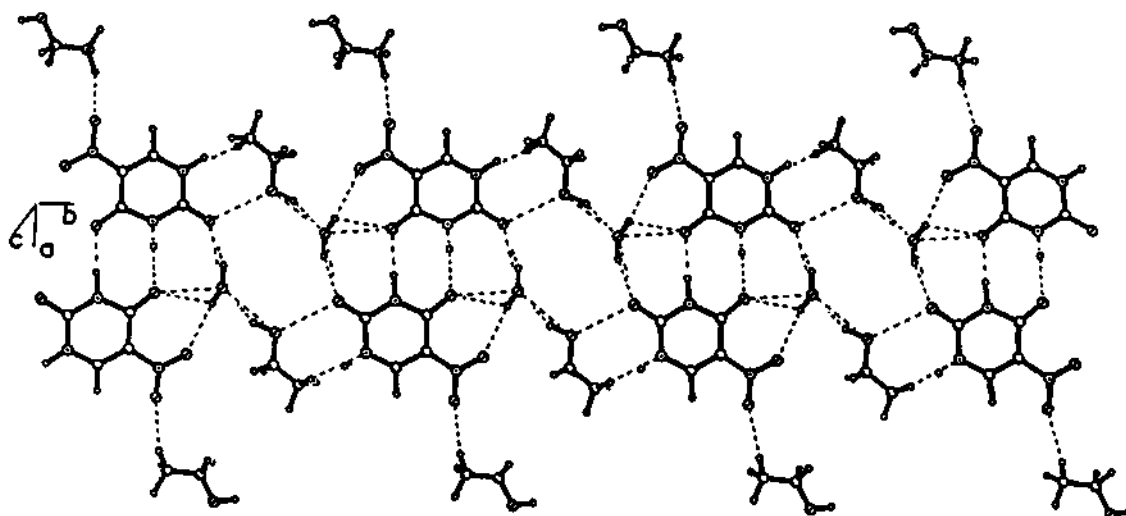
In this section, many new co-crystals obtained while trying to crystallize 5-nitouracil in different polymorphic forms are presented. These include the co-crystals with solvents and some aza aromatic compounds. The respective crystallographic information files (CIF) have been deposited with the Cambridge Crystallographic Data Centre.

6.1 Co-crystals of 5-nitouracil with solvents

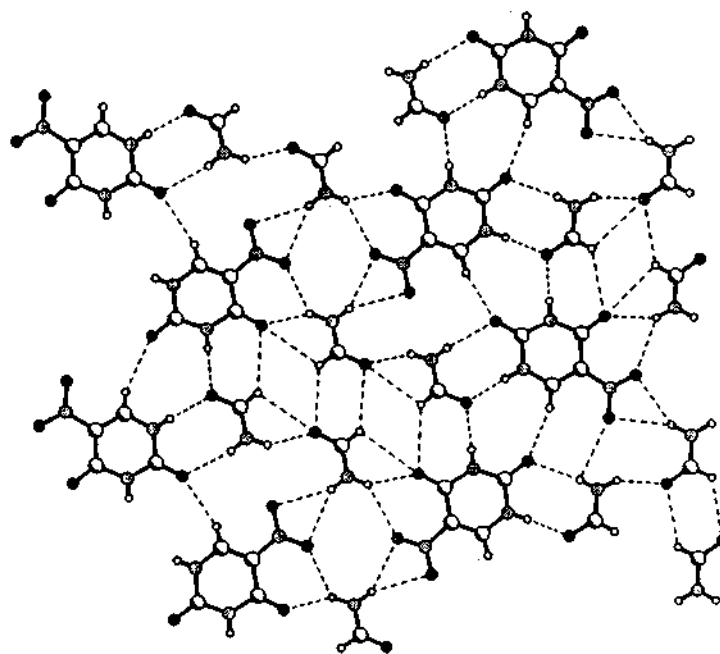
2:2:1 ternary co-crystal of 5-nitouracil, ethanol and water (I): The co-crystal exhibits N-H...O dimeric hydrogen bonds ($R_2^2(8)$) between two nitouracil molecules at moderate distances (~ 2.75 Å). In addition, water makes a bifurcated contact, $R_1^2(6)$ and a cyclic contact $R_2^2(8)$ with nitouracil. Ethanol molecules form strong C-H...O contacts at 1.85 Å with the amidic group of the nitouracil. There are other weaker contacts between them and altogether 20 contacts are found.

1:2 co-crystal of 5-nitouracil and Formamide (II): This co-crystal has a wide variety of hydrogen bonded patterns like 4-, 5- and 6-membered bifurcated hydrogen bonds ($R_1^2(4)$, $R_2^1(5)$, $R_1^2(6)$). These bifurcated hydrogen bonds in addition gives rise to a new pattern, $R_4^2(8)$. There exist other cyclic hydrogen bonds like the dimeric N-H...O bonds between uracil and formamide ($R_2^2(7)$), between two formamide molecules ($R_2^2(6)$), between two nitouracil and a formamide molecule ($R_3^2(9)$) and between two formamide molecules and a uracil molecule ($R_3^2(8)$). It thus forms 19 different hydrogen bonds all of them with moderate lengths.

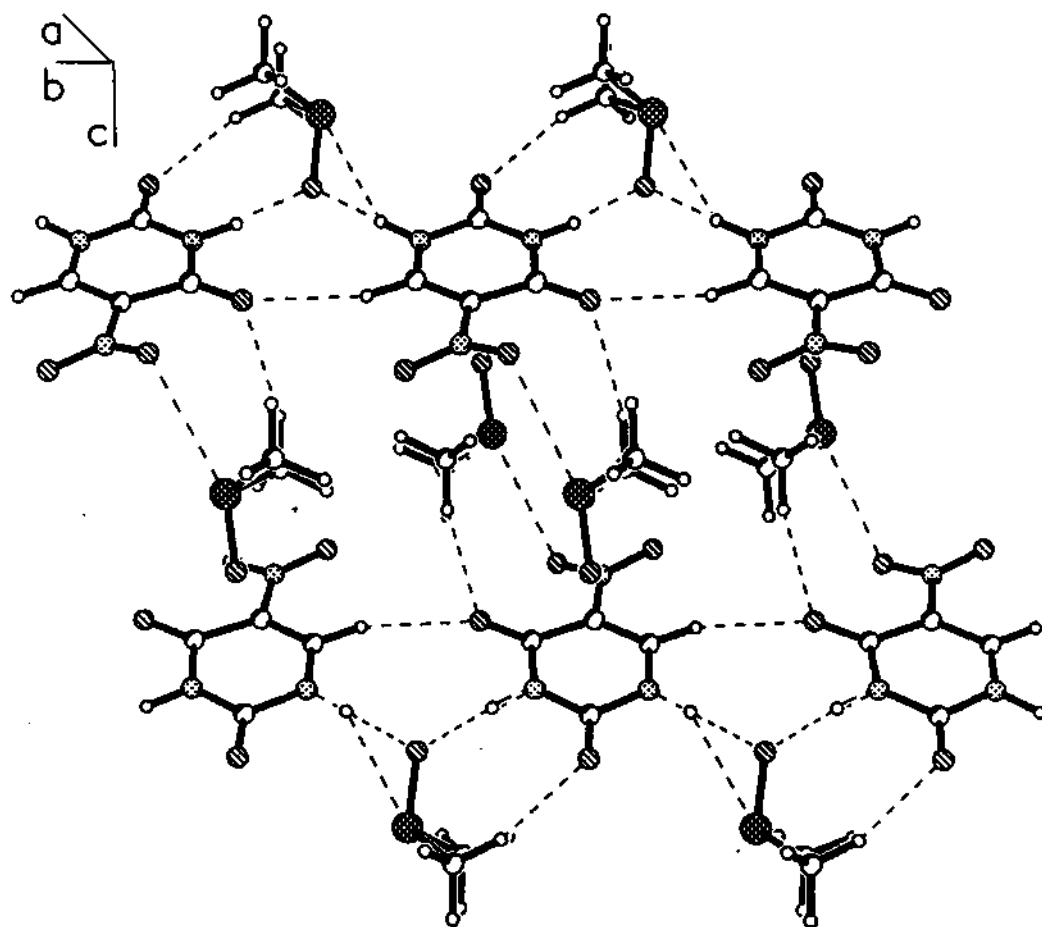
1:1 co-crystal of 5-nitouracil with DMSO (III): In this structure, the dimeric N-H...O bonds of the nitouracil are broken while new bonds those involving DMSO are formed. The most important patterns in this structure happens to be the $R_2^2(8)$ involving a DMSO molecule and a nitouracil and $R_3^2(9)$ involving two nitouracil molecules and a DMSO. The contacts appear at relatively shorter lengths and larger angles.



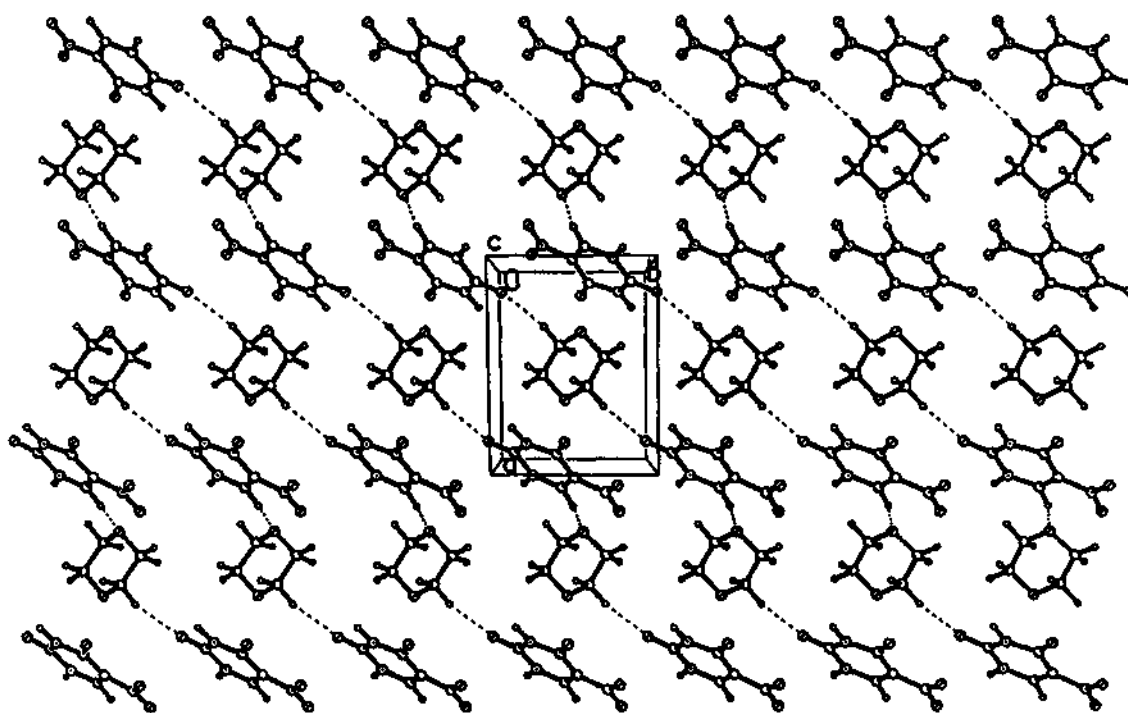
Molecular Packing diagram of I



Molecular Packing diagram of II



Molecular Packing diagram of III



Molecular Packing diagram of IV

2:1 co-crystal of 5-nitrouracil with dioxan (IV): The dimeric hydrogen bonds of 5-nitrouracil is retained in this co-crystal and a strong hydrogen bond involving the dioxan oxygen and the alkenyl hydrogen of the nitrouracil at 2.18 Å is formed. In addition, ring hydrogens of dioxan also participate in the hydrogen bonding with nitrouracil. All the contacts appear strong with short distances and large angles.

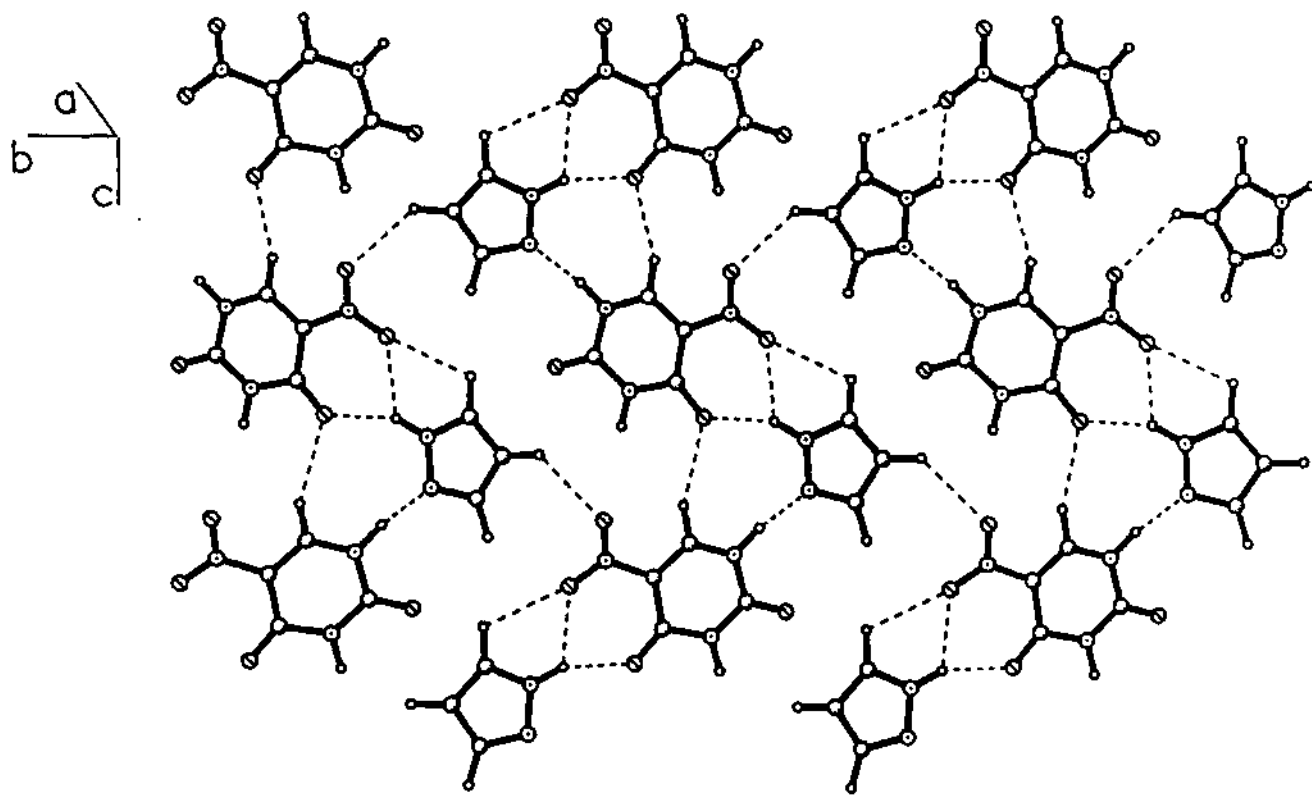
6.2 Co-crystals of 5-nitrouracil with aza aromatics

1:1 co-crystal of 5-nitrouracil with pyrazole (V): The patterns formed by this co-crystal are 5- and 6-membered bifurcated hydrogen bonds ($R_2^1(5)$ and $R_1^2(6)$), ring pattern, $R_3^2(8)$ and a finite hydrogen bond, D(2). The N-H...N and the N-H...O bonds appear at ~ 1.8 Å while the C-H...O bonds appear at ~ 2.5 Å.

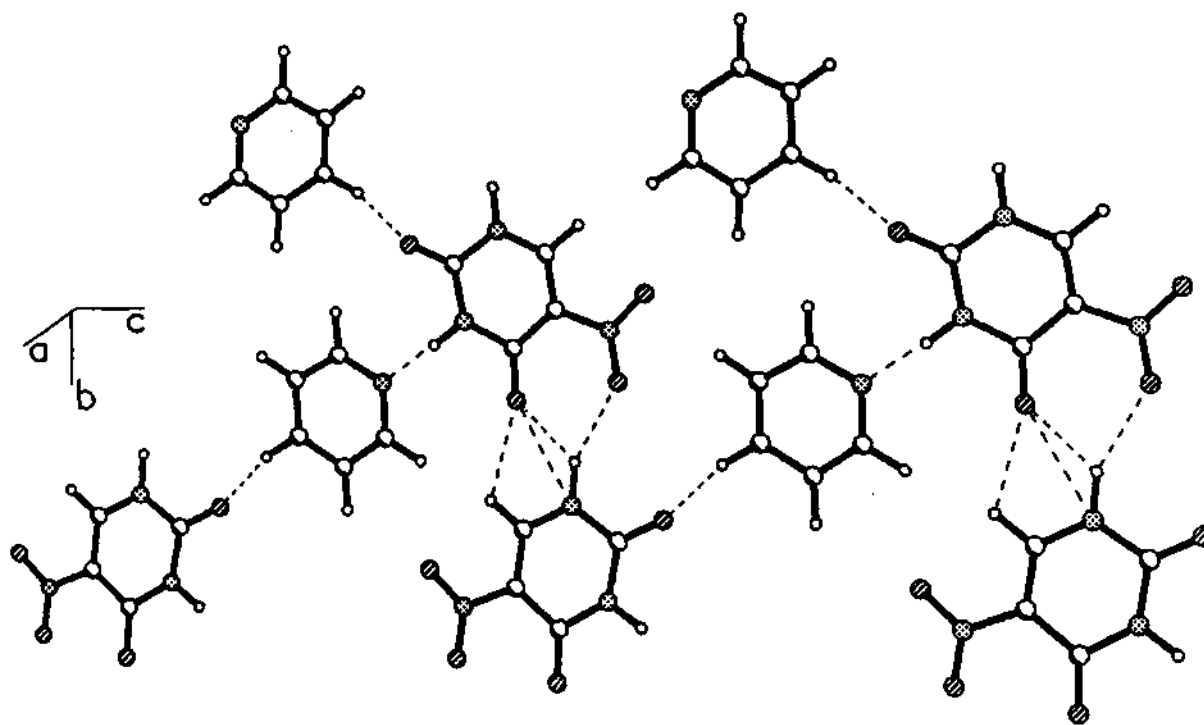
1:1 co-crystal of 5-nitrouracil with pyridine (VI): The various patterns in this structure include 5- and 6-membered bifurcated interactions ($R_2^1(5)$ and $R_1^2(6)$) and two two-centered interactions, one involving a N-H...N and the other involving a C-H...O. The interesting aspect about this structure is that the N-H...N interactions are definitely stronger than the N-H...O and C-H...O interactions.

1:1 co-crystal of 5-nitrouracil with piperazine (VII): In this structure, the nitrouracil forms chains along c-axis using N-H...O and C-H...O interactions with the piperazine molecules binding two such chains. The structure is very rich in various hydrogen-bonded patterns including rings like $R_2^2(8)$ and $R_2^2(10)$ and bifurcated hydrogen bonds like $R_1^2(6)$.

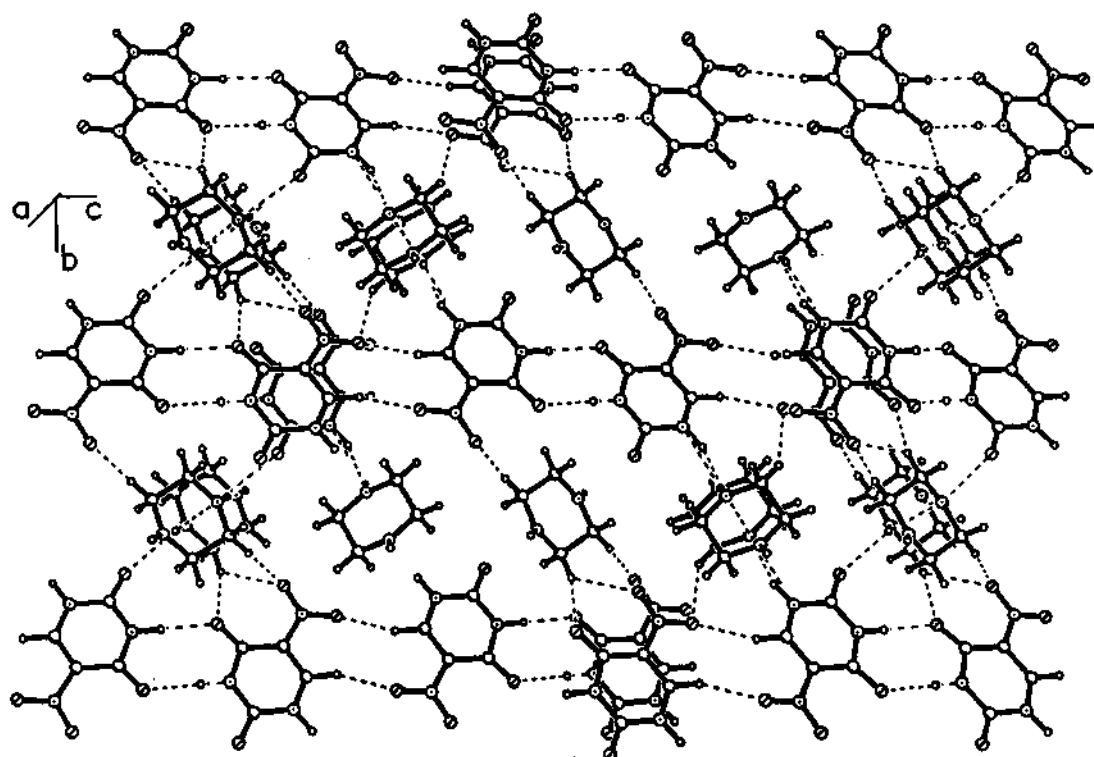
2:1 co-crystal of 5-nitrouracil with N,N-dimethylpiperazine (VIII): The dimeric N-H...O hydrogen bond of 5-nitrouracil is retained in this structure. The other interesting pattern found in this structure is a bifurcated hydrogen bond formed between the hydrogen of piperazine moiety and the nitrouracil.



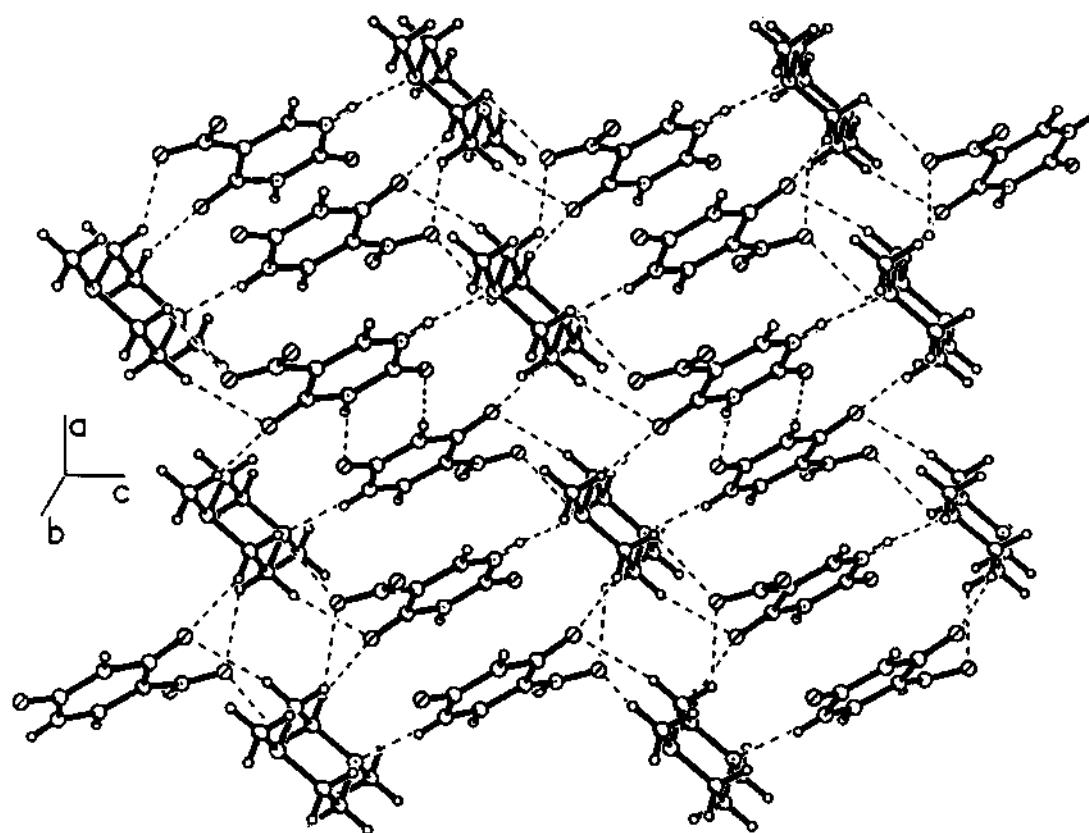
Molecular Packing diagram of V



Molecular Packing diagram of VI



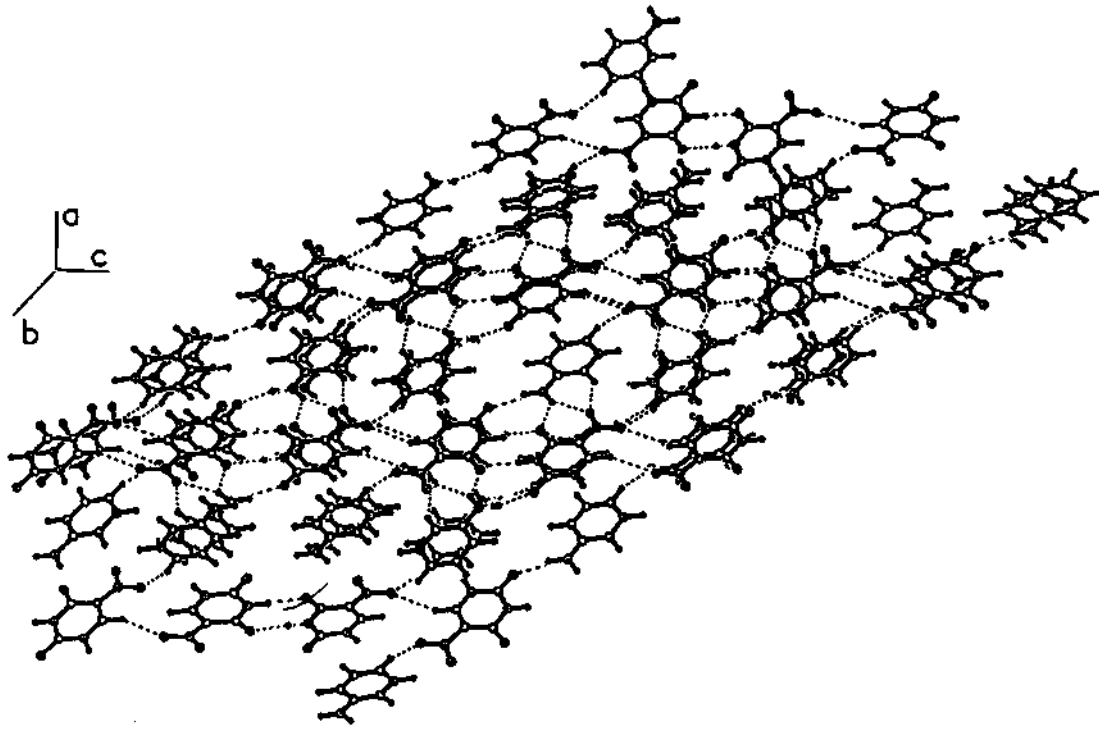
Molecular Packing diagram of VII



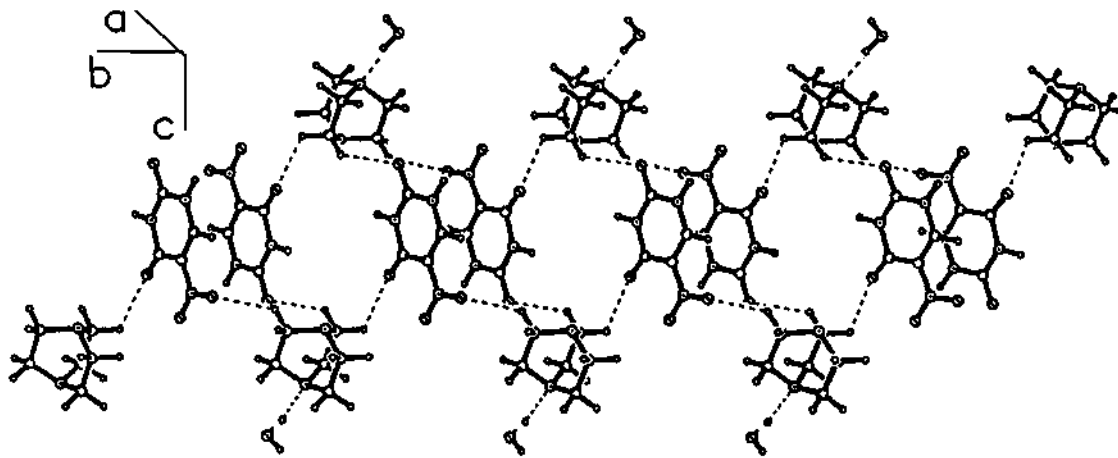
Molecular Packing diagram of VIII

1:1 co-crystal of 5-nitrouracil with 3-aminopyridine (IX): In this co-crystal, the one of the amino hydrogens of the aminopyridine exhibits a bifurcated hydrogen bond with a nitro oxygen, O(3) and a amido oxygen O(2). In addition the structure involves the dimeric N—H...O interaction found in the parent nitrouracil molecule. This also exhibits a very strong C—H...N interaction at 1.77 Å and other weak interactions.

2:2:5 ternary co-crystal of 5-nitrouracil with diazabicyclo[2.2.2]octane and water (X): This co-crystal exhibits a different types of hydrogen bonds including O—H...O, O—H...N, N—H...N, N—H...O, C—H...O and C—H...N hydrogen bonds making a total of 23 contacts. The hydrogen bonds involving the O—H and N—H groups are relatively stronger (~ 1.9 Å) than those involving C—H groups (~ 2.5 Å).



Molecular Packing diagram of IX



Molecular Packing diagram of X

SUPPLEMENTARY INFORMATION

Supplementary Table 1

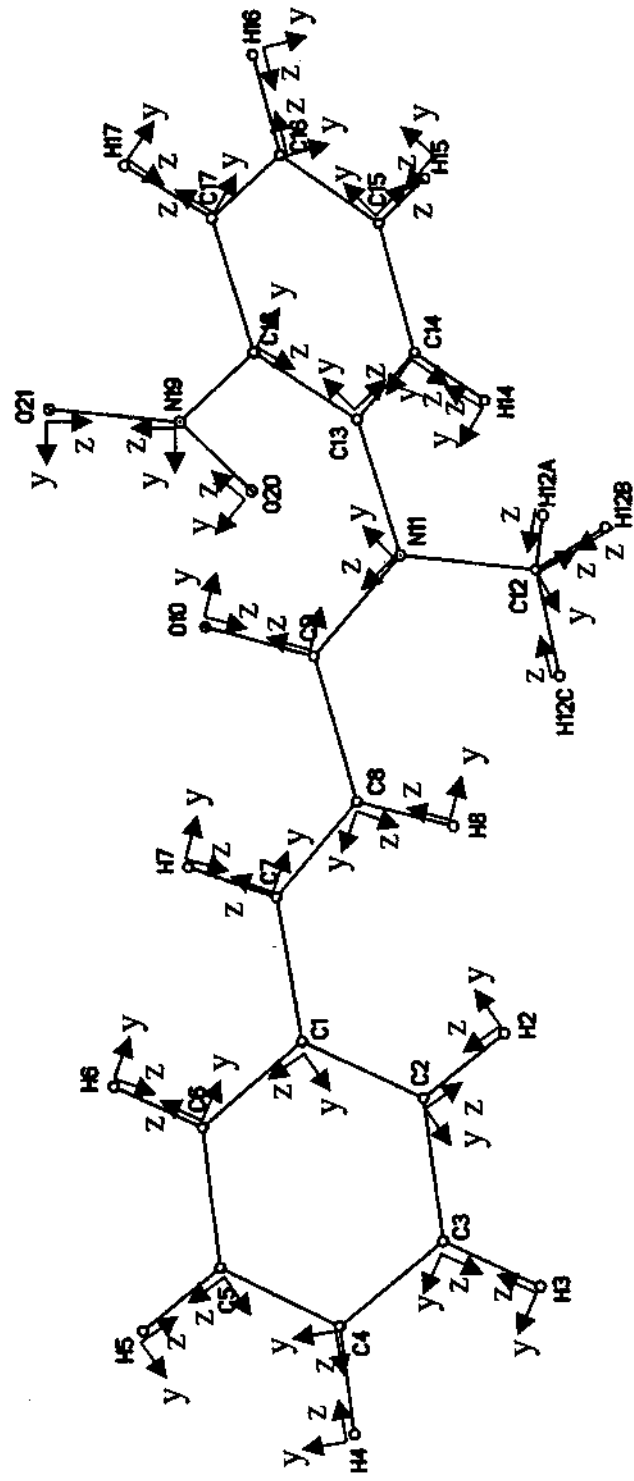
Atomic coordinates ($\times 10^4$) and anisotropic displacement parameters ($\text{\AA}^2 \times 10^3$) for N-methyl-N-(2-nitrophenyl)cinnamanilide

Atom	x	y	z	U(eq)	U11	U22	U33	U23	U13	U12
C(1)	-3355(1)	3751(1)	-383(1)	16(1)	17(1)	17(1)	16(1)	-2(1)	6(1)	-2(1)
C(2)	-4492(1)	3452(1)	-52(1)	19(1)	20(1)	20(1)	18(1)	-1(1)	8(1)	-3(1)
C(3)	-5706(1)	3009(1)	-737(1)	21(1)	19(1)	21(1)	24(1)	-1(1)	9(1)	-3(1)
C(4)	-5816(1)	2872(1)	-1768(1)	22(1)	19(1)	23(1)	23(1)	-3(1)	4(1)	-4(1)
C(5)	-4702(1)	3163(1)	-2104(1)	24(1)	24(1)	30(1)	17(1)	-5(1)	5(1)	-5(1)
C(6)	-3474(1)	3588(1)	-1415(1)	20(1)	20(1)	26(1)	17(1)	-4(1)	7(1)	-4(1)
C(7)	-2067(1)	4265(1)	306(1)	17(1)	18(1)	19(1)	16(1)	-2(1)	5(1)	-2(1)
C(8)	-1855(1)	4618(1)	1284(1)	17(1)	17(1)	20(1)	15(1)	-2(1)	6(1)	-2(1)
C(9)	-519(1)	5200(1)	1869(1)	16(1)	16(1)	18(1)	14(1)	-1(1)	5(1)	-1(1)
O(10)	390(1)	5417(1)	1471(1)	22(1)	19(1)	31(1)	18(1)	-4(1)	9(1)	-5(1)
N(11)	-302(1)	5500(1)	2873(1)	17(1)	18(1)	21(1)	14(1)	-2(1)	6(1)	-4(1)
C(12)	-1281(1)	5390(1)	3451(1)	21(1)	23(1)	25(1)	18(1)	-3(1)	11(1)	-5(1)
C(13)	1001(1)	6044(1)	3423(1)	17(1)	18(1)	18(1)	14(1)	-2(1)	5(1)	-2(1)
C(14)	1904(1)	5285(1)	4180(1)	21(1)	22(1)	22(1)	18(1)	0(1)	5(1)	2(1)
C(15)	3170(1)	5805(1)	4749(1)	24(1)	20(1)	31(1)	20(1)	-2(1)	4(1)	4(1)
C(16)	3562(1)	7074(1)	4547(1)	25(1)	18(1)	34(1)	22(1)	-6(1)	5(1)	-2(1)
C(17)	2696(1)	7829(1)	3763(1)	22(1)	19(1)	26(1)	23(1)	-6(1)	8(1)	-6(1)
C(18)	1422(1)	7314(1)	3230(1)	18(1)	18(1)	20(1)	16(1)	-1(1)	6(1)	-2(1)
N(19)	508(1)	8160(1)	2441(1)	21(1)	23(1)	20(1)	19(1)	2(1)	7(1)	-2(1)
O(20)	-706(1)	8219(1)	2398(1)	27(1)	22(1)	29(1)	30(1)	6(1)	7(1)	3(1)
O(21)	1019(1)	8782(1)	1883(1)	32(1)	35(1)	35(1)	29(1)	11(1)	12(1)	-7(1)
H(2)	-4456(17)	3590(16)	726(4)	29(4)						
H(3)	-6539(12)	2791(20)	-446(13)	42(5)						
H(4)	-6734(10)	2558(17)	-2318(10)	32(4)						
H(5)	-4777(18)	3035(18)	-2890(3)	37(4)						
H(6)	-2598(10)	3727(16)	-1673(12)	27(4)						
H(7)	-1230(9)	4422(16)	8(10)	24(4)						
H(8)	-2670(12)	4513(19)	1614(12)	39(5)						
H(12A)	-854(18)	4851(18)	4130(8)	47(5)						
H(12B)	-2145(12)	4841(18)	3043(14)	49(6)						
H(12C)	-1496(21)	6339(10)	3708(15)	52(6)						
H(14)	1598(17)	4280(6)	4278(13)	32(4)						
H(15)	3847(15)	5250(17)	5354(10)	43(5)						
H(17)	2939(16)	8822(6)	3577(12)	31(4)						
H(16)	4563(8)	7398(21)	4959(14)	45(5)						

Supplementary Table 2
Distances, corrected and uncorrected for rigid body motion for N-methyl-
N-(2-nitrophenyl)cinnamanilide

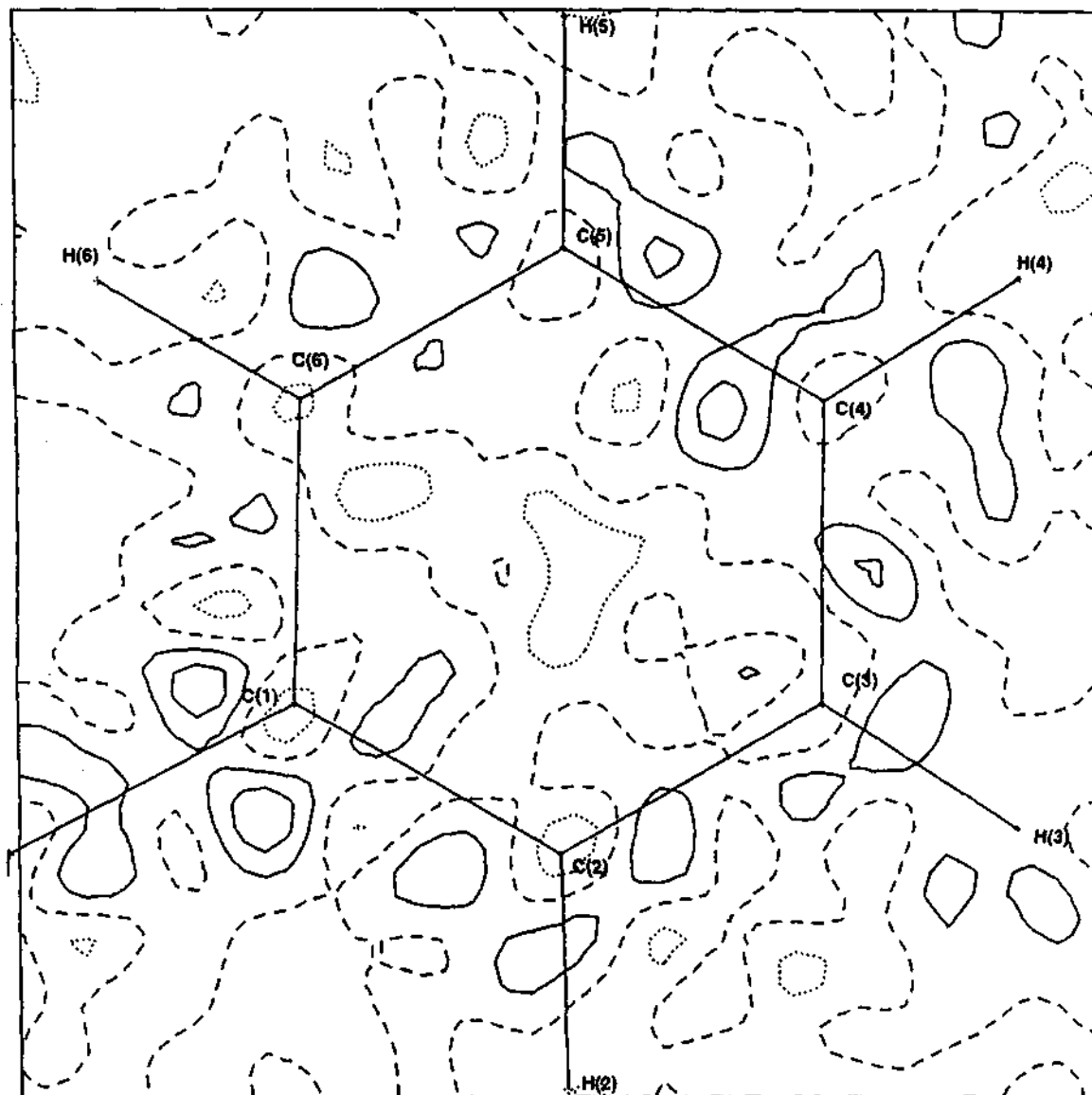
Bond	uncorrected	corrected
C1-C2	1.413	1.4142
C1-C6	1.4061	1.4072
C1-C7	1.4837	1.4847
C2-C3	1.4048	1.4057
C3-C4	1.4027	1.4038
C4-C5	1.3936	1.3948
C5-C6	1.4124	1.4134
C7-C8	1.3515	1.3523
C8-C9	1.4995	1.5005
C9-O10	1.2388	1.2399
C9-N11	1.373	1.3739
N11-C12	1.4661	1.4673
N11-C13	1.4459	1.4468
C13-C14	1.4045	1.4056
C13-C18	1.3933	1.3939
C14-C15	1.4141	1.4151
C15-C16	1.3859	1.3865
C16-C17	1.4063	1.4074
C17-C18	1.4054	1.4063
C18-N19	1.482	1.4831
N19-O20	1.2406	1.2416
N19-O21	1.2246	1.2256

N-methyl-N-(2-nitrophenyl)cinnamamide



Definition of local coordination systems

N-methyl-N-(2-nitrophenyl)cinnamanilide



Residual electron density map in the plane of the phenyl ring. (contours at $0.1 \text{ e}\text{\AA}^{-3}$)

Supplementary Table 4a

Atomic coordinates ($\times 10^4$) and anisotropic displacement parameters ($\text{\AA}^2 \times 10^3$) for the α -form of *o*-ethoxy cinnamic acid.

	x	y	z	U(eq)	U11	U22	U33	U23	U13	U12
C(1)	1261(2)	11790(1)	2980(1)	23(1)	22(1)	23(1)	24(1)	-2(1)	-8(1)	-6(1)
C(2)	2133(2)	12691(2)	3465(2)	30(1)	30(1)	27(1)	36(1)	-4(1)	-15(1)	-9(1)
C(3)	1425(3)	14466(2)	3124(2)	34(1)	37(1)	27(1)	41(1)	-6(1)	-14(1)	-12(1)
C(4)	-153(3)	15358(2)	2305(2)	33(1)	37(1)	24(1)	37(1)	-2(1)	-11(1)	-8(1)
C(5)	-1021(2)	14459(2)	1828(1)	29(1)	28(1)	26(1)	28(1)	-1(1)	-10(1)	-4(1)
C(6)	-345(2)	12673(1)	2148(1)	23(1)	20(1)	25(1)	21(1)	-2(1)	-7(1)	-4(1)
C(7)	-1279(2)	11713(2)	1673(1)	24(1)	22(1)	29(1)	21(1)	-3(1)	-9(1)	-5(1)
C(8)	-2803(2)	12396(2)	873(1)	28(1)	26(1)	31(1)	27(1)	-1(1)	-14(1)	-5(1)
C(9)	-3676(2)	11314(2)	486(1)	27(1)	22(1)	33(1)	22(1)	-2(1)	-10(1)	-5(1)
C(10)	3441(2)	9113(2)	4153(1)	26(1)	26(1)	25(1)	27(1)	-1(1)	-14(1)	-6(1)
C(11)	3856(2)	7247(2)	4282(1)	30(1)	31(1)	25(1)	31(1)	-3(1)	-13(1)	-5(1)
O(1)	-3170(2)	9744(1)	920(1)	32(1)	32(1)	32(1)	33(1)	-1(1)	-20(1)	-6(1)
O(2)	-5076(2)	12170(1)	-356(1)	35(1)	36(1)	36(1)	35(1)	-1(1)	-25(1)	-5(1)
O(3)	1864(2)	10053(1)	3268(1)	27(1)	28(1)	22(1)	34(1)	-3(1)	-19(1)	-4(1)
H(2)	3350(2)	12015(2)	4103(2)	37(5)						
H(3)	2107(3)	15153(2)	3497(2)	46(5)						
H(4)	-695(3)	16729(2)	2046(2)	54(6)						
H(5)	-2243(2)	15150(2)	1196(1)	45(6)						
H(7)	-698(2)	10347(2)	1991(1)	40(5)						
H(8)	-3391(2)	13757(2)	509(1)	45(5)						
H(10A)	2801(2)	9415(2)	5191(1)	34(4)						
H(10B)	4941(2)	9421(2)	3668(1)	30(4)						
H(11A)	2346(4)	6954(4)	4772(12)	46(5)						
H(11B)	5019(15)	6510(2)	4927(11)	47(6)						
H(11C)	4494(19)	6962(4)	3236(2)	45(5)						
H(2A)	-5587(35)	11393(4)	-564(24)	80(9)						

Supplementary Table 4b

Atomic coordinates ($\times 10^4$) and anisotropic displacement parameters ($\text{\AA}^2 \times 10^3$) for the γ -form of o-ethoxy cinnamic acid.

	x	y	z	U(eq)	U11	U22	U33	U23	U13	U12
C(1)	1615(1)	3053(2)	1493(1)	24(1)	19(1)	28(1)	24(1)	0(1)	9(1)	0(1)
C(2)	1184(1)	1370(2)	1725(1)	30(1)	23(1)	34(1)	34(1)	7(1)	12(1)	0(1)
C(3)	306(1)	1442(3)	1521(1)	31(1)	23(1)	37(1)	35(1)	2(1)	12(1)	-4(1)
C(4)	-141(1)	3187(3)	1096(1)	30(1)	19(1)	39(1)	31(1)	-2(1)	8(1)	-3(1)
C(5)	291(1)	4880(2)	872(1)	28(1)	20(1)	34(1)	27(1)	1(1)	5(1)	0(1)
C(6)	1173(1)	4843(2)	1060(1)	23(1)	20(1)	25(1)	22(1)	-2(1)	7(1)	-1(1)
C(7)	1644(1)	6560(2)	821(1)	25(1)	22(1)	27(1)	25(1)	-1(1)	7(1)	-2(1)
C(8)	1317(1)	8435(2)	440(1)	27(1)	23(1)	27(1)	28(1)	1(1)	7(1)	-1(1)
C(9)	1846(1)	10115(2)	240(1)	26(1)	25(1)	25(1)	25(1)	-1(1)	6(1)	-2(1)
C(10)	2947(1)	1157(3)	2049(1)	31(1)	21(1)	36(1)	33(1)	5(1)	7(1)	4(1)
C(11)	3858(1)	1508(3)	2110(1)	38(1)	21(1)	51(1)	41(1)	0(1)	9(1)	3(1)
O(1)	2645(1)	9940(2)	465(1)	34(1)	24(1)	38(1)	37(1)	7(1)	6(1)	-3(1)
O(2)	1462(1)	11743(2)	-158(1)	37(1)	30(1)	35(1)	43(1)	13(1)	9(1)	2(1)
O(3)	2474(1)	3099(2)	1665(1)	31(1)	18(1)	38(1)	36(1)	9(1)	10(1)	2(1)
H(2)	1528(1)	25(2)	2060(1)	36(5)						
H(3)	-26(1)	128(3)	1695(1)	33(4)						
H(4)	-818(1)	3232(3)	941(1)	47(6)						
H(5)	-59(1)	6247(2)	546(1)	45(5)						
H(7)	2314(1)	6287(2)	965(1)	40(5)						
H(8)	646(1)	8724(2)	275(1)	39(5)						
H(10A)	2722(1)	-564(3)	1844(1)	42(5)						
H(10B)	2889(1)	1226(3)	2492(1)	32(4)						
H(11A)	4065(3)	3268(10)	2295(6)	49(6)						
H(11B)	3909(2)	1350(24)	1666(1)	58(7)						
H(11C)	4236(1)	152(15)	2409(5)	53(6)						
H(2A)	1985(1)	13192(24)	-232(8)	55						

Supplementary Table 4c

Atomic coordinates ($\times 10^4$) and anisotropic displacement parameters ($\text{\AA}^2 \times 10^3$) for the photodimer of the α -form of *o*-ethoxy cinnamic acid.

Atom	x	y	z	U(eq)	U11	U22	U33	U23	U13	U12
O(1)	-3736(5)	972(6)	-497(4)	18(1)	8(1)	25(1)	22(2)	8(1)	2(1)	2(1)
O(2)	-3055(5)	-312(6)	961(3)	18(1)	10(1)	27(2)	18(1)	7(1)	6(1)	-1(1)
O(3)	2347(6)	2331(4)	779(3)	16(1)	13(2)	13(1)	17(1)	1(1)	-4(1)	-5(1)
C(1)	1680(6)	3216(5)	-63(4)	13(1)	10(2)	11(1)	16(1)	-2(1)	1(1)	-5(1)
C(2)	2341(8)	4671(5)	-242(4)	18(1)	21(2)	12(1)	22(2)	0(1)	6(2)	-5(1)
C(3)	1561(8)	5489(5)	-1130(5)	19(1)	22(2)	12(1)	24(2)	2(1)	10(2)	2(1)
C(4)	158(8)	4867(6)	-1818(4)	18(1)	21(2)	15(1)	19(2)	5(1)	8(2)	2(1)
C(5)	-453(7)	3383(5)	-1631(4)	14(1)	16(2)	14(1)	14(2)	1(1)	5(1)	2(1)
C(6)	314(6)	2523(5)	-763(3)	12(1)	10(1)	12(1)	13(1)	1(1)	4(1)	0(1)
C(7)	-353(5)	909(4)	-610(3)	10(1)	7(1)	12(1)	10(1)	0(1)	1(1)	-1(1)
C(8)	-835(5)	587(4)	359(3)	10(1)	7(1)	13(1)	11(1)	0(1)	3(1)	1(1)
C(9)	-2670(5)	410(5)	232(3)	12(1)	5(1)	14(1)	17(1)	1(1)	2(1)	0(1)
C(10)	3724(8)	2963(7)	1546(4)	20(1)	15(2)	21(2)	20(2)	-2(1)	-2(1)	-9(2)
C(11)	4087(11)	1825(9)	2416(5)	27(1)	26(3)	28(2)	18(2)	0(2)	-6(2)	-2(2)
H(2)	-4218(91)	-599(322)	752(77)	27						
H(2A)	3428(8)	5158(5)	291(4)	22						
H(3)	2058(8)	6609(5)	-1278(5)	23						
H(4)	-455(8)	5513(6)	-2486(4)	21						
H(5)	-1536(7)	2895(5)	-2166(4)	17						
H(7)	-1408(5)	637(4)	-1240(3)	12						
H(8)	-338(5)	1511(4)	892(3)	12						
H(10A)	3414(8)	4095(7)	1769(4)	24						
H(10B)	4790(8)	3080(7)	1281(4)	24						
H(11A)	5393(39)	1803(247)	2775(126)	40						
H(11B)	3676(317)	675(66)	2153(26)	40						
H(11C)	3445(279)	2200(184)	2931(101)	40						

Supplementary Table 5Distances corrected and uncorrected for rigid body motion for *o*-ethoxy cinnamic acid α -form

Bond	Uncorrected	Corrected
C1-C2	1.3955	1.3969
C1-C6	1.4119	1.413
C1-O3	1.3648	1.3658
C2-C3	1.3925	1.3935
C3-C4	1.3892	1.3903
C4-C5	1.3872	1.3885
C5-C6	1.401	1.402
C6-C7	1.4612	1.4626
C7-C8	1.3446	1.3457
C8-C9	1.4681	1.4695
C9-O1	1.2404	1.2412
C9-O2	1.3161	1.3171
C10-C11	1.5056	1.5067
C10-O3	1.4371	1.4382

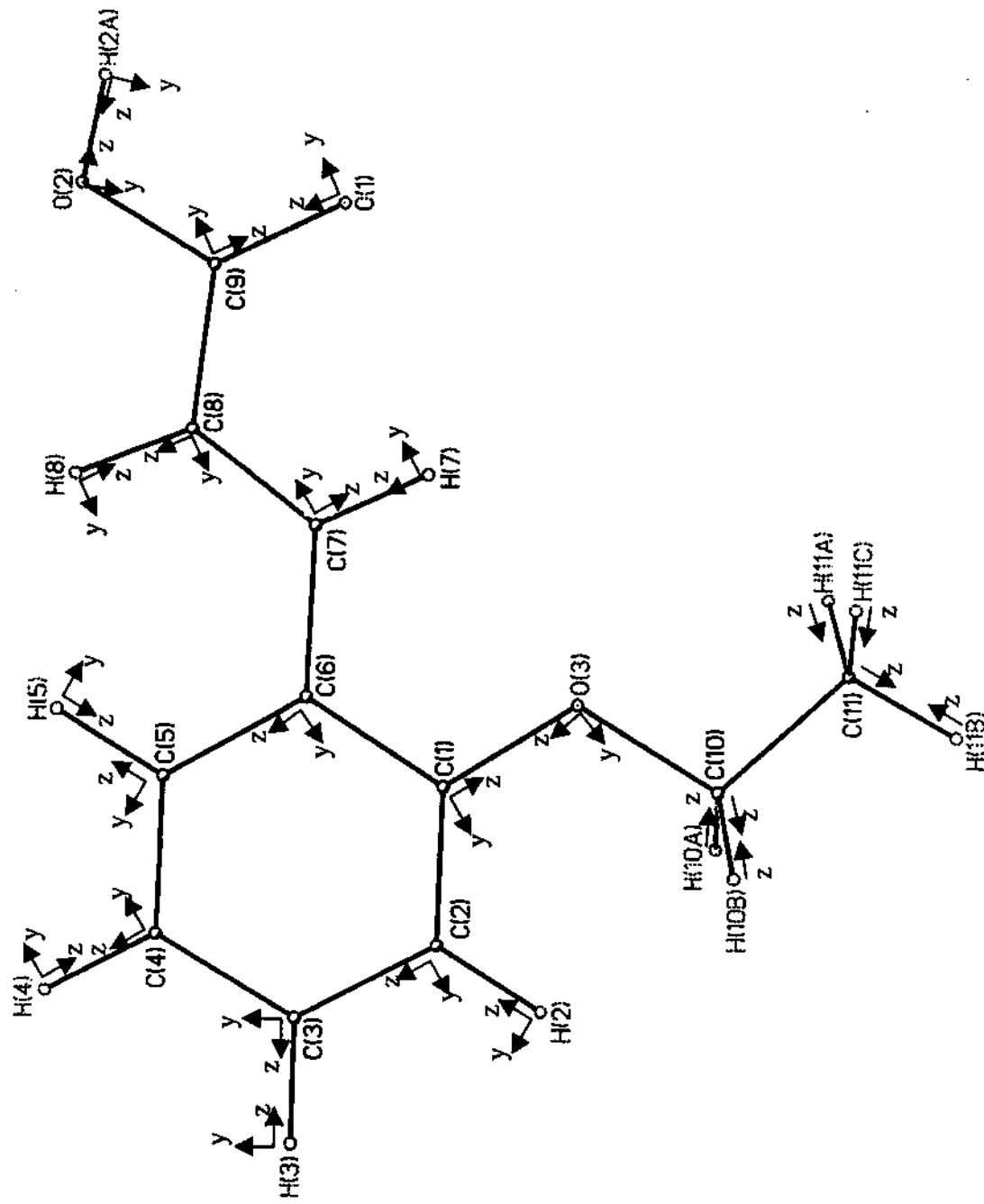
Dimer

Bond	uncorrected	corrected
C1-C2	1.3958	1.3976
C1-C6	1.4017	1.4032
O3-C1	1.3732	1.3745
C2-C3	1.396	1.3973
C3-C4	1.3816	1.3831
C4-C5	1.4013	1.4031
C5-C6	1.3982	1.3995
C6-C7	1.5091	1.511
C7-C8	1.5492	1.5504
C8-C9	1.4971	1.4987
O1-C9	1.2385	1.2397
O2-C9	1.3067	1.3079
C10-C11	1.5072	1.5087
O3-C10	1.4362	1.4376

 γ -form

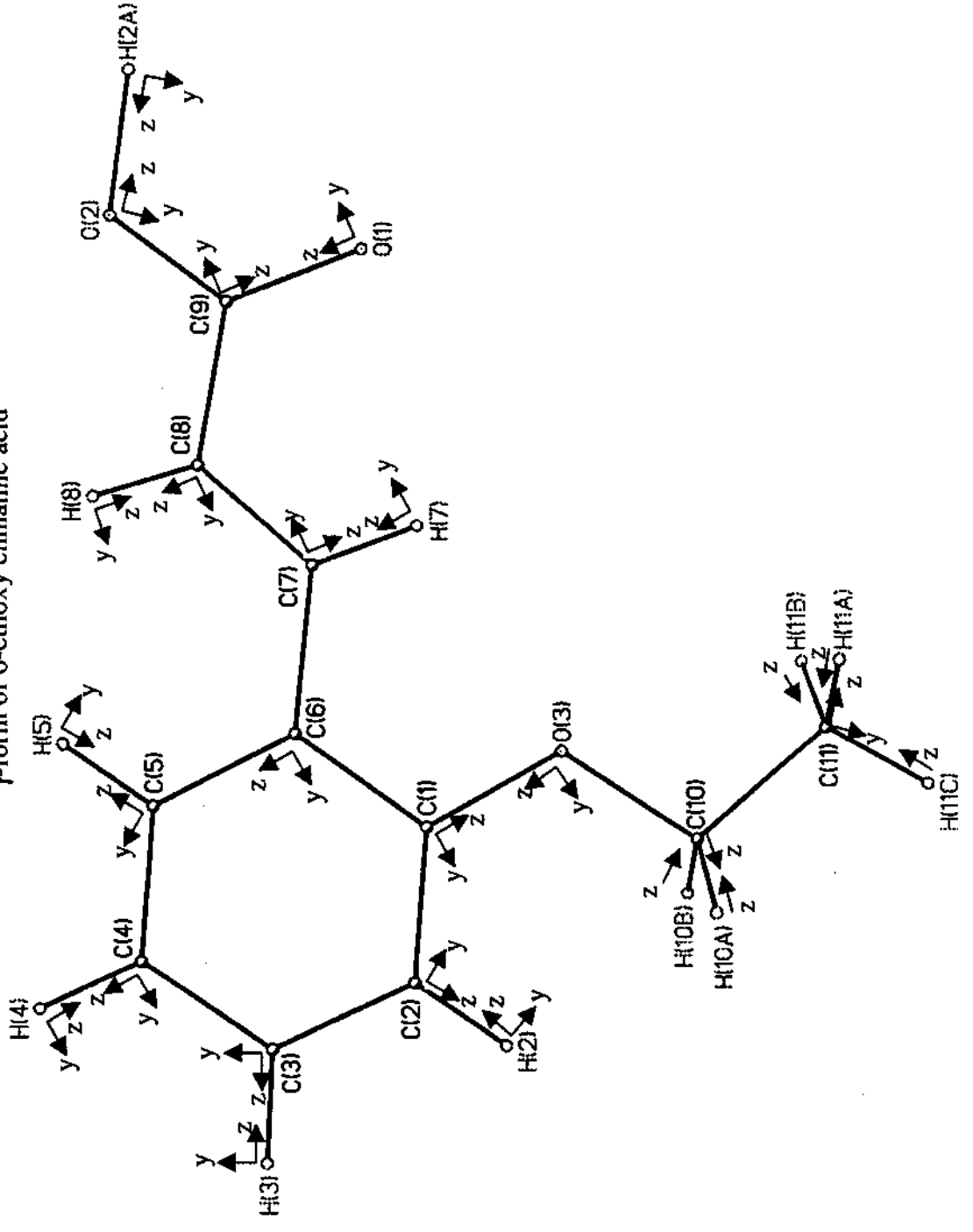
Bond	uncorrected	corrected
C1-C2	1.3946	1.3958
C1-C6	1.4083	1.4097
C1-O3	1.3675	1.3691
C2-C3	1.3941	1.3957
C3-C4	1.3834	1.3848
C4-C5	1.3893	1.3905
C5-C6	1.4027	1.4042
C6-C7	1.4622	1.4635
C7-C8	1.3353	1.3366
C8-C9	1.4685	1.4698
C9-O1	1.271	1.2725
C9-O2	1.2783	1.2796
C10-C11	1.514	1.5156
C10-O3	1.4311	1.4326

α -form of o-ethoxy cinnamic acid



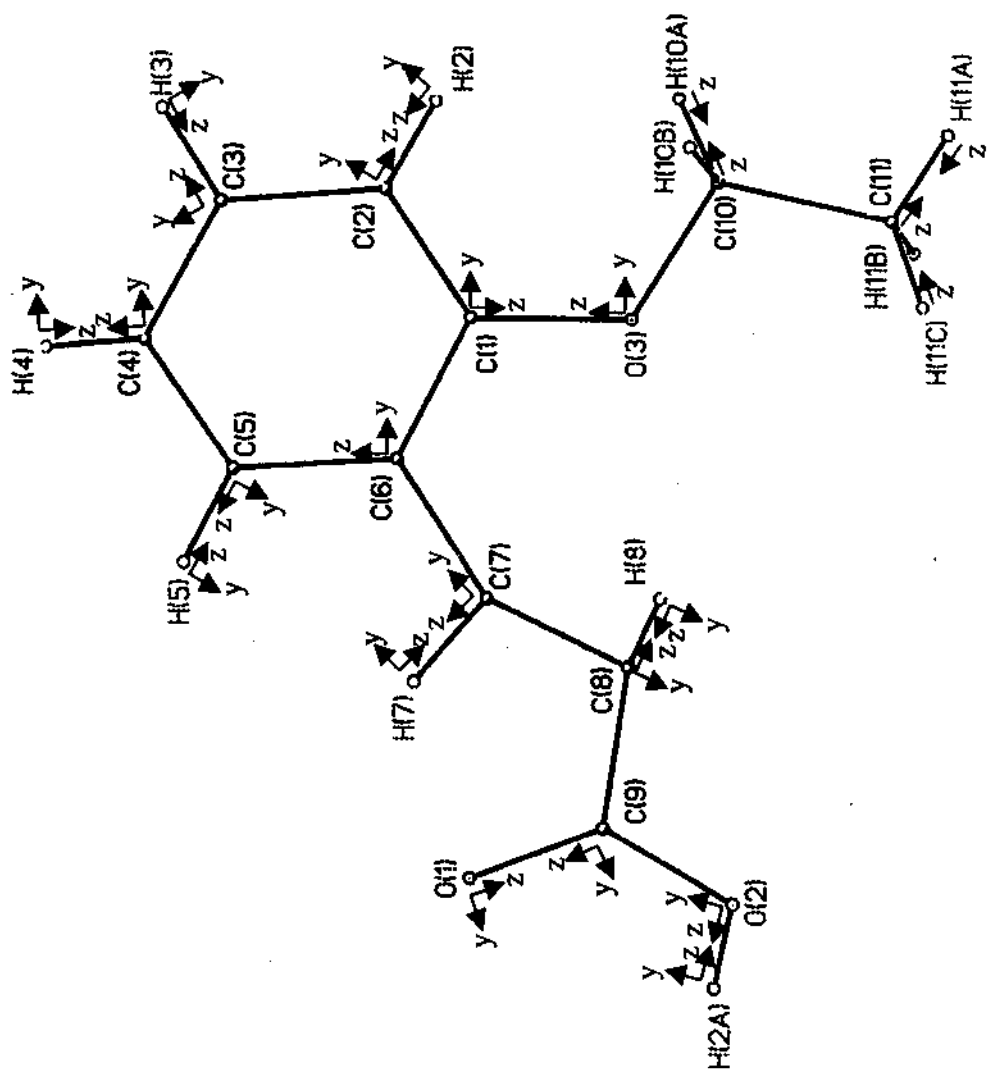
Definition of local coordination systems

γ -form of *o*-ethoxy cinnamic acid



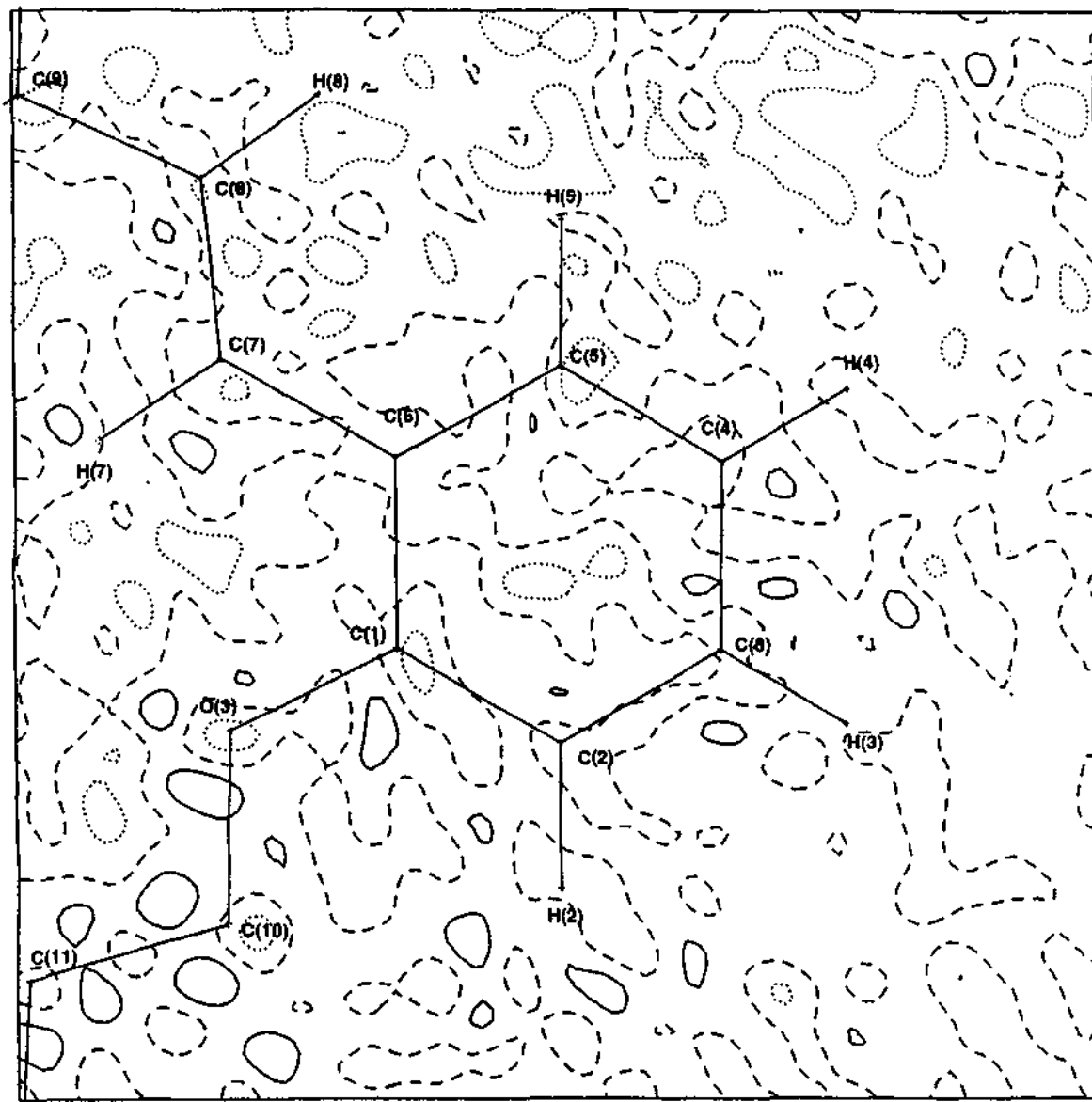
Definition of local coordination systems

Photodimer of α -form of *o*-ethoxy cinnamic acid



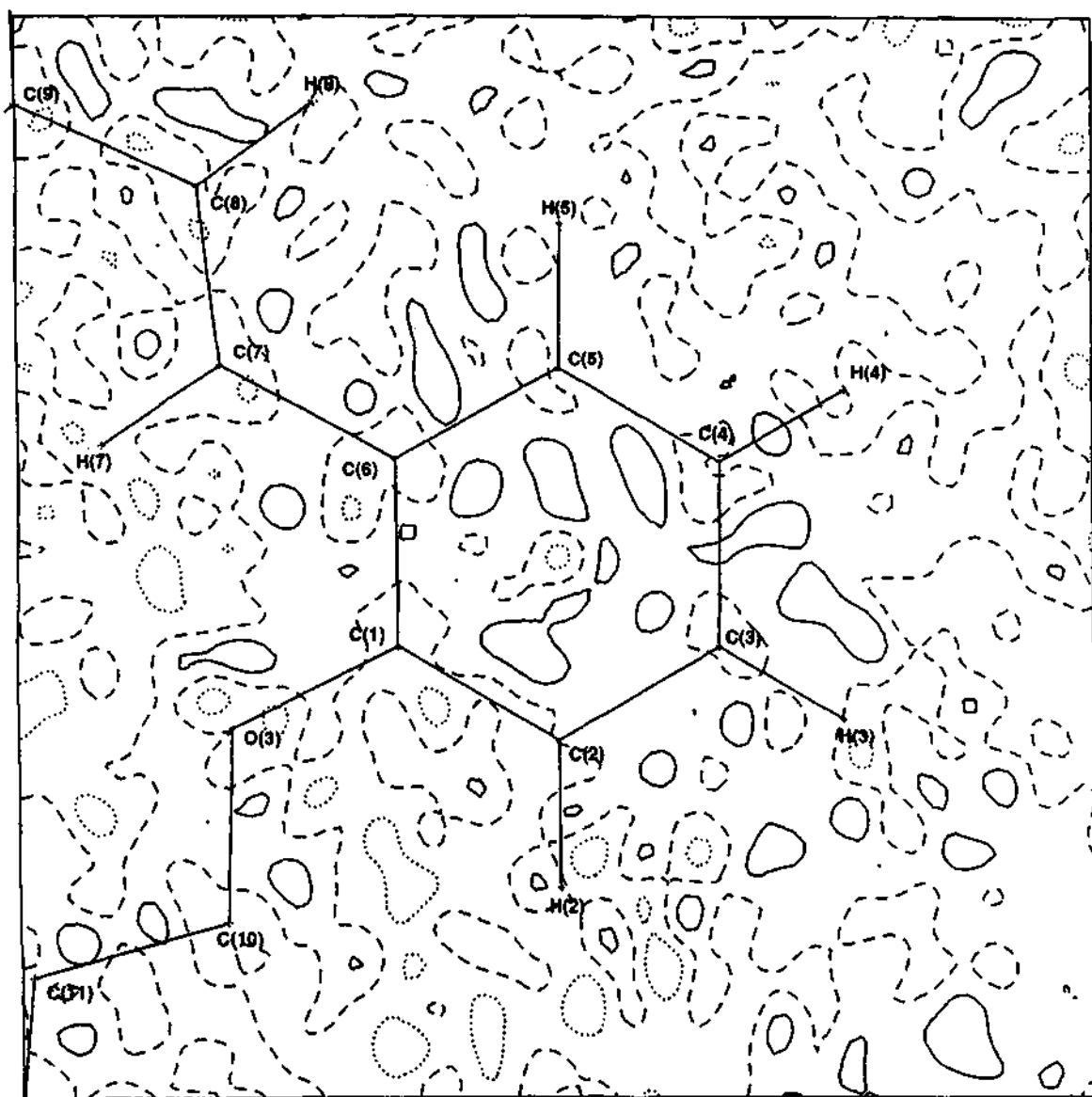
Definition of local coordination systems

α -form of o-ethoxy cinnamic acid



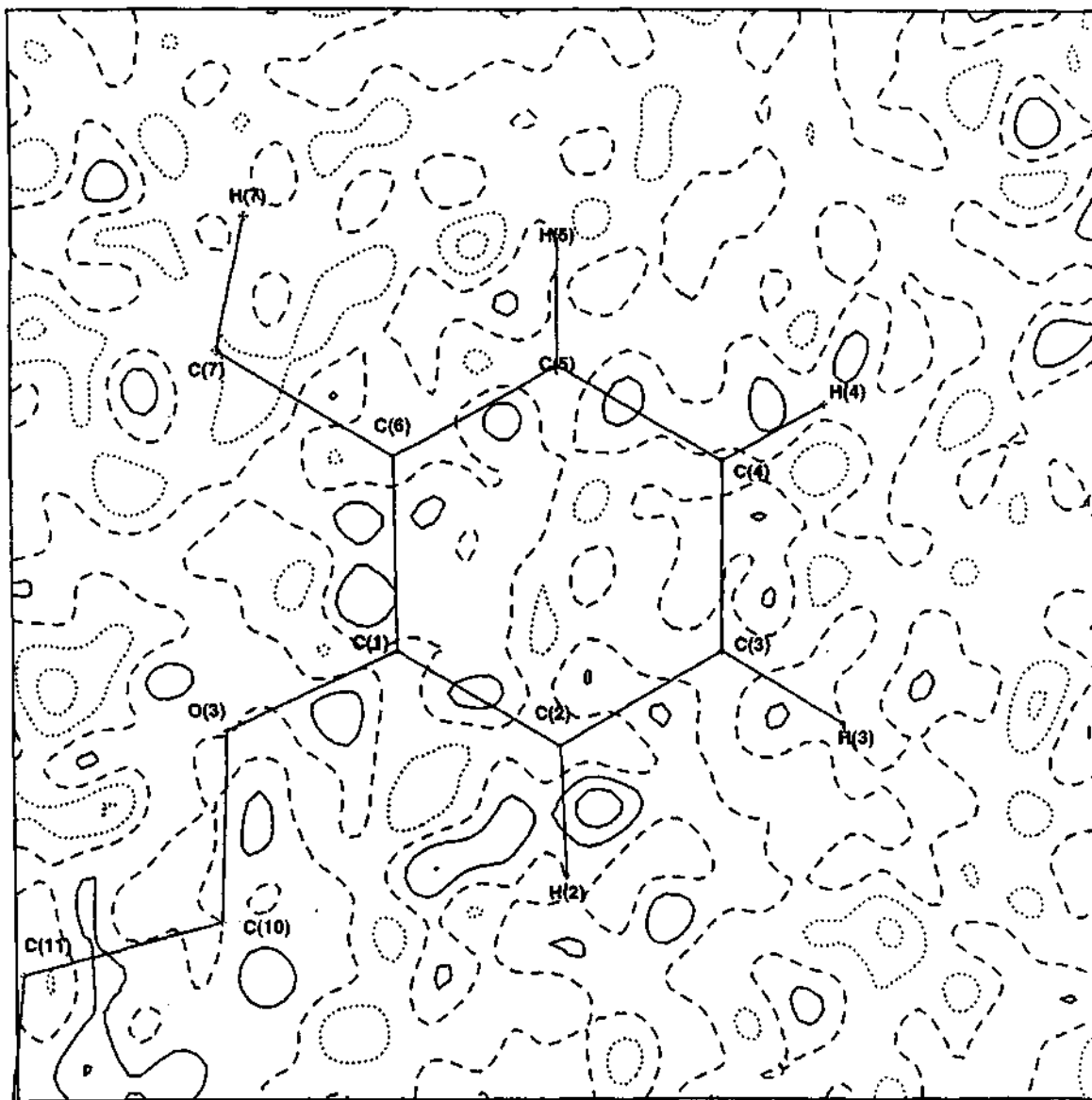
Residual electron density map in the plane of the phenyl ring. (contours at $0.1 \text{ e}\text{\AA}^{-3}$)

γ -form of *o*-ethoxy cinnamic acid



Residual electron density map in the plane of the phenyl ring. (contours at $0.1 \text{ e}\text{\AA}^{-3}$)

Photodimer of the α -form



Residual electron density map in the plane of the phenyl ring. (contours at $0.15 \text{ e}\text{\AA}^{-3}$)

Supplementary Table 7a

Atomic coordinates ($\times 10^4$) and anisotropic displacement parameters ($\text{\AA}^2 \times 10^3$) for the pristine α -form of *p*-nitrophenol.

Atom	x	y	z	U(eq)	U11	U22	U33	U23	U13	U12
O(1)	1176(1)	-235(1)	-3188(1)	23(1)	29(1)	15(1)	14(1)	-1(1)	6(1)	2(1)
O(2)	9515(1)	2070(1)	581(1)	23(1)	31(1)	22(1)	14(1)	1(1)	8(1)	-6(1)
O(3)	7090(1)	3738(1)	862(1)	24(1)	36(1)	17(1)	20(1)	-6(1)	9(1)	-7(1)
N	7601(1)	2590(1)	352(1)	16(1)	19(1)	15(1)	12(1)	0(1)	2(1)	-1(1)
C(1)	2674(1)	477(1)	-2305(1)	16(1)	15(1)	12(1)	12(1)	1(1)	2(1)	2(1)
C(2)	2095(1)	1733(1)	-1685(1)	16(1)	16(1)	12(1)	14(1)	2(1)	3(1)	-1(1)
C(3)	3707(1)	2421(1)	-796(1)	15(1)	16(1)	11(1)	13(1)	1(1)	2(1)	-1(1)
C(4)	5885(1)	1851(1)	-546(1)	14(1)	15(1)	12(1)	11(1)	1(1)	1(1)	-1(1)
C(5)	6476(1)	586(1)	-1138(1)	16(1)	14(1)	12(1)	13(1)	2(1)	2(1)	-2(1)
C(6)	4852(1)	-105(1)	-2016(1)	18(1)	16(1)	11(1)	14(1)	1(1)	1(1)	-1(1)
H(1)	-165(12)	354(11)	-3397(12)	59(5)						
H(2)	399(1)	2160(1)	-1899(1)	33(2)						
H(3)	3284(1)	3382(1)	-306(1)	33(2)						
H(5)	8170(1)	155(1)	-916(1)	33(2)						
H(6)	5267(1)	-1095(1)	-2477(1)	33(2)						

Supplementary Table 7b

Atomic coordinates ($\times 10^4$) and anisotropic displacement parameters ($\text{\AA}^2 \times 10^3$) for the β -form of *p*-nitrophenol.

Atom	x	y	z	U(eq)	U11	U22	U33	U23	U13	U12
O(1)	879(2)	5365(1)	6551(1)	19(1)	29(1)	15(1)	14(1)	-1(1)	6(1)	2(1)
O(2)	-3615(2)	6747(1)	10455(1)	22(1)	31(1)	22(1)	14(1)	1(1)	8(1)	-6(1)
O(3)	-885(2)	8399(1)	10109(1)	24(1)	36(1)	17(1)	20(1)	-6(1)	9(1)	-7(1)
N	-1900(2)	7361(1)	9923(1)	15(1)	19(1)	15(1)	12(1)	0(1)	2(1)	-1(1)
C(1)	279(2)	5894(1)	7358(1)	13(1)	15(1)	12(1)	12(1)	1(1)	2(1)	2(1)
C(2)	1060(2)	7107(1)	7541(1)	14(1)	16(1)	12(1)	14(1)	2(1)	3(1)	-1(1)
C(3)	407(2)	7592(1)	8391(1)	14(1)	16(1)	11(1)	13(1)	1(1)	2(1)	-1(1)
C(4)	-1069(2)	6852(1)	9047(1)	13(1)	15(1)	12(1)	11(1)	1(1)	1(1)	-1(1)
C(5)	-1869(2)	5644(1)	8879(1)	13(1)	14(1)	12(1)	13(1)	2(1)	2(1)	-2(1)
C(6)	-1182(2)	5166(1)	8034(1)	14(1)	16(1)	11(1)	14(1)	1(1)	1(1)	-1(1)
H(1)	2016(49)	5930(5)	6160(5)	67(7)						
H(2)	2176(2)	7668(1)	7017(1)	28(2)						
H(3)	1033(2)	8527(1)	8542(1)	28(2)						
H(5)	-3012(2)	5089(1)	9403(1)	28(2)						
H(6)	-1770(2)	4226(1)	7892(1)	28(2)						

Supplementary Table 7c

Atomic coordinates ($\times 10^4$) and anisotropic displacement parameters ($\text{\AA}^2 \times 10^3$) for the irradiated α -form of *p*-nitrophenol.

	x	y	z	U(eq)	U11	U22	U33	U23	U13	U12
O(1)	13823(1)	5233(1)	3188(1)	25(1)	23(1)	20(1)	26(1)	-3(1)	-5(1)	-2(1)
O(2)	5486(1)	2931(1)	-581(1)	24(1)	15(1)	28(1)	27(1)	-4(1)	-2(1)	6(1)
O(3)	7911(1)	1264(1)	-863(1)	25(1)	22(1)	25(1)	27(1)	-10(1)	1(1)	4(1)
N	7399(1)	2412(1)	-352(1)	18(1)	15(1)	19(1)	17(1)	-1(1)	1(1)	2(1)
C(1)	12324(2)	4520(1)	2305(1)	18(1)	18(1)	16(1)	18(1)	1(1)	1(1)	0(1)
C(2)	12902(2)	3267(1)	1686(1)	18(1)	14(1)	17(1)	21(1)	2(1)	2(1)	1(1)
C(3)	11290(2)	2578(1)	796(1)	17(1)	15(1)	16(1)	18(1)	1(1)	3(1)	2(1)
C(4)	9118(1)	3149(1)	545(1)	15(1)	13(1)	16(1)	15(1)	0(1)	2(1)	2(1)
C(5)	8523(2)	4413(1)	1135(1)	18(1)	16(1)	18(1)	18(1)	-1(1)	4(1)	4(1)
C(6)	10147(2)	5106(1)	2015(1)	19(1)	19(1)	19(1)	20(1)	-3(1)	3(1)	2(1)
H(1)	15122(19)	4604(13)	3442(17)	65(7)						
H(2)	14604(2)	2837(1)	1902(1)	31(2)						
H(3)	11715(2)	1612(1)	305(1)	31(2)						
H(5)	6823(2)	4846(1)	910(1)	31(2)						
H(6)	9730(2)	6099(1)	2478(1)	31(2)						

Supplementary Table 8
Distances, corrected and uncorrected
for rigid body motion of *p*-nitrophenol

pristine α -form

Bond	uncorrected	corrected
O1-C1	1.3607	1.3625
O2-O3	2.1768	2.1786
O2-N	1.2369	1.2381
O3-N	1.2492	1.2503
N-C4	1.4536	1.4555
C1-C2	1.4108	1.4121
C1-C6	1.4044	1.4057
C2-C3	1.3923	1.3941
C3-C4	1.4007	1.402
C4-C5	1.4014	1.4028
C5-C6	1.3903	1.3921

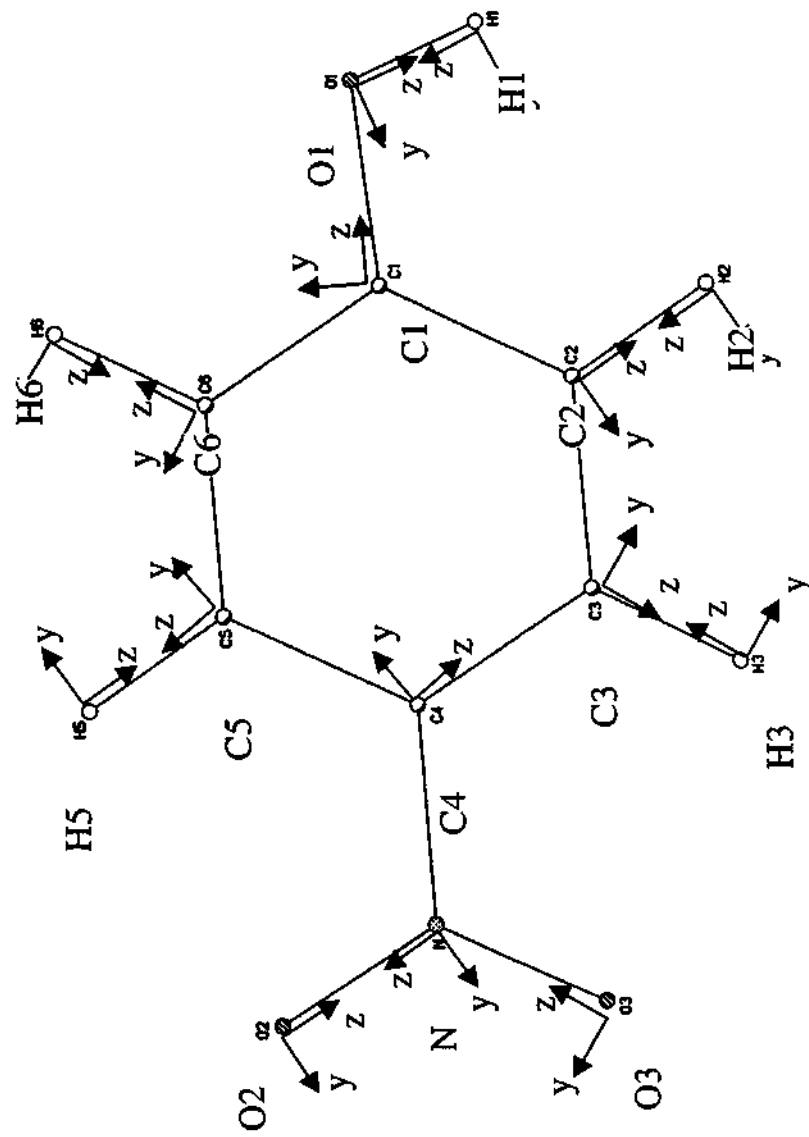
β -form

Bond	uncorrected	corrected
O1-C1	1.3478	1.3518
O2-O3	2.1652	2.1703
O2-N	1.2333	1.2364
O3-N	1.2389	1.242
N-C4	1.4478	1.4522
C1-C2	1.4021	1.4058
C1-C6	1.4061	1.4096
C2-C3	1.388	1.3921
C3-C4	1.3945	1.398
C4-C5	1.3942	1.3979
C5-C6	1.3807	1.3849

Irradiated α -form

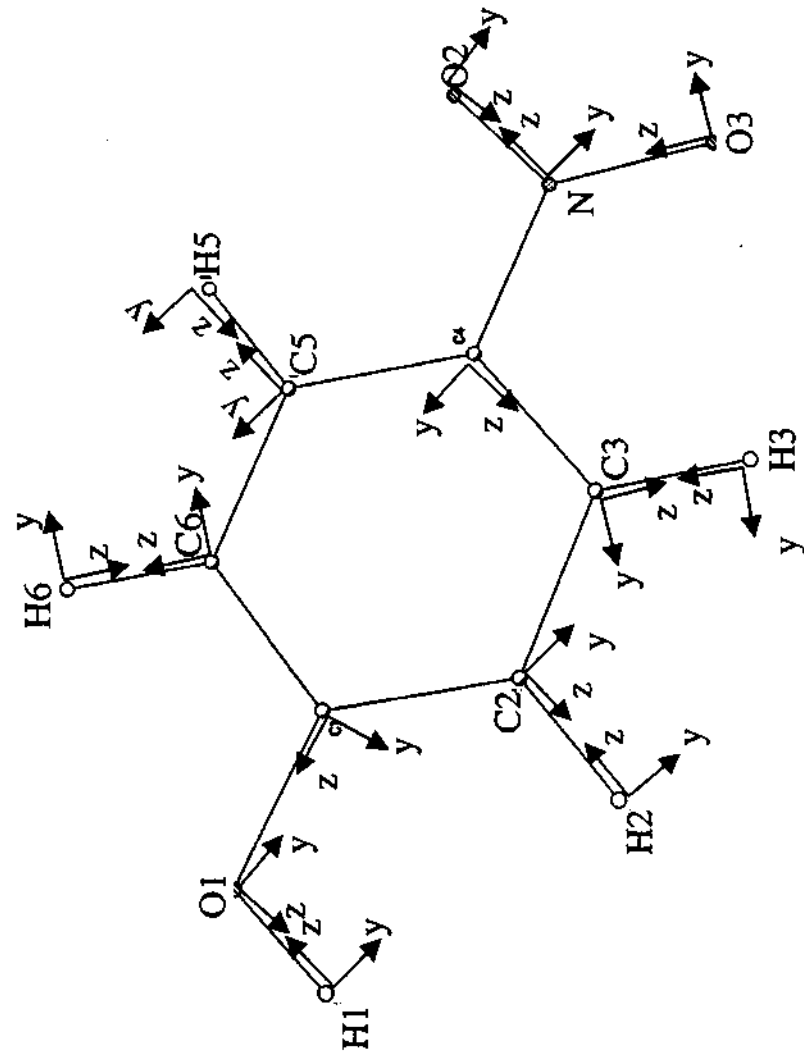
Bond	uncorrected	corrected
O1-C1	1.3571	1.3589
O2-O3	2.168	2.1699
O2-N	1.2315	1.2327
O3-N	1.2449	1.2462
N-C4	1.4485	1.4504
C1-C2	1.4026	1.404
C1-C6	1.3995	1.4008
C2-C3	1.3889	1.3908
C3-C4	1.3922	1.3935
C4-C5	1.3951	1.3965
C5-C6	1.3877	1.3896

Pristine α -form of *p*-nitrophenol



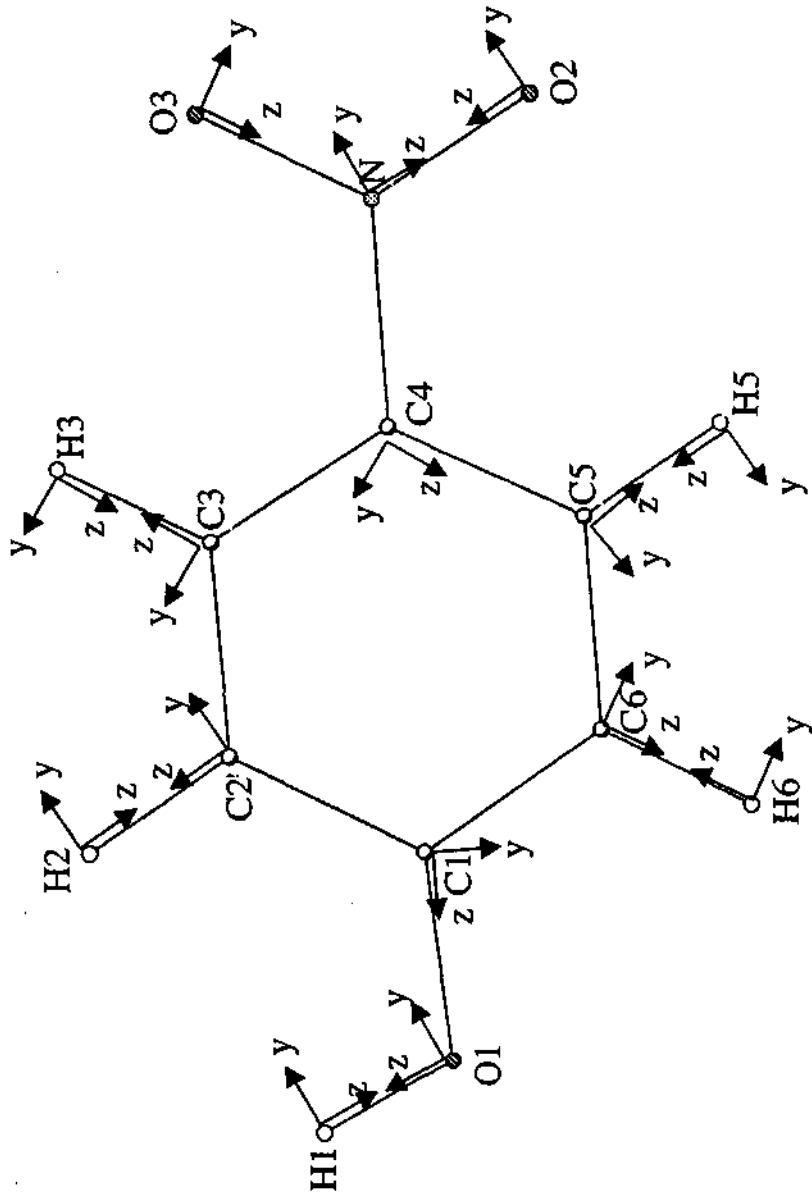
Definition of local coordination systems

β -polymorph of *p*-nitrophenol



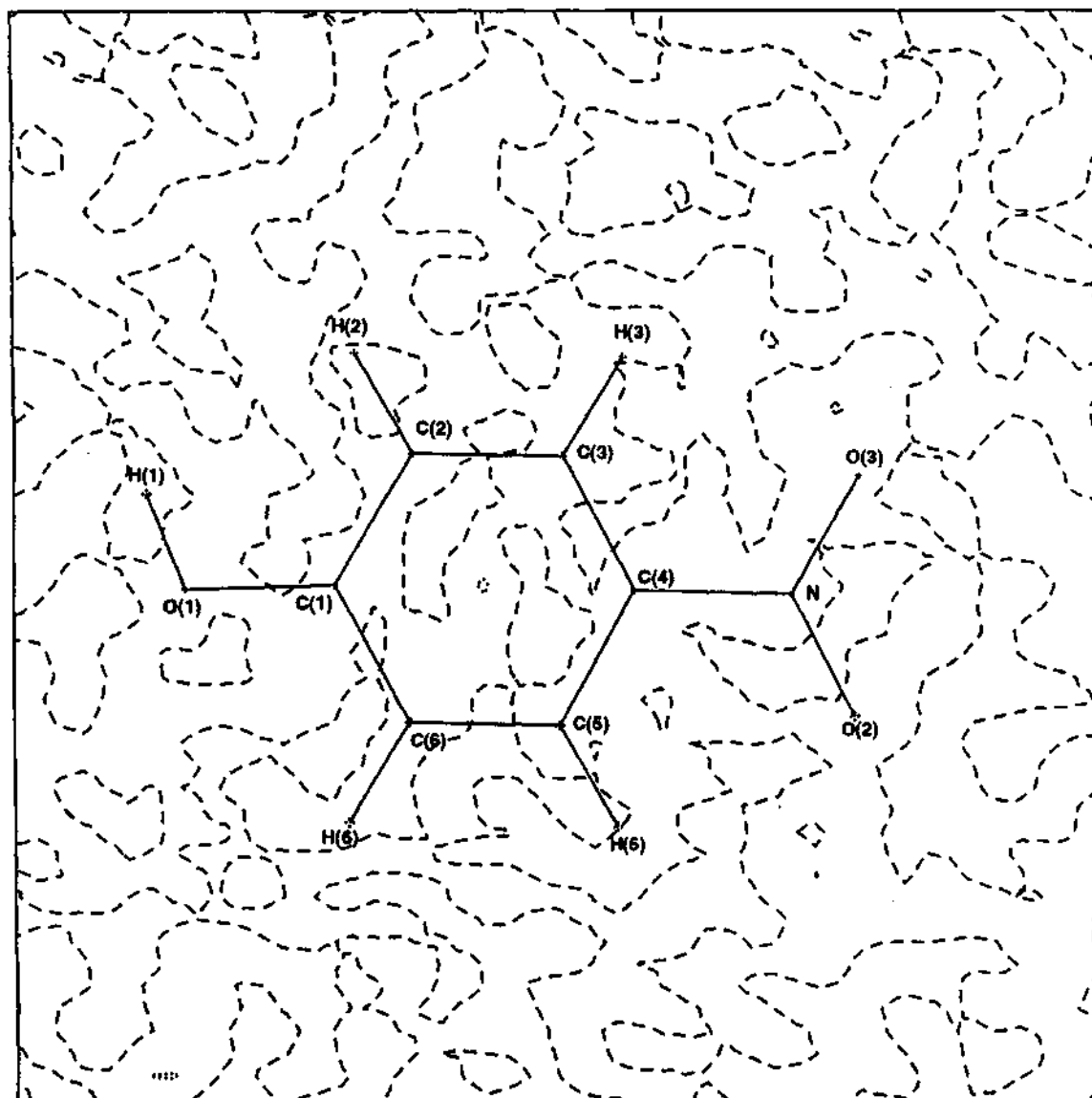
Definition of local coordination systems

Irradiated α -form of *p*-nitrophenol



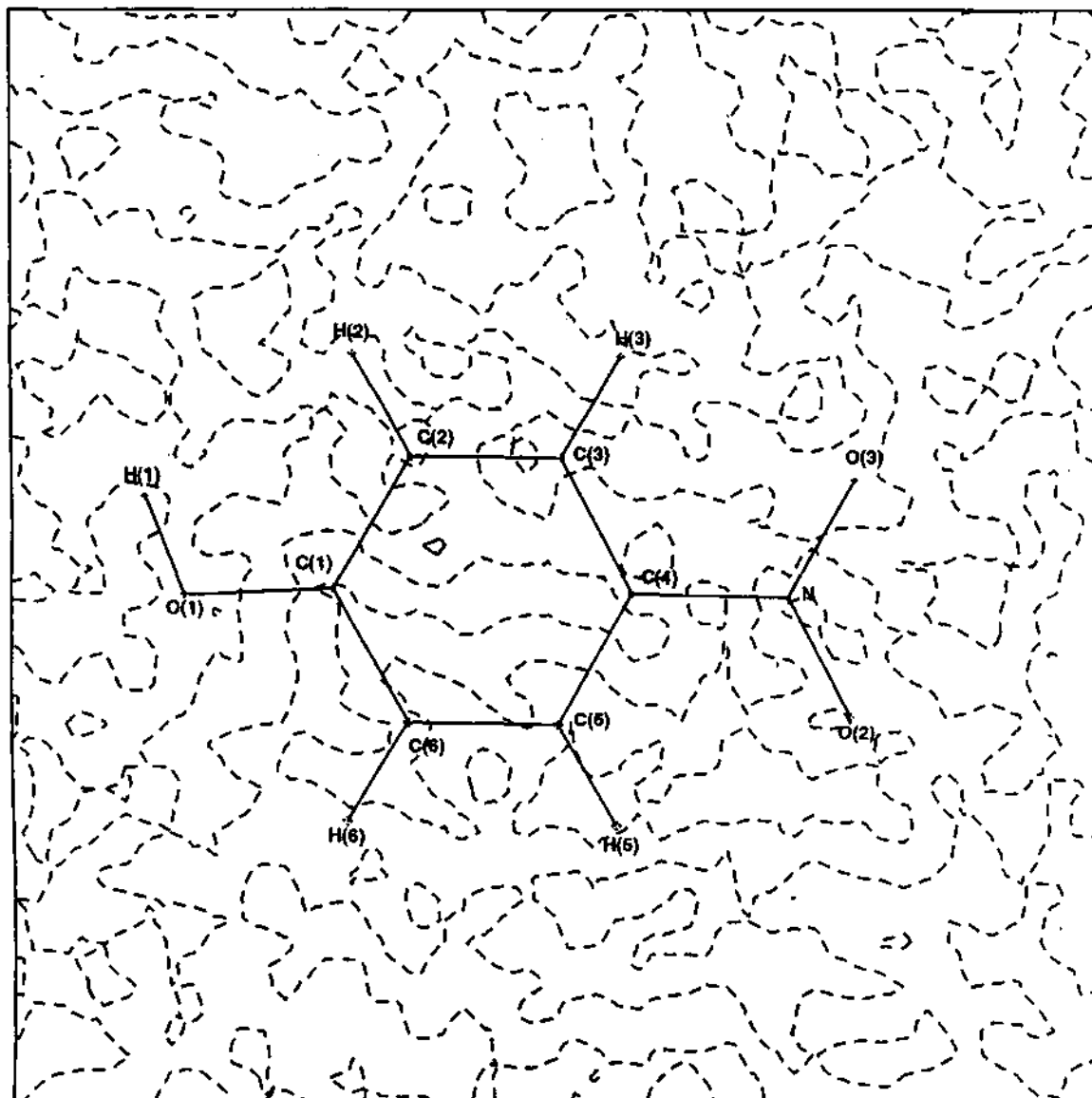
Definition of local coordination systems

Pristine α -form of *p*-nitrophenol



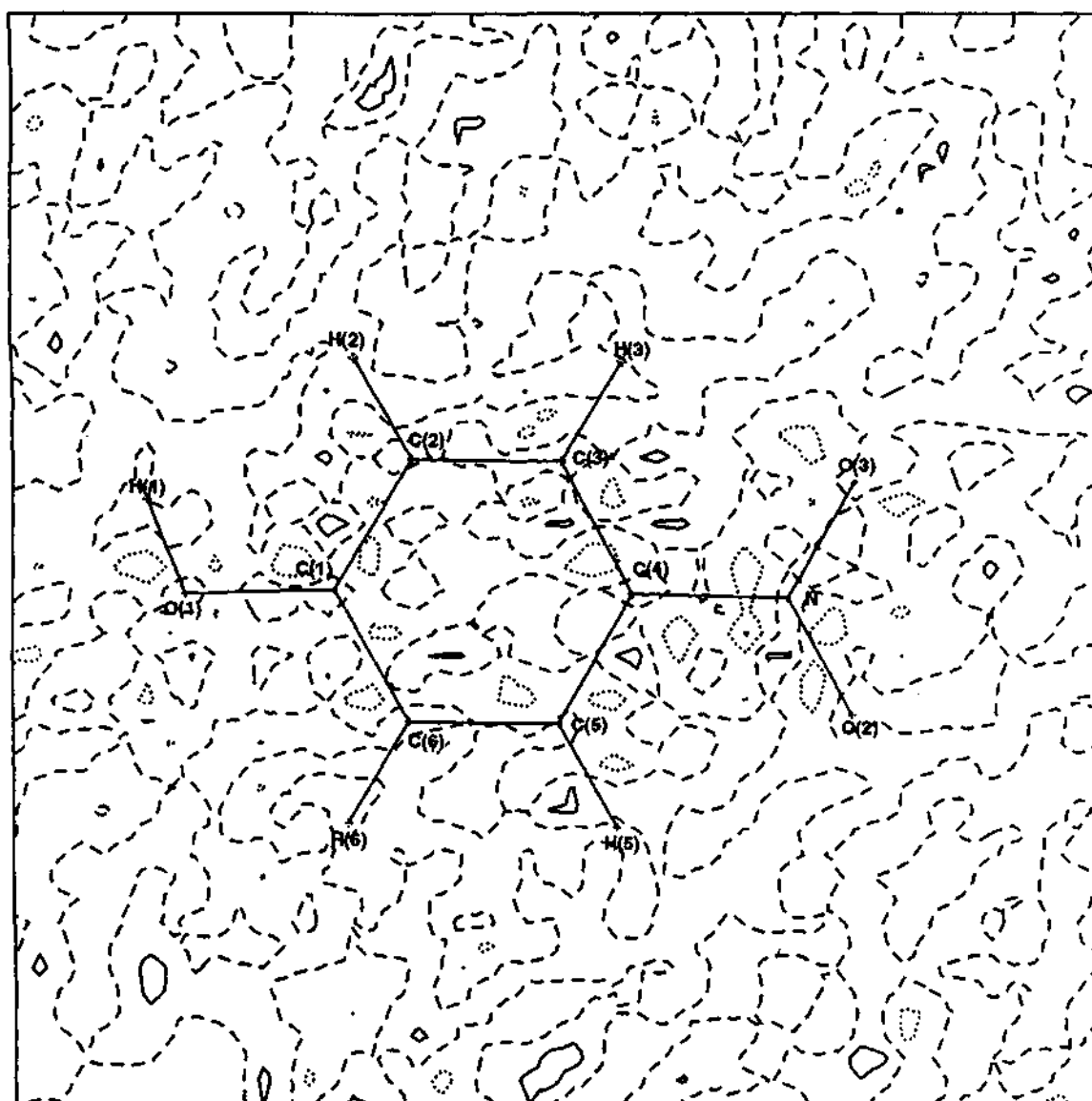
Residual electron density map in the plane of the phenyl ring. (contours at 0.15 e \AA^{-3})

β -form of *p*-nitrophenol



Residual electron density map in the plane of the phenyl ring. (contours at $0.15 \text{ e}\text{\AA}^{-3}$)

Irradiated α -form of *p*-nitrophenol



Residual electron density map in the plane of the phenyl ring. (contours at $0.15 \text{ e}\text{\AA}^{-3}$)

Supplementary Table 10aAtomic coordinates ($\times 10^4$) and anisotropic displacement parameters ($\text{\AA}^2 \times 10^3$) for Malonic acid.

Atom	x	y	z	U(eq)	U11	U22	U33	U23	U13	U12
O(1)	4561(2)	8074(2)	1248(2)	17(1)	12(1)	15(1)	23(1)	3(1)	6(1)	3(1)
O(2)	8330(2)	6771(2)	524(2)	20(1)	15(1)	14(1)	27(1)	-1(1)	9(1)	4(1)
O(3)	5821(4)	14359(3)	3134(2)	28(1)	40(1)	28(1)	27(1)	15(1)	19(1)	24(1)
O(4)	7336(4)	12576(3)	5197(2)	27(1)	34(1)	36(1)	19(1)	11(1)	12(1)	23(1)
C(1)	6983(2)	8485(2)	1365(1)	13(1)	12(1)	12(1)	16(1)	3(1)	6(1)	4(1)
C(2)	8735(2)	11105(2)	2531(2)	17(1)	13(1)	14(1)	20(1)	1(1)	6(1)	2(1)
C(3)	7166(2)	12855(2)	3651(2)	15(1)	15(1)	13(1)	17(1)	2(1)	5(1)	4(1)
H(2)	7182(44)	5078(46)	-87(89)	30						
H(4)	6059(166)	13495(202)	5754(68)	41						
H(2A)	10399(2)	10731(2)	3357(2)	20						
H(2B)	9466(2)	12100(2)	1736(2)	20						

Supplementary Table 10bAtomic coordinates ($\times 10^4$) and anisotropic displacement parameters ($\text{\AA}^2 \times 10^3$) for Succinic acid.

Atom	x	y	z	U(eq)	U11	U22	U33	U23	U13	U12
O(1)	1193(1)	4219(1)	7505(1)	16(1)	17(1)	16(1)	15(1)	-2(1)	8(1)	-4(1)
O(2)	2509(1)	6409(1)	9307(1)	18(1)	19(1)	17(1)	17(1)	-6(1)	10(1)	-4(1)
C(1)	2643(1)	5343(1)	7611(1)	11(1)	11(1)	12(1)	10(1)	0(1)	4(1)	0(1)
C(2)	4740(1)	5673(1)	5824(1)	12(1)	13(1)	13(1)	12(1)	0(1)	6(1)	-1(1)
H(2)	1127(63)	6159(27)	10385(51)	33(7)						
H(2A)	6537(1)	5973(1)	6803(1)	33(5)						
H(2B)	4130(1)	6617(1)	4729(1)	33(5)						

Supplementary Table 10cAtomic coordinates ($\times 10^4$) and anisotropic displacement parameters ($\text{\AA}^2 \times 10^3$) for Glutaric acid.

Atom	x	y	z	U(eq)	U11	U22	U33	U23	U13	U12
O(2)	2426(1)	493(2)	6129(1)	20(1)	18(1)	21(1)	24(1)	-2(1)	10(1)	-3(1)
O(1)	1340(1)	-3100(2)	5495(1)	21(1)	20(1)	21(1)	24(1)	-6(1)	10(1)	-3(1)
C(1)	1547(1)	-894(2)	6141(1)	15(1)	15(1)	16(1)	15(1)	1(1)	6(1)	0(1)
C(2)	805(1)	575(2)	6950(1)	19(1)	20(1)	18(1)	23(1)	-3(1)	12(1)	-2(1)
C(3)	0	-1287(2)	7500	18(1)	19(1)	17(1)	22(1)	0	11(1)	0
H(2)	2863(43)	-524(141)	5585(116)	53(20)						
H(2A)	406(1)	2143(2)	6305(1)	48(9)						
H(2B)	1245(1)	1610(2)	7808(1)	48(9)						
H(3A)	369	-2592(2)	8310	48(9)						
H(3B)	-369	-2592(2)	6690	48(9)						

Supplementary Table 10dAtomic coordinates ($\times 10^4$) and anisotropic displacement parameters ($\text{\AA}^2 \times 10^3$) for Adipic acid at 145K.

Atom	x	y	z	U(eq)	U11	U22	U33	U23	U13	U12
O(1)	762(2)	4015(2)	3699(1)	27(1)	34(1)	27(1)	23(1)	7(1)	13(1)	14(1)
O(2)	-1084(2)	7508(2)	3701(1)	29(1)	39(1)	27(1)	25(1)	5(1)	17(1)	13(1)
C(1)	-213(2)	5905(3)	3083(2)	19(1)	20(1)	20(1)	19(1)	1(1)	8(1)	1(1)
C(2)	-510(2)	6637(3)	1570(2)	20(1)	24(1)	18(1)	20(1)	3(1)	9(1)	2(1)
C(3)	282(2)	4657(3)	787(2)	20(1)	23(1)	20(1)	19(1)	4(1)	10(1)	4(1)
H(3B)	1858(4)	4547(49)	1276(23)	33(6)						
H(2B)	-2067(7)	6908(47)	1041(21)	31(6)						
H(2)	-1114(43)	6959(62)	4608(15)	64(9)						
H(3A)	-347(33)	2848(22)	899(26)	36(6)						
H(2A)	280(36)	8389(28)	1612(30)	53(8)						

Supplementary Table 10eAtomic coordinates ($\times 10^4$) and anisotropic displacement parameters ($\text{\AA}^2 \times 10^3$) for Pimelic acid.

Atom	x	y	z	U(eq)	U11	U22	U33	U23	U13	U12
O(1)	1642(1)	8262(2)	315(1)	19(1)	17(1)	19(1)	24(1)	5(1)	12(1)	2(1)
O(2)	2427(1)	4526(2)	1124(1)	18(1)	16(1)	20(1)	25(1)	3(1)	13(1)	3(1)
C(1)	1784(1)	6042(2)	1002(1)	14(1)	12(1)	16(1)	16(1)	0(1)	8(1)	-1(1)
C(2)	1233(1)	4697(2)	1732(1)	19(1)	17(1)	18(1)	27(1)	5(1)	16(1)	3(1)
C(3)	607(1)	6619(2)	2023(1)	17(1)	15(1)	17(1)	23(1)	1(1)	12(1)	0(1)
C(4)	0	4865(3)	2500	16(1)	14(1)	17(1)	20(1)	0	10(1)	0
H(2)	2721(16)	5333(67)	529(45)	24(8)						
H(2A)	1573(1)	3845(2)	2730(1)	44(7)						
H(2B)	946(1)	2986(2)	1084(1)	44(7)						
H(3A)	322(1)	7761(2)	1074(1)	44(7)						
H(3B)	875(1)	8095(2)	2841(1)	44(7)						
H(4A)	-302	3542(3)	1633	44(7)						
H(4B)	302	3542(3)	3367	44(7)						

Supplementary Table 11
Distances, corrected and uncorrected
for rigid body motion

Malonicacid

Bond	uncorrected	corrected
O(1)-C(1)	1.2288	1.2366
O(2)-C(1)	1.306	1.3102
O(3)-C(3)	1.2259	1.2338
O(4)-C(3)	1.308	1.3164
C(1)-C(2)	1.5109	1.5185
C(2)-C(3)	1.5053	1.51

Succinicacid

Bond	uncorrected	corrected
O(1)-C(1)	1.2275	1.2347
O(2)-C(1)	1.3233	1.3287
C(1)-C(2)	1.5027	1.5036

Glutaricacid

Bond	uncorrected	corrected
O(1)-C(1)	1.2318	1.237
O(2)-C(1)	1.32	1.3225
C(1)-C(2)	1.4994	1.5008
C(2)-C(3)	1.5239	1.5262

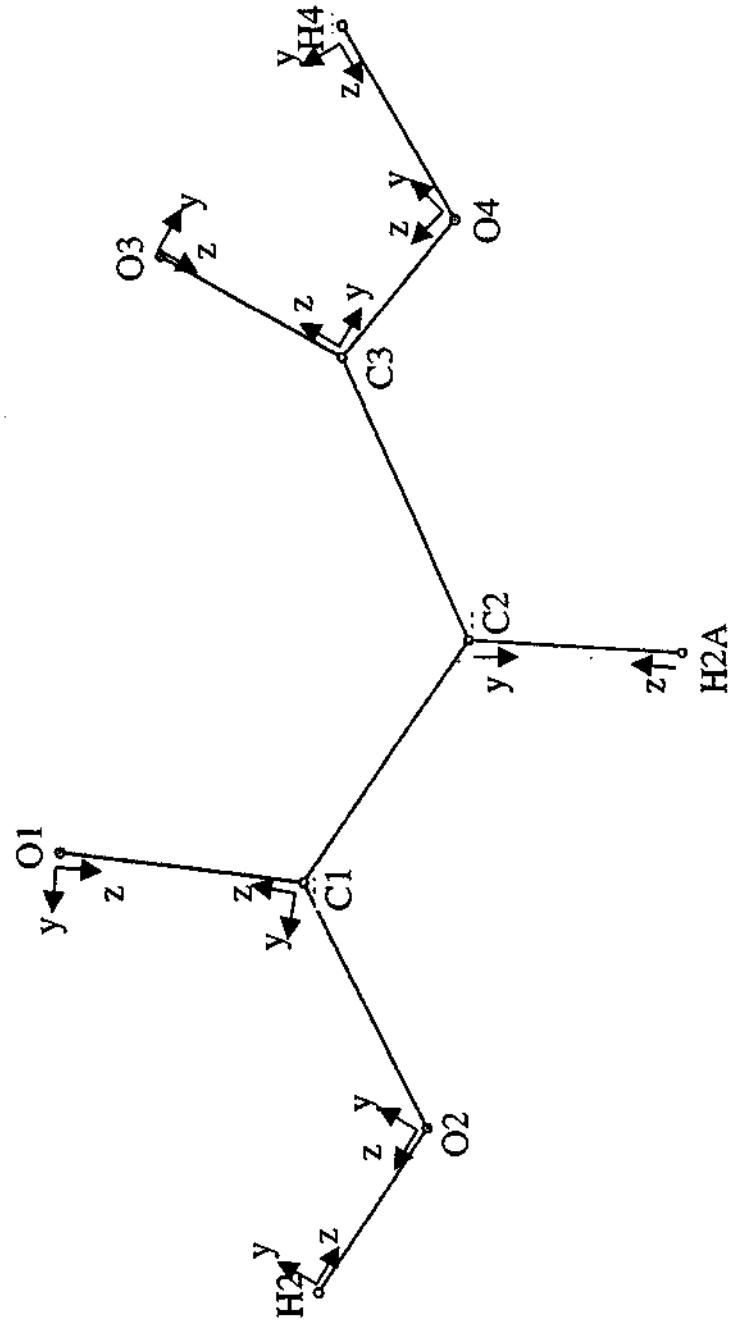
Adipicacid

Bond	uncorrected	corrected
O(1)-C(1)	1.228	1.236
O(2)-C(1)	1.3184	1.3252
C(1)-C(2)	1.5006	1.515
C(2)-C(3)	1.5181	1.5254

Pimelicacid

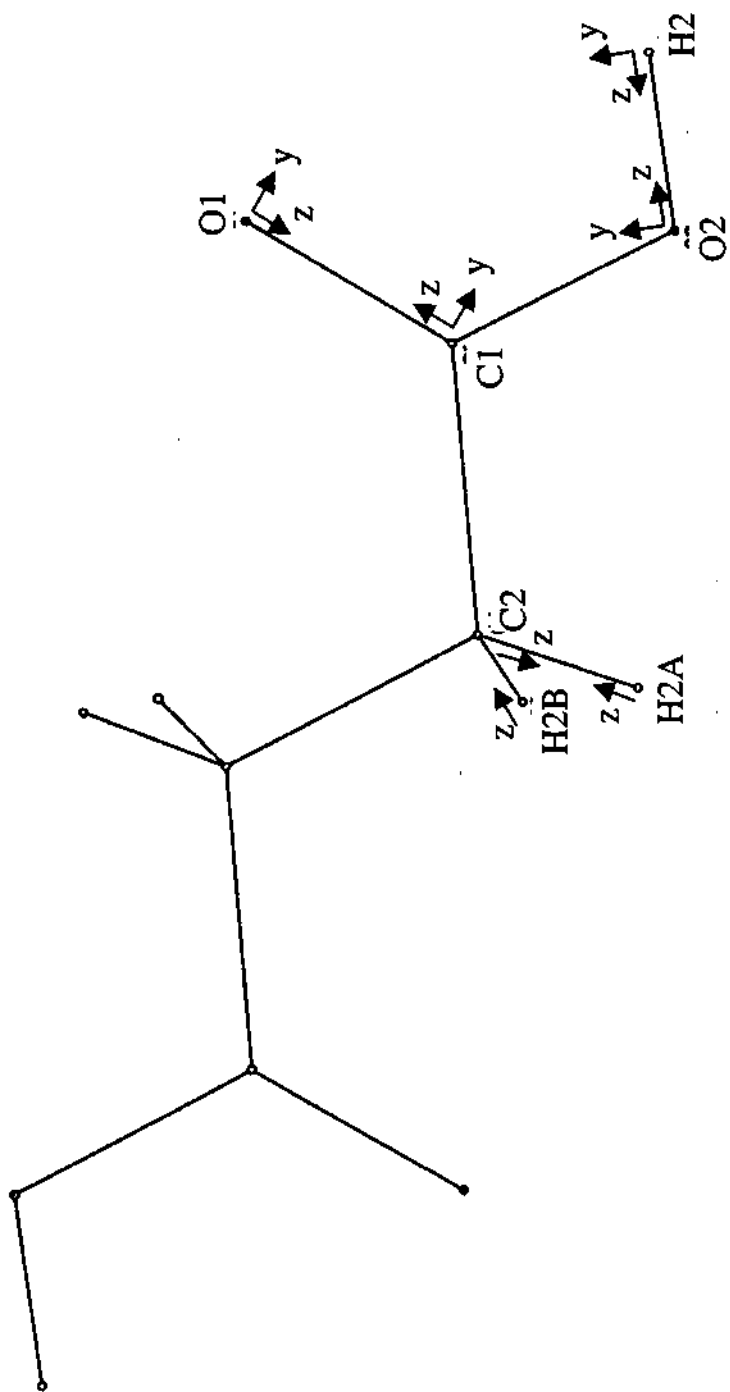
Bond	uncorrected	corrected
O(1)-C(1)	1.2295	1.2339
O(2)-C(1)	1.3214	1.3235
C(1)-C(2)	1.5003	1.5012
C(2)-C(3)	1.5226	1.5247
C(3)-C(4)	1.5299	1.5315

Malonic acid



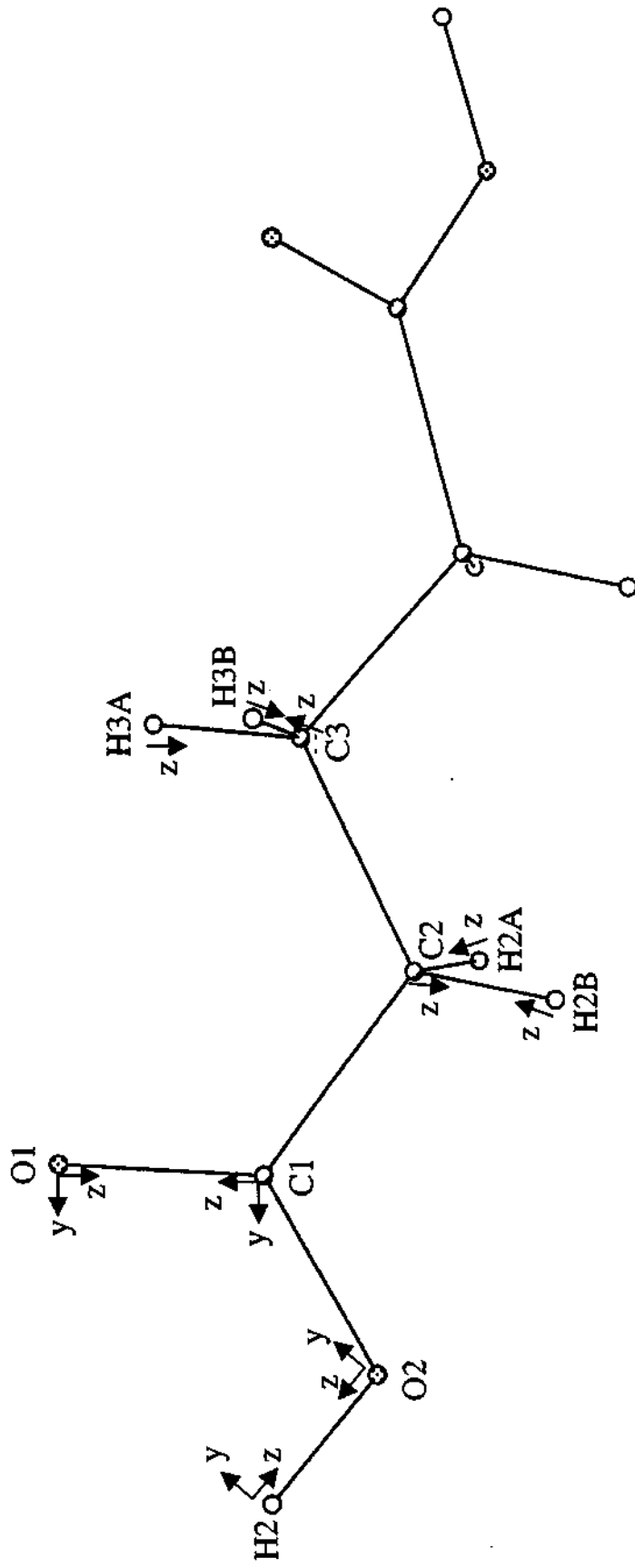
Definition of local coordination systems

Succinic acid



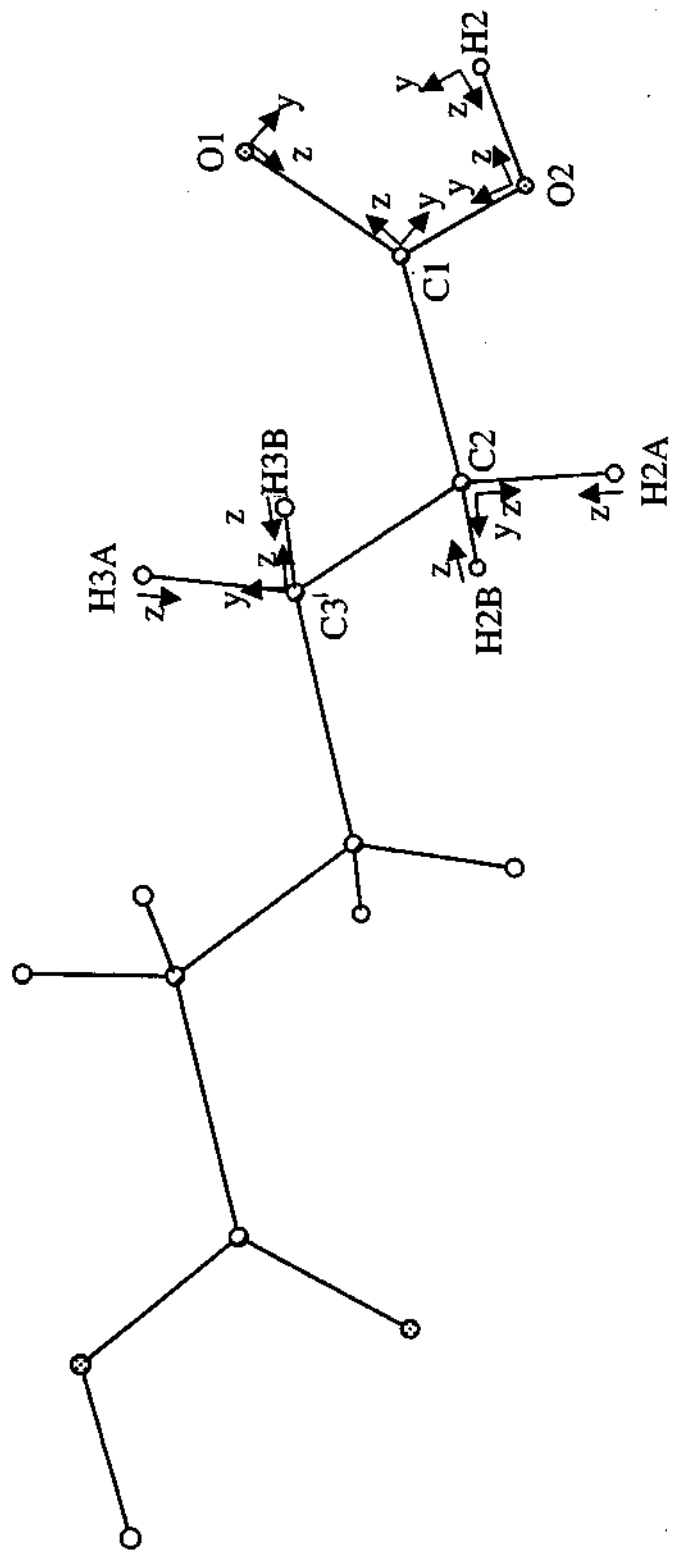
Definition of local coordination systems

Glutaric acid



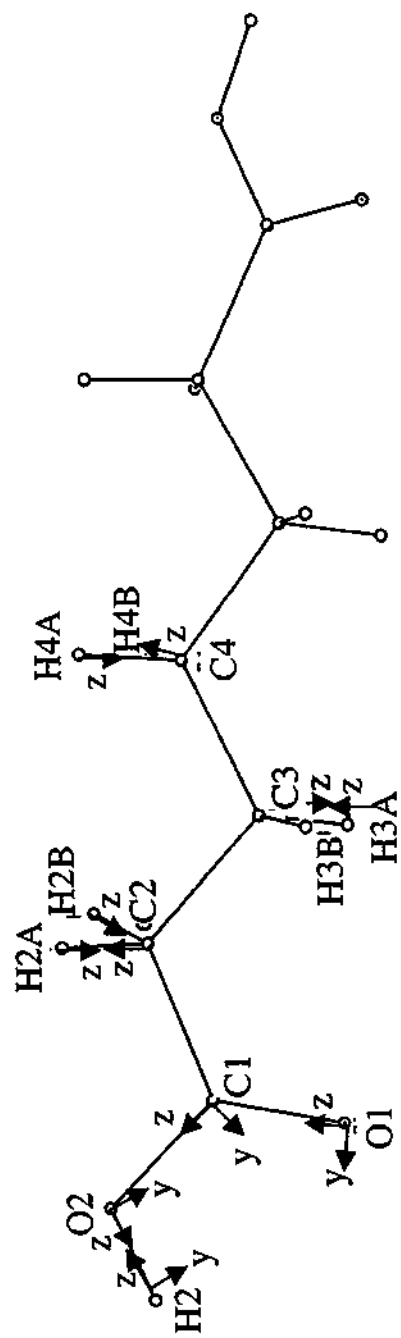
Definition of local coordination systems

Adipic acid at 145 K



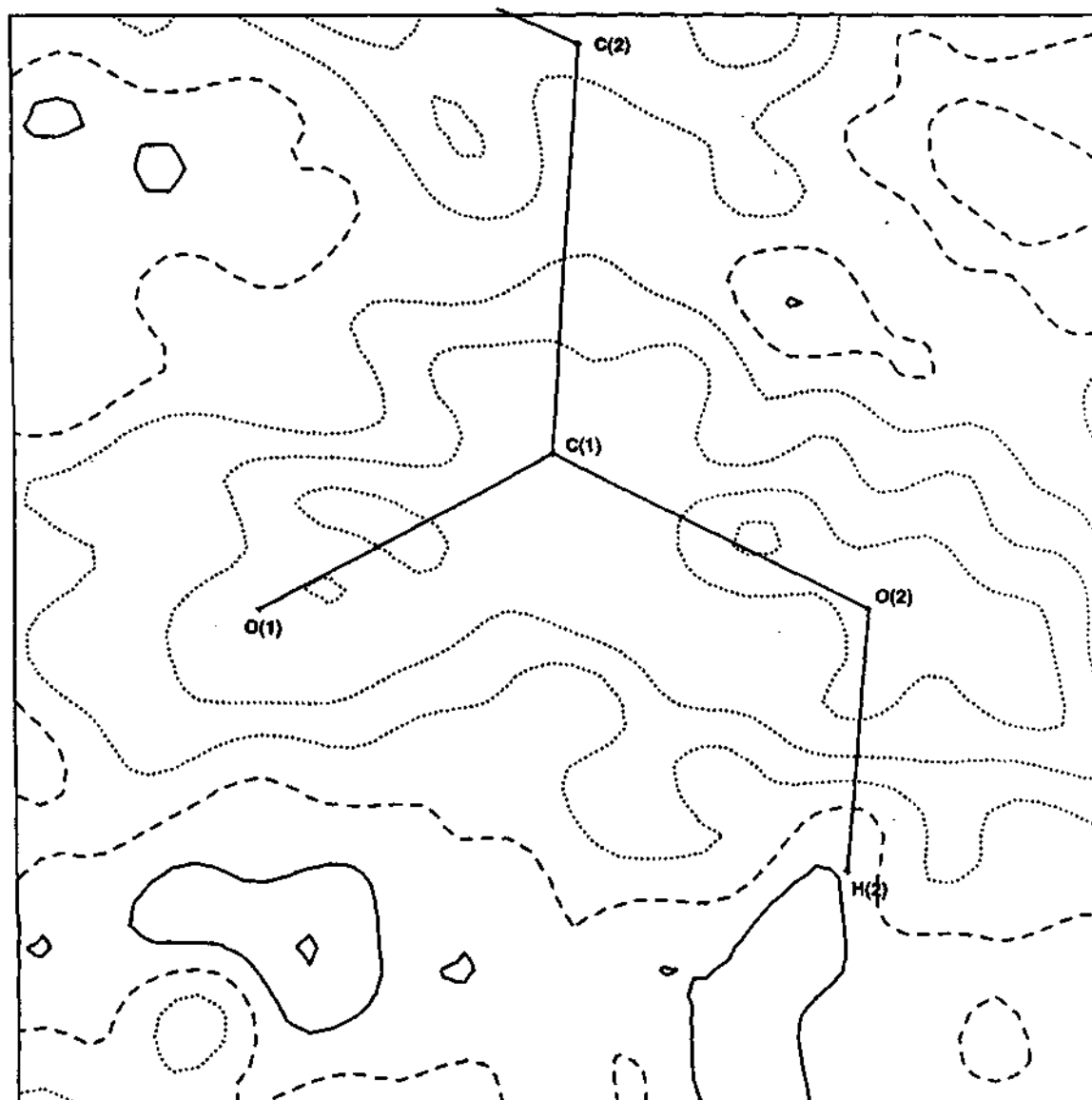
Definition of local coordination systems

Pimelic acid



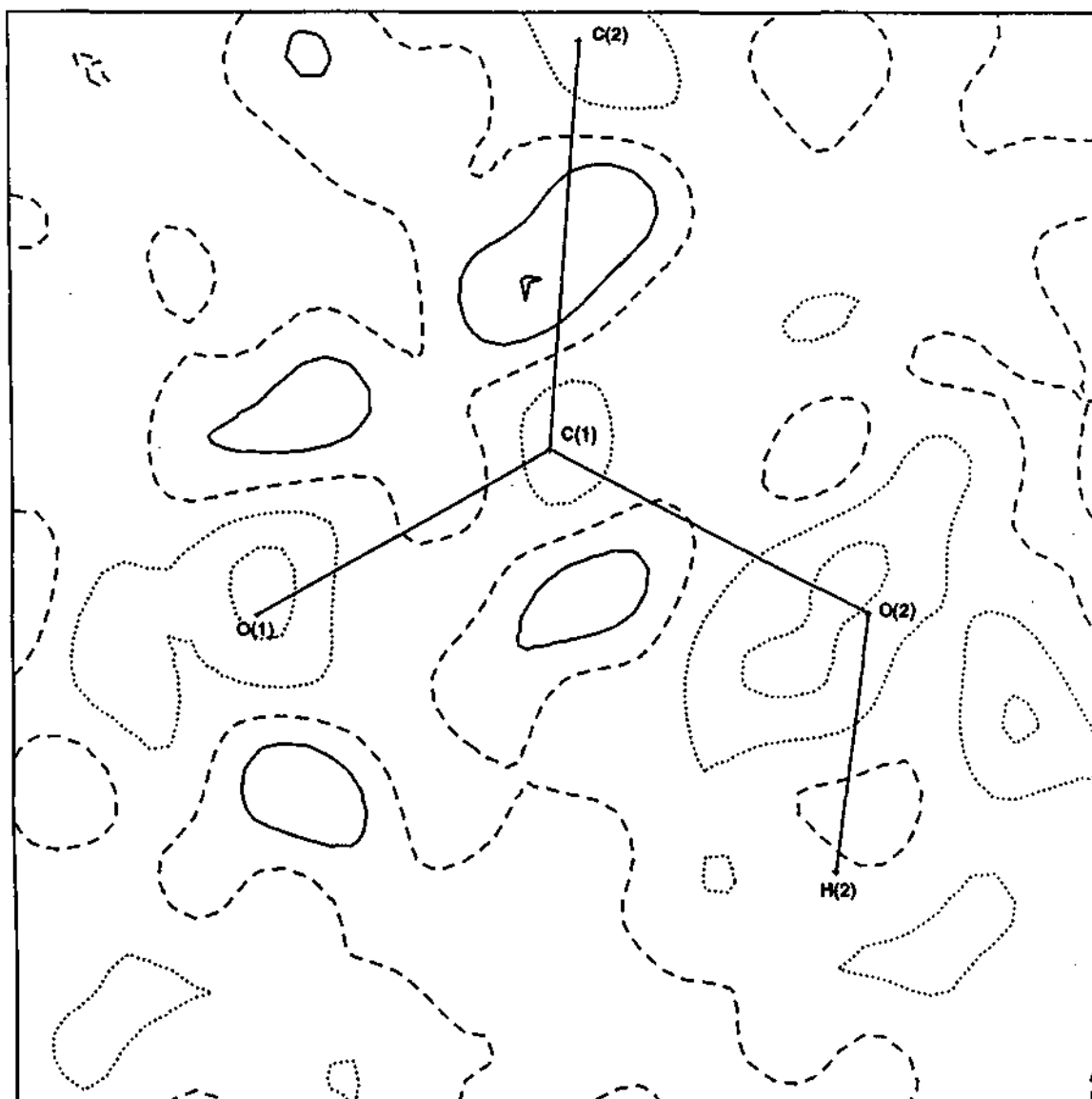
Definition of local coordination systems

Malonic acid



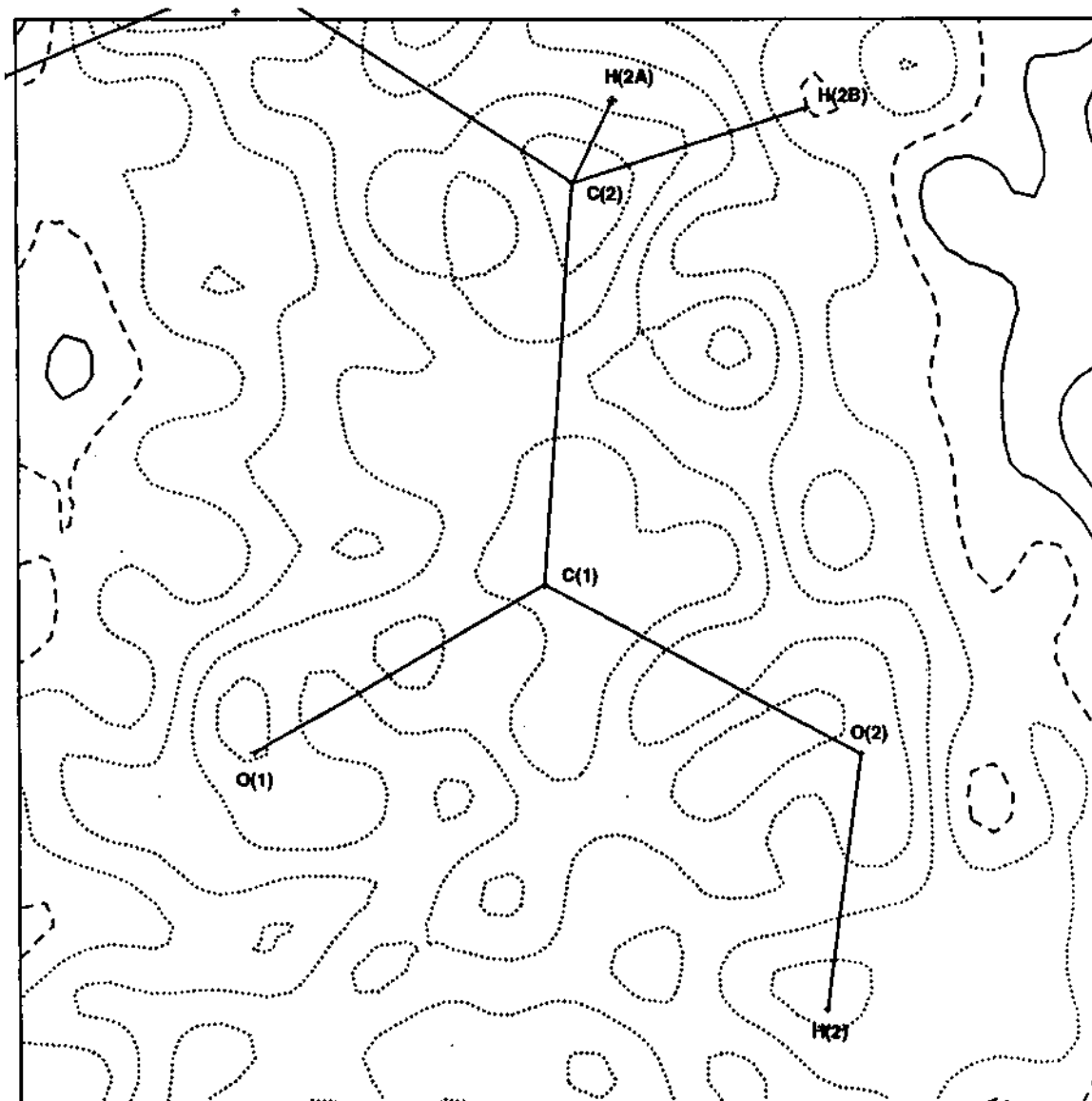
Residual electron density map in the plane containing C(1), O(1) and O(2) atoms. (contours at $0.1 \text{ e}\text{\AA}^{-3}$)

Succinic acid



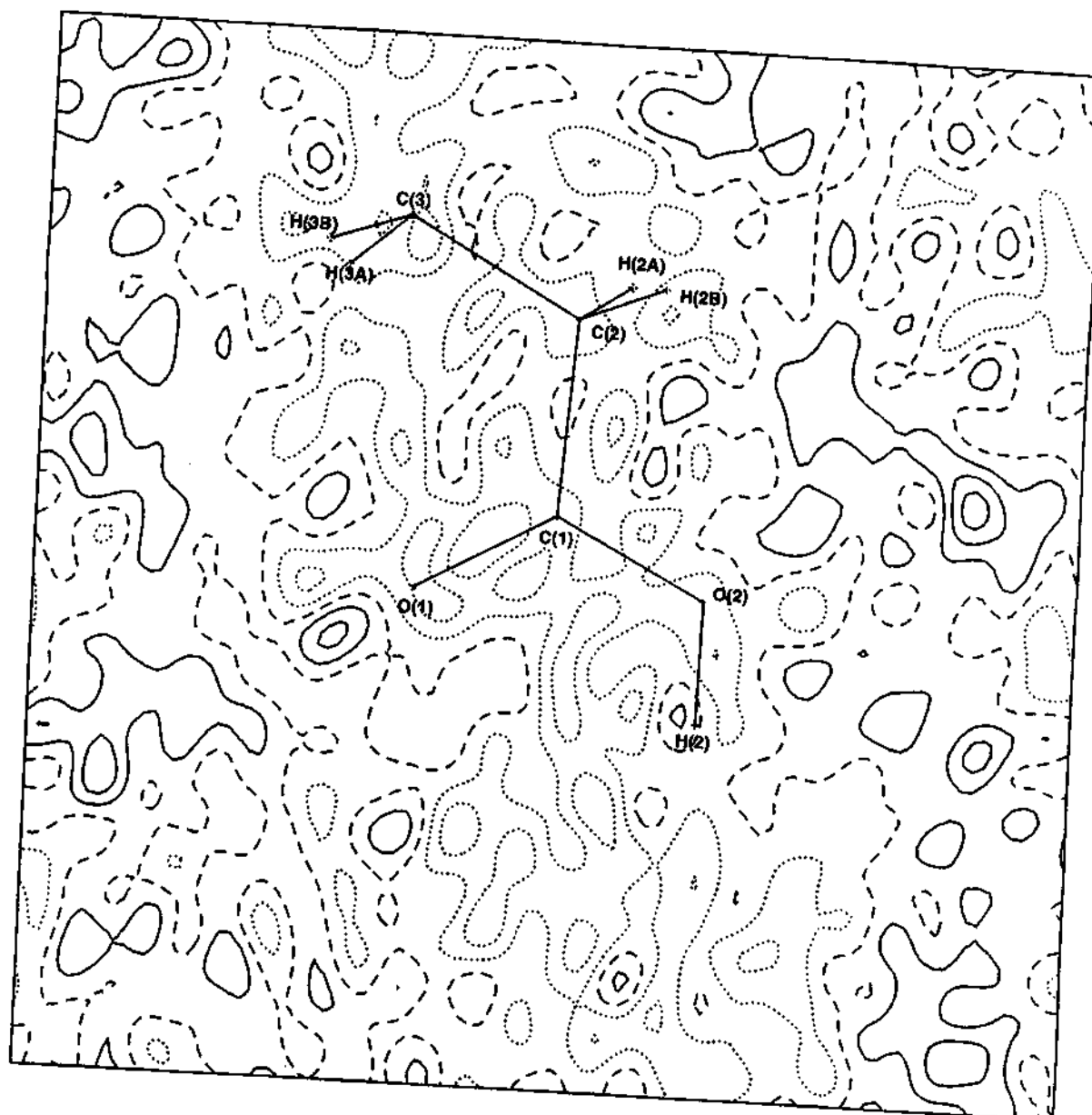
Residual electron density map in the plane containing C(1), O(1) and O(2) atoms. (contours at $0.1 \text{ e}\text{\AA}^{-3}$)

Glutaric acid



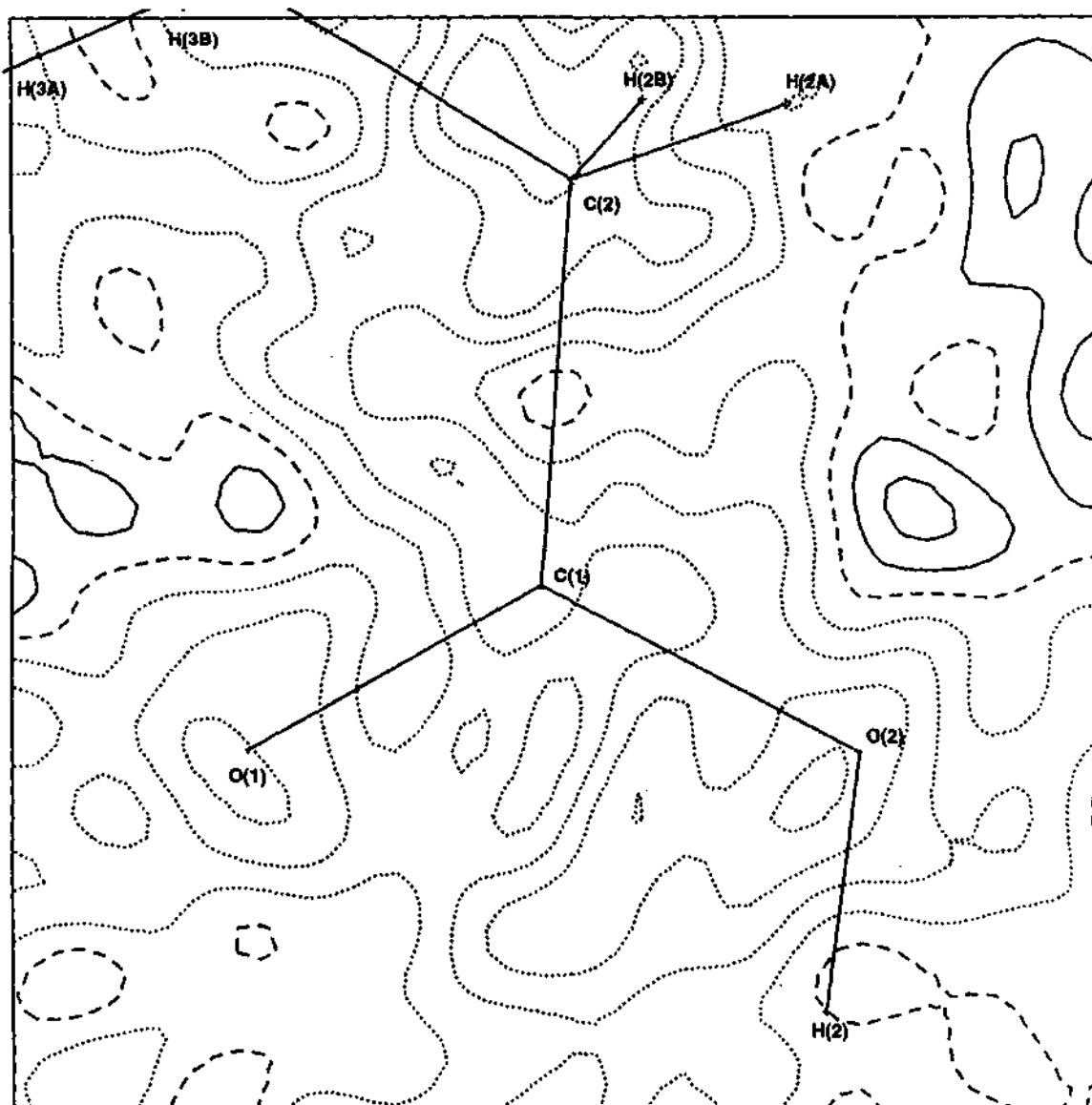
Residual electron density map in the plane containing C(1), O(1) and O(2) atoms. (contours at 0.1 eÅ⁻³)

Adipic acid at 145 K



Residual electron density map in the plane containing C(1), O(1) and O(2) atoms. (contours at $0.1 \text{ e}\text{\AA}^{-3}$)

Pimelic acid



Residual electron density map in the plane containing C(1), O(1) and O(2) atoms. (contours at 0.1 eÅ⁻³)

Supplementary Table 13a

Atomic coordinates ($\times 10^4$) and anisotropic displacement parameters ($\text{\AA}^2 \times 10^3$) for the centric polymorph of 5-nitouracil.

	x	y	z	U(eq)	U11	U22	U33	U23	U13	U12
O(1)	-612(4)	3492(2)	5617(1)	16(1)	22(1)	12(1)	14(1)	-2(1)	5(1)	1(1)
O(2)	917(4)	-4(2)	3814(2)	18(1)	28(1)	7(1)	19(1)	0(1)	6(1)	2(1)
O(4)	2367(5)	2549(3)	1538(2)	21(1)	28(2)	20(1)	16(1)	2(1)	8(1)	-2(1)
O(3)	2099(5)	538(2)	1940(2)	25(1)	42(2)	15(1)	17(1)	0(1)	5(1)	10(1)
N(2)	233(3)	1764(2)	4707(1)	13(1)	17(1)	9(1)	13(1)	0(1)	2(1)	1(1)
N(1)	555(4)	3831(2)	4095(2)	16(1)	24(1)	8(1)	15(1)	0(1)	4(1)	-1(1)
N(3)	1965(4)	1695(2)	2128(1)	15(1)	19(1)	14(1)	13(1)	1(1)	2(1)	3(1)
C(1)	17(4)	3047(2)	4854(2)	13(1)	15(1)	10(1)	14(1)	0(1)	2(1)	0(1)
C(2)	820(4)	1170(2)	3850(2)	12(1)	15(1)	9(1)	14(1)	1(1)	1(1)	0(1)
C(3)	1281(3)	2080(2)	3069(2)	12(1)	14(1)	10(1)	12(1)	0(1)	2(1)	1(1)
C(4)	1156(4)	3365(2)	3234(2)	14(1)	17(1)	10(1)	15(1)	1(1)	4(1)	0(1)
H(2)	-66(3)	1183(2)	5283(1)	16						
H(1)	497(4)	4791(2)	4189(2)	19						
H(4)	1548(4)	4023(2)	2663(2)	17						

Supplementary Table 13b

Atomic coordinates ($\times 10^4$) and anisotropic displacement parameters ($\text{\AA}^2 \times 10^3$) for the non-centric polymorph of 5-nitouracil.

	x	y	z	U(eq)	U11	U22	U33	U23	U13	U12
O(1)	3135(2)	3079(1)	3630(1)	15(1)	16(1)	20(1)	10(1)	0(1)	4(1)	2(1)
O(2)	6529(2)	1566(1)	-91(1)	16(1)	17(1)	23(1)	7(1)	-3(1)	1(1)	-2(1)
O(3)	10895(3)	152(2)	206(2)	22(1)	22(1)	25(1)	20(1)	-8(1)	5(1)	2(1)
O(4)	12139(3)	-234(2)	2163(2)	24(1)	21(1)	24(1)	28(1)	-1(1)	-3(1)	10(1)
N(2)	5039(2)	2383(1)	1785(1)	12(1)	13(1)	16(1)	6(1)	0(1)	0(1)	1(1)
N(1)	6754(2)	1896(1)	3775(1)	13(1)	16(1)	15(1)	7(1)	1(1)	-1(1)	1(1)
N(3)	10679(2)	271(1)	1381(1)	15(1)	14(1)	13(1)	19(1)	-4(1)	2(1)	0(1)
C(1)	4862(2)	2495(1)	3096(1)	11(1)	12(1)	13(1)	7(1)	0(1)	1(1)	-1(1)
C(2)	6766(2)	1652(1)	1087(1)	11(1)	11(1)	14(1)	8(1)	-1(1)	1(1)	-2(1)
C(3)	8669(2)	1051(1)	1897(1)	12(1)	12(1)	12(1)	11(1)	-1(1)	0(1)	0(1)
C(4)	8561(2)	1191(1)	3205(1)	12(1)	14(1)	12(1)	11(1)	1(1)	-2(1)	0(1)
H(2)	3764(2)	2891(1)	1265(1)	14						
H(1)	6778(2)	1992(1)	4745(1)	15						
H(4)	9959(2)	725(1)	3792(1)	15						

Supplementary Table 14
Distances, corrected and uncorrected
for rigid body motion for 5-nitouracil

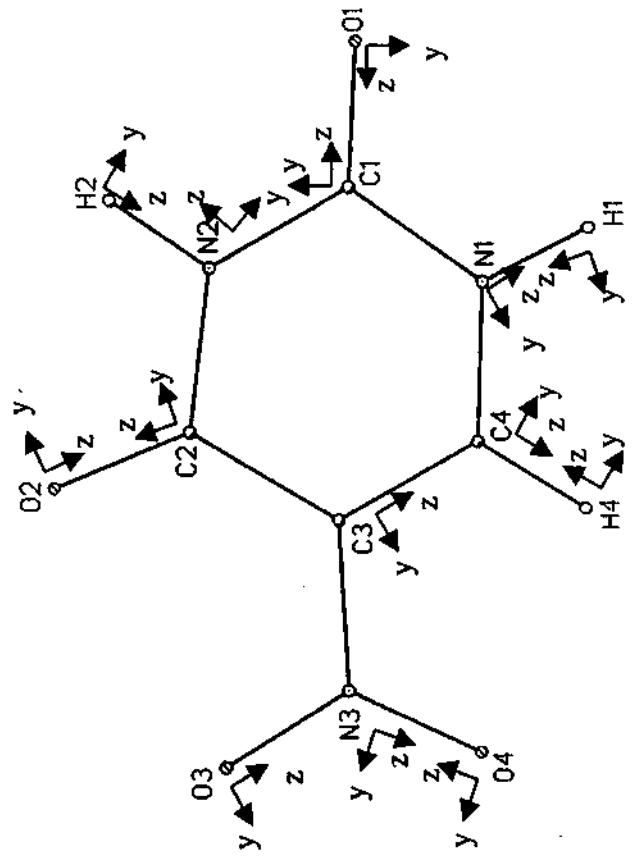
centric

Bond	uncorrected (Å)	corrected (Å)
O1-C1	1.236	1.2389
O2-C2	1.228	1.2307
O3-O4	2.1757	2.1806
O3-N3	1.2374	1.2402
O4-N3	1.2353	1.2382
N1-C1	1.3773	1.3806
N1-C4	1.3448	1.3481
N2-C1	1.3641	1.3672
N2-C2	1.3904	1.3938
N3-C3	1.4367	1.4402
C2-C3	1.4617	1.4652
C3-C4	1.3616	1.3647

non-centric

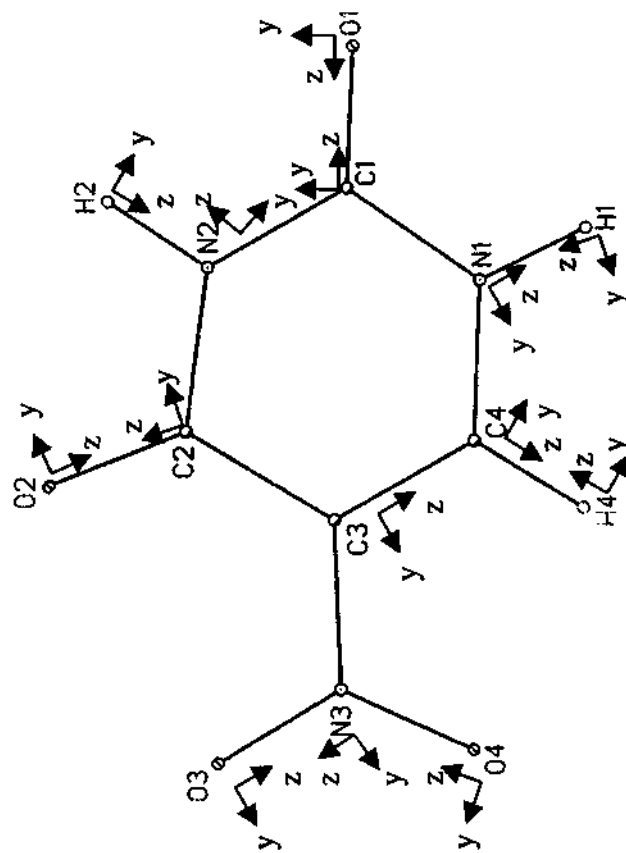
Bond	uncorrected (Å)	Corrected (Å)
O1-C1	1.2324	1.2345
O2-C2	1.2309	1.2334
O3-O4	2.1713	2.1757
O3-N3	1.2278	1.2303
O4-N3	1.2396	1.2418
N1-C1	1.3774	1.3798
N1-C4	1.3408	1.343
N2-C1	1.3669	1.3696
N2-C2	1.3855	1.3877
N3-C3	1.4385	1.4407
C2-C3	1.4577	1.4602
C3-C4	1.3634	1.3662

centric polymorph of 5-nitouracil



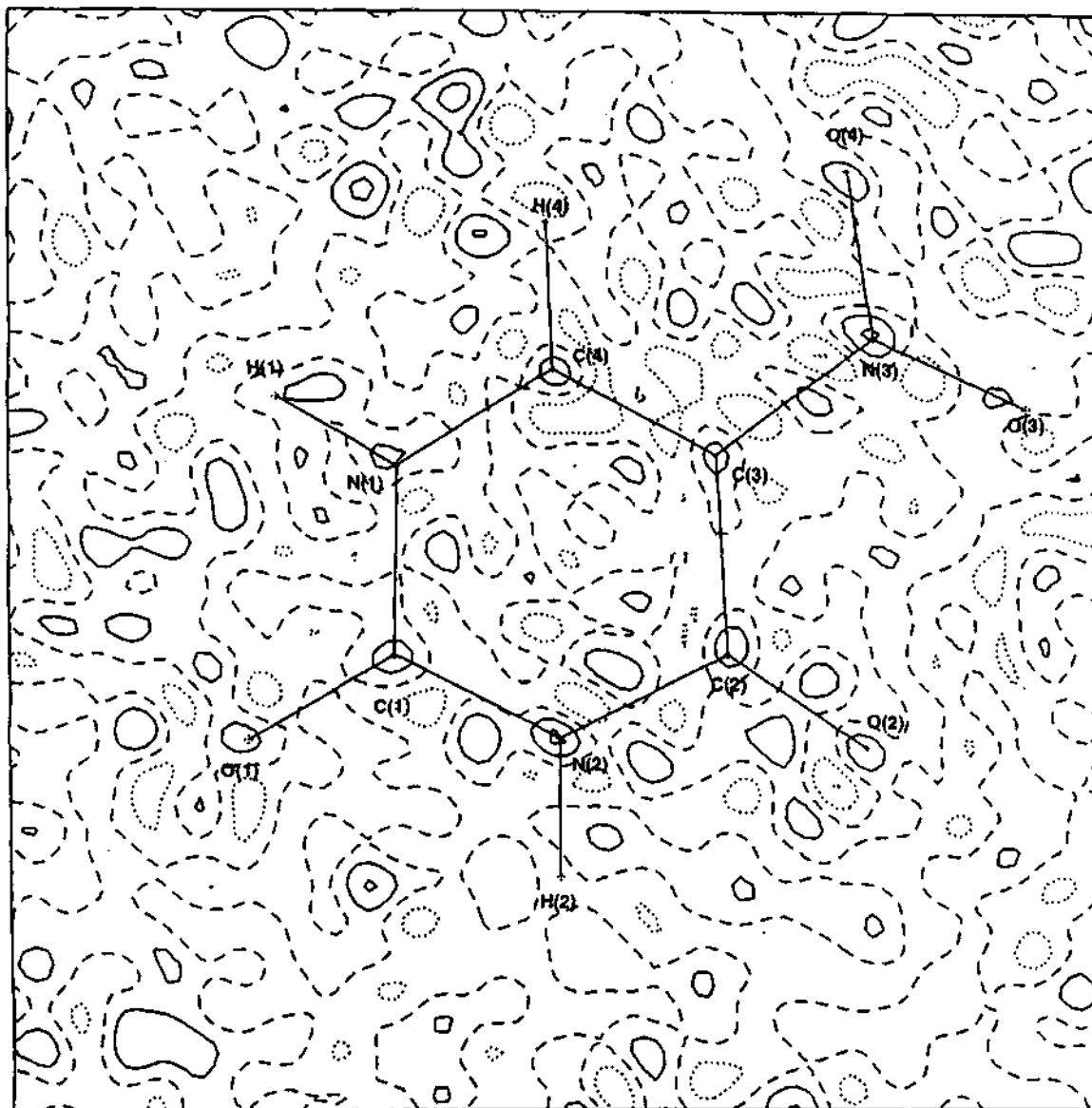
Definition of local coordination systems

non-centric polymorph of 5-nitouracil



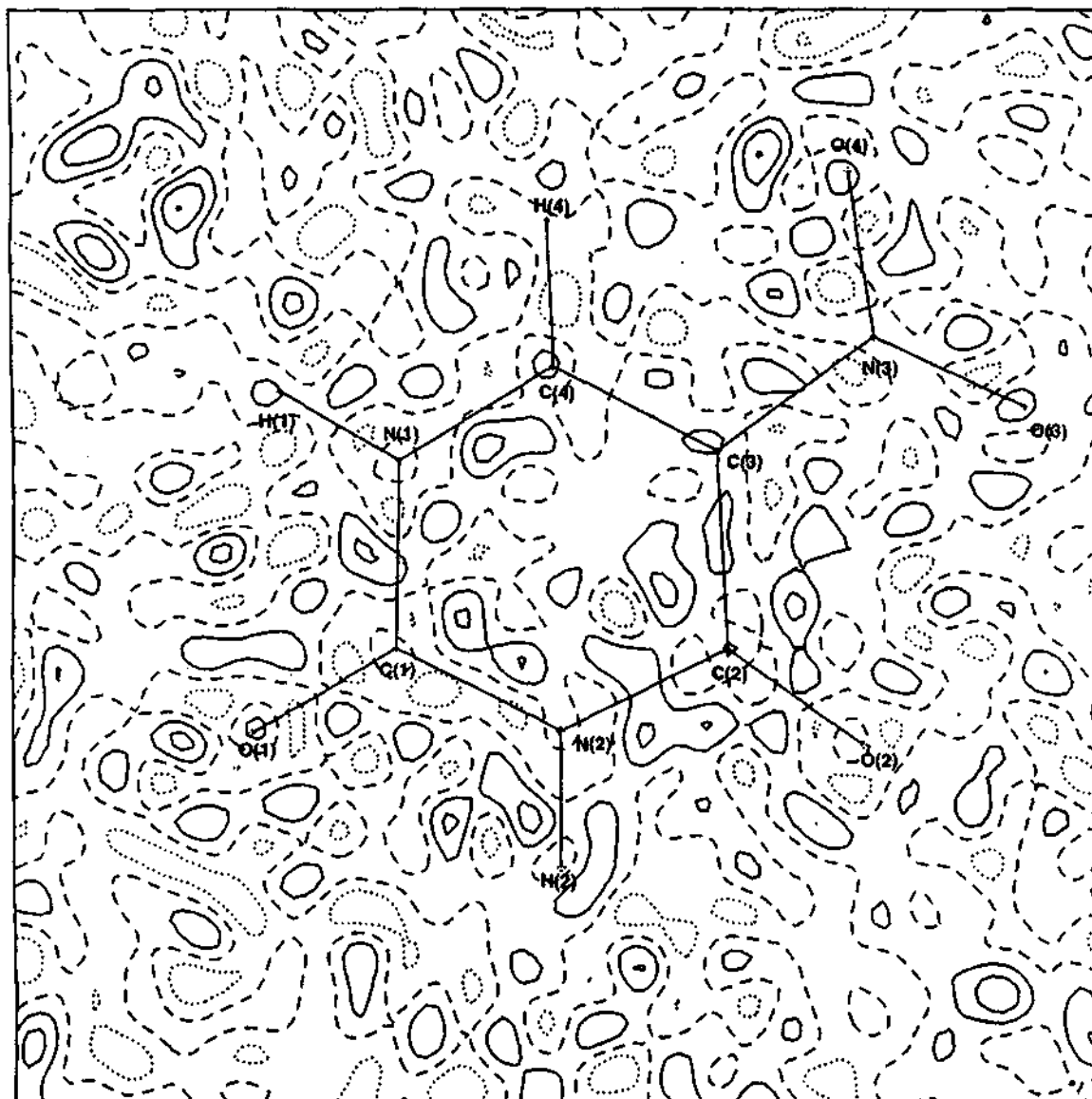
Definition of local coordination systems

Centrosymmetric form of 5-nitrouracil



Residual electron density map in the plane containing N(1), N(2) and C(3) atoms. (contours at $0.1 \text{ e}\text{\AA}^{-3}$)

Non-centrosymmetric form of 5-nitrouracil



Residual electron density map in the plane containing N(1), N(2) and C(3) atoms. (contours at 0.1 eÅ⁻³)

Supplementary Table 16a

Atomic coordinates ($\times 10^4$) and anisotropic displacement parameters ($\text{\AA}^2 \times 10^3$) for Diamino derivative of 1,1-ethylenedicarbonitrile.

Atom	x	y	z	U(eq)	U11	U22	U33	U23	U13	U12
N(1)	7524(2)	8841(1)	1150(1)	44(1)	71(1)	23(1)	38(1)	1(1)	6(1)	-2(1)
N(2)	9691(2)	7054(1)	3090(1)	46(1)	58(1)	54(1)	25(1)	2(1)	-7(1)	-16(1)
N(3)	7555(1)	5593(1)	1540(1)	27(1)	32(1)	21(1)	27(1)	3(1)	0(1)	-1(1)
N(4)	7912(1)	6464(1)	360(1)	25(1)	33(1)	24(1)	20(1)	-1(1)	-1(1)	-2(1)
C(1)	7871(1)	8108(1)	1385(1)	31(1)	45(1)	22(1)	25(1)	-2(1)	3(1)	-5(1)
C(2)	9038(1)	7122(1)	2454(1)	32(1)	41(1)	32(1)	22(1)	-1(1)	0(1)	-9(1)
C(3)	8271(1)	7206(1)	1668(1)	26(1)	36(1)	23(1)	20(1)	-1(1)	0(1)	-4(1)
C(4)	7917(1)	6416(1)	1185(1)	23(1)	27(1)	21(1)	21(1)	0(1)	0(1)	-1(1)
C(5)	6675(1)	5519(1)	2330(1)	34(1)	37(1)	32(1)	32(1)	9(1)	5(1)	-4(1)
C(6)	8077(1)	4716(1)	1169(1)	35(1)	46(1)	21(1)	39(1)	1(1)	-6(1)	4(1)
C(7)	6708(1)	5908(1)	-135(1)	32(1)	41(1)	27(1)	27(1)	-5(1)	-8(1)	0(1)
C(8)	8981(1)	7124(1)	-96(1)	31(1)	39(1)	31(1)	23(1)	3(1)	6(1)	-2(1)
H(5A)	7601(2)	5336(6)	2786(1)	51						
H(5B)	5689(8)	5003(4)	2298(2)	51						
H(5C)	6095(10)	6163(2)	2481(3)	51						
H(6A)	6964(2)	4392(3)	907(5)	53						
H(6B)	8620(11)	4279(2)	1624(1)	53						
H(6C)	9024(8)	4841(1)	708(4)	53						
H(7A)	7394(3)	5339(3)	-390(4)	48						
H(7B)	6186(8)	6321(2)	-612(3)	48						
H(7C)	5672(6)	5661(5)	238(1)	48						
H(8A)	8185(2)	7682(3)	-294(4)	47						
H(8B)	9539(9)	6791(2)	-611(3)	47						
H(8C)	9995(7)	7379(4)	286(2)	47						

Supplementary Table 16b

Atomic coordinates ($\times 10^4$) and anisotropic displacement parameters ($\text{\AA}^2 \times 10^3$) for Dithio derivative of 1,1-ethylenedicarbonitrile.

Atom	x	y	z	U(eq)	U11	U22	U33	U23	U13	U12
S(1)	2665(1)	5504(1)	4013(1)	19(1)	24(1)	18(1)	15(1)	0(1)	-1(1)	-2(1)
S(2)	1624(1)	6367(1)	2129(1)	20(1)	26(1)	16(1)	16(1)	2(1)	0(1)	-3(1)
N(1)	-4141(6)	3922(2)	1128(2)	26(1)	29(1)	26(1)	22(1)	-4(1)	-4(1)	-5(1)
N(2)	-747(8)	3107(2)	3947(2)	28(1)	42(1)	18(1)	24(1)	4(1)	2(1)	-4(1)
C(1)	-2511(5)	4194(1)	1792(1)	19(1)	21(1)	18(1)	18(1)	-2(1)	0(1)	-2(1)
C(2)	-717(5)	3716(1)	3367(1)	20(1)	27(1)	13(1)	19(1)	1(1)	3(1)	-1(1)
C(3)	-648(4)	4459(1)	2648(1)	16(1)	19(1)	14(1)	15(1)	-1(1)	1(1)	-1(1)
C(4)	999(4)	5363(1)	2851(1)	15(1)	16(1)	14(1)	14(1)	0(1)	1(1)	0(1)
C(5)	4598(5)	6732(2)	4069(1)	22(1)	23(1)	19(1)	22(1)	-4(1)	-1(1)	-2(1)
C(6)	268(6)	5995(2)	948(1)	22(1)	28(1)	21(1)	16(1)	2(1)	0(1)	0(1)
H(5A)	6101(143)	6808(21)	4711(22)	32						
H(5B)	2726(5)	7298(2)	4021(51)	32						
H(5C)	6104(143)	6813(21)	3508(29)	32						
H(6A)	893(170)	6569(26)	481(4)	33						
H(6B)	-2352(26)	5885(56)	881(14)	33						
H(6C)	1467(145)	5311(31)	789(18)	33						

Supplementary Table 16c

Atomic coordinates ($\times 10^4$) and anisotropic displacement parameters ($\text{\AA}^2 \times 10^3$) for Thioamino derivative of 1,1-ethylenedicarbonitrile.

Atom	x	y	z	U(eq)	U11	U22	U33	U23	U13	U12
S(1)	7493(1)	3085(1)	7467(1)	21(1)	23(1)	23(1)	16(1)	-1(1)	1(1)	3(1)
N(1)	8886(3)	844(2)	3905(1)	41(1)	63(1)	38(1)	20(1)	-8(1)	2(1)	2(1)
N(2)	9570(3)	5197(2)	5412(1)	34(1)	50(1)	27(1)	25(1)	6(1)	1(1)	-5(1)
N(3)	8270(2)	224(2)	6808(1)	25(1)	34(1)	18(1)	23(1)	1(1)	-8(1)	-2(1)
C(1)	8855(3)	1490(2)	4685(1)	26(1)	35(1)	26(1)	18(1)	-2(1)	-1(1)	2(1)
C(2)	9215(3)	3923(2)	5535(1)	23(1)	28(1)	26(1)	16(1)	1(1)	-1(1)	0(1)
C(3)	8813(2)	2339(2)	5630(1)	20(1)	23(1)	21(1)	15(1)	-2(1)	-1(1)	1(1)
C(4)	8263(2)	1719(2)	6585(1)	18(1)	20(1)	18(1)	16(1)	-1(1)	-4(1)	-2(1)
C(5)	8241(3)	2401(2)	8722(1)	25(1)	25(1)	36(1)	15(1)	-1(1)	0(1)	-2(1)
C(6)	7099(3)	-475(2)	7565(2)	38(1)	48(1)	30(1)	34(1)	11(1)	-11(1)	-19(1)
C(7)	9363(4)	-874(2)	6247(2)	42(1)	70(2)	22(1)	32(1)	-4(1)	-12(1)	16(1)
H(5A)	7828(3)	3169(2)	9314(1)	38						
H(5B)	9581(3)	2356(2)	8719(1)	38						
H(5C)	7750(3)	1278(2)	8867(1)	38						
H(6A)	7335(3)	-1682(2)	7616(2)	56						
H(6B)	5835(3)	-289(2)	7319(2)	56						
H(6C)	7284(3)	42(2)	8304(2)	56						
H(7A)	9173(4)	-2006(2)	6545(2)	62						
H(7B)	10646(4)	-551(2)	6347(2)	62						
H(7C)	9056(4)	-856(2)	5445(2)	62						

Supplementary Table 17
Distances, corrected and uncorrected for rigid
body motion for 1,1-ethylenedicarbonitriles

diamino

Bond	uncorrected (Å)	corrected (Å)
N1-C1	1.1684	1.1715
N2-C2	1.1651	1.1682
N3-C4	1.3537	1.3577
N3-C5	1.4586	1.4628
N3-C6	1.4523	1.4563
N4-C4	1.3501	1.354
N4-C7	1.4624	1.4665
N4-C8	1.4593	1.4635
C1-C3	1.4145	1.4183
C2-C3	1.4086	1.4124
C3-C4	1.417	1.4212

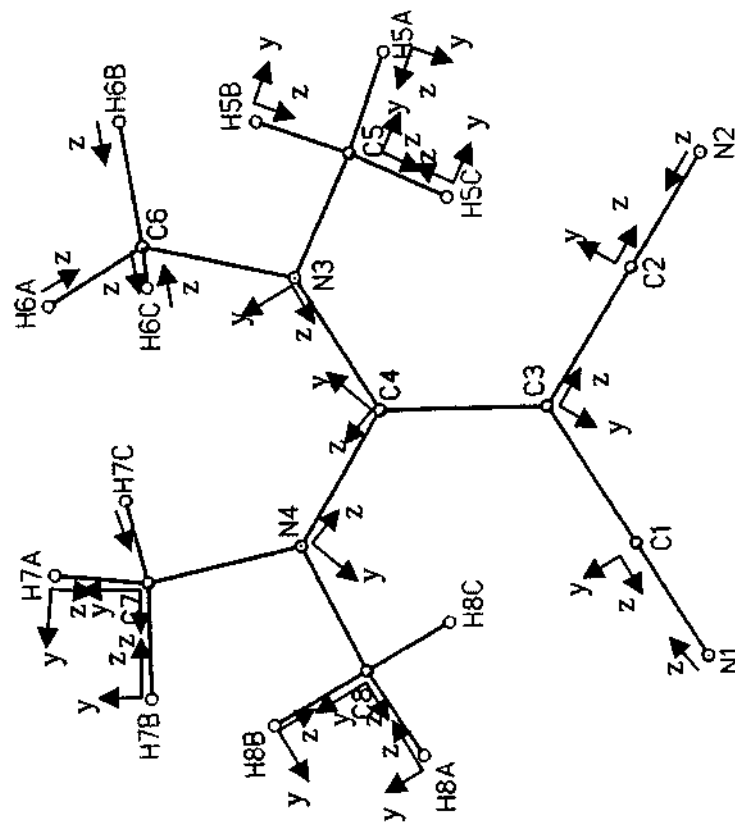
dithio

Bond	uncorrected (Å)	Corrected (Å)
S1-C4	1.7507	1.7531
S1-C5	1.7998	1.8027
S2-C4	1.7196	1.7221
S2-C6	1.8027	1.8052
N1-C1	1.1635	1.1653
N2-C2	1.162	1.1636
C1-C3	1.4238	1.4259
C2-C3	1.4289	1.4309
C3-C4	1.3851	1.3874

thioamine

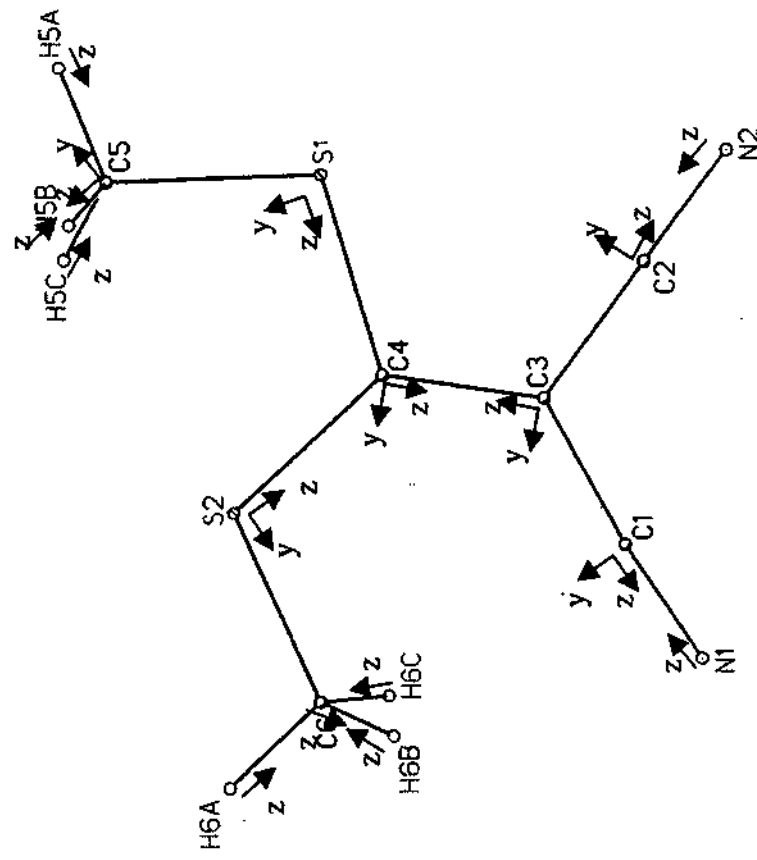
Bond	uncorrected (Å)	corrected (Å)
S1-C4	1.7377	1.7431
S1-C5	1.8191	1.8242
N1-C1	1.1628	1.1668
N2-C2	1.1452	1.1489
N3-C4	1.3144	1.3185
N3-C6	1.4986	1.5028
N3-C7	1.4445	1.4482
C1-C3	1.4077	1.4125
C2-C3	1.4115	1.4162
C3-C4	1.4198	1.4241

diamino derivative of 1,1-ethylenedicarbonitrile



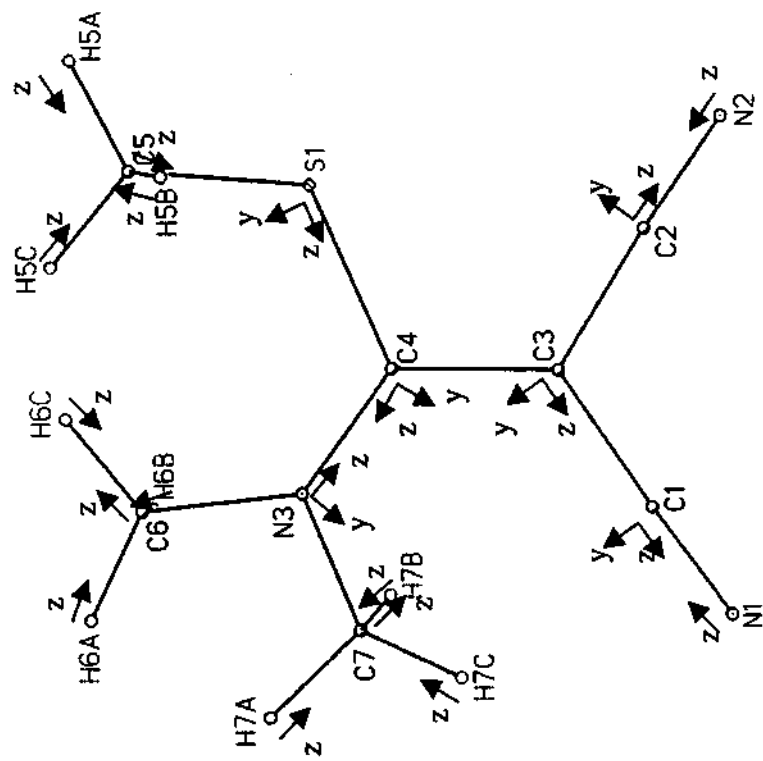
Definition of local coordination systems

dithio derivative of 1,1-ethylenedicarbonitrile



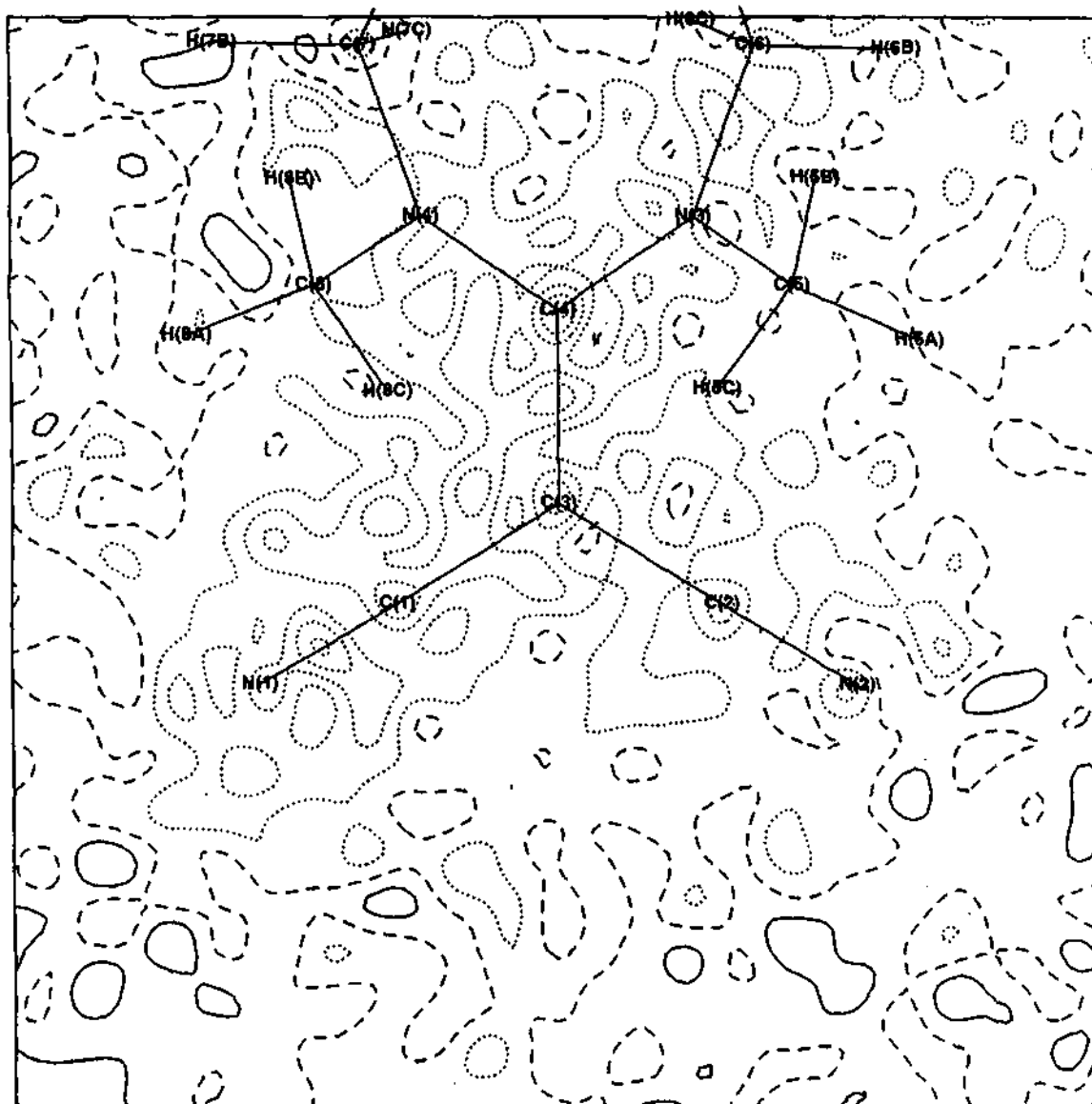
Definition of local coordination systems

thioamino derivative of 1,1-ethylenedicarbonitrile



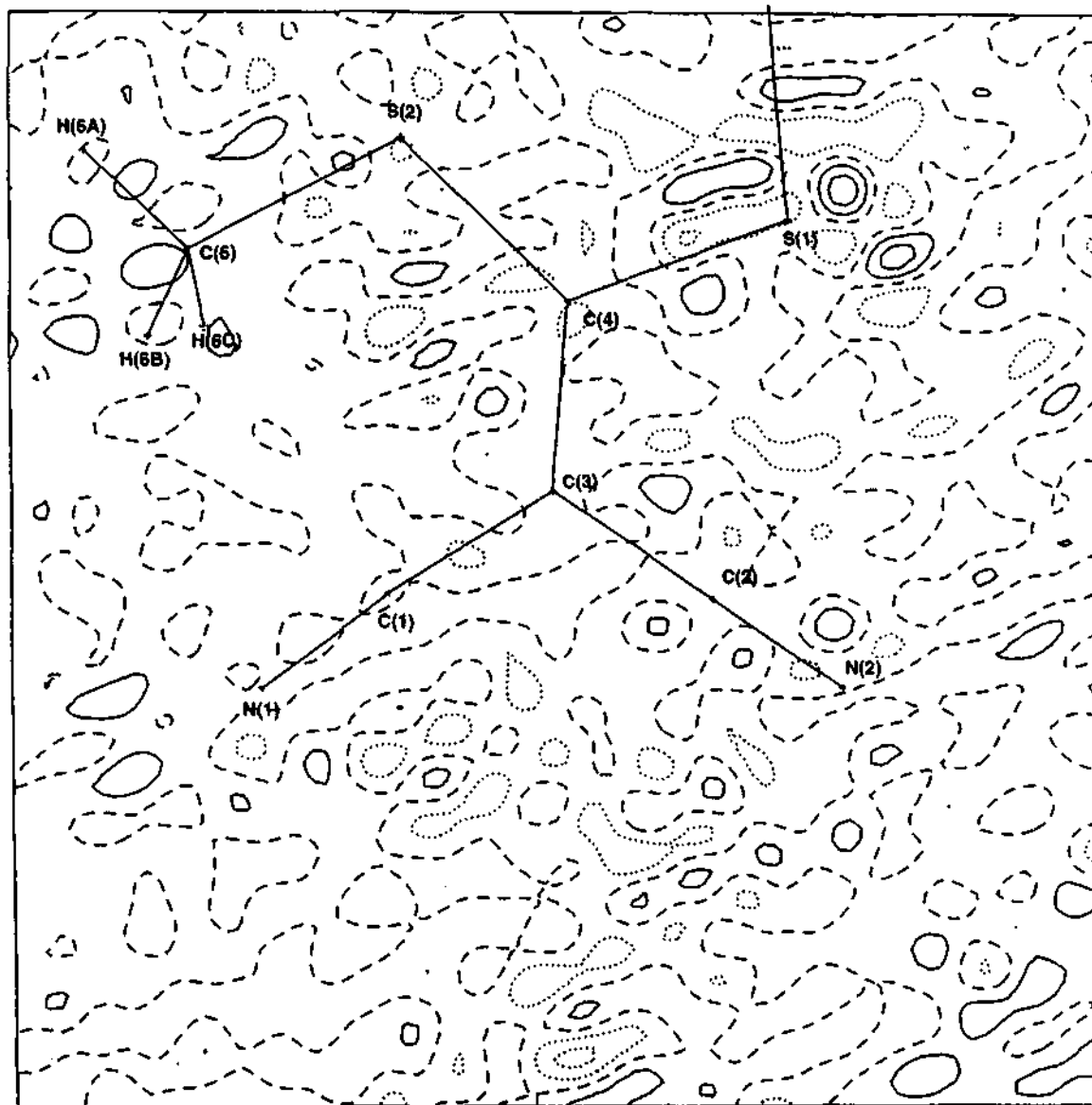
Definition of local coordination systems

Diamino derivative of 1,1-ethylenedicarbonitrile



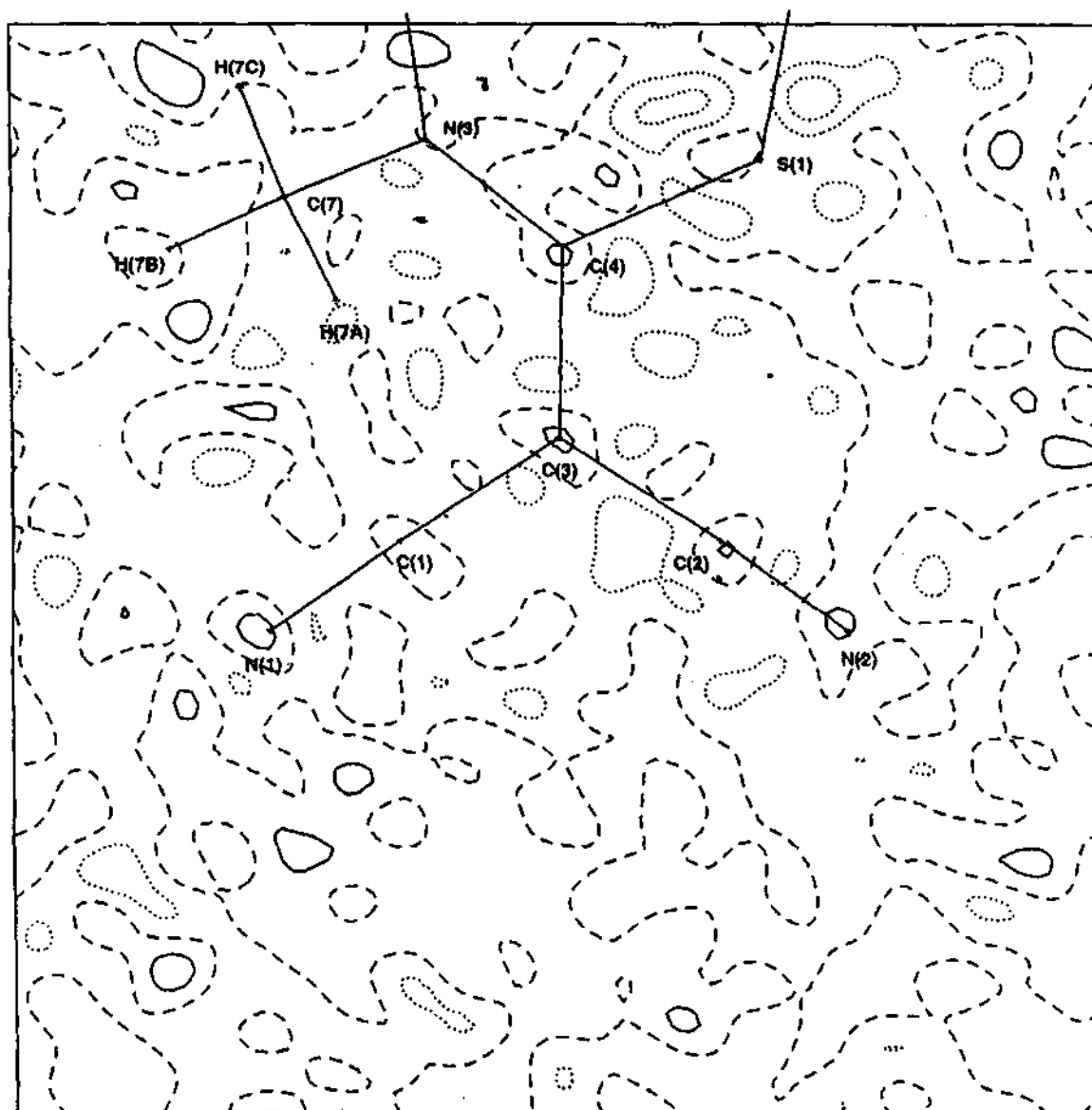
Residual electron density map in the plane containing N(1), C(3) and N(2) atoms. (contours at $0.1 \text{ e}\text{\AA}^{-3}$)

Dithio derivative of 1,1-ethylenedicarbonitrile



Residual electron density map in the plane containing N(1), C(3) and N(2) atoms. (contours at $0.1 \text{ e}\text{\AA}^{-3}$)

Thioamino derivative of 1,1-ethylenedicarbonitrile



Residual electron density map in the plane containing N(1), C(3) and N(2) atoms. (contours at $0.1 \text{ e}\text{\AA}^{-3}$)

Supplementary Table 19

Atomic coordinates ($\times 10^4$) and anisotropic displacement parameters ($\text{\AA}^2 \times 10^3$) for 7,7-di(S(+)-2-(methoxymethyl)pyrrolidino)-8,8-dicyanoquinodimethane.

Atom	x	y	z	U(eq)	U11	U22	U33	U23	U13	U12
O(1)	1121(2)	13072(2)	4575(1)	33(1)	25(1)	33(1)	44(1)	0(1)	15(1)	-4(1)
O(2)	2937(2)	15073(2)	508(1)	32(1)	30(1)	34(1)	35(1)	2(1)	14(1)	-2(1)
N(1)	2808(2)	14097(2)	3261(1)	18(1)	19(1)	16(1)	17(1)	-1(1)	3(1)	2(1)
N(2)	1638(2)	13160(2)	1712(1)	18(1)	18(1)	17(1)	18(1)	-2(1)	3(1)	3(1)
N(3)	10364(2)	9889(3)	2712(2)	38(1)	23(1)	34(1)	58(2)	-2(1)	14(1)	0(1)
N(4)	7416(2)	5676(3)	2287(2)	40(1)	26(1)	24(1)	69(2)	-3(1)	13(1)	0(1)
C(1)	4004(2)	11925(2)	2528(1)	16(1)	15(1)	17(1)	17(1)	1(1)	4(1)	3(1)
C(2)	3793(2)	10238(2)	2350(2)	18(1)	14(1)	17(1)	21(1)	0(1)	-4(1)	0(1)
C(3)	5001(2)	9226(3)	2356(2)	17(1)	16(1)	16(1)	21(1)	0(1)	6(1)	1(1)
C(4)	6461(2)	9846(3)	2516(1)	15(1)	14(1)	18(1)	14(1)	1(1)	5(1)	-1(1)
C(5)	6651(2)	11561(3)	2679(2)	18(1)	16(1)	18(1)	21(1)	0(1)	6(1)	-1(1)
C(6)	5447(2)	12565(3)	2698(2)	18(1)	17(1)	16(1)	20(1)	0(1)	6(1)	0(1)
C(7)	2760(2)	13073(2)	2498(1)	16(1)	16(1)	15(1)	17(1)	1(1)	5(1)	0(1)
C(8)	7708(2)	8792(3)	2512(2)	18(1)	15(1)	17(1)	22(1)	0(1)	5(1)	2(1)
C(9)	3504(2)	13669(3)	4304(1)	18(1)	18(1)	21(1)	15(1)	1(1)	3(1)	1(1)
C(10)	3591(3)	15327(3)	4856(2)	23(1)	27(1)	24(1)	18(1)	-2(1)	4(1)	-3(1)
C(11)	3335(3)	16629(3)	4036(2)	25(1)	31(1)	19(1)	24(1)	-2(1)	3(1)	-3(1)
C(12)	2236(2)	15800(3)	3185(2)	21(1)	25(1)	15(1)	22(1)	-2(1)	4(1)	3(1)
C(13)	2557(3)	12402(3)	4688(2)	24(1)	28(1)	23(1)	23(1)	5(1)	8(1)	0(1)
C(14)	157(3)	12000(4)	4949(2)	44(1)	39(1)	56(2)	40(1)	-6(1)	18(1)	-24(1)
C(15)	1695(2)	12574(3)	701(2)	23(1)	28(1)	22(1)	16(1)	-3(1)	-1(1)	6(1)
C(16)	138(3)	13042(3)	84(2)	29(1)	31(1)	29(1)	21(1)	-2(1)	-8(1)	2(1)
C(17)	-839(2)	13029(3)	838(2)	28(1)	23(1)	28(1)	30(1)	-2(1)	-5(1)	-1(1)
C(18)	160(2)	13816(3)	1747(2)	23(1)	16(1)	24(1)	26(1)	-1(1)	-1(1)	5(1)
C(19)	2958(3)	13357(3)	336(2)	28(1)	31(1)	34(1)	18(1)	-1(1)	6(1)	10(1)
C(20)	4149(3)	15887(4)	230(2)	38(1)	28(1)	56(2)	30(1)	2(1)	6(1)	-11(1)
C(21)	9164(2)	9400(3)	2625(2)	23(1)	22(1)	20(1)	28(1)	2(1)	9(1)	4(1)
C(22)	7543(2)	7084(3)	2391(2)	23(1)	17(1)	23(1)	31(1)	0(1)	7(1)	3(1)
H(2)	2686(2)	9724(2)	2208(2)	21						
H(3)	4818(2)	7921(3)	2233(2)	21						
H(5)	7749(2)	12092(3)	2790(2)	21						
H(6)	5623(2)	13864(3)	2846(2)	21						
H(9)	4624(2)	13182(3)	4353(1)	22						
H(10A)	2739(3)	15401(3)	5285(2)	28						
H(10B)	4675(3)	15485(3)	5355(2)	28						
H(11A)	2866(3)	17746(3)	4274(2)	30						
H(11B)	4366(3)	16931(3)	3820(2)	30						
H(12A)	1107(2)	15854(3)	3295(2)	25						
H(12B)	2268(2)	16350(3)	2472(2)	25						
H(13A)	2511(3)	11264(3)	4267(2)	29						
H(13B)	3030(3)	12134(3)	5467(2)	29						
H(14A)	-904(3)	12546(4)	4850(2)	65						
H(14B)	595(3)	11787(4)	5713(2)	65						
H(14C)	66(3)	10871(4)	4561(2)	65						
H(15)	1821(2)	11234(3)	709(2)	28						
H(16A)	152(3)	14255(3)	-247(2)	35						
H(16B)	-251(3)	12148(3)	-503(2)	35						
H(17A)	-1845(2)	13747(3)	577(2)	34						
H(17B)	-1143(2)	11780(3)	996(2)	34						
H(18A)	136(2)	15152(3)	1693(2)	27						
H(18B)	-162(2)	13448(3)	2427(2)	27						
H(19A)	4012(3)	12839(3)	730(2)	33						
H(19B)	2831(3)	13118(3)	-453(2)	33						
H(20A)	4095(3)	17161(4)	370(2)	57						
H(20B)	4091(3)	15695(4)	-533(2)	57						
H(20C)	5161(3)	15409(4)	649(2)	57						

Supplementary Table 20

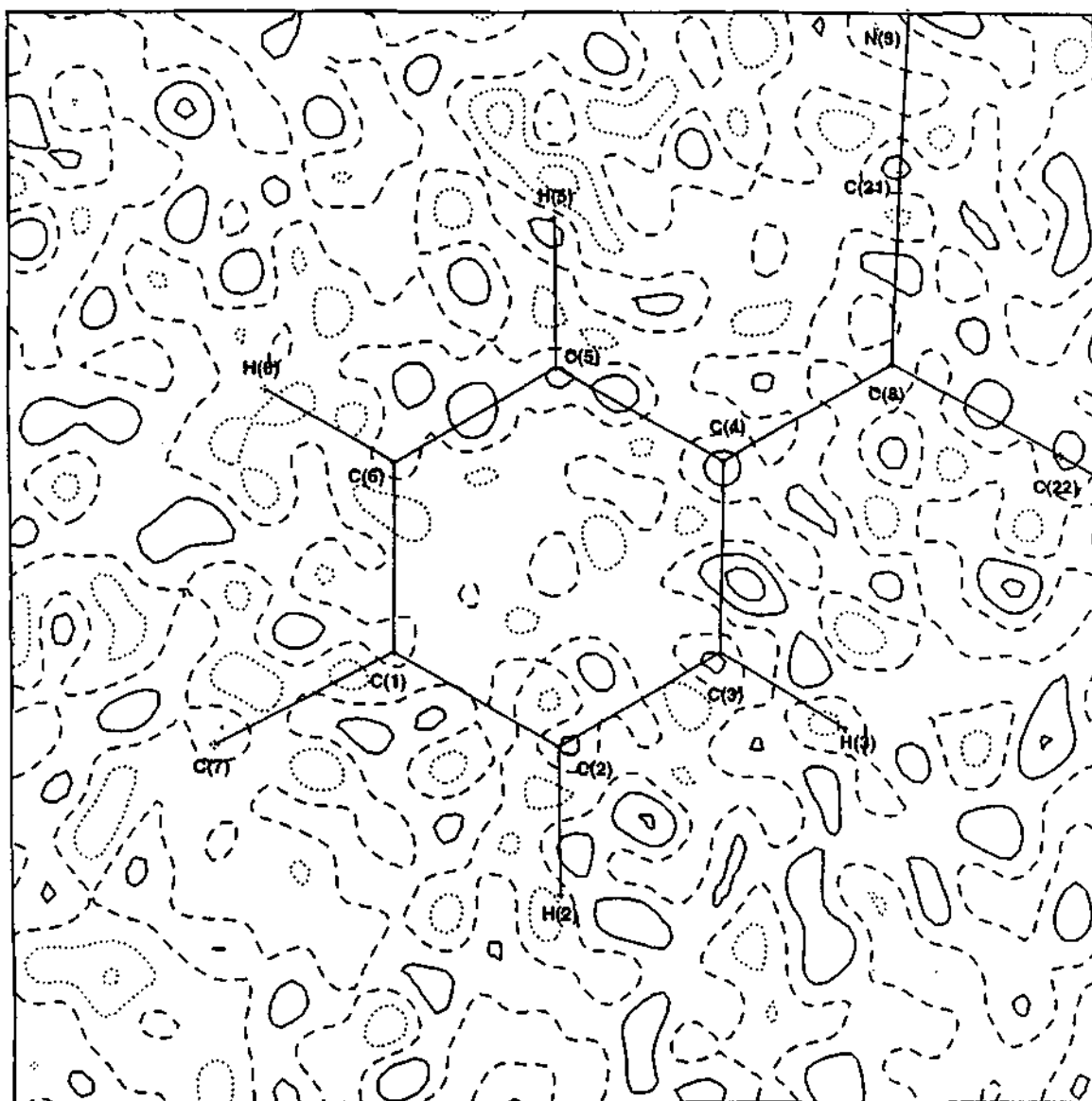
Distances, corrected and uncorrected for rigid body motion for 7-di(S(+)-2-(methoxymethyl)pyrrolidino)-8,8-dicyanoquinodimethane.

Bond	uncorrected	corrected
O1-C13	1.4149	1.4158
O1-C14	1.428	1.4293
O2-C19	1.421	1.4225
O2-C20	1.4307	1.432
N1-C7	1.3408	1.3421
N1-C9	1.4871	1.4882
N1-C12	1.4821	1.4834
N2-C7	1.329	1.3299
N2-C15	1.4933	1.4946
N2-C18	1.4815	1.4825
N3-C21	1.1621	1.1631
N4-C22	1.1603	1.1616
C1-C2	1.4036	1.4051
C1-C6	1.4049	1.4061
C1-C7	1.478	1.4791
C2-C3	1.3893	1.3903
C3-C4	1.4148	1.416
C4-C5	1.4217	1.4233
C4-C8	1.4418	1.4428
C5-C6	1.3891	1.3901
C8-C21	1.4128	1.414
C8-C22	1.4077	1.4092
C9-C10	1.5464	1.5481
C9-C13	1.5273	1.5288
C10-C11	1.5347	1.5359
C11-C12	1.5316	1.533
C15-C16	1.5505	1.5515
C15-C19	1.5159	1.5172
C16-C17	1.5295	1.5307
C17-C18	1.5284	1.5298

Supplementary Table 21
Multipole populations in 7,7-di(S(+)-2-(methoxymethyl)pyrrolidino)-8,8-dicyanoquinodimethane

Atom	M1	D1+	D1-	D0	Q0	Q1+	Q1-	Q2+	Q2-	Q0	O1+	O1-	O2+	O2-	O3+	O3-
O(1)	6.25(3)	0.05(2)	-0.06(2)	-0.03(2)	0.13(2)	0.00(2)	0.09(2)	0.20(2)	0.03(2)	0.20(3)	-0.03(3)	0.01(3)	0.07(3)	-0.01(3)	-0.03(3)	-0.02(3)
O(2)	6.25(3)	0.05(2)	-0.06(2)	-0.03(2)	0.13(2)	0.00(2)	0.09(2)	0.20(2)	0.03(2)	0.20(3)	-0.03(3)	0.01(3)	0.07(3)	-0.01(3)	-0.03(3)	-0.02(3)
N(1)	5.05(5)	-0.03(2)	-0.04(2)	0.03(2)	-0.02(3)	-0.05(2)	0.04(2)	-0.02(2)	0.02(2)	0.20(3)	-0.01(3)	-0.02(4)	0.15(3)	-0.02(3)	-0.02(3)	0.01(3)
N(2)	5.05(5)	-0.03(2)	-0.04(2)	0.03(2)	-0.02(3)	-0.05(2)	0.04(2)	-0.02(2)	0.02(2)	0.20(3)	-0.01(3)	-0.02(4)	0.15(3)	-0.02(3)	-0.02(3)	0.01(3)
N(3)	5.22(7)	0.01(3)	-0.04(3)	0.08(4)	0.14(4)	-0.05(3)	0.04(3)	-0.02(3)	0.02(3)	0.09(4)	-0.02(4)	-0.05(4)	-0.03(4)	-0.03(4)	-0.04(3)	-0.04(3)
N(4)	5.22(7)	0.01(3)	-0.04(3)	0.08(4)	0.14(4)	-0.05(3)	0.04(3)	-0.02(3)	0.02(3)	0.09(4)	-0.02(4)	-0.05(4)	-0.03(4)	-0.03(4)	-0.04(3)	-0.04(3)
C(1)	3.97(9)	0.00(3)	-0.08(4)	0.03(3)	0.20(4)	0.08(3)	0.10(4)	-0.01(3)	0.03(3)	0.24(5)	0.02(4)	-0.06(5)	0.20(5)	-0.04(5)	0.05(4)	0.03(4)
C(2)	4.27(8)	0.00(2)	-0.08(2)	0.04(3)	0.11(3)	-0.05(2)	0.01(2)	-0.21(3)	0.03(3)	0.28(4)	0.02(3)	-0.05(4)	0.20(4)	-0.06(4)	0.06(3)	0.01(3)
C(3)	4.23(8)	-0.02(2)	0.00(3)	-0.01(3)	0.06(3)	-0.03(2)	-0.04(3)	-0.16(3)	0.02(2)	0.27(4)	0.01(3)	0.02(4)	0.25(3)	-0.03(3)	-0.03(3)	-0.03(3)
C(4)	3.9(1)	0.01(3)	0.07(4)	0.05(3)	0.14(4)	-0.03(3)	0.03(4)	0.00(3)	0.00(3)	0.25(5)	-0.03(4)	-0.06(4)	0.13(5)	0.02(4)	-0.05(4)	-0.01(4)
C(5)	4.23(8)	-0.02(2)	0.00(3)	-0.01(3)	0.06(3)	-0.03(2)	-0.04(3)	-0.16(3)	0.02(2)	0.27(4)	0.01(3)	0.02(4)	0.25(3)	-0.03(3)	-0.03(3)	-0.03(3)
C(6)	4.27(8)	0.00(2)	-0.08(2)	0.04(3)	0.11(3)	-0.05(2)	0.01(2)	-0.21(3)	0.03(3)	0.28(4)	0.02(3)	-0.05(4)	0.20(4)	-0.06(4)	0.06(3)	0.01(3)
C(7)	4.02(9)	0.02(3)	-0.03(4)	-0.07(3)	-0.09(4)	-0.01(4)	-0.05(4)	-0.07(4)	-0.02(3)	0.35(6)	-0.03(5)	-0.07(4)	0.29(5)	0.09(4)	0.02(4)	0.00(4)
C(8)	4.6(1)	0.02(3)	-0.03(4)	-0.07(3)	-0.09(4)	-0.01(4)	-0.05(4)	-0.07(4)	-0.02(3)	0.35(6)	-0.03(5)	-0.07(4)	0.29(5)	0.09(4)	0.02(4)	0.00(4)
C(9)	4.08(6)	0.00(2)	-0.09(2)	0.04(3)	0.01(3)	0.00(3)	0.04(2)	0.03(2)	0.03(2)	0.35(4)	0.05(4)	0.04(3)	0.00(3)	-0.03(3)	-0.06(4)	-0.30(3)
C(10)	4.42(7)	-0.08(3)	0.15(3)	0.01(3)	-0.01(3)	0.06(3)	0.07(3)	-0.16(3)	-0.07(3)	0.25(4)	0.01(4)	-0.04(4)	0.02(4)	0.02(4)	-0.01(4)	-0.29(4)
C(11)	4.26(7)	-0.08(2)	0.14(3)	0.02(3)	-0.01(3)	-0.02(3)	-0.03(3)	-0.04(3)	-0.08(2)	0.33(4)	-0.10(4)	0.01(4)	-0.05(4)	0.02(3)	0.05(3)	-0.25(4)
C(12)	4.44(7)	-0.07(2)	0.12(3)	0.04(3)	0.04(3)	0.13(3)	0.05(3)	-0.10(3)	0.07(3)	0.26(4)	0.05(4)	0.00(4)	0.04(3)	0.04(3)	0.00(4)	-0.29(3)
C(13)	4.38(7)	-0.04(2)	0.19(3)	0.11(3)	0.08(3)	0.02(3)	-0.09(3)	-0.05(3)	-0.10(3)	0.37(4)	-0.01(4)	-0.02(4)	-0.01(4)	-0.05(3)	-0.05(4)	-0.30(4)
C(14)	4.3(1)	0.07(4)	0.18(4)	0.08(4)	0.07(4)	0.10(3)	-0.07(4)	-0.13(4)	0.04(4)	0.24(4)	0.16(5)	-0.03(5)	-0.04(4)	-0.22(4)	0.04(5)	-0.33(4)
C(15)	4.08(6)	0.00(2)	-0.09(2)	0.04(3)	0.01(3)	0.00(3)	0.04(2)	0.03(2)	-0.05(2)	0.35(4)	0.05(4)	0.04(3)	0.00(3)	-0.03(3)	-0.06(4)	-0.30(3)
C(16)	4.42(7)	-0.08(3)	0.15(3)	0.01(3)	-0.01(3)	0.06(3)	0.07(3)	-0.16(3)	-0.07(3)	0.25(4)	-0.04(4)	-0.04(4)	0.02(4)	0.02(4)	-0.01(4)	-0.29(4)
C(17)	4.26(7)	-0.08(2)	0.14(3)	0.02(3)	-0.01(3)	-0.02(3)	-0.03(3)	-0.04(3)	-0.08(2)	0.33(4)	-0.10(4)	0.01(4)	-0.05(4)	0.02(3)	0.05(3)	-0.25(4)
C(18)	4.44(7)	-0.07(2)	0.12(3)	0.04(3)	0.04(3)	0.13(3)	0.05(3)	-0.10(3)	0.07(3)	0.26(4)	0.05(4)	0.00(4)	0.04(3)	0.04(3)	0.00(4)	-0.29(3)
C(19)	4.38(7)	-0.04(2)	0.19(3)	0.11(3)	0.08(3)	0.02(3)	-0.09(3)	-0.05(3)	-0.10(3)	0.37(4)	-0.01(4)	-0.02(4)	-0.01(4)	-0.05(3)	-0.05(4)	-0.30(4)
C(20)	4.3(1)	0.07(4)	0.18(4)	0.08(4)	0.07(4)	0.10(3)	-0.07(4)	-0.13(4)	0.04(4)	0.24(4)	0.16(5)	-0.03(5)	-0.04(4)	-0.22(4)	0.04(5)	-0.33(4)
C(21)	4.15(9)	-0.06(3)	0.06(3)	0.10(5)	0.27(4)	0.03(3)	0.00(3)	0.03(2)	-0.03(2)	-0.01(5)	0.03(5)	0.04(5)	0.01(4)	-0.05(4)	0.05(3)	0.02(3)
C(22)	4.15(9)	-0.06(3)	0.06(3)	0.10(5)	0.27(4)	0.03(3)	0.00(3)	0.03(2)	-0.03(2)	-0.01(5)	0.03(5)	0.04(5)	0.01(4)	-0.05(4)	0.05(3)	0.02(3)

7,7-di(S(+)-2-(methoxymethyl)pyrrolidino)-8,8-dicyanoquinodimethane



Residual electron density map in the plane containing C(1), C(3) and C(5) atoms. (contours at $0.1 \text{ e}\text{\AA}^{-3}$)

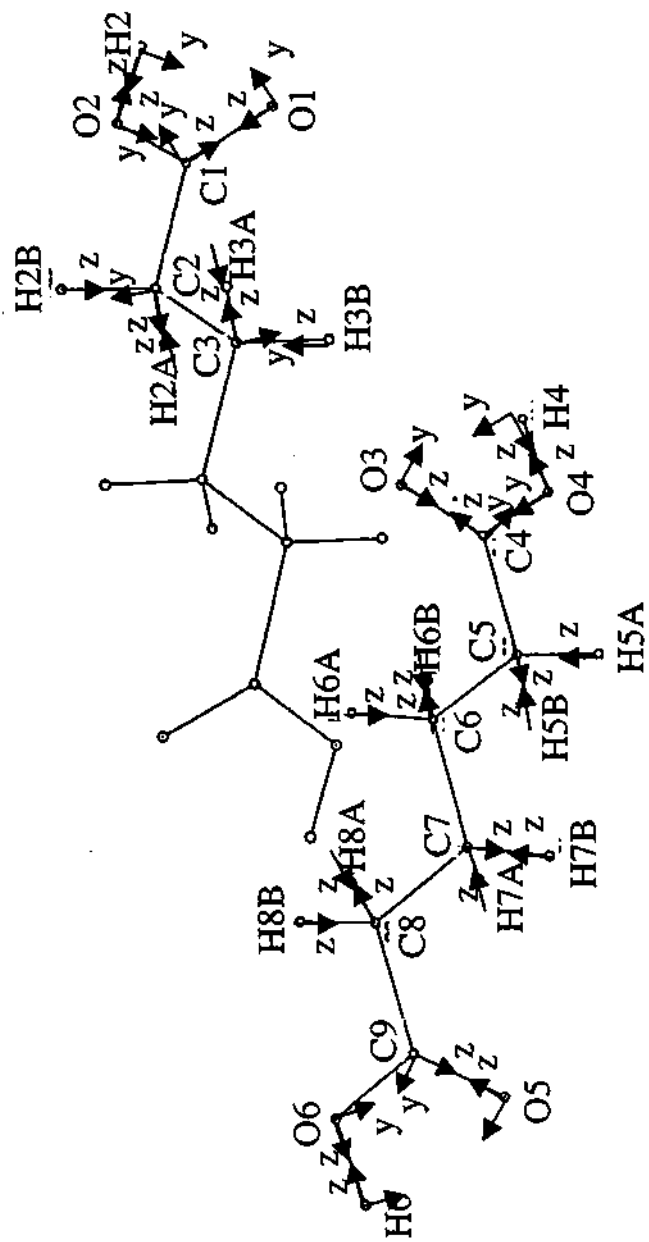
Supplementary Table 22Atomic coordinates ($\times 10^4$) and anisotropic displacement parameters ($\text{\AA}^2 \times 10^3$) for Adipic acid at 116 K.

Atom	x	y	z	U(eq)	U11	U22	U33	U23	U13	U12
O(1)	5690(4)	366(2)	13680(3)	18(1)	23(1)	21(2)	11(1)	-4(1)	9(1)	-9(1)
O(2)	3902(5)	-846(2)	13683(3)	19(1)	28(1)	19(2)	11(1)	-1(1)	11(1)	-8(1)
O(3)	741(5)	1356(3)	9326(3)	20(1)	28(1)	22(2)	12(1)	5(1)	10(1)	11(1)
O(4)	-997(5)	2587(3)	9320(3)	21(1)	32(1)	21(2)	12(1)	4(1)	12(1)	12(1)
O(5)	-602(5)	2104(3)	1961(3)	21(1)	33(1)	19(2)	15(1)	5(1)	14(1)	13(1)
O(6)	1009(5)	835(2)	1920(3)	19(1)	30(1)	18(2)	12(1)	3(1)	12(1)	9(1)
C(1)	4702(4)	-283(3)	13058(3)	13(1)	13(1)	18(2)	7(1)	-2(1)	4(1)	-3(1)
C(2)	4282(5)	-502(3)	11511(3)	14(1)	19(1)	16(2)	10(1)	-2(1)	7(1)	-2(1)
C(3)	5268(5)	119(3)	10786(3)	16(1)	23(1)	18(2)	9(1)	-3(1)	8(1)	-4(1)
C(4)	-161(4)	2022(3)	8715(3)	13(1)	16(1)	17(2)	8(1)	1(1)	6(1)	2(1)
C(5)	-395(5)	2281(2)	7218(3)	14(1)	21(1)	12(2)	10(1)	1(1)	7(1)	2(1)
C(6)	336(4)	1593(3)	6424(3)	14(1)	17(1)	17(2)	10(1)	3(1)	7(1)	2(1)
C(7)	-153(5)	1855(3)	4868(3)	15(1)	22(1)	16(2)	9(1)	2(1)	8(1)	4(1)
C(8)	411(5)	1137(3)	4024(3)	15(1)	23(1)	15(2)	10(1)	3(1)	9(1)	4(1)
C(9)	209(5)	1415(2)	2542(3)	13(1)	19(1)	12(2)	10(1)	0(1)	8(1)	2(1)
H(2)	4220(5)	-673(2)	14661(3)	28						
H(4)	-798(5)	2386(3)	10270(3)	31						
H(6)	840(5)	1044(2)	979(3)	28						
H(2A)	2762(5)	-473(3)	10947(3)	17						
H(2B)	4735(5)	-1169(3)	11441(3)	17						
H(3A)	6794(5)	74(3)	11315(3)	19						
H(3B)	4850(5)	790(3)	10871(3)	19						
H(5A)	354(5)	2892(2)	7257(3)	16						
H(5B)	-1887(5)	2399(2)	6629(3)	16						
H(6A)	-296(4)	962(3)	6470(3)	17						
H(6B)	1862(4)	1529(3)	6933(3)	17						
H(7A)	-1664(5)	1977(3)	4387(3)	18						
H(7B)	580(5)	2458(3)	4825(3)	18						
H(8A)	1872(5)	950(3)	4593(3)	18						
H(8B)	-466(5)	564(3)	3953(3)	18						

Supplementary Table 23
Distances, corrected and uncorrected
For rigid body motion for Adipic acid at 116K

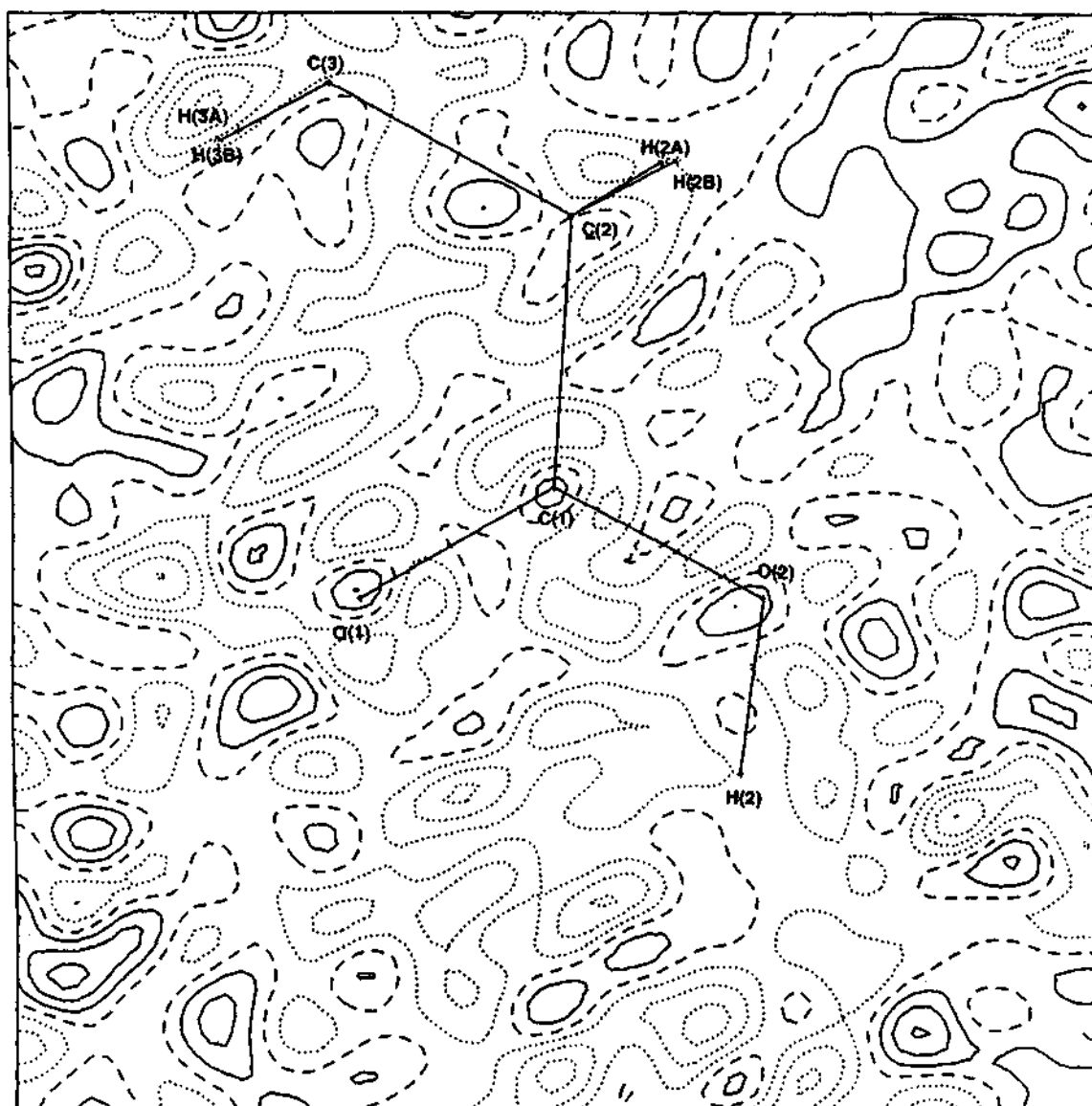
Bond	Uncorrected	Corrected
O1-C1	1.237	1.2374
O2-C1	1.3123	1.3128
O3-C4	1.2288	1.2297
O4-C4	1.3174	1.3183
O5-C9	1.2257	1.2266
O6-C9	1.3261	1.3269
C1-C2	1.506	1.507
C2-C3	1.52	1.5206
C4-C5	1.5007	1.5017
C5-C6	1.5161	1.5171
C6-C7	1.522	1.5231
C7-C8	1.5157	1.5167
C8-C9	1.5001	1.5012

Adipic acid at 116 K



Definition of local coordination systems

Adipic acid at 116 K



Residual electron density map in the plane containing C(1), O(1) and O(2) atoms. (contours at $0.1 \text{ e}\text{\AA}^{-3}$)

548.8
P